Exploring the molecular determinants of behavioral changes induced by ketamine at the nanoscale

Floriane Uyttersprot

université de BORDEAUX

THÈSE PRÉSENTÉE

POUR OBTENIR LE GRADE DE

DOCTEURE DE

L'UNIVERSITÉ DE BORDEAUX

ÉCOLE DOCTORALE SCIENCES DE LA VIE ET DE LA SANTÉ

SPÉCIALITÉ NEUROSCIENCES

Par Floriane Uyttersprot

CARACTERISATION DES DETERMINANTS MOLECULAIRES DES CHANGEMENTS COMPORTEMENTAUX INDUITS PAR LA KETAMINE A L'ECHELLE NANOMETRIQUE

EXPLORING THE MOLECULAR DETERMINANTS OF BEHAVIORAL CHANGES INDUCED BY KETAMINE AT THE NANOSCALE

Sous la direction de : Julien Dupuis

Soutenue le 19 septembre 2024

Membres du jury :

M. Julien DUPUIS	Chargé de Recherche, Université de Bordeaux,	Directeur de thèse
Mme. Ana Luisa CARVALHO	Professeure, Université de Coimbra,	Rapportrice
Mme. Julie PERROY	Directrice de Recherche, Université de Montpellier,	Rapportrice
M. Thomas FRERET	Professeur, Université de Caen,	Examinateur
M. Stéphane OLIET	Directeur de Recherche, Université de Bordeaux	Président

Titre : Caractérisation des déterminants moléculaires des changements comportementaux induits par la kétamine à l'échelle nanométrique

Résumé : Au sein du système nerveux central (SNC), les récepteurs glutamatergiques de type NMDA (RNMDA) sont les principaux acteurs de la transmission neuronale excitatrice, permettant l'entrée massive de calcium dans les cellules neuronales et l'activation subséquente de voies de signalisation spécifiques. Les récents progrès de la microscopie super résolution ont révélé qu'au-delà de leur fonction ionotropique, leur organisation précise et dynamique à l'échelle nanométrique au niveau des synapses contribuent aux phénomènes de plasticité synaptique sous-tendant la cognition et la mémoire. Ces observations soulèvent la question de l'intérêt thérapeutique potentiel de l'organisation synaptique des NMDAR. De plus, les antagonistes compétitifs et non compétitifs tels que les bloqueurs de canaux ouverts (OCB) provoquent une inhibition similaire de la signalisation des RNMDA mais différents résultats comportementaux, ce qui suggère l'implication de mécanismes indépendants de la fonction ionotropique. En utilisant une combinaison de techniques de microscopie super résolution et de tests comportementaux, nous démontrons que la kétamine, un antagoniste non compétitif des RNMDA, favorise la rétention synaptique des récepteurs et atténue ainsi les déficits comportementaux de type anxiété/dépression provoqués par les auto-anticorps de patients psychotiques. Nous avons ensuite examiné si ces modifications de distribution synaptique des RNMDA pouvaient contribuer aux réarrangements de la connectivité cérébrale soutenant les propriétés antidépresseurs de la kétamine. La dépression est souvent attribuée à une activité anormale dans les structures clés soutenant l'humeur et la récompense, à savoir les structures cortico-méso-limbiques. Les traitements monoaminergiques actuels présentent un long délai d'efficacité et jusqu'à un tiers des patients sont résistants. Ainsi, la découverte qu'une dose sous-anesthésique de kétamine induit un effet antidépresseur rapide et durable a fait naître de nouvelles perspectives thérapeutiques. Cependant, les mécanismes par lesquels la kétamine agit sur la signalisation des RNMDA dans le réseau cortico-méso-limbique pour produire son effet antidépresseur ne sont toujours pas clairs. Les expériences ont été menées sur un modèle pharmacologique basé sur l'exposition chronique à la corticostérone (CORT). Une batterie de tests comportementaux a tout d'abord été réalisée pour évaluer l'impact de la kétamine sur les différentes modalités du phénotype dépressif chez la souris. Nous avons ensuite évalué à l'échelle mésoscopique les changements d'activité et les réarrangements des réseaux neuronaux au début (90 minutes) et à la fin (24 heures) de l'établissement de l'effet antidépresseur de la kétamine en couplant la détection de gène précoce immédiate et la microscopie à feuillet de lumière. Des expériences parallèles de suivi de RNMDA uniques par microscopie de localisation photoactivée (PALM) ont été réalisées sur des neurones

corticaux chroniquement incubés avec de la corticostérone pour examiner les changements de diffusion des GluN2A-RNMDA et des GluN2B-RNMDA au niveau des synapses, 90 minutes ou 24 heures après la kétamine. Dans l'ensemble, nous démontrons l'implication de nouveaux mécanismes moléculaires pour expliquer les changements comportementaux induits par la kétamine. Notre travail propose la manipulation de la distribution synaptique des RNMDA comme stratégie thérapeutique ciblant les déficits pathologiques induits par les auto-anticorps et les déficits associés à la dépression.

Mots clés : récepteurs NMDA, kétamine, nano-organisation, dépression

---

Title: Exploring the molecular determinants of behavioral changes induced by ketamine at the nanoscale

Abstract: In the central nervous system (CNS), NMDA receptors (NMDAR), part of the ionotropic glutamate receptors family, mediate the majority of fast excitatory neuronal transmission. By allowing calcium influx into neuronal cells and subsequent activation of signaling pathways, NMDAR play a central role in synaptic plasticity events that occur during development and underly cognition and memory processes. Recent advances in super resolution microscopy have revealed unexpected dimensions of NMDAR signaling beyond their ionotropic function, which contribute to synaptic physiology. Indeed, NMDAR adopt a precise and dynamically regulated nanoscale organization at synapses which regulates their plasticity and controls memory formation, thereby raising the question whether NMDAR synaptic organization can be of therapeutic interest. Moreover, competitive and non-competitive antagonists like open channel blockers (OCBs) elicit similar inhibition of NMDAR signaling but result in distinct behavioral outcomes, suggesting mechanisms independent of ion flux blocking. Using a combination of super resolution microscopy techniques and behavioral testing, we demonstrate that the non-competitive NMDAR antagonist ketamine enhances the synaptic trapping of receptors, and thereby alleviates anxiety/depression-like behavioral deficits caused by autoantibodies from psychotic patients. We then examined whether these changes in NMDAR distribution at synapses may contribute to ketamine-elicited rearrangements in brain connectivity supporting its antidepressant properties. Major depressive disorder is a leading cause of disability worldwide and is believed to be the consequence of abnormal activity in key structures supporting mood and reward, namely cortico-meso-limbic structures. Current treatments, such as serotonin-based pharmacotherapies and

psychotherapies, have a delayed onset of action and still up to one-third of patients are resistant. Thus, the recent discovery that a subanesthetic dose of ketamine induce a rapid-acting and sustained antidepressant effect has risen new hopes for the treatment of depression. Despite intense investigation, the mechanisms through which ketamine acts on NMDAR signaling within the cortico-meso-limbic network to produce its antidepressant effect remain unclear. To address this, we have developed a multi-level approach combining single-molecule imaging to monitor NMDAR synaptic redistributions and detection of immediate early gene expression in a pharmacological model of depression using light-sheet microscopy to identify network rearrangements induced by ketamine. Among all existing depression model, experiments were performed on a pharmacological model using corticosterone (CORT). A battery of behavioral tests was performed to evaluate ketamine impact on different modalities of the depression-like phenotype. We then assessed activity changes and network rearrangements at early (90 min) and later (24 hours) stages of ketamine antidepressant effect establishment. Parallel single-particle tracking using photoactivated localization microscopy (PALM) experiments were performed on cortical neurons chronically incubated with corticosterone to examine changes in GluN2A-NMDAR and GluN2B-NMDAR organization at synapses, 90 min or 24 hours after ketamine. Overall, we provide new molecular mechanisms supporting ketamine-elicited behavioral changes, offering NMDAR synaptic distribution manipulation as a therapeutic strategy for both autoantibody-induced pathological deficits and depressive-associated deficits.

Keywords: NMDA receptor, ketamine, nanoscale organization, depression

---

Unité de recherche

Institut Interdisciplinaire de Neurosciences, Université de Bordeaux, UMR5297, Centre Broca Nouvelle Aquitaine, 146 rue Léo Saignat 33076 Bordeaux Cedex (France)

Remerciements

Firstly, I would like to thank the members of my PhD defense committee for accepting to review and discuss my work, and for providing their valuable feedback: Dr Ana Luisa Carvalho, Dr Julie Perroy, Dr Thomas Freret and Dr Stéphane Oliet.

Dr Laurent Groc, merci de m'avoir accepté au sein de ton équipe et de m'avoir ouvert les portes à un immense champs de possibilités. Merci de ton soutien et de l'intérêt que tu as porté à mes recherches et pour nos riches discussions.

Je tiens à remercier mon directeur de thèse, Dr Julien Dupuis. Un grand merci pour m'avoir fait confiance et d'avoir été toujours disponible lorsque j'en avais besoin. Tu as été un réel guide lors de cette aventure qu'est la thèse, peu importe le nombre et la nature de mes questions, mes idées, mes inquiétudes, mes frustrations parfois, tu étais là pour me rebooster. Merci pour ces heures de discussions à parler concepts, ton expertise m'a beaucoup apporté. Merci pour ton soutien, ta bonne humeur, mais aussi tes conseils running !

Merci à tous les anciens et actuels membres de la team GROC, pour les conseils, discussions et réflexions scientifiques qui ont grandement nourri ma réflexion. À Delphine, Frédéric et Hélène. À Olivier pour le temps que tu m'as accordé à me former sur diverses manips et surtout ta bonne humeur constante. Merci à Lina qui a contribué aux manips *in vitro* dans le cadre de son stage de master 2. À tous les collègues : Léa, Flávia, Laurine, Adèle, Camille, Magalie, Morgane, Romain, Thomas L, Thomas G, Ivo, Juan, Nathan, Daniel, Mar, Zoë, Dominique... Pour tous les bons moments passés au lab, les happy hours, et le package lunch-rires-discussions mémorables. À ceux qui sont devenus beaucoup plus et pour tous les moments passés en dehors du lab. Grâce à vous, j'ai notamment maintenu mes compétences en judo, enfin appris la best technique pour arrêter le hoquet, et surtout beaucoup dansé, chanté et ris !

Je souhaiterai également remercier l'équipe du GRAP à Amiens, que j'ai intégré au cours de mes stages de Master, et plus particulièrement Pr Mickaël Naassila, Pr Olivier Pierrefiche et Dr Chloé Deschamps. Mickaël, merci pour votre confiance et les opportunités offertes. Olivier, merci pour votre investissement dans ma construction en tant que jeune chercheuse et votre soutien. Et bien sûr merci à toi Chloé pour ta patience (je pense qu'il en fallait lors des calculs de dose d'injection) ta pédagogie et ton amitié.

Merci au Dr Frédéric Bretzner de m'avoir accueilli au sein de son équipe à Québec pendant quelques mois il y a maintenant plus de 3 ans et offert une superbe expérience. Merci au Dr Marie Roussel, alias Marrou, qui m'a pris sous son aile et partagé son savoir scientifique et technique. Tu es devenue une amie très chère, ta présence, ta guidance et ton soutien permanent même à des milliers de kilomètres sont vraiment précieux.

Un immense fancy massive merci aux membres successifs de mon bureau, ce qui lui a d'ailleurs valu différents petits noms et aménagements ; the MDZF office, the office of dead plants and finally, the office of secrets... Je suis heureuse d'avoir croisé votre chemin et de vous compter parmi mes amis, vous tenez une place toute particulière dans mon cœur alors allez let's go pour quelques épanchements.

First of all, a big thank you to the first person that warmly welcomed me in this cozy office, Madame Maria del Mar. "Do you want to come for a coffee or tea Floriane?" No offense for the other little dragon and the shy little boy at the time. Thank you for the laughs, your professional and personal advices, the craziness (we definitely have unexploited talent for parkour). It's weird because I definitely feel that these few months

with you were too short (you could have stayed more quoi) but at the same time I keep so many great memories of our time together. Next time big reunion in Barcelona!

A big thanks and bisous bisous to the second “left too early” person, the one and only Daniboy Chasseur. I have countless amazing memories with you, and our evening discussions are what I miss the most. You have been my favorite person to annoy on a daily basis. Thank you for letting me express myself in the most unbearable and crazy ways. At some point, we were just two kids messing with each other, and I loved it. At the same time, you were and still are a brilliant scientist to whom I never hesitated to ask any questions, even the stupidest ones, without ever feeling judged. See you soon, my friend.

Thank you to Madame Domimi, it was a pleasure to share a daily life in the office with you. Thank you for being a daily support and a fair mama gnocchi, for pushing me when it was necessary, and for insisting on having a beer when that was necessary too, voilà. When I wasn’t able to put things into perspective (relativiser quoi), I am so grateful that you did it for me. Thank you for taking care of our well-being and supporting even our craziest ideas. Don’t be surprised if I randomly reach out for your advice in the future, as well as to plan some fancy week end abroad!

Merci mon cher Nathou, pour ton soutien sans faille pendant ces 3 ans mais surtout d’avoir accepté ma demande en colocation de bureau ! En même temps on a passé tellement de moment café-thé le matin ensemble dans le bureau avant ton emménagement, c’était la suite logique ! Mille mercis pour ton écoute, d’avoir toujours les bons mots, et surtout ta capacité à prendre les choses en main dans mes moments de détresse (et aussi quelques suprenants zoomies). Comme on a été dans le même bateau, j’espère t’avoir rendu au moins la moitié du soutien que tu m’as apporté ces derniers mois. En écrivant ses lignes, tu es à quelques jours de soumettre toi aussi ta thèse et ce n’est que le début, une grande carrière t’attend j’en suis certaine ! Et aussi merci à toi et Sissi pour nos super moments passés ensembles, j’espère qu’il y en aura pleins d’autres !

Un grand merci à la constante de ma daily life de ces dernières années (Z = 33/36 soit 0.916...), ma chère Zozi. Tu es définitivement devenu le repère de ma vie de thésarde ici à Bordeaux, j’ai toujours pu compter sur ton soutien à toute épreuve (même d’une voiture hantée ou d’une gourde aquarium), ma target préférentielle de bidirectional big lances et pour enfin répondre à la question que tu te poses depuis longtemps, ouais I think it’s veri funny ! Sincèrement, une page s’est tournée quand tu as quitté the office, je souhaite à tout new PhD student arrivant dans une nouvelle équipe de tomber sur une Zozi. Merci pour ton amitié et pour tous ces lunch runs, d’ailleurs merci aussi au début de ne pas avoir cessé de m’inviter aux running sessions du mercredi soir jusqu’à ce qu’un beau jour j’accepte de venir joyeusement souffrir avec toi, Mathou, Didi et Coco. J’en profite pour également vous remercier, Mathou pour ta constante bienveillance mais pas pour les pyramides ni pour les excentriques, Didi pour ton rire communicatif et Coco pour les Elmaleh vibes, je suis très succincte mais sachez que vous m’avez beaucoup apporté (il faut se prévoir une course ensemble fissa). Une pensée pour Laure, alias Lolo, merci pour ta douceur, je me suis toujours sentie apaisée après un moment avec toi et promis je vais prendre des cours de rock !

Merci à mes amis pour tous les moments partagés ensemble et leur soutien. Aux anciens rencontrés sur les bancs de la fac et qui sont still here, les pedros Alex et Baptiste, pour le fun, les vacances, les week-ends, les péripéties rocambolesques, tellement de choses partagées ensemble depuis la licence que je ne sais quoi dire ! Ces moments sont de véritables bulles d’air frais (c’est plus joli que des bols) et mes abdos mettent toujours trois jours à s’en remettre tellement j’ai ris. Et à un moment donné aussi, petite pensée pour la dernière recrue Emma, merci de m’avoir soutenu dans ces derniers mois de thèse, une notif d’un réel de boubou et j’oubliai les deadlines pendant quelques secondes ! Merci à Bastien et Anaïs pour m’avoir fait attendre le week-end avec impatience pour nos journées plages et super soirées apéros grands débats

et jeux de société, ils nous restent une belle liste d'escape game à faire ! Merci aux ministres Jeff et Julien pour leur soutien, les sorties vélos (bon en fait LA sortie vélo, c'est quand le rdv decathlon ?) et le fun ensemble, vivement qu'on fête ça autour d'une bièraubeurre !

Un merci plein d'amour pour l'homme qui partage ma vie et son indéfectible soutien, le seul et unique Ninou. Merci de ne pas t'enfuir en courant devant Gremlinsprot qui ne gère plus la pression, de croire en moi lorsque je n'y arrive pas. Je ne sais que dire tellement il y a de choses pour lesquelles je te suis reconnaissante, merci d'épanouir ma vie, d'être le sel sur la tartine d'avocat, d'être ma maison. En fait je pourrai presque écrire une deuxième thèse, « Caractérisation des bénéfices induits par le Ninou à l'échelle de la Sprot ». J'en profite pour également vous remercier, Jean-Michel et Florence, de me soutenir et m'encourager depuis déjà plusieurs années, nos discussions au coin du feu autour d'un thé (et de chocolat) sont mes instants préférés. Une pensée de gratitude et des bisous pour Perrine, Paul et Gabriel, dont les moments passés ensemble ont toujours rechargé mes batteries.

J'aimerai terminer par remercier ma famille. Merci à vous, Maman et Papa, de m'avoir toujours laissé le choix et donné les moyens de faire ce que je voulais, même si j'avais voulu aller étudier les éléphants au bout du monde, j'aurai pu compter sur votre soutien. Merci de m'avoir transmis vos valeurs, le respect, l'ambition, le travail appliqué. Je ne serai jamais arrivée jusqu'ici sans vous. Merci aussi pour les heures passées à me faire réviser mes cours, à m'avoir appris à ne pas considérer mes échecs comme tels et m'avoir reboosté dans ces moments-là, merci également pour m'avoir appris la différence entre les torchons et les serviettes, merci pour les tupperware du dimanche soir, merci pour Jazz, Aragorn et Ocean, et particulièrement Aragorn pour tout l'amour et l'apaisement qu'il m'apportait quand je rentrais le week end, merci pour tout et bien plus encore. Merci à mon chouchou de petit frère plus grand que moi, Allan, de m'avoir donné de la force quand j'en avais besoin et de toujours croire en moi, merci de ne jamais m'avoir rendu la pareille avec Gollum, mais surtout de me faire marrer comme personne à kékéland ! Prépare-moi ta meilleure playlist stp, qu'on fête ça dignement.

Une pensée pour mes grands-parents qui m'ont toujours soutenu. À ma mamie Colette et les incalculables parties de scrabble, le jeu des panneaux et le best of de Brassens. Merci d'être restée fière de moi et supportrice pour 4. À ma mamie Monique, j'aurai aimé que tu ne connaisses pas seulement la petite fille que j'étais, mais que tu sers dans tes bras la jeune femme tout juste diplômée de son doctorat. À mon papi Bernard, ta caille aurait bien eu besoin de plusieurs après-midi tv et de ta crème de cassis au cours de ces dernières années (et de ton aide pour convertir les gens à la cancoillotte). À mon papi Maurice, j'aurais tout donné pour que tu sois là le 19 septembre prochain et entendre ton « ohhh c'est bien ma grande ! », puis fêter ça autour d'une de tes meilleures bouteilles et de quelques huitres (évidemment je n'en prendrais qu'une ou deux, pour fayoter).

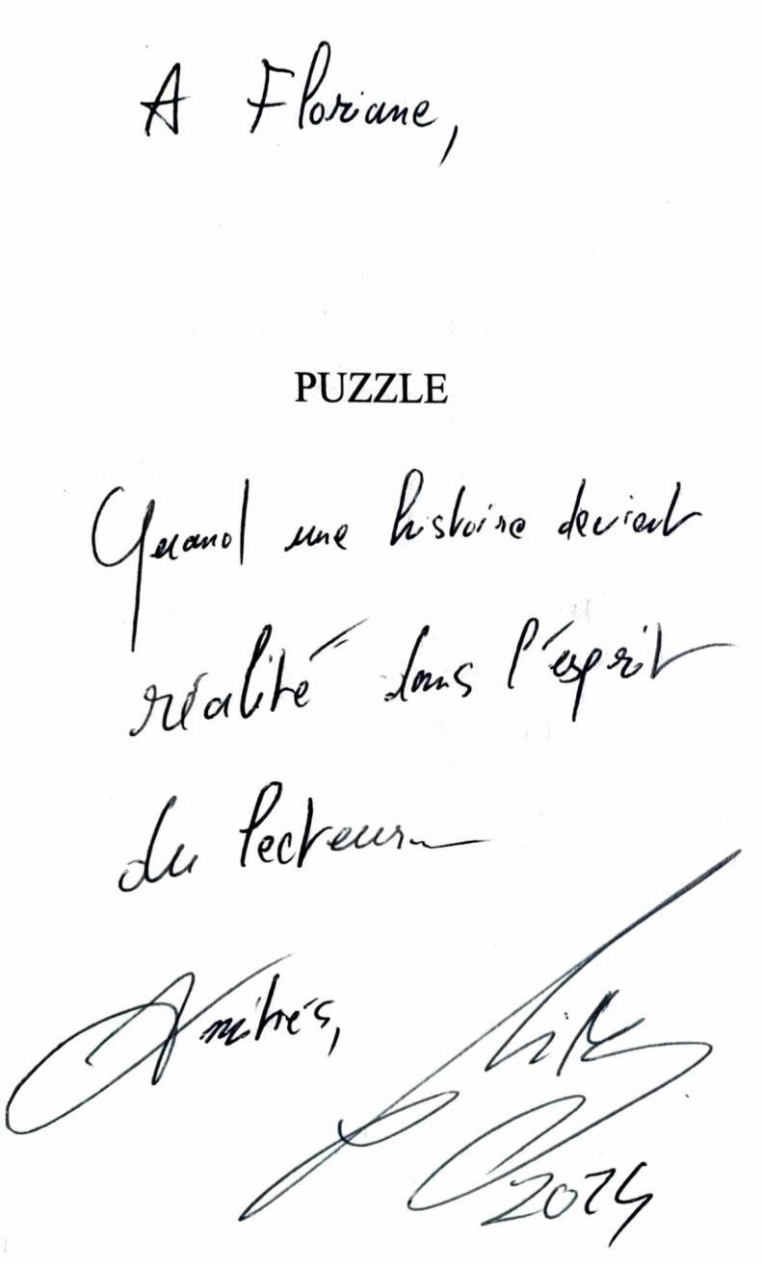

Franck Thilliez.

Table of contents

Introduction

CHAPTER I: NMDA RECEPTORS IN BRAIN FUNCTIONS AND MENTAL DISORDERS

A. A glutamatergic overview

The brain is a complex organ responsible for the gathering and processing of various types of signals coming from the body and the environment. Its cellular components, neurons and glial cells, are able to communicate between each other at contact points called synapses, notably by the release of chemical messengers called neurotransmitters that cross the synaptic cleft to reach out specific receptors. This interneuronal communication underlies brain function (Lovinger, 2008). To guarantee a good and stable communication, neuronal circuits keep a balance between excitation processes and inhibition events, where two major types of systems intervene: an excitatory system supported by excitatory neurotransmitters and an inhibitory system supported by inhibitory neurotransmitters. Glutamate is the main excitatory neurotransmitter of the central nervous system, which makes the glutamatergic system the principal excitatory system of the brain (Orrego and Villanueva 1993).

The glutamatergic system is a dynamic system, meaning that it involves different types of actors that are presynaptic, postsynaptic, neurotransmitters. Moreover, the quantity, the sensitivity and the level of activity displayed by these different actors define the strength of the synaptic transmission. The glutamatergic system also involves the action of two categories of glutamatergic receptors, i.e. ionotropic receptors and metabotropic receptors. Metabotropic glutamate receptors (mGluR) regulate synaptic neuronal transmission through the activation of G proteins modulating second messenger systems. On the contrary, ionotropic glutamate receptors (iGluR) are fast-acting ion channels composed of different subunits organized around a central pore. They are directly activated upon glutamate binding, causing ion flux modifications and consequent changes in the electrical potential of the membrane and neuronal excitability. Ionotropic glutamate receptors are divided in several categories depending on the binding ligand, including N-methyl-D-aspartate receptors (NMDAR), α-amino-3-hydroxy-5-methyl-4-isoxazolepropionic acid (AMPA) receptors and kainate receptors (Ottersen and Landsend 1997; Reiner and Levitz, 2018). Rapid mobilization of glutamatergic receptors at the synapse and its signaling interactors is possible thanks to a specific zone organized in the postsynaptic neuron called the postsynaptic density (PSD).

The PSD is a 30 to 50 nm thick protein-concentrated zone that is connected to actin filaments of the cytoskeleton. Indeed, hundreds of proteins supporting synaptic transmission are located in the PSD including receptors, scaffolding proteins and cytoskeletal proteins (Sheng and Kim, 2011). More precisely, the PSD is divided into a core layer and a pallial layer. The core layer of the PSD is directly located below the postsynaptic membrane and contains membrane associated guanylate kinases (MAGUK), of which the most abundant is postsynaptic density protein 95 (PSD-95). PSD-95 is binding to receptors of the postsynaptic membrane, NMDA and AMPA receptors with their N-terminal tail, and to a guanylate kinase-associated protein (GKAP) at their C-terminal (Dosemeci et al., 2016). The core layer of the PSD is followed by the pallial layer, more cytoplasmic. This pallial layer is mainly composed of Shank and Homer proteins that are able to bind each other to functionally connect post synaptic receptors to intracellular calcium stores of the endoplasmic reticulum (Sheng 2011). Upon excitation, the PSD undergoes morphological changes triggered by bonding of its different components, leading to the activation and accumulation of calmodulin-dependent protein kinase II (CaMKII) in the pallial layer of the PSD, where functioning coupling to NMDA receptors and subsequent calcium ion influx become possible (Petersen et al., 2003).

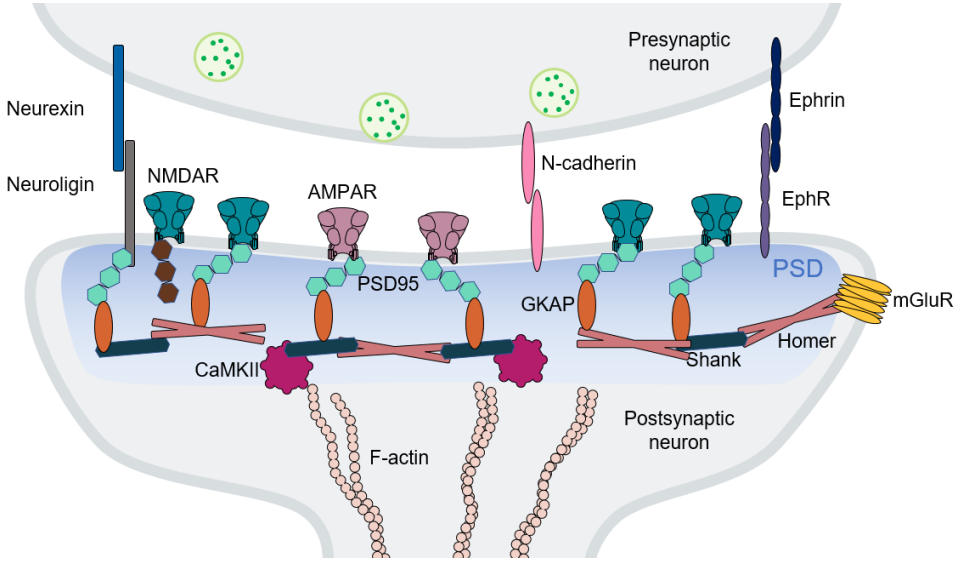

Figure 1: The glutamatergic synapse and its main actors. Postsynaptic receptors (NMDAR, AMPAR, EphR) and transmembrane proteins (Neuroligin, N-cadherin) are anchored to the membrane by interactors of the core layer of the PSD, i.e. PSD95 and GKAP. These proteins interact with the pallial layer of the PSD containing SHANK and Homer proteins. The pallial layer of the PSD is connected to the cytoskeleton via filaments of F-actin.

In order to bring structural stability and signal transmission efficiency, multiple synaptic protein complexes and transmembrane receptors are inserted into the phospholipid bilayer. Synaptic cell adhesion molecules (CAM) have a direct control over the organization of molecules at both presynaptic and postsynaptic sites. Indeed, they regulates excitatory synaptic transmission through interactions with glutamate receptors. CAM usually form trans-synaptic adhesion complexes that shape postsynaptic properties. For example, neurexin-neuroligin

complexes, N-cadherin- β-cadherin associations and Ephrin-B-EphBs (EphB receptor tyrosine kinase) complexes are known to tightly regulate synaptic plasticity notably by interacting with NMDA receptors and AMPA receptors (Figure 1)(de Wit and Ghosh, 2016; Jang et al., 2017; Kim et al., 2022). mGluR are G-protein-coupled dimers activated involved in slower and complex modulation of synaptic transmission and protein-protein interactions (Niswender and Conn, 2010). In the end, iGluR and more precisely NMDA receptors, are the greater contributors to synaptic plasticity; NMDAR display unique properties including for instance a wide subunit diversity and calcium permeability, making them one of the biggest vulnerable targets in favor of synaptic dysfunctions, rooting for neuropsychiatric disorders.

B. NMDA receptors (NMDAR)

NMDAR are glutamate-gated ion channels selectively permeant to sodium, potassium and calcium. Calcium permeability is a key feature of NMDAR that plays pivotal role in several receptor functions, including the initiation of NMDAR-mediated forms of synaptic plasticity as well as learning and memory formation (Hansen et al., 2021).

1. Architecture and ionotropic function

a. NMDAR topology

NMDAR are heterotetrameric assemblies composed of two glycine- or D-serine-binding GluN1 obligatory subunits combined with two additional glutamate-binding GluN2 or, less commonly, glycine-binding GluN3 subunits. Eight different variants of the GluN1 subunit (GluN1-[1-4]a and GluN1-[1-4]b) are produced through alternative splicing of the GRIN1 gene at exons 5 (N-terminal domain), 21 and 22 (C-terminal domain). They can assemble with four possible GluN2 (A-D) and two possible GluN3 (A-B), each encoded by a single gene, resulting in a large diversity of NMDAR encompassing several hundreds. The various combinations of GluN2 and GluN3 subunits allow the formation of either diheteromeric (two GluN1 and two identical GluN2 or GluN3 subunits) or triheteromeric (two GluN1 and two different GluN2 and GluN3 subunits) receptors and result in a multitude of NMDAR complexes with unique trafficking, biophysical, pharmacological, and signaling properties (Hansen et al., 2021; Paoletti et al., 2013; Zhou and Tajima, 2023). While GluN2A and GluN2B subunit-containing receptors predominate in the forebrain, the composition of NMDAR evolves during development and varies across brain regions, and the respective proportions of diheteromeric versus triheteromeric NMDAR complexes remain a matter of intense debate.

Each GluN subunit is articulated in four structural and functional domains: the amino-terminal domain (NTD), the ligand-binding domain (LBD; also called agonist-binding domain, ABD), the transmembrane domain (TMD) and the carboxyl-terminal domain (CTD) (Figure 2).

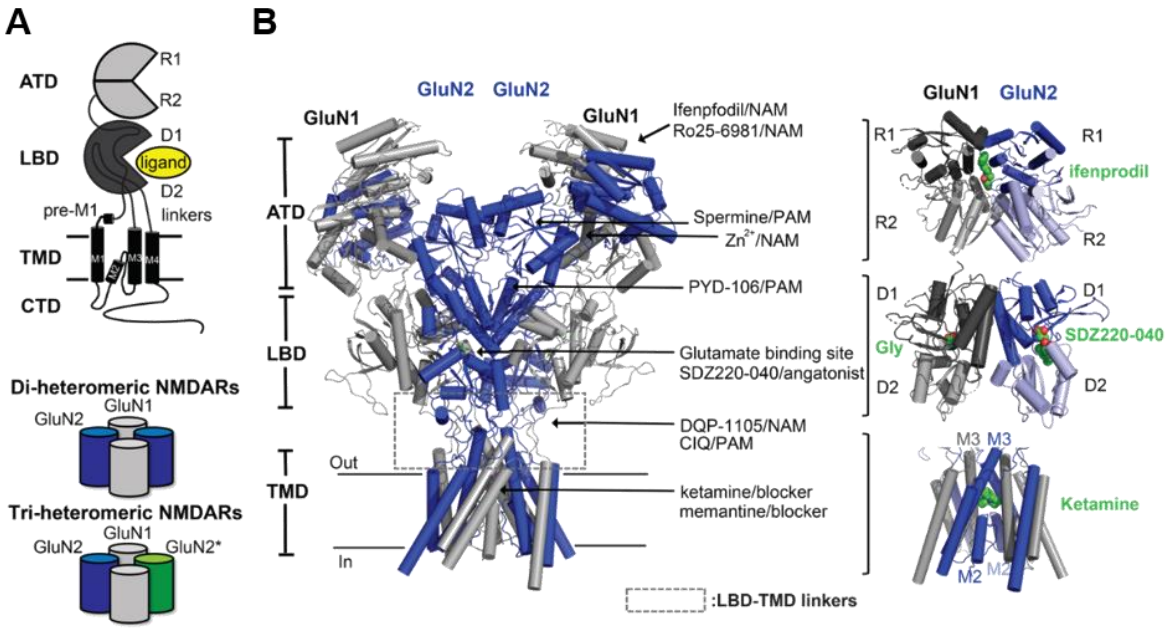

Figure 2: NMDAR molecular architecture. (A) Upper panel, NMDAR topology: subunits are organized in domains: the extracellular N-terminal-domain (NTD), the ligand-binding domain (LBD), the transmembrane domain (TMD) and the intracellular C-terminal-domain (CTD). Bottom panel, representations of di-heteromeric and tri-heteromeric NMDAR assemblies. (B) Cryo-electron microscopy resolved structure of a di-heterotetrameric GluN1-GluN2 NMDAR. Fixation sites of the different modulators are targeted by arrows. (from Zhou and Tajima, 2023)

Compared to other iGluR, NMDAR have a more compact extracellular region, conceding a tight coupling between NTD and LBD. Consequently, these two domains interact with each other in a reciprocal manner and operate as a single cohesive unit, which is crucial for allosteric signaling and channel gating modulation. The NMDAR NTD controls biophysical parameters such as channel open probability (Po) and deactivation kinetics. It also plays a role in NMDAR assembly in the endoplasmic reticulum, and is involved in protein-protein interactions influencing the trafficking and signaling of receptors (Zhu and Paoletti, 2015). NMDAR NTD display a clamshell-like structure composed of two lobes, the upper lobe (UL or R1) and the lower lobe (LL or R2) connected by a three-peptide link (Krieger et al., 2015). Globally, NMDAR NTD function under two conformations, i.e. an open state in the absence of ligand and a closed state when a ligand is bound. Subunit-specific allosteric modulators can bind to different sites displayed by NTD, the best-characterized examples so far targeting GluN2A- and GluN2B-containing receptors. As an example, zinc binding to the NTD of GluN2A triggers a conformational transition of the domain to a closed stated that directly impacts the LBD and decreases the open probability of the receptor (Romero-Hernandez et al., 2016). Thus, zinc is defined as a negative allosteric modulator (NAM), a category that also includes

drugs like ifenprodil and Ro25-6981 which bind at the GluN1-GluN2B NTD heterodimer interface (Figure 2). On the contrary, positive allosteric modulators (PAM), such as polyamines (e.g. spermine), bind to the GluN1-GluN2B NTD interface and stabilize it in an open-cleft conformation, thus increasing channel Po and subsequent excitatory transmission (Mony et al., 2011).

Connected to the NTD by a linker, the LBD displays binding sites for glutamate on GluN2 subunits and for the co-agonists glycine and D-serine on GluN1 and GluN3 subunits, whose concomitant binding allow full activation of the receptor through subsequent channel opening (Furukawa et al., 2005). The LBD is also the binding site for competitive antagonists such as D-AP5. Like NTD, the GluN1-GluN2 ABD heterodimer is folded in a clamshell shape mostly interacting through upper lobes (D1 lobes). Movements of this D1 lobes interface controls channel Po and agonist affinity. Indeed, their interaction (closed cleft conformation) or dissociation (open cleft conformation), as occurring in the presence of agonists or antagonists, are involved in a potentiation or an inhibition of the receptor, respectively (Regan et al., 2015). Attached to the LBD by specific peptide linkers, the transmembrane domain (TMD) is composed of three hydrophobic transmembrane helices (M1 M3 and M4), and a reentrant loop M2 forming the cation-selective (Na^+, K^+, Ca^{2+}) pore of the channel where Mg^{2+} ions get trapped and occlude ion fluxes at hyperpolarized resting membrane potentials, a distinctive feature of NMDAR on which relies their voltage sensitivity (Hansen 2021). The pore is also the site of action of activity-dependent blockers, also referred to as non-competitive antagonists, such as ketamine, dizocilpine (MK-801) or phencyclidine (PCP) which trap NMDAR in an agonist-bound but ionotropically-silent conformation. Finally, the C-terminal domain (CTD) of NMDAR encompasses the cytosolic amino acid stretches connected to the TMD helices, including the C-terminal tail of the receptors whose size and roles vary dramatically depending on subunits. In particular, the large CTD of GluN2 subunits are major sites of post-translational modifications (e.g. phosphorylation, palmitoylation) and protein-protein interactions, and contribute to the regulation of NMDAR assembly, surface trafficking, synaptic trapping channel gating and downstream signaling, as well as targeting for degradation (Warnet et al., 2021).

b. Subtype-dependent biophysical and pharmacological properties

At hyperpolarized resting membrane potential, NMDAR are essentially closed due to the obstruction of ion pore by Mg^{2+} ions (Mayer et al., 1984). NMDAR activation can only take place when three conditions occur concomitantly, i.e. (i) glutamate binding to the LBD of GluN2 subunits, (ii) glycine or D-serine binding to the LBD of GluN1 subunits, and (iii) AMPAR-mediated post-synaptic depolarization allowing the voltage-dependent removal of Mg^{2+} from

the pore (Seeburg et al., 1995). Since both presynaptic neurotransmitter release and post-synaptic membrane depolarization are required for their activation, NMDAR are commonly considered as molecular coincidence detectors of simultaneous pre and post-synaptic activity which is believed to be the basis for Hebbian changes in synaptic strength underlying learning and memory. The first step of receptor activation is the binding of agonists and co-agonists to the cleft between the S1 and S2 segments of GluN2 and GluN1 LBD, respectively. All four agonist/co-agonist binding sites must be occupied for receptor activation to occur, which leads to closure of the S1/S2 clamshell and separates LBD one from another, creating tension in the linkers resulting in the reorganization of the TMD and opening of the ion pore (Mony and Paoletti, 2023).

Calcium influx permeability and Mg^{2+} blockade can vary in function of the subunit composition of the receptor. For instance, GluN2A- and GluN2B-containing receptors display a higher sensitivity to magnesium and permeability to calcium than GluN2C- and GluN2D-containing receptors (Paoletti et al., 2013). Because of this double requirement and their kinetics properties, NMDAR are able to integrate and transduce signals into modifications of synaptic strength, i.e. synaptic plasticity. During long-term potentiation (LTP), NMDAR are activated and allowing the entry of calcium ion flux, participating to the rise of intracellular calcium levels. This leads to the activation of specific signaling cascades eliciting the insertion of AMPAR at the post-membrane, thereby increasing synaptic strength. On the contrary, when the activated signaling cascades promotes removal of AMPAR from the post-synaptic membrane, synaptic strength decreases to form long-term depression (LTD) (Citri and Malenka, 2008). Synaptic plasticity occurs at specific locations and times within the brain, triggering diverse cognitive processes, thus highlighting NMDAR changes in terms of spatial distribution and neuronal development.

2. NMDAR distribution and functions

NMDAR heteromers are produced in the endoplasmic reticulum (ER) by ribosomes with the particularity that GluN1 subunits are oversynthetized compared to GluN2 and GluN3 subunits, guaranteeing their availability for other subunits production. GluN2 subunits, along with certain GluN1 splice variants, remain within the endoplasmic reticulum (ER) until they are assembled into functional complexes. Once out of the ER, receptors are transported through the Golgi apparatus. Subsequently, they are either inserted directly into vesicles and sent to the plasma membrane or delivered into dendrites to reach spines (Horak et al., 2014; Wenthold et al., 2003). Subunit composition within NMDAR is a dynamic process that evolve and is modified along with neuronal development.

a. NMDAR distribution throughout the brain

NMDAR are ubiquitously expressed throughout the brain. However, the expression patterns of NMDAR subunits - and thereby of NMDAR subtypes - are not uniform and vary across cell types, brain regions and developmental stages (Monyer et al., 1994). The obligatory GluN1 subunit is ubiquitously expressed in the brain and particularly concentrated in the forebrain and cerebellum, with isoform-specific regional and developmental expression patterns which are mostly fixed from birth and show little variations throughout life (Figure 3). However, expression levels and patterns of GluN2 and GluN3 auxiliary subunits are tightly regulated in time and space (Monyer et al., 1994; Watanabe et al., 1993). GluN2B and GluN2D expression only are detected at embryonic stages. At birth, GluN2B expression is widespread and peaks at the end of the first postnatal week, after which it decreases and remains essentially abundant in the forebrain.

During early postnatal development and throughout all the central nervous system, the subunit composition of NMDAR switches from predominant GluN2B subunits to mostly having GluN2A subunits. While GluN2B subunits persist in many adult CNS regions, GluN2A increased presence brings distinct alterations in NMDAR-mediated synaptic currents, including faster decay kinetics and changes in pharmacology. This shift is marked by increased sensitivity to zinc and reduced response to GluN2B-specific antagonists. The exact molecular mechanisms underlying this switch remain unclear, but it seems to be driven by neuronal activity and sensory experiences, therefore in concomitance with the critical period of development (Monyer et al., 1994; Paoletti et al., 2013). Furthermore, GluN1, GluN2A and GluN2D are found in high levels from P7 to P14, then decrease until more moderate levels in adult. In the contrary, GluN2B and GluN2C have the inverse tendency, meaning that their levels are initially very but increase from P7 until reaching high levels in adulthood (Lau et al., 2003; Monyer et al., 1994). GluN2C expression is quite restricted to the cerebellum while GluN2D is mainly expressed in the basal ganglia (Figure 3) (Monyer et al., 1994; Watanabe et al., 1993; Wyllie et al., 2013). Regarding GluN3 subunit expression, GluN3A and GluN3B present an opposite pattern of expression, i.e. high expression of GluN3A at birth followed by a decrease until adulthood and low initial expression of GluN3B that increases through development. GluN3A and GluN3B subunits are notably expressed in the hippocampus, entorhinal cortex, striatum and cerebellum (Murillo et al., 2021; Pachernegg et al., 2012; Wee et al., 2016).

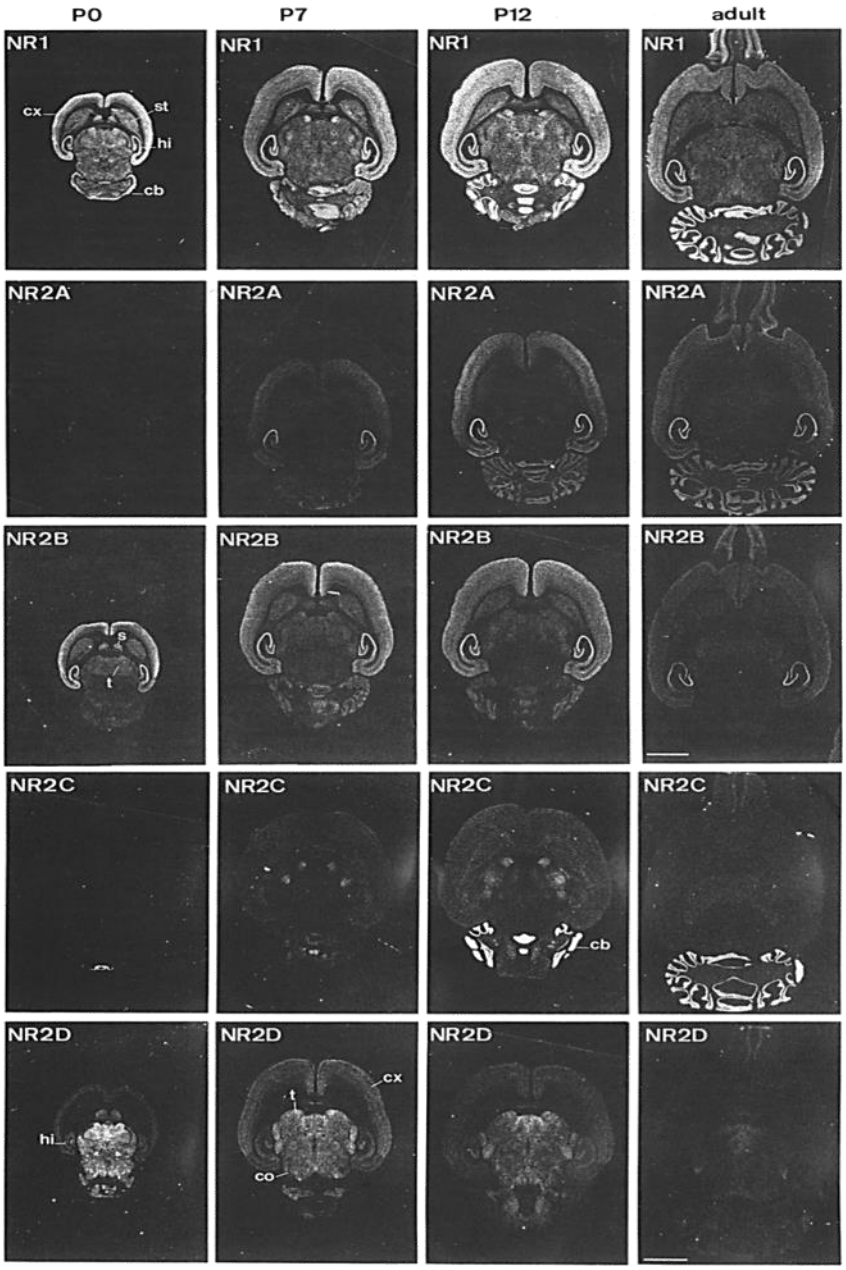

Figure 3: NMDAR subunits expression through brain development. GluN1 is ubiquitous, GluN2A and GluN2B containing NMDAR undergo developmental switch. GluN2C expression is mainly restricted to cerebellum and GluN2D initial expression in midbrain is barely inexistent at mature state (Scalebar, 3.4 mm, adapted from Monyer et al., 1994).

GluN3A and GluN3B subunits display opposite evolutions. Indeed, GluN3A expression is widespread and increases from birth until P8, after which it decreases until adulthood. Instead, GluN3B expression is barely detectable at early stages and peaks at adulthood where it can be detected in the brainstem, hippocampus, entorhinal cortex, striatum and cerebellum (Murillo et al., 2021; Pachernegg et al., 2012; Wee et al., 2016). GluN3A- and GluN3B-containing NMDAR are expressed in multiple cell types including pyramidal cells, interneurons and motor neurons (Crawley et al., 2022).

b. NMDAR subcellular distribution and functions

Electron microscopy studies reveal that NMDAR are widely distributed at the surface of neurons where they have been detected on the cell body, axon, and dendritic shafts (Petralia et al., 2010).

Axonal NMDAR: regulation of glutamate release and presynaptic plasticity

While NMDAR are particularly abundant at postsynaptic level, there has been increasing evidence of their axonal expression at presynaptic terminals in specific brain regions where they regulate synaptic transmission (Banerjee et al., 2016). For instance, implication of presynaptic NMDAR in the regulation of glutamate release has been reported at excitatory synapses in the visual cortex, the hippocampus, the entorhinal cortex, the somatosensory cortex as well as the cerebellum. Furthermore, presynaptic NMDAR have been shown to participate in short-term and long-term plasticity processes together with mGluR, IP3R-gated internal stores of the presynaptic terminal and retrograde endocannabinoid signaling to build functional circuits during development (Bouvier et al., 2015).

Dendritic NMDAR: controlling cell survival and post-synaptic strength

Dendritic NMDAR expression can be detected both at synaptic and extrasynaptic compartments. At a given time point, between 20% and 50% of NMDAR are extrasynaptic and located in dendritic shafts where they are not anchored to specific scaffold-dense zones, unlike in the synaptic compartment where they associate with the PSD (Blanpied et al., 2008; Harris and Pettit, 2007). In adults, the extrasynaptic compartment contains predominant GluN2B-NMDAR with high affinity to glutamate while synapses mainly host GluN2A-NMDAR. This can be partially explained by the preferential association between GluN2A-NMDAR and PSD95 scaffolding protein of the synapse (Papouin and Oliet, 2014). Regarding GluN2C/2D-containing NMDAR, their presence is predominant in the extrasynaptic compartment (Groc et al., 2009; Wu and Johnson, 2015). It is also true for GluN3A-NMDAR, which can parenthetically reduce GluN2A-NMDAR dwelling time in synapses to expel it in extrasynaptically (González-González et al., 2023). Overall, it has been established that synaptic NMDAR promote the release of neurotrophic factors while NMDAR located in the extrasynaptic compartment are more prone to activate signaling pathways related to apoptosis, shaping an NMDAR controlling survival/death equilibrium through intracellular mechanisms (Hardingham et al., 2002). However, the role of NMDAR subunits or locations in inducing excitotoxicity-mediated cell death is still debated. Indeed, excitotoxicity would not exhibit preferential engagement with either 2A- or 2B-containing NMDAR (Papouin and Oliet, 2014; Zhou et al., 2013). On a functional aspect, synaptic and extrasynaptic NMDAR mediate different signaling properties. Synaptic NMDAR generate phasic currents and calcium influxes

at the origin of intracellular signaling cascades while extrasynaptic NMDAR produce tonic currents that enhance neuronal excitability (Dupuis et al., 2023; Hansen et al., 2021). Additionally, the co-agonist control of NMDAR differs between the two compartments: D-serine gates synaptic receptors while glycine binds extrasynaptic receptors (Papouin et al., 2012). Finally, NMDAR are mobile and can travel laterally from a compartment to another, shaping their dynamic organization (Bard and Groc, 2011; Groc et al., 2006; Tovar and Westbrook, 2002).

It is well established that NMDAR ionotropic function is a key actor of synaptic plasticity supporting learning and other cognitive processes. Synaptic plasticity refers to the ability of a synapse to modulate its efficacy of transmission, whose most prominent forms are long-term potentiation (LTP) and long term depression (LTD) (Citri and Malenka, 2008). LTP and LTD have been described as involving high and low calcium entry respectively in the post-synapse (Lüscher and Malenka, 2012; Regehr and Tank, 1990). Yet, agonist binding to NMDAR, even without ion flux, has been later shown to be sufficient to initiate LTP and LTD mechanisms. By using NMDAR blockers like MK-801 and 7-chlorokynurenic acid (7-CK), it has been shown that inhibition of ion flux does not prevent the induction of NMDAR dependent LTD whereas in presence of competitive antagonists that hinder glutamate binding, NMDAR dependent LTD is not induced. Further research demonstrated that when ionotropic activity is blocked, glutamate binding is still able to trigger intracellular signaling notably through the activities of p38 mitogen-activated protein kinase (p38 MAPK) and CaMKII, highlighting metabotropic properties of NMDAR (Nabavi et al., 2013; Park et al., 2022; Stein et al., 2020). Moreover, NMDAR metabotropic activity can trigger an increase of synaptic strength, i.e. LTP, in absence of ionotropic activity, through glycine-elicited postsynaptic modifications. More precisely, glycine binding to GluN2A-NMDAR enhances phosphorylation of extracellular signal-regulated protein kinase (ERK1/2) leading to an increase in AMPAR currents (Li et al., 2016; Park et al., 2022).

3. Mechanisms controlling NMDAR distribution and organization at synapses

The development of single-molecule localization microcopy (SMLM) at the beginning of the century has allowed nanoscopic explorations of the organization of pre- and post-synaptic elements. These studies have revealed that glutamatergic receptors are not uniformly distributed and everlastingly stable at synapses. Instead, they aggregate within nanometric clusters that are structured by cytosolic scaffolding proteins and aligned with the presynaptic glutamate release machinery through the contribution of cell adhesion molecules, forming trans-synaptic functional units which have named nanocolumns (Groc and Choquet, 2020; Kellermayer et al., 2018; MacGillavry et al., 2013; Nair et al., 2013; Tang et al., 2016).

Moreover, receptors are only transiently trapped within these domains and continuously undergo dynamic redistributions through lateral diffusion within the membrane plane following a Brownian motion regime driven by thermal agitation, allowing a powerful control of receptor numbers and composition that shapes the intensity of synaptic transmissions (Dupuis et al., 2023; Groc and Choquet, 2020).

a. NMDAR nanoscale organization

Within the PSD, NMDAR clusters contains from 10 to 40 receptors and are mainly central and surrounded by AMPAR clusters of 15 to 100 receptors (Maynard et al., 2023). Synaptic GluN2A-NMDAR and GluN2B-NMDAR differ in their nanoscale organization, they each form 1 to 4 clusters of about 60 nm diameter, with 30% overlapping. It is believed that distinct synaptic anchoring mechanisms explains this different and non-overlapping nanoscale organization (Dupuis et al., 2023; Kellermayer et al., 2018). Furthermore, synaptic GluN2B-NMDAR nanoscale organization varies along the dendrite ; more proximal synapses display larger and denser GluN2B-NMDAR nanodomains because of its interaction with CaMKII (Ferreira et al., 2020). Even if the function of this NMDAR nanoscale organization remains unknown, one hypothesis propose that it may negatively couple NMDAR currents within a nanodomain via calcium-dependent inactivation. The degree of negative coupling would be dependent of the distance between NMDAR, the closer they are, the more efficiently they inhibit each other (Iacobucci and Popescu, 2019).

b. Diffusion-based NMDAR redistributions

NMDAR move in different manners whether they are located inside, at the interface or outside neurons, tuning synaptic functioning in both healthy and disease conditions. Overall, they undergo long and rapid intracellular transportation and shorter Brownian diffusion once at the surface. Usually, movements of NMDAR adapts during change of compartment (intracellular and surface, synaptic and extrasynaptic) (Groc and Choquet, 2020, 2006). Once produced and assembled, NMDAR-vesicles are actively trafficking along the cytoskeleton to reach plasma membranes or endosomes. More precisely, NMDAR-vesicles are transported on microtubules by kinesin motor proteins on the longest distance from the soma to dendrites. NMDAR are thus first reaching extrasynaptic membranes, additional short-distance transport system is needed into spines. Indeed upon arrival to the synapse, trafficking is slower and involves myosin motors transport on actin filaments (Horak et al., 2014; Kapitein and Hoogenraad, 2011; Petralia et al., 2009; Setou et al., 2000). Once inserted in the plasma membrane, NMDAR can travel long distances along the dendritic arborization by lateral diffusion and they can eventually reach synapses and the PSD (Choquet and Triller, 2013). Thus, exocytosis, endocytosis and lateral diffusion processes finely regulate and adjust the

number, composition and distribution of NMDAR, making them extremely dynamic and subject to constant renewal (Dupuis et al., 2023). Furthermore, the surface dynamics GluN2A-NMDAR and GluN2B-NMDAR are differently regulated at synapses, GluN2A-NMDAR being more stable (Bard et al., 2010; Groc et al., 2006). GluN2B-NMDAR are more mobile and display higher level of exchanges between synaptic and extrasynaptic compartments, regulating LTP by CaMKII redistributions at hippocampal synapses (Dupuis et al., 2014). NMDAR diffusion is tightly regulated by different types of interactors, intracellular transmembrane and extracellular.

c. Regulators of NMDAR synaptic trapping and surface redistributions

Intracellular modulators

The lateral diffusion of NMDAR can be regulated by interaction of their C-term tail with MAGUK proteins. Indeed, these protein-protein interactions support NMDAR synaptic organization and anchoring at the PSD (Bard et al., 2010; Dupuis et al., 2023). More precisely, the PSD-95 family of PDZ-containing scaffold proteins are the main MAGUK interactors of NMDAR. This family is composed of 4 different type of proteins encoded by 4 distinct genes : PSD-95, PSD-93, SAP102 and SAP97 (Sheng and Kim, 2011). These PSD-MAGUK protein share a similar organization and contain three PDZ domains at their N-term extremity, a SH3 domain and a guanylate cyclase domain at their C-term extremity (Elias and Nicoll, 2007). PSD-MAGUK proteins are able to interact with GluN2 subunits, with a preferential association of GluN2A to PSD-95, PSD-93 and SAP97 and of GluN2B with PSD-95 and SAP102 (Gardoni and Di Luca, 2021; Sans et al., 2000). Besides modulating NMDAR surface diffusion, PSD-MAGUK are also interacting with NMDAR during their intracellular trafficking; SAP97 is mainly driving NMDAR traffic through the endoplasmic reticulum and Golgi from soma to dendrites (Gardoni and Di Luca, 2021).

Protein kinases located at the PSD are also privileged interactors of NMDAR, with Ca2+/calmodulin-dependent protein kinase II (CaMKII) being the predominant one. The interplay between the C-term tail of GluN2B subunit and the activated form of CaMKII (i.e. αCaMKII) modulates NMDAR function and diffusion. Indeed, upon NMDAR activation, CaMKII preferentially bind GluN2B to increase GluN2B-NMDAR lateral diffusion into spines, causing CaMKII redistributions at synapse supporting LTP processes (Dupuis et al., 2023, 2014; Ferreira et al., 2020).

Transmembrane modulators

Transmembrane interactors participate in surface protein-protein cis-interactions with NMDAR, thus play a role in receptor functioning and organization. Neurotransmitter receptors

and ion channels mostly constitute the NMDAR surface cis-interactome. Overall, these interactions have been shown to regulate synaptic plasticity as well as NMDAR organization and diffusion, supporting glutamatergic synapse functioning in physiological and pathological conditions. These interactions are regulated by neurotransmitters like dopamine, acetylcholine, and opioids (Figure 4)(Petit-Pedrol and Groc, 2021).

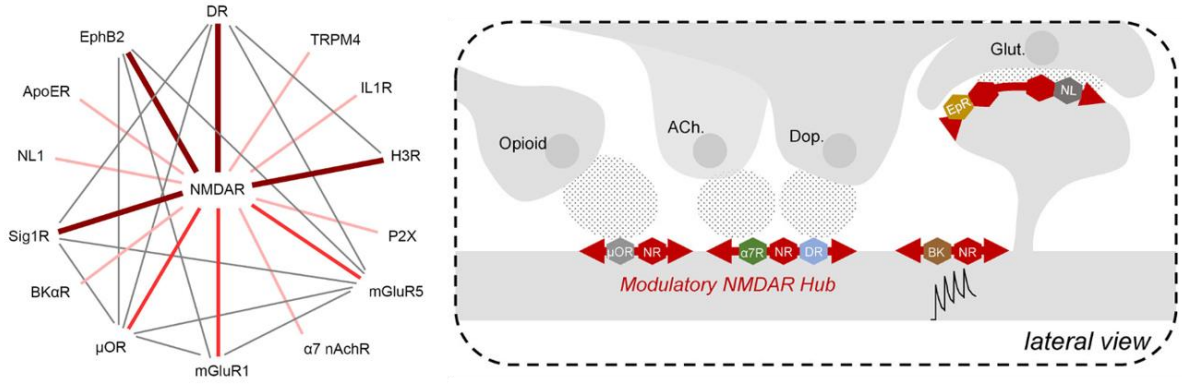

Figure 4: NMDAR transmembrane interactors and their regulatory action. The NMDAR surface cis-interactome is composed of different neurotransmitter receptors and ion channels that are involved in protein-protein interactions with NMDAR. Together, they form nanodomains dynamically evolving in organization as a function of neurotransmitter release from projecting neurons (DR: dopamine receptors, TRPM4: transient receptor potential cation channel subfamily M member 4, IL1R: IL-1 receptor, H3R: histamine 3 receptor, P2X: purinergic P2X receptors, mGluR: metabotropic glutamate receptors subtype, nAChR: nicotinic acetylcholine receptors, μOR: μ-Opioid receptors, BK: voltage-activated potassium, Sig1R: Sigma-1 receptor, NL1: neuroligin 1, ApoER: Apolipoprotein E receptor, EphB2: Ephrin B2 receptor)(From Petit-Pedrol and Groc, 2021).

For example, mGluR5-NMDAR interaction reciprocally regulate the trafficking and respective activities of both receptors (Perroy et al., 2008). Interactions with Ephrin-B2 receptors (EphB2R) favor NMDAR synaptic retention and its disruption is a feature of autoimmune antibody-induced neurological symptoms (Mikasova et al., 2012; Petit-Pedrol and Groc, 2021). Among the most studied, dopamine receptors, especially the D1 subtype (D1R), physically interact with GluN1-NMDAR at their C-term tails to mainly maintain NMDAR into the extrasynaptic compartment, forming a reserve pool (Bénac et al., 2024; Ladepeche et al., 2013; Lee et al., 2002). Indeed, when D1R are activated by dopamine release, the interaction with NMDAR breaks and induces an increase in NMDAR surface lateral diffusion causing an increase in NMDAR synaptic content and amplitude of synaptic currents, favoring LTP and memory processes (Ladepeche et al., 2013; Nai et al., 2010). Furthermore, it has recently been demonstrated that besides that functional role, D1R-NMDAR interaction is increased at immature state, inducing NMDAR clustering and synaptogenesis independently of D1R activation (Bénac et al., 2024).

Extracellular modulators

The extracellular environment surrounding NMDAR contains a variety of molecules regulating receptor dynamics. Components of the extracellular matrix ECM - a meshwork of proteins providing structural and functional support to neurons (Dityatev et al., 2010) - have a robust impact on the surface diffusion of extracellular NMDAR. For instance, accumulation of the secreted glycoprotein reelin across development selectively enhances GluN2B-NMDAR diffusion and thus decreases their synaptic trapping and contribution to NMDAR-mediated currents. Conversely, reelin inhibition enhances the synaptic trapping of GluN2B-NMDAR and prevents the developmentally-regulated reduction in their synaptic contribution (Groc et al., 2007). Alike, modulation of integrin β1-dependent signaling by the matrix metalloproteinase-9 (MMP-9) enhances NMDAR surface diffusion, a mechanism which may contribute to the involvement of MMP-9 in synaptic plasticity (Michaluk et al., 2009). Diffusible molecules present in the extracellular space also influence NMDAR surface dynamics. As an example, local variations in the concentrations of the co-agonists glycine and D-serine trigger subtype-selective modulations of the diffusion and trapping of synaptic and extrasynaptic NMDAR. Indeed, higher synaptic concentrations of D-serine and extrasynaptic concentrations of glycine selectively decrease the surface diffusion of GluN2A- and GluN2B-NMDAR, respectively, a mechanism that could contribute to the spatial segregation of the two NMDAR subtypes and to participate in their developmental switch (Ferreira et al., 2017; Papouin et al., 2012). Typically, D-serine binding changes the conformation of NMDAR cytosolic domains, thereby weakening interactions between GluN2B-NMDAR and PSD-95 and impacting their trapping and synaptic content (Ferreira et al., 2017). The serine protease tissue plasminogen activator (tPA) binds to the NTD of the GluN1 subunit and promotes the diffusion and clustering of extrasynaptic receptors as well, thereby modulating NMDAR-mediated signaling and neurotoxicity (Lesept et al., 2016). Hormones can also regulate NMDAR surface diffusion properties in a subtype-selective manner, as illustrated by the estrogen 17β-estradiol E2 and the glucocorticoid corticosterone which both selectively enhance the synaptic trapping of GluN2B-NMDAR, thereby favoring synaptic potentiation causing spine density and associative memory formation in the hippocampus (Mikasova et al., 2017; Potier et al., 2016). Thus, numerous extracellular modulators contribute to the fine-tuning of receptor diffusion, and it is likely that other molecules present in the ECS, such as polyamines and zinc, may also act on NMDAR surface redistributions which appears to be an essential component of excitatory neurotransmission (Petit-Pedrol and Groc, 2021).

Interestingly, diffusible modulators of NMDAR surface trafficking can also emerge in pathological contexts. Indeed, anti-NMDAR circulating antibodies from patients with anti-NMDAR encephalitis and psychosis have been reported to impair NMDAR surface diffusion

and synaptic organization properties, resulting in NMDAR-mediated signaling and plasticity deficits which lead to major cognitive and behavioral deficits (Jézéquel et al., 2017; Mikasova et al., 2012). Thus, impairment in NMDAR synaptic organization and diffusion-based surface redistributions may contribute to the etiology of neuropsychiatric conditions.

4. NMDAR diffusion impairment in psychiatric disorders

Dysfunction of NMDAR signaling is a main feature of neuropsychiatric disorders and intense efforts have been made to investigate the mechanisms underlying its contribution to brain illnesses. Indeed, pathological NMDAR hyper- or hypofunction have been reported in a variety of neurological conditions including epilepsy, ischemic stroke, Parkinson's, Huntington's and Alzheimer's disease. They also been associated with mental disorders such as intellectual disability, autism, schizophrenia and depression. Interestingly, pathological NMDAR dysfunctions do not necessarily result from channel gating deficits. In Alzheimer's disease for instance, it appears that synaptic plasticity deficits and dendritic spine loss may result from non-ionotropic NMDAR signaling initiated by β-amyloid oligomers which cause changes in the conformation of cytosolic domains of the receptors and affect their interaction with scaffolds (Kessels et al., 2013; Lacor et al., 2007; Shankar et al., 2008). Moreover, the recent discovery of an autoimmune disorder affecting NMDAR surface trafficking further highlighted the fact that channel dysfunctions cannot be considered as the sole etiological factor in brain conditions associated with NMDAR dysfunction. Since then, it has been demonstrated that the surface dynamics and organization of NMDAR are altered in various neurological and psychiatric disorders (Figure 5) (Dupuis et al., 2023; Groc and Choquet, 2020). Most of our knowledge regarding NMDAR surface trafficking impairment in psychiatric diseases comes from an autoimmune disorder called NMDAR encephalitis where NMDAR are targeted by autoantibodies (NMDAR-Abs) directed against the GluN1 obligatory subunit. NMDAR encephalitis is characterized by a viral-like prodromal phase followed by psychotic symptoms and a later stage including seizures and autonomic dysfunction (Dalmau et al., 2007; Hunter et al., 2021). Early single molecule imaging studies have shown that NMDAR-Abs induce a rapid dispersal of synaptic NMDAR and a rearrangement and internalization of extrasynaptic receptors, causing alterations in NMDAR-mediated synaptic plasticity that may underlie some of the psychotic symptoms observed in patients (Jézéquel et al., 2017; Mikasova et al., 2012; Dupuis et al., 2023). The sequence of antibody-elicited events leading to NMDAR hypofunction was recently better characterized in a study reporting that NMDAR-Abs primarily affect the diffusion, nanoscale organization and interactions of extrasynaptic NMDAR which in turn leads to the disruption of NMDAR synaptic organization, highlighting the major

physiological importance of maintaining balanced surface exchanges between the two compartments (Jamet et al., 2024).

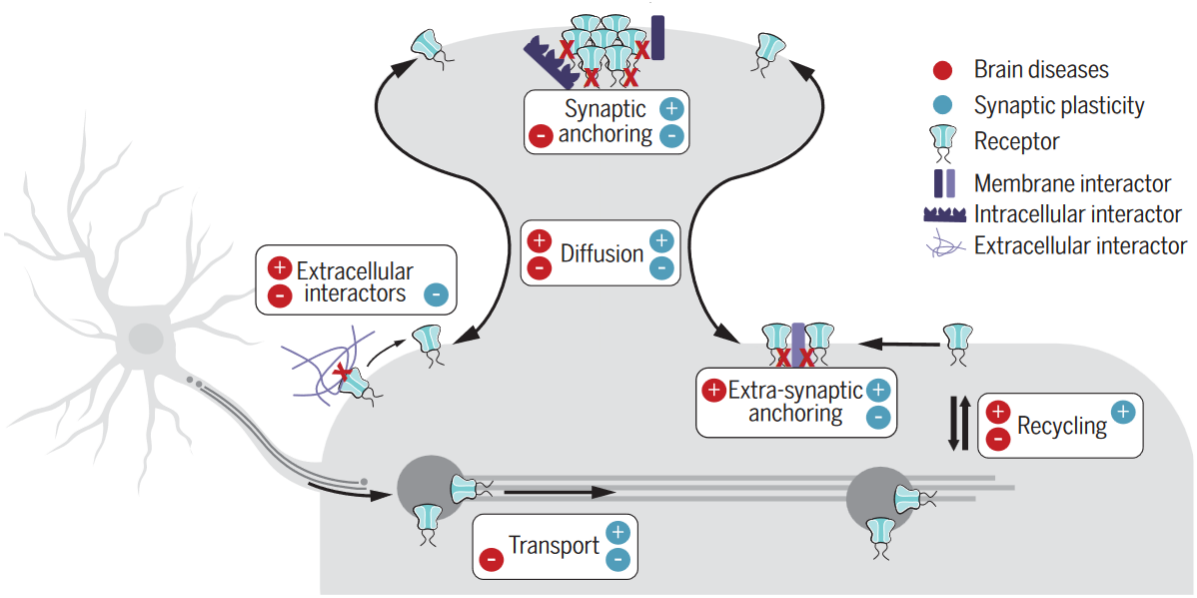

Figure 5: NMDA receptors dynamics into the different neuronal compartments. NMDAR move in different manners whether they are located inside, at the interface or outside neurons, tuning synaptic functioning in both healthy (blue) and disease (red) conditions. "+" refers to positive modulation while "-" refers to negative modulation (from Groc and Choquet, 2020).

Consistently, NMDAR surface diffusion and organization impairment have been reported in other models of psychosis such as (i) knock-down of the susceptibility gene DISC1, (ii) exposure to CSF samples from psychotic patients or (iii) to the envelop protein of the human endogenous retrovirus (HERV) type W found in patients with neuropsychiatric conditions, all of which result in abnormal redistribution patterns and plasticity deficits (Espana et al., 2021; Jézéquel et al., 2017; Johansson et al., 2020). Thus, besides impairment of the ionotropic function of the receptors, alterations of NMDAR surface trafficking also emerge as a hallmark of neuropsychiatric conditions and could represent a valuable target for therapeutic intervention. Thus, NMDAR surface dynamics, independently of receptor ionotropic function, became a strong target of action to develop therapeutic strategies within psychiatric and neurological diseases.

5. NMDAR as pharmacological targets

Antagonization of NMDAR occurs naturally in presence of endogenous molecules like magnesium or zinc, or by exposure of an exogenous synthetized drug. NMDAR antagonists

can broadly be classified according to their binding site on the receptor into competitive and uncompetitive antagonists (Figure 6).

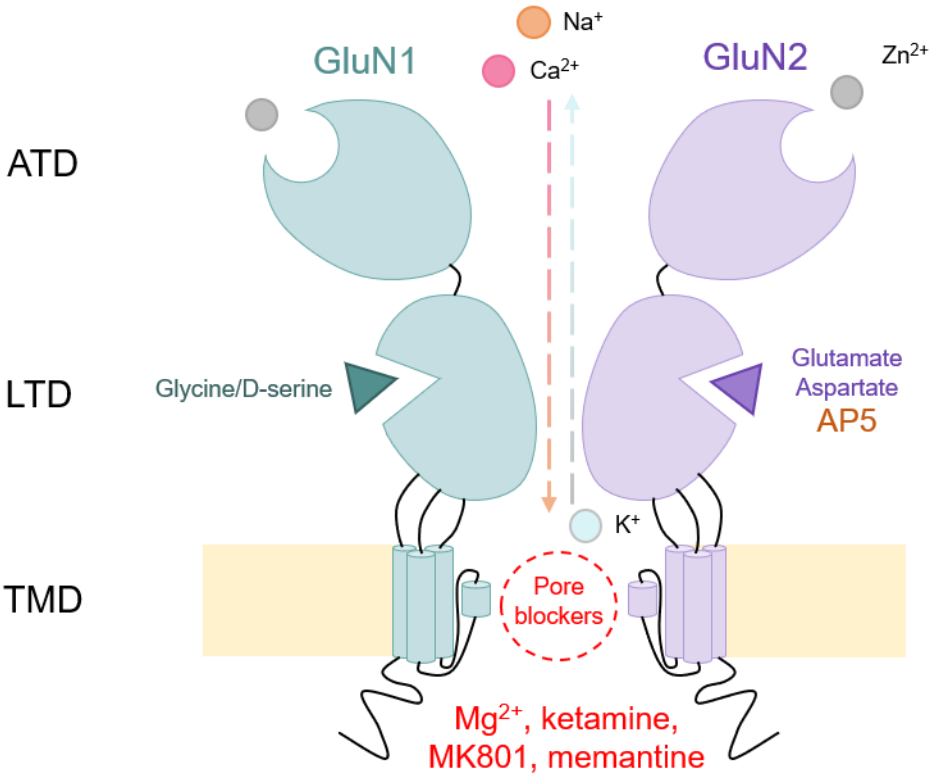

Figure 6: The NMDAR and its antagonists. Zinc, along with ifenprodil and Ro25-698 are NAMs that bind the ATD/NTD of GluN2B subunits. D-AP5, competitive antagonist, prevent NMDAR agonist binding. Open-channel blockers like magnesium, ketamine, MK-801 and memantine, block ion flux through the receptor.

Competitive ligands block receptor activation by binding the fixation site of GluN1-NMDAR agonists (glutamate and NMDA). NMDAR-LBD is therefore maintained in an open cleft conformation, preventing channel gating (Hansen et al., 2021). 2-amino-5-phosphonovalerate (AP5) is the first discovered and most selective NMDAR competitive antagonist and is still extensively used in fundamental research, D-AP5 being the active isomer of the racemic mixture (Collingridge et al., 1983; Lodge et al., 2019). Collingridge and collaborators have demonstrated in the early 1980s thatD-AP5 prevents synaptic potentiation in CA1 after high frequency stimulation (HFS) of Schaffer collaterals in hippocampal slices, highlighting the important involvement of NMDAR in synaptic plasticity processes. Since then, the drug has been used to study NMDAR roles in multiple brain regions (Dawbarn and Pycock, 1981; Fox and Armstrong-James, 1986; Kimura et al., 1985; Lodge et al., 2019). 3-(2-Carboxypiperazin-4-yl)propyl-1-phosphonic acid (CPP) has been synthetized as a more potent analogue of AP7, acting similarly as D-AP5 (Carmack et al., 2013; Davies et al., 1986).

Other physiological (e.g. kynurenic acid) and pharmacological (e.g. 7-chlorokynurenic, 7-CK) competitive antagonists can bind the obligatory co-agonist site located on the GluN1 subunit (Cai, 2006). Kynurenic acid (KA) has neuroprotective properties and is able to block most of iGluRs with a higher affinity for NMDAR. Its neuroprotective effect is conferred by presynaptic glutamate release inhibition, thus preventing excitotoxicity (Majláth et al., 2016).

Uncompetitive antagonists obstruct the channel pore, occluding ion flows through the receptor. Extracellular magnesium ions (Mg^{2+}) are endogenous pore-channel blocker at rest (Mayer et al., 1984; Nowak et al., 1984). Binding sites for NMDA open-channel blockers are defined by the type of present residues in the M2 pore loop and the pre-M1 region. Clinically relevant open-channel blockers (OCB) mostly include ketamine, dizocilpine (MK-801) and memantine. Ketamine and MK-801 have higher affinity for NMDAR than memantine (Hansen et al., 2021). Regarding their pharmacological properties, drug potency and affinity are reflected by the half maximal inhibitory concentration (IC50) and the inhibition constant (Ki) (Table 1). For example, D-AP5 display some heterogeneity regarding its Ki values among subunits, making it quite unable to use for dissection of subunit composition. Furthermore, an NMDAR antagonist is considered as specific of a subunit when its IC50 is at least 50 fold lower than for other subunits (Ogden and Traynelis, 2011).

	GluN2A	GluN2B	GluN2C	GluN2D
Competitive antagonists	Ki (µM)			
AP5	0.28	0.46	1.6	3.7
CPP	0.041	0.27	0.63	1.99
Open-channel blockers	IC50 (µM)			
Ketamine	5.4	5.1	1.2	2.9
MK-801	0.015	0.009	0.024	0.038
Memantine	13	10	1.6	1.8

Table 1: Ki and IC50 values for different competitive and uncompetitive NMDAR antagonists according to NMDAR different subunits (adapted from Ogden and Traynelis, 2011).

Over the last decades, NMDAR antagonists gained interest regarding their therapeutic potential, notably following to the discovery of the antidepressant properties of ketamine (Berman et al., 2000). Ketamine has been initially synthetized as an anesthetic drug, it is still widely used in clinical and veterinary medicine. Along with MK-801, ketamine has further been shown to produce psychomimetic effects including sedation, acute psychosis and hallucinations, confusion in humans and rodents (Mion and Villevieille, 2013). On the other

hand, memantine possessed a very low potential for psychomimetic effect and substance abuse in general. Memantine has been approved by the FDA to treat moderate to severe Alzheimer's dementia. Indeed, memantine is well tolerated compared to MK-801 and ketamine due to its fast-open channel blocking/unblocking kinetics. Indeed, memantine is able to unbound NMDAR quickly before channel closure and agonist release whereas MK-801 and ketamine stay completely trapped into the receptor, leading to a long-lasting inhibition of the receptor therefore unavailable for agonist binding (Aljuwaiser et al., 2023; Parsons et al., 2007). Thus, competitive antagonists and OCBs elicit similar inhibition of NMDAR signaling function but they trigger distinct behavioral responses, indicating that might affect differently on another dimension of NMDAR.

CHAPTER II: TARGETING NMDAR FOR THE TREATMENT OF MAJOR DEPRESSIVE DISORDER

A. Major Depressive Disorder (MDD)

1. Definition

A mood disorder is a medical condition that is characterized by significant disruptions in mood and its associated functions. In the Diagnostic and Statistical Manual of Mental Disorders (DSM-5), mood disorders are classified in two distinct sections, i.e. bipolar disorders and depressive disorders, diseases that overall affect an individual emotional content. People that have mood disorders experience mood fluctuations, either low ones like in depressive disorders or high ones like in manic episodes of bipolar disorders (Parker, 2014). Indeed, bipolar disorders are characterized by an alternation of depressive episodes (low mood and energy) and manic or hypomanic episodes (elevated mood and increased activity) while depressive disorders only encompass low mood episodes. Overall, the diminished quality of life experienced by individuals with mood disorders is primarily linked to symptoms of depressive episodes rather than those of mania (“Bipolar disorders,” 2018).

According to the DSM-5, we can distinguish three main categories of depressive disorders that are disruptive mood dysregulation disorder, major depressive disorder (MDD) and persistent depressive disorder (PDD, also called dysthymia). All of these diseases share a common feature that only varies in terms of duration, timing or presumed etiology: the cohabitation of sad mood with somatic and cognitive alterations that substantially impact a patient's functional capacities (*DSM-5*). Disruptive mood dysregulation disorder is mainly defined by a chronic and persistent irritability, i.e. persistent anger punctuated by severe temper outbursts. Dysthymia is a chronic condition that lasts for at least two years in adults with less intense but more persistent symptoms than those of MDD (Ventriglio et al., 2020). It is notable that individuals who exhibit symptoms consistent with the criteria for MDD over a two-year period with no periods of remission lasting longer than 2 months should additionally be diagnosed with persistent depressive disorder (Parker, 2014). Finally, major depressive disorder, commonly known as depression, is the depressive disorder where individual symptoms are the most severed ones. It is also the most common depressive disorder as it affects each year approximately 7% of the global population, whereas dysthymia touches 1,5% (Kessler et al., 2005).

2. Epidemiology

Major depressive disorder is a chronic and severe disease. According to the World Health Organization (WHO), depression is now the greatest contributor to burden of disability,

measured by years lived with disability (YLD). Indeed, depression represents 7.5% of all years lived with disability in 2015 (WHO 2017). This metric captures the extent to which an illness impairs daily quality of life before its resolution or the individual's death. The global prevalence of MDD over a 12-month period is approximately about 7% of adults worldwide. Around one third of the susceptibility to depression is attributed to genetic factors, while the remaining two thirds is influenced by environmental factors (Nemeroff, 2008). Moreover, after puberty, women have 50% more chances to experience depression over the course of their lives compared to men. This can be explained by a stronger genetic risk, hormonal fluctuations, lower gender equality or higher prevalence of violent stress exposure like childhood sexual abuse (Kuehner, 2017). The annual prevalence doesn't significantly vary between high-income countries (5,5%) and low- and middle-income countries (5,9%), suggesting that depression is independent of economic status (De Aquino et al., 2018). Moreover, depression is quite common, as almost one person over five is going through it at some point during their life (Malhi and Mann, 2018). The global prevalence of MDD has increased by 60% between 1990 and 2019. Furthermore, the Global Burden of Disease 2020 study estimates a 30% increase in the prevalence of MDD due to the COVID-19 pandemic ("Global, regional, and national burden of 12 mental disorders in 204 countries and territories, 1990–2019," 2022). It is therefore very concerning and the urgent need of new antidepressants is undeniable.

3. Symptoms

As a disorder, depression is defined as a collection of symptoms forming a syndrome, which results in functional impairment. Importantly, none of the symptoms are pathognomonic of depression, i.e. specific indicators, because they can also be found at various intensities in many other psychiatric and medical conditions. The DSM-5 describes the current diagnostic criteria for major depressive disorder (Table 1). In other words, major depressive disorder can be defined as an alternation of major depressive episodes of at least 2 weeks with remission periods. Indeed, the recurrence of major depressive episodes is a hallmark feature of MDD and this alternation of depressive episodes followed by remission can persist throughout an individual's life. Both depressed mood and anhedonia (reduced pleasure) are fundamental symptoms of MDD, patients must present at least one of them to be diagnosed with MDD. Once the diagnostic has been made, a major depressive episode can be further characterized by specifiers, which are standardized supplementary descriptors provided by the DSM-5 (Table 2).

DIAGNOSTIC CRITERIA FOR MAJOR DEPRESSIVE DISORDER (DSM-5)
A. Five (or more) of the following symptoms have been present during the same 2-week period and represent a change from previous functioning; at least one of the symptoms is either (1) depressed mood or (2) loss of interest of pleasure. 1. Depressed mood most of the day, nearly every day, as indicated by either subjective report (e.g., feels sad, empty, hopeless) or observation made by others (e.g., appears tearful). 2. Markedly diminished interest or pleasure in all, or almost all, activities most of the day, nearly every day (as indicated by either subjective account or observation). 3. Significant weight loss when not dieting or weight gain (e.g., a change of more than 5% of body weight in a month), or decrease or increase in appetite nearly every day. 4. Insomnia or hypersomnia nearly every day. 5. Psychomotor agitation or retardation nearly every day (observable by others, not merely subjective feelings of restlessness or being slowed down). 6. Fatigue or loss of energy nearly every day. 7. Feelings of worthlessness or excessive or inappropriate guilt (which may be delusional) nearly every day (not merely self-reproach or guilt about being sick). 8. Diminished ability to think or concentrate, or indecisiveness, nearly every day (either by subjective account or as observed by others). 9. Recurrent thoughts of deaths (not just fear of dying), recurrent suicidal ideation without a specific plan, or a suicide attempt or a specific plan for committing suicide.
B. The symptoms cause clinically significant distress or impairment in social, occupational, or other important areas of functioning.
C. The episode is not attributable to the physiological effects of a substance or to another medical condition.
D. The occurrence of the major depressive episode is not better explained by schizoaffective disorder, schizophrenia, schizophreniform disorder, delusional disorder, or other specified and unspecified schizophrenia spectrum and other psychotic disorders.
E. There has never been a manic episode or a hypomanic episode.

Table 1: Current diagnostic criteria for MDD described in the DSM-5. In blue, emotional symptoms; in green, neurovegetative symptoms; In yellow, neurocognitive symptoms (Parker 2014).

SPECIFIERS FOR MAJOR DEPRESSIVE DISORDER (DSM-5)
A. **Severity**: based on the number of criterion symptoms, the severity of those symptoms, and the degree of functional disability. 1. Mild: few symptoms, the intensity is distressing but manageable and the symptoms result in minor impairment in social or occupational functioning. 2. Moderate: number and intensity of symptoms and/or functional impairment are between those specified for “mild” and “severe”. 3. Severe: number of symptoms in excess of that required to make the diagnosis, intensity of symptoms seriously distressing and unmanageable and the symptoms markedly interfere with social and occupational functioning.
B. **Clinical features**: different supplementary symptoms. 1. Anxious distress 2. Mixed features: at least three of manic/hypomanic symptoms are present nearly every day during the majority of days of a major depressive disorder. 3. Melancholic features 4. Atypical features: for example, mood reactivity. 5. Psychotic features: delusions and/or hallucinations are present. 6. Catatonia
C. **Disease’s pattern**: 1. Single episode 2. Recurrent episode 3. Rapid cycling 4. Seasonal
D. **Remission**: 1. Partial: full criteria of the depressive episode not met or period lasting less than 2 months without any significant symptoms of a major depressive episode following the end of such one. 2. Full: during the past 2 months, no significant signs or symptoms of the disturbance were present.

Table 2: Summary of the main specifiers for MDD described in the DSM-5 (Parker 2014).

These diagnostic specifiers help clinicians in selecting the more appropriate treatment for a patient in particular and also in being able to inform the patient with a prognosis. It is well known that mental disorders are the highest vulnerability factor to attempted and completed suicides, depression being notably the main risk factor (Roca et al., 2019). Furthermore, comorbid anxiety is a predictor for suicide attempts and suicide-related deaths among MDD patients (Li et al., 2022).

4. Some comorbidities

The consequences of major depressive disorder on human health goes beyond its impact on daily quality of life and functioning. Indeed, depression has also somatic consequences. First, the initiation of major depressive disorder has been linked to abdominal obesity. Furthermore, once MDD sets in, the presence of metabolic syndrome (that refers to the combination of abdominal obesity, lipid abnormalities, hypertension and hyperglycemia) significantly increases the persistency of depressive episodes by 3-fold (Vogelzangs et al., 2011). Given that the metabolic syndrome is a major risk factor for type 2 diabetes, studies have investigated the relationship between MDD and type 2 diabetes and revealed that MDD patients have a 37% increased risk of developing type 2 diabetes (Campayo et al., 2011). The estimate prevalence of depression in type 1 diabetes is lower but still present; overall, diabetes doubles the odds of major depressive disorder (Anderson et al., 2001). There is also a strong association between depression and cardiovascular outcomes. Indeed, 20% of patients with cardiovascular disease also suffer from MDD, where inflammation may mediate this association (Elderon and Whooley, 2013). Not surprisingly, depression and dementia (encompassing Alzheimer's disease, vascular dementia, dementia with Lewy bodies and fronto-temporal dementia) are extremely linked: depressed patients present an increased risk of dementia but dementia as well can potentially lead to a resurgence of symptoms in formerly depressed patients. Indeed, depression is present in 25% of people with dementia, the central theory explaining this connection is that inflammatory neurodegeneration underlies this association (Kuring et al., 2018). Patients with cancer are three to five times more susceptible to develop depression, and undeniably this prevalence rate increases with severity of the disease, with higher rates for breast and pancreatic cancers. The development of MDD in patients with cancer is not only attributable to the emotional repercussions of their diagnosis, but also to inflammatory processes (Sotelo et al., 2014). Finally, psychiatric comorbidities often co-occur with MDD, with anxiety disorders being the most frequent. Besides, about 50% of depressed patients have a lifetime diagnosis of at least one anxiety disorder (Kessler et al., 2005). Other psychiatric comorbidities include attention-deficit hyperactivity disorder (ADHD), substance use disorder (SUD) and psychotic disorders like schizophrenia (Kim and Schwartz,

2020). Psychiatric comorbidities generally increase MDD severity and worsen symptoms, progression and outcomes.

5. Treatments

Historically, psychotherapy, i.e. sessions guided by a therapist, has been the first type of treatment approach used to treat MDD, as for the majority of psychiatric diseases. Regarding pharmacotherapy, medications emerged during the second half of the 20th century, allowing a deeper understanding of the pathological mechanisms underlying MDD. Whether to use psychotherapy, pharmacotherapy or the combination of both mainly depends of the severity experienced by the patient, as classified in the DSM-5. For instance, psychotherapy alone can be efficiently sufficient for patients with mild depression while the combination of both psychotherapy and pharmacotherapy is the most effective option for patients suffering from the moderate to severe forms of MDD (Prescott and White, 2017).

Psychotherapy

All of the psychotherapies used to treat depressed patients are not specific and are also used for other psychiatric diseases. Behavioral therapy is a type of psychotherapy whose aim is to change patient behavior in order to change their cognition. For instance, patients that follow a behavioral activation treatment are encouraged to do enjoyable activities to improve their mood. Cognitive-behavioral therapy (CBT) combines behavioral therapy and cognitive therapy to allow patients to recognize and challenge their negative thoughts and behaviors. Other types of cognitive therapies can also be efficient, like psychodynamic therapy which is more unconscious focused, and interpersonal therapy that targets the improvement of patients social functioning ((Barth et al., 2013; Cuijpers et al., 2019).

Pharmacotherapy

First generation antidepressants were fortuitously discovered in the 1950s. At the time, American chemists synthetized an antituberculotic agent, iproniazid which surprisingly enhanced mood, appetite and sleep in patients. This observation led to clinical trials on depressed patients, which confirmed iproniazid efficiency in treating MDD (Kiloh et al., 1960). The antidepressant properties of imipramine were discovered soon after, initially in schizophrenic patients then confirmed in depressed patients, leading to its commercialization as an MDD treatment (Carrillo et al., 2020). Investigations in rodents exploring the hypothesis that iproniazid and imipramine may counteract chemical imbalances causing depression later revealed that (i) iproniazid inhibits the monoamine oxidase (MAO) and thereby prevents the degradation of catecholamines, and that (ii) imipramine blocks serotonin and noradrenaline re-uptake transporters. Combined with clinical observations, these discoveries shaped the

foundations of the monoaminergic theories of depression postulating that the disease results from reduced noradrenergic or serotonergic neurotransmission in key brain areas (Carrillo et al., 2020; Lopez-Munoz and Alamo, 2009). Based on the knowledge built from iproniazid and imipramine, monoamine oxidase inhibitors (MAOI) and tricyclic antidepressants (TCA), respectively, became mainstream compounds to treat depression, and second-generation medications targeting monoaminergic systems more selectively were developed in the 1970s to limit adverse effects.

Fluoxetine hydrochloride was the first selective serotonin reuptake inhibitor (SSRI) described, and obtained FDA approval as an antidepressant under the name Prozac in the 1980s. Since then, other SSRIs have been developed, sharing the same mechanism of action: selective inhibition of the serotonin re-uptake transporters to increase synaptic serotonergic levels. While SSRIs are still the most prescribed antidepressants, they display similar side effects as their precursors and a slow onset of action of at least several weeks (Lochmann and Richardson, 2018). Besides serotonergic hypofunction, the catecholamine hypothesis of depression postulating a noradrenaline deficiency led to the development of a new class of antidepressants in the 1990s: the serotonin-noradrenaline re-uptake inhibitors (SNRIs). However, no measurable efficiency improvement has been reported compared to the SSRIs.

Despite these advancements, challenges persist in antidepressant pharmacotherapy. Side effects like dry mouth, weight gain, sleep disturbances, sexual dysfunction and others are common (Brunello et al., 2002). In addition, the onset of efficiency is long and more than one treatment often have to be prescribed. Furthermore, up to one-third of patients resist to treatment, with treatment-resistant depression (TRD) being defined as the lack of response (minimum 50% improvement in depression severity) after two treatments by two different antidepressant classes at optimal dose after a minimum duration of six weeks (Fava and Davidson, 1996; Li, 2023). This highlights an urgent demand for more potent antidepressants, recently underscored by investigations into fast-acting options like ketamine and psilocybin.

B. Neurobiological basis of MDD

1. General features of the disease in humans

Depression pathophysiology is characterized by a complex dysregulation of multiple systems of the human body beyond brain functioning damages. Indeed, major features includes alterations of the hypothalamo-pituitary-adrenal (HPA) axis, immune system, autonomic nervous system, cardiovascular and metabolic systems (Figure 1)(Otte et al., 2016).

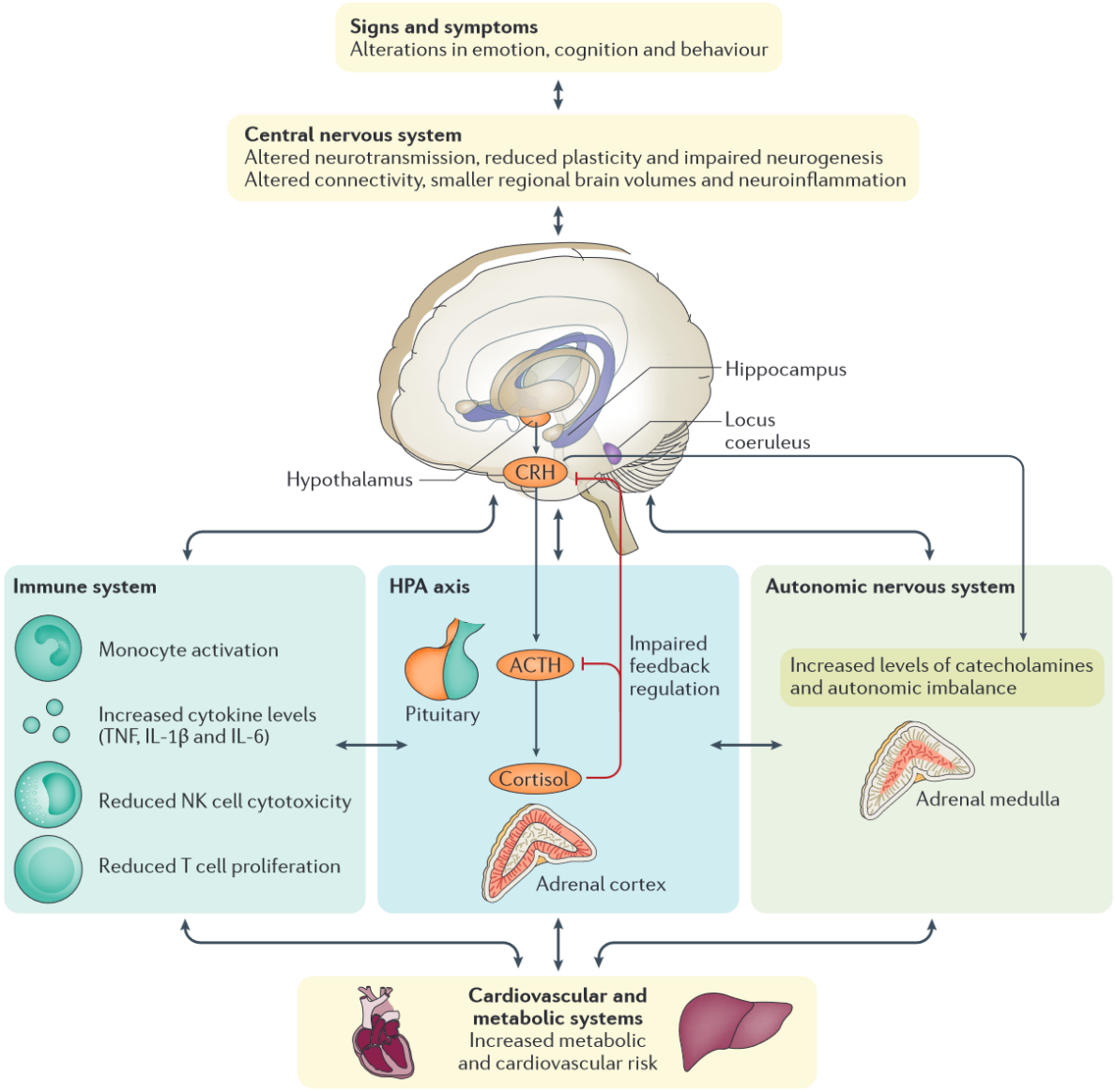

Figure 1: Major pathophysiological features of depression. Depression results from a general dysregulation of multiples systems of the human body. Patients present altered emotion, cognition and behavior with concomitant impaired neurotransmission and connectivity in specific brain areas. Overall, a general activation of systems is occurring, involving circulation of pro-inflammatory markers, autonomic imbalance and above all, a hyperactivation of the HPA axis leading to excess of stress hormones (from Otte et al, 2016).

Depression and stress are overlapping, as acute or chronic stress often contribute to the development of the disease through hyperactive response to stress, i.e. HPA axis overactivation (Dean and Keshavan, 2017). In depressed patients, HPA axis alterations include hypersecretion of corticotropin-releasing factor (CRF) and vasopressin (AVP) from the hypothalamus, resulting in high secretions of adrenocorticotropic hormone (ACTH) from the pituitary, leading to hypercortisolemia through adrenal cortex stimulation (Ferrari and Villa, 2017). Furthermore in healthy conditions, cortisol levels autoregulates by inhibiting

hypothalamic CRH and pituitary ACTH productions whereas in the context of depression, this negative feedback is impaired as the inhibition of brain structure is lost, leading to constant production of cortisol (Dean and Keshavan, 2017). In reality, immune, autonomic nervous and HPA systems are closely related in the disease, i.e. psychosocial stress firstly activates stress responses through corticotropin-releasing hormone (CRH) and pro-inflammatory sympathetic nervous system (SNS) pathways (Miller et al., 2009). Catecholamines are then released by the SNS, thereby enhancing NF-kB activation in immune cells. This leads to the release of pro-inflammatory markers such as IL-1, tumor necrosis factor alpha (TNF-α), and IL-6, responsible for the promotion of inflammation (Mössner et al., 2007). In healthy conditions, the parasympathetic nervous system (PNS) would counteract this inflammatory response through cortisol secretion. However, in the context of MDD, due to cytokines-mediated dysfunction of glucocorticoid receptors, inhibitory effect of cortisol is less efficient and results in a chronic imbalance favoring inflammation maintenance (Krishnan and Nestler, 2008). Ultimately, this establishment of stress-related endocrine and inflammatory environment impact brain functioning both at the cellular and circuit levels (Otte et al., 2016).

2. Central nervous system alterations

Thanks to neuroimaging, post-mortem studies and rodent studies, a lot of cellular brain processes and brain areas have been reported to be involved in the pathophysiology of depression.

Human studies greatly uncovered brain areas that are demonstrating modifications of structure and metabolic activity in depressed patients, i.e. the reward circuit. This circuit include meso-cortico-limbic structures such as the medial prefrontal cortex (mPFC), the hippocampus (Hipp), the basolateral amygdala (BLA), the nucleus accumbens (Nac) and the ventral tegmental area (VTA) (Russo and Nestler, 2013). Prefrontal cortex alterations in depressed patients are well characterized, demonstrated a consistent large volume reduction, particularly in anterior cingulate cortex (ACC) and bilateral orbito-frontal cortex (OFC), abnormal coupling of connectivity within its subregions and global decrease in activity (Koolschijn et al., 2009; Pizzagalli and Roberts, 2022). Results are similar and consistent regarding the hippocampus and associated to impairment in encoding memories. These hippocampal volume reductions generally occur after the onset of the disease (Schmaal et al., 2016). Findings are either inconsistent or lacking regarding the BLA, Nac and VTA. BLA volume and gray matter density tend to decrease while its activity tends to increase in depressed patients (Russo and Nestler, 2013). Obtaining data regarding potential alterations of VTA in depressed patients is still a challenge, as its limits are not clearly defined yet due to technical limitations and variability in its composition (Morris et al., 2022). The nucleus

accumbens is a major brain region involved in reward processing, its dysregulation of connectivity being associated to anhedonia (Pan et al., 2022). Indeed, reward task–based functional MRI (fMRI) have revealed that reduced activity in the Nac is significant in the etiology of depression; moreover it serves both as a predictor and a consequence of the disease (Pan et al., 2017). These main structural and functional alterations observed in depressed patients are summarized in table 3.

Brain reward region	Morphometric changes	Functional changes	Impaired processes
mPFC	Volume reduction	Reduced activity	Executive functions and emotional regulation
Hipp	Volume reduction	NA	Memory and stress response regulation
BLA	Volume reduction (but rather inconsistent)	Increased activity	Emotions
Nac	Volume reduction	Reduced activity	Reward system

Table 3: Major focal morphometric changes and functional changes occurring in depressed patients and their associated cognitive deficits, revealed by both neuroimaging technique and postmortem studies (Adapted from Russo and Nestler, 2013; Savitz and Drevets, 2009).

3. Experimental models of major depressive disorder

One of the biggest challenges in psychiatric research is the use of clinically relevant animal models. An animal model is valid if it encompasses the predictive (response to treatments), face (symptoms and underlying mechanisms) and construct (etiology) validities (Willner and Mitchell, 2002). Indeed, major depressive disorder is a highly heterogeneous disease and human symptomatology is hardly reproducible in animals. Nevertheless, some modalities of the pathology can be mimicked in animals by replicating typical behavioral, physiological and neurochemical aspects of depression observed in human (Figure 2). These animals are then described as presenting “depressive-like behavior”.

Genetic models

Numerous genetic factors contribute to major depressive disorder; indeed, it is also highly improbable that depression is only caused by a single gene modification. Thus, even if genetic models of depression have poor face and predictive validity, still some mice line - mainly knock-out mice - have been generated in order to identify candidate genes for depression, to study its pathogenesis and to design new therapeutic strategies (Urani et al., 2005). Three main categories of targeted genes can roughly be distinguished, i.e. (i) genes encoding

proteins involved in the monoaminergic system, (ii) genes encoding BDNF or its receptor, or (iii) genes encoding proteins involved in the HPA axis regulation.

Briefly, the monoaminergic system has been targeted in different ways; either through inactivation of the vesicular monoamine transporter (Vmat) (Fukui et al., 2007), silencing of the tryptophan hydroxylase (TPH) involved in serotonin biosynthesis (Gutknecht et al., 2015), downregulation of the serotonin (SERT), noradrenaline (NAT) or dopamine (DAT) transporters (Haenisch and Bönisch, 2011), or manipulation of 5-HT receptors (Yohn et al., 2017). The neurotrophic hypothesis of depression, and potential role of neurogenesis in the etiology and physiopathology of MDD have been explored using BDNF mutant and inducible BDNF KO mice lines (Gardier et al., 2009). Finally, mimicking dysregulations of the HPA axis – a key feature of depression – has been achieved by targeting genes encoding the corticotropin-releasing factor (CRF), the glucocorticoid receptor or the mineralocorticoid receptor (Urani et al., 2005). Overall, genetic models constitute a robust strategy to study the functional enhancement or impairment of specific genes in major depressive disorder. The main weakness of this strategy is that genetic manipulation can cause lack and loss of functions across various biological systems other that the targeted one, which may not necessarily manifest at the same degree in human depression (Becker et al., 2021).

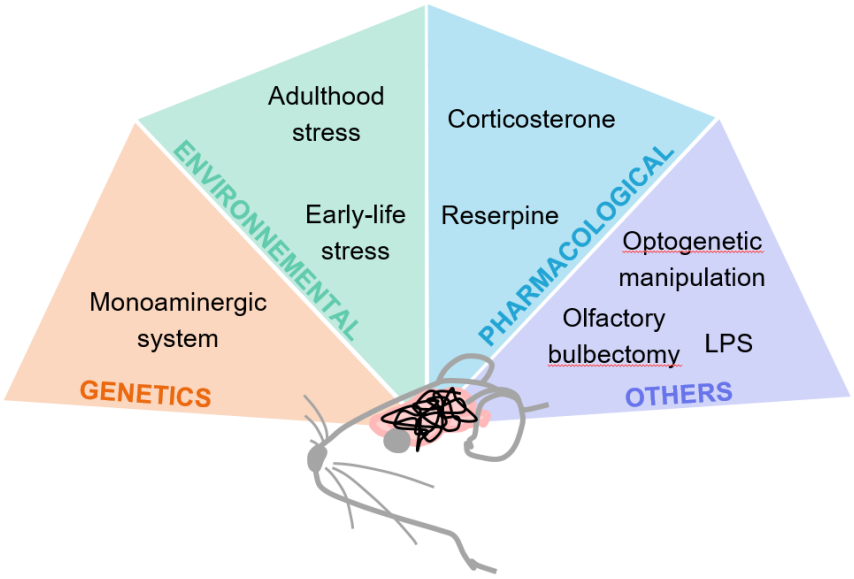

Figure 2: Representation of different ways of modeling modalities of major depressive disorder in mice. These models can be categorized into genetic, pharmacological, environmental and neurobiological (others) strategies. Genetic models mainly target manipulation of monoaminergic systems, environmental models involve animals undergoing acute or chronic stressful procedures, pharmacological models consist of inducing depression-like behavior by exposing animals to compounds while other notable models include neurobiological manipulation through surgery or optogenetic and inflammation-induced depression-like phenotype. LPS: lipopolysaccharide.

Behavioral models: exposure to stressors

The development of major depressive disorder is predominantly linked to both short-term and prolonged exposure to stressful factors. Accordingly, stress-based behavioral models are considered the more ethologically relevant and are the most commonly used ones as they induce a phenotype in animals that closely resembles MDD. It is known that individuals who have experienced early life stress (ELS) are 2,5 times more prone to develop major depressive disorder in the future (LeMoult et al., 2020). Of course, it is not possible nor ethical to reproduce those kinds of early life stressful events, i.e. sexual abuse, physical abuse or emotional abuse for example. Thus, maternal stress during pregnancy and maternal separation are the main rodent models of early life stress used for depression (Schmidt et al., 2011). Regarding adulthood stress, there are different ways to environmentally stress a rodent, mainly chronically. The chronic mild stress (CMS) model is the most commonly used, which relies on the continuous exposure of rats or mice to unpredictable micro-stressors, leading to the emergence of various behavioral alterations. The CMS model is highly regarded as the animal model of depression with the highest validity and potential for translation into human research, despite early concerns about its reliability (Willner, 2017). Several micro-stressors can be used : social stress, mice restraint and disturbance of the light-dark cycle, wet cage and/or sawdust, empty cage, inclined cage (Burstein and Doron, 2018)… Social stress can be used by its own in the context of another model called the social defeat model where an animal is placed into the cage of an aggressive individual leading to confrontations.

Pharmacological models

While drug-elicited depressive-like manifestations may appear as ethologically less relevant models of MDD, they allow powerful multiscale investigations spanning from in vitro dissections of molecular mechanisms up to pathological rearrangements of brain circuitry supporting disease-related behavioral deficits.

Animals were found to present depressive-like behaviors after being exposed to specific pharmacological compounds, for example reserpine or corticosterone. Reserpine is an alkaloid extracted from the root of the plant *Rauwolfia serpentina* and was initially used as a first line treatment to reduce blood pressure in patients with hypertension. Reserpine is in fact acting on the monoaminergic system by depleting noradrenalin, dopamine and serotonin from synapses, at the origin of severe side effects causing its prescription decline (Shamon and Perez, 2016). In mice, intraperitoneal injections of reserpine (0,5 mg/kg) once per day for two weeks induce depressive-like behaviors, hippocampal and prefrontal cortex volume reductions and increase the levels of inflammatory cytokines (Qian et al., 2023). Alike, daily subcutaneous reserpine injections (1 mg/kg) in rats during three weeks, cause reductions in

serotonin and dopamine level and increase immobility time in the forced swim test (FST) highlighting reinforced despair behavior (Ikram and Haleem, 2017). Nevertheless, it is important to note that reserpine also causes major motor impairment which were successfully used to develop experimental models of Parkinson's disease, but limit its validity as a relevant model of depression.

Increased HPA axis activity is a main feature of MDD that involves hypothalamic corticotropin-releasing hormone (CRH) and vasopressin hypersecretion causing increase in glucocorticoids levels. This is responsible for behavioral symptoms observed in MDD, such as anxiety, disrupted sleep, changes in psychomotor activity, decreased appetite and libido, and cognitive impairment (Antonijevic, 2006). In rodents, the main glucocorticoid is corticosterone, an analog of cortisol in humans. Corticosterone (CORT) is binding two types of receptors: mineralocorticoid receptors (MR) mainly found in the hippocampus, isocortex and amygdala and glucocorticoid receptors (GR) that are more ubiquitous. CORT tends to naturally bind MR with a high affinity, but it also activates GR – although with a 10-fold lower affinity - at higher concentrations during stress (Joëls et al., 2018). Exposing mice to a low dose of corticosterone (35 µg/ml/day or 5 mg/kg/day) for 4 to 8 weeks produces an depressive-live behavioral phenotype accompanied by decrease of hippocampal neurogenesis and serotonin serum levels (Brachman et al., 2016; David et al., 2009; Hache et al., 2012). One limitation of the chronic CORT model, however, is that it may produce a more systemic metabolic and biochemical alteration in animals that is hardly comparable to what is observed human patients with MDD (Becker et al., 2021).

Other notable models

Another feature of depression is a systemic immune activation. Indeed, MDD patients display increased proinflammatory cytokine levels, thought to alter neurotransmitter signaling in structures and circuits involved in mood regulation and to activate the HPA-axis. Cytokines imbalances and neuroinflammation would trigger and/or maintain depression (Beurel et al., 2020; Jeon and Kim, 2016). Lipopolysaccharide (LPS) triggers inflammation, notably through monocytes and macrophages activation, that cross the blood-brain-barrier (BBB) to produce neuroinflammation (Yin et al., 2023). Mice that receive LPS intraperitoneally for 3 days (2mg/kg) display a depressive-like phenotype, microglial activation, spine loss and reductions in the of genes involved in synaptogenesis (Li et al., 2021a, 2021b). Even a single injection of LPS at a dose of 1mg/kg is sufficient to induce depressive-like behavior, abolish LTP and reduce BDNF expression in the hippocampus (Tang et al., 2020).

Olfactory deficits can be observed in MDD patients, showing odor identification impairment, reduced olfactory sensitivity and even anosmia (Lombion-Pouthier et al., 2006; Pause et al.,

2001). By performing bilateral olfactory bulbectomy (OBX) in rodents, causing anosmia and loss of detection of pheromones at the origin of depressive-like behavior, noradrenergic and serotonergic systems are perturbed through altered neurotransmission to cortex, hippocampus, amygdala and dorsal raphe nuclei (Hellweg et al., 2007; Song and Leonard, 2005). Olfactory bulbs are usually removed by aspiration during a surgery, which can be traumatic, but it has recently been shown that chemogenetically inhibiting the olfactory bulbs induces a depressive-like state with desynchronization of neuronal activity in the limbic system (Fattore et al., 2023; Li et al., 2023).

4. NMDAR dysfunction in MDD

a. Clinics

Various neuroanatomical on post-mortem human brains and neuroimaging studies support an involvement of NMDAR dysfunctions in depression. Depressed patients consistently exhibit decreased prefrontal cortex and hippocampus volumes, which includes thickness and cell density reductions reflecting a loss of excitatory synapses (Rajkowska et al., 1999). The levels of NMDAR subunits and their interactors are altered in post-mortem brains. Enhanced expression of GluN2A have been found in the amygdala of MDD patients, suggesting dysfunction of glutamatergic system in this structure (Karolewicz et al., 2009). In the perirhinal cortex, GluN2A and GluN2B mRNAs are decreased in MDD patients (Beneyto et al., 2007). In the prefrontal cortex (PFC), global diminutions of GluN1, GluN2A, GluN2B expressions have been observed in depressed patients along with reduction in PSD-95 levels. Besides, receptor autoradiography indicated stable receptor number, suggesting a possible change of subunit composition (Beneyto and Meador-Woodruff, 2008; Feyissa et al., 2009). In locus coeruleus (LC), while levels of GluN1 were not altered in depressed patients compared to healthy subjects, the amount of GluN2C was significantly increased. GluN2C is also enhanced in the cerebellum of MDD patients (Karolewicz et al., 2005). At the level of the body, MDD patients present increased levels of circulating glutamine in the cerebrospinal fluid (CSF) and glutamate in plasma (Levine et al., 2000; Mauri et al., 1998).

b. Antidepressant effect of NMDAR antagonists

Recently, several compounds targeting NMDAR have been shown to exert antidepressant properties. Ketamine and to a less extent, memantine, are the more studied glutamatergic agents aimed for treatment. Ketamine has been the first NMDA receptor used in clinic and exhibiting in a few hours antidepressant properties in depressed patients (Berman et al., 2000). This first double-blind randomized study has been conducted on 4 men and 5 women from 23 to 56 years, diagnosed with major depressive disorder according to the DSM-IV at the

time. All participants received a subanesthetic dose of 0.5 mg/kg of ketamine intravenously. From 4 hours after the infusion, half of the patients presented reduced symptoms, as demonstrated by a 50% reduction in the Hamilton Depression Rating Scale (HDRS) scores. This effect persisted until 1 to 2 weeks after the infusion depending of the patient (Berman et al., 2000). Following this study, ketamine has been extensively tested in different clinical trials for depression. MDD patients that received an intravenous infusion (0.5 mg/kg) exhibited reduced scores 80 minutes post-treatment, with the improvement lasting for one week (Carlos A Zarate et al., 2006). The antidepressant effect of ketamine occurs even if the route of administration is changed. For instance, Lapidus and colleagues have shown significant decreased in the Montgomery-Asberg Depression Rating Scale (MADRS) from 40 min and persisted for 2 days after an intranasal intake of ketamine (50 mg) in depressed patients (Lapidus et al., 2014). Ketamine is not the only NMDAR antagonist reported to have an antidepressant action. Indeed, memantine has been shown to exert antidepressant and mood stabilizing effects but less consistently than ketamine (Ghasemi et al., 2014). For instance, this effect is occurring in bipolar depressive patients following daily administrations of memantine (10mg/day to 20 mg/day) for a few weeks but failed to be reproduced in MDD patients at the same range of doses and duration (5 to 20 mg/day for 8 weeks)(Smith et al., 2013; Teng and Demetrio, 2006; Carlos A. Zarate et al., 2006). In rodents, NMDAR allosteric modulators have also been shown to exert antidepressant properties. Indeed a single dose of rapastinel, an NMDAR-PAM, produces antidepressant effect through mTORC1 pathway activation in the mPFC of rats (Liu et al., 2017). Antagonists targeting GluN2B-NMDAR, such as CP-101,606 and MK-0657, have shown potential in reducing depression symptoms, with CP-101,606 causing ketamine-like side effects that decrease at lower doses, while MK-0657 does not cause these psychomimetic effects (Burgdorf et al., 2015). Similarly to ketamine, lanicemine, a low-trapping NMDAR channel blocker, has the ability to produce antidepressant efficacy but concomitantly with psychomimetic side effects (Downey et al., 2016; Sanacora et al., 2014).

C. Ketamine as a treatment of major depressive disorder

1. History of ketamine

Ketamine is a derivative of a dissociative drug developed in the fifties called phencyclidine (PCP, denomination: CI-395). PCP was the first synthetized molecule aimed for anesthesia and analgesia uses. Its anesthetic properties were indeed confirmed and the compound was safe and reliable but side effects were too important, with patients experiencing a massive and long-lasting emergence delirium (Li and Vlisides, 2016). Hence, chemists focused on synthetizing an analog compound of PCP presenting similar anesthetic power with less

emergence delirium. This derivative was denominated CI-581 and commonly called ketamine, and its anesthetic properties were rapidly confirmed in animals. To ensure its human use and efficacy, ketamine was administrated for the first time intravenously to volunteered prisoners from Jackson, Michigan USA (Domino et al., 1965). The following year, a first clinical trial validated its clinical use on patients and confirmed its unique anesthetic properties: a specific state of altered consciousness called “dissociative anesthesia” along with deep analgesia and a limited effect that can be controlled by modulating the number of administrations. Moreover, ketamine is devoid of the deleterious adverse effects of PCP such as the emergence delirium (Domino, 2010; Le Daré et al., 2022). Since approval by the American Food and Drug Administration (FDA), ketamine has been widely used as a surgical anesthetic for soldiers during Vietnam War in the seventies, thanks to its fast onset of action and its sympathomimetic properties (Mion, 2017). Apart from its clinical and veterinary uses, ketamine is also used since a few decades as a recreational drug because of its reinforcing and rewarding properties (Liu et al., 2016).

2. Structure

Ketamine is an arylcyclohexylamine that contains a chiral center at C2 position of the cyclohexane ring, producing two isomers. Indeed, ketamine exists as a racemic mixture of two enantiomers, (S)-ketamine and (R)-ketamine, meaning each isomer is identically present at 50%. These two enantiomers share the same chemical and physical properties, they only differ in their ability to turn polarized light; (R)-ketamine rotates it in a clockwise direction while (S)-ketamine turns it in a counterclockwise direction. However, both isomers display different binding affinities for receptors, a phenomenon called stereoselective binding, and cause different clinical outcomes (Sinner and Graf, 2008). For instance, (S)-ketamine has a three- to four-fold more powerful anesthetic action than (R)-ketamine, and may thus cause harsher psychiatric side effects (White et al., 1980). Besides blocking the ion channel pore of NMDAR, ketamine is able to inhibit other types of receptors like adrenergic receptors, acetylcholine adrenergic and nicotinic receptors and dopaminergic receptors (Peltoniemi et al., 2016).

3. Pharmacokinetics

Depending of its route of administration, ketamine displays different bioavailabilities, i.e. the amount of drug available in the blood stream to produce its desired effects. Naturally, intravenous injection is the most efficient route of administration, allowing a bioavailabitlity of 100% and a rapid onset of action of 30 seconds. Intramuscularly and intranasally, ketamine reaches a bioavailability of 93% and 50% respectively. Finally, oral and rectal routes are the less efficient, allowing a ketamine bioavailability of 17% and 25% only, respectively (Dinis-Oliveira, 2017; Mion and Villevieille, 2013). Ketamine is water- and lipid-soluble and presents

a low binding affinity for plasma proteins (about 20 to 30%). Consequently, the drug can distribute in a large volume of 3 to 5 L/kg with a 10-15min a half-life and it is able to rapidly cross the BBB to produce its effects (Dinis-Oliveira, 2017). Its clearance is relatively fast, as it takes between 2 to 4 hours for the drug to decrease by half by intravenous route (Domino et al., 1982).

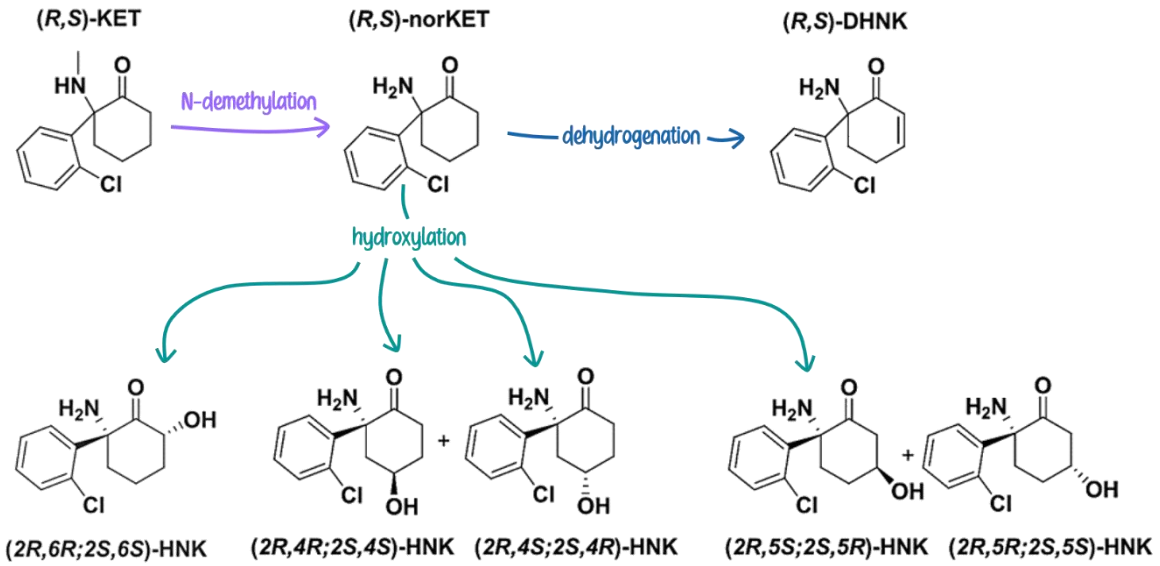

Figure 3: Ketamine and its major metabolic pathways. Ketamine is primarily metabolized in the liver to form norketamine ((R,S)-norKET) through N-demethylation, this metabolite undergoes hydroxylation to form different other metabolites, main ones being (2R-6R)-HNK and (2S-6S)-HNK (Adapted from (Zanos et al., 2018).

The liver is the principal site of ketamine metabolization through the action of different types of cytochromes, but this process also involves the lungs, intestine and kidneys. About 80% of ketamine undergo N-demethylation to form norketamine (norKET). Then, 15% of norketamine are hydroxylated to hydroxynorketamine (HNK) that are ultimately excreted in bile and urine. The elimination half time of norketamine is superior to the one of ketamine, allowing the persistency of the analgesic effect of the drug (Figure 3). Finally, ketamine clearance follows liver blood flow, i.e. between 12 and 20 ml/min/kg, with a clearance being about 20% higher in women (Mion and Villevieille, 2013). All these metabolites are detected in human plasma following a 40-min subanesthetic dose of ketamine, but (2R;6R)-HNK and (2S;6S)-HNK stand out as the predominant ones (Zarate et al., 2012).

4. <u>Ketamine dosing</u>

Ketamine is able to produce a short-term dissociative anesthesia that is characterized by a functional dissociation between thalamocortical and limbic systems without systematic loss of

consciousness (Mion, 2017). Anesthetic doses in human adults typically range from 1-2 mg/kg by intravenous route and 3-9 mg/kg for intranasal administration (Gao et al., 2016). When given at lower doses than the anesthetic ones, a single ketamine administration has the ability to produce persistent antidepressant effect in depressed patients, including treatment-resistant-depressed (TRD) patients (Berman et al., 2000). Subanesthetic doses are mostly administered intravenously and, depending of the patient, they typically range from 0.1 mg/kg to 0.75 mg/kg, with the most common dose being 0.5 mg/kg. Administration commonly lasts around 40 minutes, with the range of safe and efficient use being between 2 and 100 minutes (Andrade, 2017). As a comparison, when used recreationally, ketamine powder is preferentially snorted or inhaled and produces mild dissociative effects associated to hallucinations and time and space distortions. Nonetheless, ketamine provokes a severe dissociation called the “K-hole” when consumed at large doses over 150 mg ; consciousness and reality are fractured and users experience severe hallucinations and temporal memory loss (Muetzelfeldt et al., 2008).

5. Proposed mechanisms for the antidepressant action of ketamine

To date, three different molecular pathways have been proposed to support the antidepressant properties of ketamine on the glutamatergic system, including direct actions of the drug on NMDAR or indirect actions of its metabolites on AMPAR. Whether these processes occur synergistically or independently remains unknown. However, they all share common outcomes involving enhanced protein synthesis hence increased excitatory neurotransmission which is believed to support the antidepressant action of ketamine (Thompson, 2023).

a. Inhibition of NMDAR localized on GABAergic interneurons

Disinhibition was the first hypothesis proposed to explain the antidepressant action of ketamine. According to this hypothesis, ketamine may selectively antagonize NMDAR expressed by GABAergic interneurons projecting in the mPFC and hippocampus, thereby inducing a disinhibition of glutamatergic excitatory neurotransmissions in these brain regions. This action appears to be specific of low subanesthetic ketamine doses, as higher anesthetic doses instead reduce glutamate release (Moghaddam et al., 1997; Zanos and Gould, 2018). Ketamine may preferentially target GluN2B-NMDAR on interneurons in the mPFC (Gerhard et al., 2020; Pothula et al., 2021). In addition to increased glutamate levels, ketamine’s binding on NMDAR of interneurons induce increased glutamate cycling and enhanced probability of action potential generation (Borsellino et al., 2023; Chowdhury et al., 2017). It is well known that BDNF release, along with TrkB receptors activation, are directly and dose-dependent influenced by glutamate release (Falkenberg et al., 1996). Hence, disinhibited presynapses

release more glutamate, that binds and activates post-synaptic AMPAR, causing increased BDNF release and TrkB receptors activation (Qu et al., 2021). BDNF-TrkB signaling leads to downstream activation of the PI3K/AKT pathway notably responsible for cell growth, proliferation and survival. The stimulation of the PI3K/AKT pathway results in activation of mTOR signaling, ultimately producing enhanced synthesis of proteins involved in synapse maturation and formation like the GluA1 subunit of AMPAR and the scaffolding protein PSD95 (Duman et al., 2016; Li et al., 2010; Sarbassov et al., 2005). Overall, these pathways recruited by ketamine have been shown to decrease the inhibition/excitation balance (Widman and McMahon, 2018; Zhang et al., 2021).

b. Inhibition of NMDAR expressed by pyramidal cells

Inhibition of spontaneous NMDAR-mediated synaptic transmission

Neurotransmission is not only driven by action potentials, and stochastic spontaneous neurotransmission occurs at all synapses at lower frequency and amplitude. This so-called miniature neurotransmission involves spontaneous presynaptic neurotransmitter release triggering postsynaptic miniature excitatory synaptic currents (mEPSCs). NMDAR spontaneous neurotransmission is essential in the stabilization of synapse function (Sutton et al., 2006). Upon binding to synaptic NMDAR, ketamine has been shown to inhibit NMDAR-mediated mEPSCs and to trigger by inhibition of eukaryotic elongation factor 2 kinase (eEF2K), ultimately leading to enhanced BDNF release, activation of TrkB, and increased postsynaptic expression of GluA1- and GluA2-containing AMPAR supporting synaptic potentiation (Autry et al., 2011; Nosyreva et al., 2013). While GluN2B-NMDAR have initially been considered as preferential targets, it is now established that both GluN2A- and GluN2B-NMDAR are required for the antidepressant action of ketamine. Indeed, administration of a GluN2A- (NVP AAM077) or a GluN2B-selective (Ro 25-6981) antagonist both elicit antidepressant responses in the force swimming test (FST) (Jiménez-Sánchez et al., 2014), suggesting that inhibition of either GluN2A- or GluN2B-NMDAR is sufficient to alleviate depressive-like behavioral phenotypes. Furthermore, the antidepressant action of ketamine was recently reported to be occluded in both GluN2A KO and GluN2B KO mice (Miller et al., 2014; Su et al., 2023). Thus, the antidepressant action of ketamine likely involves both subtypes of receptors. However, the nature and timing of their respective contributions remains elusive.

Inhibition of extrasynaptic NMDAR

Extrasynaptic glutamate concentrations are tightly buffered by surrounding astrocytes through the action of glutamate transporters, which are responsible for keeping extracellular glutamate

levels low and preventing glutamate-induced neurotoxicity (Rothstein et al., 1996). At basal state, extrasynaptic NMDAR can be activated by these low ambient glutamate levels, which recruit the mTOR pathway to prevent protein synthesis and maintain synaptic homeostasis. Ketamine-elicited blockade of extrasynaptic GluN2B-NMDAR in the mPFC was shown to suppress mTOR activation, leading to a disinhibition of protein synthesis that enhances excitatory transmission and alleviates motivational and anxiety-related behavioral deficits in rodents (Miller et al., 2014; Zanos and Gould, 2018).

c. NMDAR-independent action of HNK metabolites

The metabolites hydroxynorketamines were also reported to support the antidepressant action of ketamine, especially (2R-6R)-HNK and to a lesser extent, (2S-6S)-HNK. Like ketamine, they display a rapid onset and persistent antidepressant effect. For example, intraperitoneal injection of (2R-6R)-HNK (10 mg/kg) decreases immobility of mice in the FST (Zanos et al., 2016). It is believed to be underlined by an increase in extracellular glutamate levels in the prefrontal cortex and a direct activation of AMPAR triggering the BDNF/TrKB pathway and subsequent mTOR signaling initiating protein synthesis (Fukumoto et al., 2019; Pham et al., 2018). Importantly, the antidepressant action of (2R-6R)-HNK exposures is totally occluded following administration of an anti-BDNF antibody or an antagonist of the mTORC1 signaling pathway in the PFC (Borsellino et al., 2023; Nordvall et al., 2022). The milder antidepressant action of (2S-6S)-HNK appears to rely on different mechanisms and has recently been proposed to involve modulation of $GABA_AR$-mediated tonic inhibition in glutamatergic neurons located in the anterior part of the paraventricular nucleus of the thalamus (aPVT) (Kawatake-Kuno et al., 2024).

Objectives of the thesis

The general aims of this work were to provide new insights into the action mechanisms of clinically-relevant NMDAR antagonists, and to investigate whether their behavioral outcomes involve drug-induced changes in NMDAR synaptic trapping, organization, and signaling.

Objective I: Impact of ketamine and other open channels blockers on NMDAR synaptic trapping

Beyond ionotropic considerations, NMDAR organization and diffusion-based redistributions at synapses play important roles in synaptic physiology and adaptation, and their alterations have been associated with the emergence of psychosis. However, whether targeting NMDAR synaptic trapping and organization is of clinical relevance for the treatment of brain conditions remains an open question. Interestingly, competitive, non-competitive, and glycine-site antagonists of NMDAR elicit comparable channel inhibition of the receptors but trigger distinct behavioral outcomes and have diverging therapeutic potential, suggesting that they impact NMDAR signaling through different mechanisms, some of which may be independent of ion flux blockade. These discoveries prompted us to investigate whether specific subclasses of NMDAR antagonists may act upon NMDAR trafficking and trapping at synapses, and to assess if this action could somehow contribute to their therapeutic properties.

Does the action of clinically-relevant antagonists involve modifications of NMDAR synaptic trapping and organization? We combined single molecule imaging and immunocytochemistry approaches to investigate whether acute exposure to competitive (D-AP5), non-competitive (ketamine, MK-801, memantine) and glycine-site antagonists (kynurenic acid) affect the synaptic trapping and organization of NMDAR. We then used fluorescence lifetime imaging of Förster resonance energy transfer (FLIM-FRET) to dissect the mechanisms (conformational rearrangement, protein-protein interaction) supporting drug-elicited changes in NMDAR synaptic trapping.

Can ketamine-elicited NMDAR synaptic trapping be of interest to restore synaptic function? We combined single molecule imaging, immunocytochemistry, and FLIM-FRET-based monitoring of enzymatic activity to investigate whether synaptic anchoring promoted by ketamine could counteract the pathological destabilization and signaling impairments of synaptic NMDAR caused by autoantibodies from patients with anti-NMDAR encephalitis. Using a battery of assays to monitor locomotion, sensorimotor gating and anxiety/depression manifestations, we then explored if behavioral deficits provoked by patient antibodies can be alleviated by the action of ketamine.

Objective II: Exploring the contribution of drug-evoked NMDAR redistributions in the antidepressant action of ketamine

Major depressive disorder is a leading cause of disability worldwide and is believed to be the consequence of abnormal activity in key structures supporting mood and reward, namely cortico-meso-limbic structures (Chaudhury et al., 2015). Current treatments, that is serotonin-based pharmacotherapies and psychotherapies, have a delayed onset of action and still up to one-third of patients are resistant. Thus, the recent discovery that a subanesthetic dose of ketamine, a non-competitive N-methyl-D-aspartate glutamate receptor (NMDAR) antagonist, induce a rapid-acting and sustained antidepressant effect has raised new hopes for the treatment of depression (Berman et al., 2000; Carlos A Zarate et al., 2006). Although intensely investigated, the mechanisms through which ketamine acts on NMDAR signaling within the cortico-meso-limbic network to produce its antidepressant effect are still unclear. Based on the results gathered in the first objective of this work, we hypothesized that ketamine may elicit changes in NMDAR synaptic distribution allowing rearrangements in the functional connectivity of cortico-meso-limbic structures, thereby alleviating the symptoms of depression. To tackle this question, we developed a multi-level approach combining behavioral tests, whole-brain imaging of immediate early gene expression and super resolution microscopy in a pharmacological model of depression based on the chronic administration of corticosterone.

Our main questions were:

How are brain networks rearranged in response to antidepressant doses ketamine? Neural circuits activated by a behavior or a pharmacological treatment can be visualized by combining tissue clearing, immediate early gene (IEG) immunolabelling and light sheet microscopy (Renier et al., 2016, 2014). Using chronic corticosterone (CORT) administration as a pharmacological model of depression (David et al., 2009), we aimed at deciphering activity changes and brain network rearrangements acutely (90 min) after ketamine administration, and at later stages (24 h) when its antidepressant action is fully established.

Does ketamine impact NMDAR organization at synapses? Single molecule imaging using photoactivated localization microscopy (PALM) on dissociated cortical neurons was used to explore subtype-dependent changes in NMDAR synaptic trapping across time following administration of ketamine or its metabolites.

Results I: IMPACT OF KETAMINE AND OTHER OPEN CHANNELS BLOCKERS ON NMDA RECEPTOR SYNAPTIC DYNAMICS

Villéga*, Fernandes*, Jézéquel*, **Uyttersprot** et al, accepted in Neuron.

I directly contributed to PALM experiments investigating the effects of competitive and non-competitive antagonists on NMDAR surface diffusion (Figure S2).

Ketamine alleviates NMDA receptor hypofunction through synaptic trapping

Frédéric Villéga[1,2#], Alexandra Fernandes[1#], Julie Jézéquel[1#], Floriane Uyttersprot[1], Nathan Benac[1], Sarra Zenagui[1], Laurine Bastardo[1], Hélène Gréa[1], Delphine Bouchet[1], Léa Villetelle[1], Olivier Nicole[1], Véronique Rogemond[3,4], Jérôme Honnorat[3,4], Julien P. Dupuis[1*], Laurent Groc[1,5*]

[1]University of Bordeaux, CNRS, Interdisciplinary Institute for Neuroscience, IINS, UMR 5297, F-33000, Bordeaux, France
[2]Department of Pediatric Neurology, CIC-1401, University Children's Hospital of Bordeaux, Bordeaux, France.
[3]Synaptopathies and Autoantibodies Team, Institut NeuroMyoGene-MeLis, INSERM U1314, CNRS UMR 5284, Université Claude Bernard Lyon1, F-69373, Lyon, France
[4]French Reference Centre on Paraneoplastic Neurological Syndromes and Autoimmune Encephalitis, Hospices Civils de Lyon, Hôpital Neurologique Pierre Wertheimer, F-69677, Bron, France
[5]Lead contact

[#] These authors contributed equally

*Correspondence: julien.dupuis@u-bordeaux.fr (JD), laurent.groc@u-bordeaux.fr (LG)

SUMMARY

Activity-dependent modulations of N-methyl-D-aspartate glutamate receptor (NMDAR) trapping at synapses regulate excitatory neurotransmission and shape cognitive functions. While NMDAR synaptic destabilization has been associated with severe neurological and psychiatric conditions, tuning NMDAR synaptic trapping to assess its clinical relevance for the treatment of brain conditions remains a challenge. Here, we report that ketamine and other clinically-relevant NMDAR open channel blockers (OCBs) promote interactions between NMDAR and PDZ domain-containing scaffolding proteins and enhance NMDAR trapping at synapses. We further show that ketamine-elicited trapping enhancement compensates for depletion in synaptic receptors triggered by autoantibodies from patients with anti-NMDAR encephalitis. Preventing synaptic depletion mitigates impairment in NMDAR-mediated CaMKII signaling and alleviates anxiety- and sensorimotor gating-related behavioral deficits provoked by autoantibodies. Altogether, these findings reveal an unexpected dimension of OCB action and stress the potential of targeting receptor anchoring in NMDAR-related synaptopathies.

INTRODUCTION

The vast majority of fast excitatory transmission between nerve cells occurs through the synaptic release of glutamate and subsequent activation of postsynaptic ionotropic AMPA, kainate, and NMDA glutamate receptors (NMDAR). NMDAR functions encompass the regulation of neuronal migration, synaptogenesis and maturation during development, as well as the initiation of long-term synaptic plasticity and fine-tuning of brain network activities and behaviors.[1] NMDAR are tetrameric receptors incorporating two obligatory GluN1 subunits, which bind the co-agonists glycine or D-serine, and two glutamate-binding GluN2(A-D) or less commonly glycine-binding GluN3(A-B) subunits.[2] These complexes form glutamate-gated ion channels permeant to sodium, potassium and calcium contributing to post-synaptic depolarization and initiating activity-dependent changes in synapse structure and function. While NMDAR-mediated calcium influxes allow the recruitment of proteins that are essential for adaptive cellular processes,[2] an increasing corpus of studies unveils that NMDAR-dependent functions also involve mechanisms that do not require their ion channel features.[3,4] As such, non-ionotropic signaling[5,6] participates in structural plasticity, and diffusion-based surface redistributions control the amount, composition and organization of synaptic receptors and allow the recruitment of protein kinases to post-synaptic densities (PSD).[7,8] Thus, NMDAR-mediated signaling relies on a complex mosaic of ionotropic, non-ionotropic and trafficking-based processes.

Consistent with their crucial role in cell communication, NMDAR dysfunctions have been associated with some of the most devastating human pathologies, including cancer, diabetes and brain diseases. NMDAR expressed by cancer cells contribute to tumor growth and brain metastasis,[9,10] while pancreatic NMDAR on beta cells are putative targets to regulate insuline secretion.[11] In the brain, NMDAR dysfunctions have long been suspected to participate in neurological and psychiatric disorders such as Alzheimer's disease, depression, stroke, epilepsy, and schizophrenia,[1,2] based on genetic mutations found in patients and pharmacological studies showing that activating or antagonizing NMDAR can mimick core symptoms of these illnesses. However, direct evidence for a central contribution of NMDAR dysfunctions in brain disorders only recently emerged from the description of anti-NMDAR encephalitis,[12] in which patients develop autoantibodies directed against an extracellular N-terminal domain of the obligatory GluN1 subunit (NMDAR-IgG).[13] Clinically, patients suffer from cognitive deficits, major psychiatric symptoms (e.g. psychosis), seizures, abnormal movements and other clinical presentations,[14] all of which can be ameliorated through immunotherapy which allows the removal of pathogenic NMDAR-IgG and the functional resetting of synapses and neuronal network functions.[13,15-17] From a mechanistic point-of-view, NMDAR-IgG do not harm NMDAR channel properties but cause their synaptic destabilization

and disorganization at the plasma membrane.[16-19] Over time, these impairment disrupt AMPAR- and $GABA_AR$-mediated neurotransmissions, leading to an excitation/inhibition inbalance that alters network activity and promotes oscillations.[20,21] These discoveries marked a significant step forward in our understanding of the mechanisms underpinning NMDAR contributions to the etiology of brain disorders. However, despite intense efforts from academic and private actors, therapeutic attempts to counteract NMDAR dysfunction using compounds modulating NMDAR activity have yielded rather disappointing outcomes so far.[22-25]

Common explanations include the facts that targeting NMDAR channel properties often comes with major adverse effects, and NMDAR agonists and antagonists elicit a variety or responses at the synaptic, network and behavioural levels.[2] For instance, open channel blockers (OCBs) induce behavioural responses that are not observed with competitive antagonists, suggesting that they affect different dimensions of NMDAR signaling.[26] Among OCBs, ketamine has sparked sustained attention from physicians and neuroscientists over the past decades. Depending on the dose, ketamine exhibits powerful anesthetic or psychoactive properties, including an unmatched ability to alleviate the symptoms of treatment-resistant depression upon a single administration.[27] However, the molecular mechanisms supporting these therapeutic attributes remain misunderstood and appear not to rely on its pore-blocking capacities only as they cannot be replicated by other NMDAR antagonists. Recently, surface diffusion-based spatiotemporal rearrangements in the organization and trapping of NMDAR at synapses emerged as a key regulatory mechanism controlling the initiation of activity-dependent synaptic adaptations supporting cognitive functions.[7,8,28] These discoveries prompted us to investigate whether specific subclasses of NMDAR antagonists may act upon NMDAR trafficking and trapping at synapses. Here, we demonstrate that OCB binding induces conformational rearrangements promoting interactions between NMDAR and PDZ domain-containing scaffolding proteins, resulting in enhanced trapping of the receptors at synapses. Furthermore, we show that enhanced trapping elicited by OCBs compensates for depletion in synaptic receptors caused by NMDAR-IgG, thereby restoring CaMKII signaling and alleviating behavioral deficits provoked by patient autoantibodies. These data suggest that the action of OCBs on brain functions may involve the promotion of NMDAR synaptic trapping.

RESULTS

Open channel blockers enhance the synaptic trapping of NMDAR

NMDAR synaptic trapping is ensured by a complex combination of extracellular, transmembrane and cytosolic protein-protein interactions finely tuned through post-translational modifications and binding of ligands such as NMDAR agonists and co-agonists.[29] Based on these discoveries, we examined whether alike receptor activation, inhibition might impact NMDAR trapping and organization at excitatory synapses. To do so, we compared the actions of several classes of NMDAR antagonists with therapeutical interest, i.e. the competitive antagonist D-2-amino-5-phosphonovalerate (D-AP5), the glycine binding site antagonist kynurenic acid (KA), and the uncompetitive open channel blockers (OCBs) dizocilpine (MK-801), ketamine (KET) and memantine (MEM) (Figure 1A). While all of them exhibited comparable inhibition of NMDAR-mediated calcium influx in hippocampal cultured neurons (Figure S1A, B), single-particle tracking (SPT) revealed that a 1h exposure to KET and MK-801 strongly reduced the surface diffusion and enhanced the confinement of endogenous NMDAR at synapses, thereby increasing their synaptic residency time (Figure 1B-G; Figure S1C-G). Noteworthy, similar results were obtained in the presence of tetrodotoxin (TTX) following an acute (5 min) co-application of the drugs with NMDA to allow OCB action despite the absence of action potential firing (Figure 1F-H; Figure S1H-J), showing that enhanced receptor trapping does not result from a drop in network activity caused by the antagonists but arises from a direct action of the drugs on the receptors. These observations were further confirmed using photoactivated localization microscopy (PALM) to track GluN1-mEos3.2-NMDAR before and 5 min after exposure to the drugs co-applied with NMDA in the presence of TTX (Figure S2). Interestingly, MEM enhanced receptor confinement at synapses in these experimental conditions (Figure S2B, C), suggesting that it might also provoke some intermediate level of receptor trapping. Extrasynaptic receptors remained unaffected by OCBs whatever the experimental configuration (Figure S2C). We then assessed whether OCBs also affect the synaptic behavior of other transmembrane proteins. Neither the diffusion nor the residency time at excitatory synapses of EphB2 receptors (EphB2R) or voltage-gated potassium channels $K_V1.3$ were affected by prolonged exposure to KET (Figure S3A, B). Alike, the diffusion, residency time and surface explored by $\gamma2$ subunit-containing $GABA_A$ receptors at inhibitory synapses remained unaffected after acute exposure to KET co-applied with NMDA in the presence of TTX (Figure S3C-F). Together, these results demonstrate that OCBs selectively enhance the trapping of NMDAR at excitatory synapses.

Acute exposure to OCBs has a limited impact on NMDAR synaptic numbers and organization

We next assessed if enhanced receptor trapping caused by OCBs alters the amount and distribution of NMDAR at synapses. None of the drugs modified the number of dendritic spines after a 1h exposure (Figure S4A, B). Accordingly, the linear density of NMDAR clusters and their macroscopic features remained unchanged (Figure 2A, B; Figure S4C-E), suggesting that acute exposure to NMDAR antagonists does not affect the amount of receptors at synapses. Rearrangements of NMDAR synaptic organization and subsequent signaling adjustements may occur without obvious changes in the number of synaptic receptors.[8] Thus, we examined this possibility using stochastic optical reconstruction microscopy (STORM), a single-molecule localization microscopy approach that can provide the nanoscale map of surface NMDAR. Interestingly, a 1h exposure to D-AP5 caused a significant contraction and an increase in the density of synaptic NMDAR clusters and nanodomains (Figure 2C-E). This reorganization likely resulted from an inhibition of neuronal activity triggered by D-AP5, as TTX exhibited a similar action on NMDAR clusters (Figure 2D-E). On the contrary, neither KET nor MK-801 affected NMDAR synaptic cluster properties. To note, MEM did not affect the size or density of NMDAR synaptic clusters and nanodomains (Figure S4F, G). Altogether, these data indicate that short-term exposure to OCBs increase NMDAR synaptic trapping and thus prevent activity-dependent receptor reorganizations.

KET drives conformational changes in NMDAR cytosolic domains and favors synaptic trapping through enhanced interaction with PDZ domain scaffolding proteins

NMDAR trapping at excitatory synapses involves a variety of interactions with intracellular proteins.[29] Thus, we investigated whether OCBs would enhance NMDAR synaptic stabilization by modulating interactions with its cytosolic partners. For this, we used fluorescence lifetime imaging of Förster resonance energy transfer (FLIM-FRET) between GluN1 C-termini as a proxy for their conformation.[30,31] We first explored whether the binding of antagonists change the conformation of NMDAR cytosolic domains. In hippocampal neurons expressing recombinant NMDAR incorporating GFP- and mCherry-tagged GluN1 subunits (Figure 3A), we monitored evolutions in GFP lifetime before and 5 min after co-exposure to NMDA (5 µM) and antagonists as a proxy for conformational changes in the cytosolic domains of the receptors.[31,32] None of the experimental conditions affected GFP fluorescence lifetimes in NMDAR clusters expressing GluN1-GFP alone (Figure S5A, B). The co-expression of the donor (GluN1-GFP) and acceptor (GluN1-mCherry) fluorophores yielded significant FRET within dendritic spine receptor clusters in all conditions (Figure 3B, C). However, unlike D-AP5 and MEM, exposure to KET and MK-801 enhanced FRET efficiency within NMDAR clusters co-expressing GluN1-GFP and GluN1-mCherry (Figure 3B, C; Figure S5C, D). Furthermore,

incorporating a point mutation (N616A) within the binding site for KET abolished the action of the drug,[33] indicating that changes in FRET efficiency proceed from drug binding to the receptors (Figure 3D-F; Figure S5E). Together, these results indicate that the binding of KET and MK-801 drives conformational rearrangements in the cytosolic domains of NMDAR.

PDZ domain-containing scaffolding proteins of the membrane-associated guanylate kinase (MAGUK) family are central organizers of the post-synaptic density (PSD).[34] MAGUK are abundantly expressed at excitatory synapses where they contribute to stabilize NMDAR through the binding of GluN2 subunit C-terminal motifs to PDZ domains.[31,32,35] Thus, we next explored whether conformational rearrangements caused by OCBs would translate into modifications of NMDAR interactions with MAGUK. We first examined if disrupting interactions with MAGUK had any impact on OCB-elicited changes in NMDAR conformation. Infusing TAT-conjugated peptides mimicking the C-terminal sequences of GluN2B-NMDAR subunits to interfere with the binding of NMDAR to PDZ domains[8,35] prevented the ability of KET to increase FRET efficiency between GluN1-GFP and GluN1-mCherry within NMDAR clusters (Figure 4A-C; Figure S6A-C), suggesting that this mechanism requires a physical interplay with MAGUK.

We further investigated the contribution of MAGUK to drug-induced NMDAR synaptic trapping by quantifying FLIM-FRET between GluN1-GFP and mCherry-labelled PSD-95, a prototypical example of PDZ domain-containing protein providing a major contribution to NMDAR anchoring at the PSD[35] (Figure 4D). As previously reported,[32] acute exposure to NMDA decreased FRET efficiency in dendritic spine clusters co-expressing GluN1-GFP and PSD-95-mCherry, reflecting a dissociation of NMDAR/PSD-95 complexes upon receptor activation (Figure 4E, F; Figure S6D). While this decrease persisted in the presence of MEM and was partially restrained by D-AP5, co-application with KET and MK-801 prevented the action of NMDA, indicating that the binding of these drugs avoided dissociation and favored the persistence of NMDAR/PSD-95 complexes (Figure 4E, F; Figure S6D, E). Finally, we probed the role of these interactions in drug-elicited NMDAR synaptic trapping using SPT to track WT or recombinant flag-tagged GluN2A- and GluN2B-NMDAR (Figure 4G, H). While acute co-exposure to NMDA and KET in the presence of TTX enhanced the confinement and increased the residency time of WT receptors at excitatory synapses, introducing a single point mutation in GluN2A (S1462A) and GluN2B (S1480A) cytosolic domains to prevent the binding to PDZ domain-containing scaffolds occluded the action of the drug (Figure 4G, H). Together, these findings indicate that KET and MK-801 enhance the synaptic trapping of NMDAR by driving conformational rearrangements in cytosolic receptor domains that strengthen interactions with PDZ domain-scaffolding proteins.

KET prevents impairment in NMDAR synaptic anchoring and signaling caused by patient-derived anti-NMDAR antibodies

Deciphering the molecular mechanisms underlying the multiple therapeutic properties of KET is a major challenge. Building on our results, we wondered if some of these properties might result from its ability to trap NMDAR at synapses. To address this question, we took advantage of our understanding of anti-NMDAR encephalitis, a severe brain condition in which NMDAR-IgG directed against NMDAR extracellular domains cause psychotic-like manifestations and life-threatening neurological dysfunctions.[36] From a mechanistic point-of-view, NMDAR-IgG do not compromise NMDAR channel properties but disrupt protein-protein interactions between NMDAR and transmembrane partners, thereby triggering a dispersal of synaptic receptors and a hypofunction of NMDAR-mediated transmission and plasticity.[13,15,17] Thus, we explored whether synaptic anchoring promoted by KET could counteract the pathological destabilization of synaptic NMDAR caused by patient-derived NMDAR-IgG using a higher drug concentration (10 µM) that ensured rapid and efficient targeting of a large fraction of receptors. Using SPT, we first confirmed that exposure to purified NMDAR-IgG or cerebrospinal fluid (CSF) from patients with anti-NMDAR encephalitis impaired receptor trapping at excitatory synapses (Figure 5A-D; Figure S7A-C).[17] Strikingly, co-application of KET - but not D-AP5 - prevented the destabilizing action of NMDAR-IgG and favored NMDAR synaptic anchoring (Figure 5A-D; Figure S7B-D). Ensemble imaging of super-ecliptic pHluorin (SEP)-tagged GluN2A-NMDAR populations through fluorescence recovery after photo-bleaching (FRAP) further confirmed these observations and showed that while NMDAR-IgG increased the fraction of mobile receptors at synapses, exposing neurons to KET averted this deleterious action (Figure 5D, E). Noteworthy, the benzodiazepine midazolam currently used as a sedative treatment for patients with anti-NMDAR encephalitis did not replicate the compensatory action of KET, advocating for a selective operation on NMDAR (Figure S7D). This reversal likely involved drug-induced cytosolic rearrangements in the C-terminal domains of the receptors as depicted above (Figure 3) since FLIM-FRET monitoring from GluN1-GFP/GluN1-mCherry-incorporating NMDAR complexes showed that exposure to NMDAR-IgG caused an increase in the lifetime of GFP fluorescence within dendritic spine receptor clusters that was abolished by co-exposure with KET but persisted upon co-exposure with D-AP5 (Figure 5F-H; Figure S7E). At the macomolecular level, KET -unlike D-AP5- administration compensated for NMDAR-IgG-elicited impairment in the number of NMDAR-containing synapses and in the abundance of receptors within synaptic clusters without affecting the density of synapses or the properties of PSD scaffolding protein clusters (Figure 6A, B; Figure S8A-C). Altogether, these results demonstrate that enhanced synaptic trapping elicited by KET counterbalances the pathological destabilization of NMDAR caused by NMDAR-IgG.

NMDAR-IgG-induced removal of synaptic receptors results in severe hypofunction of NMDAR-mediated signalling.[37] To explore whether the stabilizing action of KET could prevent such impairment, we monitored the activity of Ca^{2+}/calmodulin-dependent protein kinase II α (CaMKIIα), one of the main downstream effectors associated with NMDAR and a central initiator of synaptic plasticity. Using the FRET-based sensor Green-Camuiα,[38] we measured intramolecular FLIM-FRET as a proxy for kinase activity (Figure 6C). Exposure to NMDAR-IgG significantly reduced the amplitude of glutamate-elicited (25 µM, 2 min) increase in mEGFP fluorescence lifetime, consistent with an autoantibody-induced hypofunction of NMDAR and CaMKIIα (Figure 6D, E). Remarkably, co-application of KET counteracted the impact of NMDAR-IgG and restored CaMKIIα activity to baseline levels, while KET alone at this concentration had no impact and co-application of D-AP5 worsened impairment in CaMKIIα activity (Figure 6D, E). Thus, enhanced synaptic trapping promoted by KET mitigates impairment in NMDAR synaptic anchoring and signaling elicited by encephalitis patient NMDAR-IgG.

KET alleviates anxiety- and sensorimotor gating-related behavioral deficits caused by patient antibodies

Building on the ability of KET to compensate for the synaptic impairment occurring upon exposure to NMDAR-IgG *in vitro*, we finally assessed if KET also displayed the ability to improve behavioral deficits caused by patient NMDAR-IgG. We developed a rat model based on a 14-days continuous delivery of NMDAR-IgG into the CSF through the subcutaneous implantation of an osmotic pump connected to a cannula unilaterally implanted in a cerebral ventricle (Figure 7A).[39] After surgery, rats were allowed to recover for a period of 10 days before undertaking a battery of behavioral assays in order to characterize potential manifestations of anhedonia (sucrose consumption), anxiety (elevated plus maze), despair (forced swim test) or evidence of locomotion (open field), memory (novel object recognition), or sensorimotor gating (prepulse inhibition) deficits (Figure 7A). Comparison with saline-exposed animals (sham) showed that infusing IgG from healthy individuals (Healthy-IgG) alone or combined with KET did not affect behavioral performances in any of the tests (Figure S9). Alike, infusing Healthy-IgG, NMDAR-IgG alone or combined with KET or CPP (an analog of D-AP5) did not substantially impact locomotor activity as illustrated by Z-scores calculated on the basis of horizontal activity and velocity in the open field test (Figure 7B-E), and none of the experimental conditions affected memory performances in the novel object recognition test either (Figure 7L).

Assessing behavioral features related to anxiety and depression, we observed that the time spent in open arms of the elevated plus maze and in the center zone of the open field were

not affected by NMDAR-IgG infused alone or together with KET or CPP (Figure 7F-H). However, rats infused with NMDAR-IgG displayed lower sucrose consumption compared to those exposed to Healthy-IgG. Strikingly, sucrose consumption in NMDAR-IgG + KET-treated and Healthy-IgG-treated rats was not different when NMDAR-IgG + CPP-treated and NMDAR-IgG-treated animals were undistinguishable, suggesting that patient NMDAR-IgG trigger manifestations of anhedonia that are compensated by KET (Figure 7I). Consistently, rats exposed to NMDAR-IgG were more immobile in the forced swim test, and this feature was alleviated both by KET and CPP (Figure 7J). Most importantly, we combined all data from sucrose consumption, forced swim, open field and elevated plus maze tests to yield a Z-score for each condition (Figure 7K). The Z-score value was significantly lower in animals exposed to NMDAR-IgG when compared to the Healthy-IgG condition, indicating that patient NMDAR-IgG favor the development of behavioral features of anxiety and depression. The NMDAR-Ig effect was fully reversed by KET, whereas NMDAR-Ig and NMDAR-Ig + CPP score values were statistically not different (Figure 7K). In addition, rats infused with NMDAR-IgG or NMDAR-IgG + CPP responded poorly to the prepulse inhibition test when compared to animals receiving Healthy-IgG or NMDAR-IgG + KET, indicative of sensorimotor gating deficits triggered by patient NMDAR-IgG that were improved by KET (Figure 7M). Collectively, these data indicate that KET alleviates anxiety- and sensorimotor gating-related behavioral deficits provoked by patient NMDAR-IgG.

DISCUSSION

NMDAR are targeted by several therapeutic drugs daily used in the clinics, ranging from general anesthetics (e.g. KET) to cognitive enhancers prescribed for the treatment of Alzheimer's disease (e.g. MEM).[2] Unfortunately, our understanding of their action mode is fragmented and deciphering whether the sedative, psychotomimetic or antidepressant properties of clinically-relevant NMDAR modulators originate from identical or distinct molecular mechanisms remains challenging. The recent repurposing of KET as an antidepressant has put the spotlight on NMDAR antagonism as a strategy for the treatment of mental illnesses. However, most attempts so far to identify better tolerated drugs sharing the beneficial properties of KET and devoid of its adverse effects have yielded disappointing outcomes, suggesting that the psychoactive actions of NMDAR antagonists do not result exclusively from modulations of channel gating and involve additional features. Recent advances in the structural biology of NMDAR provided insightful information on the binding mechanisms and conformational rearrangements of extracellular and transmembrane domains caused by OCBs.[33,40] However, the labile nature of cytosolic domains makes them less amenable to structural studies and still limits our understanding of how drug-elicited conformational rearrangements may translate into modulations of interactions with cytosolic proteins. Our comparative exploration of the impact of competitive (D-AP5), uncompetitive (KET, MK-801, MEM) and glycine site (KA) antagonists provides evidence that while all drugs efficiently block NMDAR-mediated ion fluxes, changes in the conformation of cytosolic domains selectively elicited by short-term exposures to OCBs promote interactions with PDZ domain-containing scaffolds and thereby enhance receptor trapping at synapses. Thus, the action of OCBs may encompass an unsuspected mosaic of ionotropic- and non-ionotropic processes.

How could the trapping of ionotropically-silenced NMDAR by OCBs be of any benefit to synaptic function? Activity-dependent adjustments in NMDAR synaptic trapping and organization emerge as powerful mechanisms allowing rapid adaptations of NMDAR signaling without necessary changes in synaptic receptor numbers.[4,29] Surface diffusion-based rearrangements in NMDAR localization play a major structural role in NMDAR-mediated CaMKII signaling as the physical interaction between receptors and the kinase allows its translocation and stabilization to dendritic spines, a molecular mechanism that shapes the plastic fate of synapses and allows memory formation and persistence.[41] Reciprocally, interactions with CaMKII shape the organization of NMDAR synaptic clusters, and destructuring receptor nanodomains has profound consequences on synaptic plasticity, suggesting that the nanoscale organization of CaMKII/NMDAR complexes contributes to the

spatiotemporal orchestration of biochemical reactions supporting synaptic signaling.[8,42,43] Here, we show that low doses of KET do not silence basal CaMKIIα synaptic activity but instead prevent its impairment caused by NMDAR-IgG, indicating that OCBs preserve glutamate-driven NMDAR signaling despite precluding NMDAR-mediated calcium influx. It further suggests that by maintaining the pool and nanoscale architecture of NMDAR synaptic complexes, OCBs could stabilize NMDAR signaling at synapses that are exposed to damaging stimuli. Interestingly, the ability of OCBs to favor the synaptic anchoring of membrane proteins may extend beyond NMDAR. Indeed, KET was recently reported to bind the tropomyosin receptor kinase B (TrkB), i.e. the receptor of brain-derived neurotrophic factor (BDNF), and to favour its synaptic stabilization and signaling. This allosteric facilitation of BDNF signalling involves the binding of KET to a cholesterol-sensitive domain within the receptor transmembrane segment and the formation of receptor multimers.[44] Since KET also rapidly redistributes cholesterol within the plasma membrane[45] and can modulate NMDAR *via* a hydrophobic membrane path through a gated fenestration,[46] it is plausible that KET may alter NMDAR intracellular domain conformation and synaptic trapping through cholesterol/lipid-mediated mechanisms. Though, the fact that KET did not affect the synaptic trapping and organization of K_V1.3, EphB2R or $GABA_AR$ indicates that its action is selective and not a mere change in membrane properties that would affect all membrane proteins undistinctively.

Over the past decades, substantial progress has been made in dissecting how impairment in NMDAR function may participate in the onset of brain diseases. However, endeavors aiming at rescuing these dysfunctions through pharmacological intervention on NMDAR channel gating have repeatedly failed, either because of limited efficacy or as a result of damaging adverse effects, urging the need for alternative therapeutic approaches. Accumulating evidence from pre-clinical animal models suggests that abnormalities affecting channel-unrelated features of NMDAR function may contribute to the etiology of mental and neurological illnesses. Convincing illustrations include the participation of non-ionotropic NMDAR-mediated signaling mechanisms in glutamate-elicited excitotoxicity,[47-50] the implication of aberrant NMDAR redistributions at the surface of striatal neurons in L-DOPA-induced dyskinesia and Huntington's disease,[51,52] or the description of Aβ-initiated disruption of NMDAR synaptic anchoring[53,54] and non-ionotropic NMDAR-mediated synaptic depression and dendritic spine loss in Alzheimer's disease.[55-58]

The discovery of neuropsychiatric conditions such anti-NMDAR encephalitis, in which NMDAR-IgG cause a severe hypofunction of NMDAR-mediated signaling that gives rise combination of psychiatric and neurological manifestations without altering channel gating,[19,36,59] further fed this new field of investigation. Raising the expression of transmembrane and/or cytosolic scaffolds (i.e. EphB2R, PSD-95) or administering ligands

(e.g. ephrin B2) to promote the stabilization of NMDAR have been proposed as therapeutic options to alleviate the synaptic and cognitive deficits associated with the Alzheimer's disease and anti-NMDAR encephalitis, respectively.[53,56,60] Additionnally, recent studies in genetic-, developmental- and immune-based models of psychosis suggest that manipulating NMDAR synaptic redistributions could represent a powerful strategy to counterbalance molecular deficits associated with mental disorders.[61,62] Here, we show that enhanced NMDAR synaptic trapping triggered by KET compensates for depletion in synaptic receptors and corrects signaling and behavioral deficits caused by NMDAR-IgG from patients with anti-NMDAR encephalitis. KET appears particularly efficient at alleviating behavioral features of anxiety and depression as well as sensorimotor gating deficits provoked by NMDAR-IgG. While using an antagonist to compensate for symptoms resulting from NMDAR hypofunction may sound counterintuitive, two decades of investigations have revealed that the antidepressant action of KET paradoxically relies on a wave of neural plasticity in the corticomesolimbic circuitry supporting reward and mood.[63,64] These mechanisms involve either NMDAR inhibition on principal cells or interneurons causing release of BDNF, or direct binding of the drug to TrkB, all of which elicit TrkB activation and mammalian target of rapamycin (mTOR) signaling allowing protein synthesis and synaptic adaptation.[65] Remarkably, enhanced synaptic trapping of plasticity-related receptors emerges as a common feature of several antidepressants, as the direct binding of KET and fluoxetine to TrkB or the actions of tianeptine and ketamine on AMPA glutamate receptors were both reported to promote interactions with PDZ domain-containing scaffolds and to extend the transient anchoring of these receptors at excitatory connections.[44,66-69] Thus, targeting the synaptic trapping of neurotransmitter and neurotrophin receptors appears as a promising research track to compensate for molecular impairment associated with psychiatric illnesses. While the molecules described to promote receptor anchoring so far exhibit a polypharmacological profile limiting their clinical use, developing compounds acting on synaptic trapping exclusively without harming other receptor functions or secondary targets could provide innovative therapeutic strategies for the treatment of brain disorders involving glutamatergic dysfunction.

Limits of the study

Here, we characterized OCB-elicited changes in conformation, interactions, synaptic trapping and nanoscale organization of all NMDAR without subtype-based distinction. Given the variety of composition and subsequent functions of these receptors, and considering recent reports suggesting that psychotomimetic and antidepressant properties of OCBs might result from subtype-selective targeting,[70] exploring whether OCBs preferentially affect the synaptic trapping and organization of NMDAR incorporating specific sets of GluN2 and/or GluN3 subunits will be of major interest. Furthermore, while we limited our investigations to

hippocampal pyramidal cells, repeated reports of dysfunctions affecting NMDAR expressed by interneurons in neuropsychiatric disorders and a growing body of evidence proposing them as preferential targets supporting the psychoactive properties of KET call for similar investigations on other cell types. Exploring whether specific brain areas may be more prone to OCB action will also be important step, as recent reports indicate that the antidepressant action of KET specifically involves a use-dependent trapping of KET in NMDAR in the lateral habenula.[71,72] Finally, whether magnesium - i.e. the physiological NMDAR pore blocker - shares similar properties as OCBs and acts as an endogenous regulator controlling not only channel gating but also NMDAR synaptic trapping to ensure receptor activation at right time and location is an exciting question that will need to be addressed.

ACKNOWLEDGMENTS

We thank the Bordeaux Imaging Center, a service unit of the CNRS-INSERM and Bordeaux University, member of the national infrastructure France BioImaging (ANR-10-INBS-04-01), in particular Christel Poujol, Magali Mondin, Fabrice Cordelières and Sébastien Marais. We also thank the Pole In Vivo for animal care, especially Hajer El Oussini-Ben Chaabane and Guillaume Dabee, as well as the Cell Biology Facility for managing cell biology-related activities, especially Constance Manso, Morgane Meras, Rémi Sterling, Emeline Verdier and Natacha Retailleau. We thank Paul de Koninck and Kim Doré for providing GluN1-GFP, GluN1-mCherry and PSD-95-mCherry constructs and giving us precious advice for FLIM-FRET experiments. We would like to thank Corey Butler, Adel Kechkar, Florian Levet and Jean-Baptiste Sibarita for the development of PALMTracer and SR-Tesseler analysis softwares and lab members for constructive discussions. This work was supported by the Centre National de la Recherche Scientifique, the Institut National de la Santé et de la Recherche Médicale, the University of Bordeaux, the Agence Nationale de la Recherche (ANR-19-CE16-0005 and ANR-20-CE16-0023 to J.P.D., ANR-18-RHUS-0012 to J.H. and V.R.), a NARSAD Young Investigator Grant from the Brain & Behavior Research Foundation (2019 NARSAD YIG #27942 to J.P.D.), the Bordeaux Neurocampus Seed program (TACTIK/2020 to J.P.D.), the Fondation pour la Recherche Médicale (PhD fellowship to F.V. and PhD extension grants to A.F. J.J.), the Ministère de l'Enseignement Supérieur et de la Recherche (PhD fellowships to A.F. and J.J.), the Labex Bordeaux BRAIN and IDEX Bordeaux (to L.G.), the Fondation FondaMental, the Conseil Régional d'Aquitaine, the Human Frontier Science Program (RGP0019 to L.G.), and the European Research Council Synergy grant (ENSEMBLE, #951294 to L.G.).

AUTHOR CONTRIBUTIONS

F.V., A.F., J.J., S.Z., L.B. and J.P.D. performed and analysed SPT experiments. F.V., A.F., J.J., N.B. and J.P.D. performed and analysed FLIM-FRET experiments. A.F. performed and analysed calcium imaging and spine counting experiments. FU performed and analysed PALM experiments. F.V. performed and analysed FRAP experiments. A.F. and S.Z. performed and analysed STORM experiments. A.F. and F.V. performed and analysed immunocytochemistry experiments. F.V., H.G., O.N. performed surgeries and behaviour experiments and analysis. D.B. and L.V. generated molecular biology constructs. V.R. and J.H. performed clinical assessments, purified immunoglobulins and provided patient samples. J.P.D. and L.G. acquired the funding, conceived and supervised the project, designed the experiments, and wrote the manuscript with input from co-authors.

DECLARATION OF INTERESTS

The authors declare that they have no conflict of interest.

REFERENCES

1. Paoletti, P., Bellone, C., and Zhou, Q. (2013). NMDA receptor subunit diversity: impact on receptor properties, synaptic plasticity and disease. Nat Rev Neurosci 14, 383-400. nrn3504 [pii] 10.1038/nrn3504.
2. Hansen, K.B., Wollmuth, L.P., Bowie, D., Furukawa, H., Menniti, F.S., Sobolevsky, A.I., Swanson, G.T., Swanger, S.A., Greger, I.H., Nakagawa, T., et al. (2021). Structure, Function, and Pharmacology of Glutamate Receptor Ion Channels. Pharmacol Rev 73, 298-487. 10.1124/pharmrev.120.000131.
3. Park, D.K., Stein, I.S., and Zito, K. (2022). Ion flux-independent NMDA receptor signaling. Neuropharmacology 210, 109019. 10.1016/j.neuropharm.2022.109019.
4. Dore, K., Stein, I.S., Brock, J.A., Castillo, P.E., Zito, K., and Sjostrom, P.J. (2017). Unconventional NMDA Receptor Signaling. J Neurosci 37, 10800-10807. 10.1523/JNEUROSCI.1825-17.2017.
5. Stein, I.S., Gray, J.A., and Zito, K. (2015). Non-Ionotropic NMDA Receptor Signaling Drives Activity-Induced Dendritic Spine Shrinkage. J Neurosci 35, 12303-12308. 10.1523/JNEUROSCI.4289-14.2015.
6. Stein, I.S., Park, D.K., Claiborne, N., and Zito, K. (2021). Non-ionotropic NMDA receptor signaling gates bidirectional structural plasticity of dendritic spines. Cell Rep 34, 108664. 10.1016/j.celrep.2020.108664.
7. Dupuis, J.P., Ladepeche, L., Seth, H., Bard, L., Varela, J., Mikasova, L., Bouchet, D., Rogemond, V., Honnorat, J., Hanse, E., and Groc, L. (2014). Surface dynamics of GluN2B-NMDA receptors controls plasticity of maturing glutamate synapses. EMBO J 33, 842-861. embj.201386356 [pii]10.1002/embj.201386356.
8. Kellermayer, B., Ferreira, J.S., Dupuis, J., Levet, F., Grillo-Bosch, D., Bard, L., Linares-Loyez, J., Bouchet, D., Choquet, D., Rusakov, D.A., et al. (2018). Differential Nanoscale Topography and Functional Role of GluN2-NMDA Receptor Subtypes at Glutamatergic Synapses. Neuron 100, 106-119 e107. 10.1016/j.neuron.2018.09.012.
9. Li, L., and Hanahan, D. (2013). Hijacking the neuronal NMDAR signaling circuit to promote tumor growth and invasion. Cell 153, 86-100. 10.1016/j.cell.2013.02.051.
10. Zeng, Q., Michael, I.P., Zhang, P., Saghafinia, S., Knott, G., Jiao, W., McCabe, B.D., Galvan, J.A., Robinson, H.P.C., Zlobec, I., et al. (2019). Synaptic proximity enables NMDAR signalling to promote brain metastasis. Nature 573, 526-531. 10.1038/s41586-019-1576-6.
11. Marquard, J., Otter, S., Welters, A., Stirban, A., Fischer, A., Eglinger, J., Herebian, D., Kletke, O., Klemen, M.S., Stozer, A., et al. (2015). Characterization of pancreatic NMDA receptors as possible drug targets for diabetes treatment. Nat Med 21, 363-372. 10.1038/nm.3822.
12. Dalmau, J., and Graus, F. (2018). Antibody-Mediated Encephalitis. N Engl J Med 378, 840-851. 10.1056/NEJMra1708712.
13. Hughes, E.G., Peng, X., Gleichman, A.J., Lai, M., Zhou, L., Tsou, R., Parsons, T.D., Lynch, D.R., Dalmau, J., and Balice-Gordon, R.J. (2010). Cellular and synaptic mechanisms of anti-NMDA receptor encephalitis. J Neurosci 30, 5866-5875. 30/17/5866 10.1523/JNEUROSCI.0167-10.2010.
14. Dalmau, J., Armangue, T., Planaguma, J., Radosevic, M., Mannara, F., Leypoldt, F., Geis, C., Lancaster, E., Titulaer, M.J., Rosenfeld, M.R., and Graus, F. (2019). An update on anti-NMDA receptor encephalitis for neurologists and psychiatrists: mechanisms and models. Lancet Neurol 18, 1045-1057. 10.1016/S1474-4422(19)30244-3.

15. Gleichman, A.J., Spruce, L.A., Dalmau, J., Seeholzer, S.H., and Lynch, D.R. (2012). Anti-NMDA receptor encephalitis antibody binding is dependent on amino acid identity of a small region within the GluN1 amino terminal domain. J Neurosci 32, 11082-11094. 32/32/11082 10.1523/JNEUROSCI.0064-12.2012.
16. Ladepeche, L., Planaguma, J., Thakur, S., Suarez, I., Hara, M., Borbely, J.S., Sandoval, A., Laparra-Cuervo, L., Dalmau, J., and Lakadamyali, M. (2018). NMDA Receptor Autoantibodies in Autoimmune Encephalitis Cause a Subunit-Specific Nanoscale Redistribution of NMDA Receptors. Cell Rep 23, 3759-3768. 10.1016/j.celrep.2018.05.096.
17. Mikasova, L., De Rossi, P., Bouchet, D., Georges, F., Rogemond, V., Didelot, A., Meissirel, C., Honnorat, J., and Groc, L. (2012). Disrupted surface cross-talk between NMDA and Ephrin-B2 receptors in anti-NMDA encephalitis. Brain 135, 1606-1621. aws092 10.1093/brain/aws092.
18. Dean, C.A., Metzbower, S.R., Dessain, S.K., Blanpied, T.A., and Benavides, D.R. (2022). Regulation of NMDA Receptor Signaling at Single Synapses by Human Anti-NMDA Receptor Antibodies. Front Mol Neurosci 15, 940005. 10.3389/fnmol.2022.940005.
19. Jezequel, J., Johansson, E.M., Dupuis, J.P., Rogemond, V., Grea, H., Kellermayer, B., Hamdani, N., Le Guen, E., Rabu, C., Lepleux, M., et al. (2017). Dynamic disorganization of synaptic NMDA receptors triggered by autoantibodies from psychotic patients. Nat Commun 8, 1791. 10.1038/s41467-017-01700-3.
20. Ceanga, M., Rahmati, V., Haselmann, H., Schmidl, L., Hunter, D., Brauer, A.K., Liebscher, S., Kreye, J., Pruss, H., Groc, L., et al. (2023). Human NMDAR autoantibodies disrupt excitatory-inhibitory balance, leading to hippocampal network hypersynchrony. Cell Rep 42, 113166. 10.1016/j.celrep.2023.113166.
21. Hunter, D., Petit-Pedrol, M., Fernandes, D., Benac, N., Rodrigues, C., Kreye, J., Ceanga, M., Pruss, H., Geis, C., and Groc, L. (2024). Converging synaptic and network dysfunctions in distinct autoimmune encephalitis. EMBO Rep 25, 1623-1649. 10.1038/s44319-024-00056-2.
22. Lipton, S.A. (2006). Paradigm shift in neuroprotection by NMDA receptor blockade: memantine and beyond. Nat Rev Drug Discov 5, 160-170. 10.1038/nrd1958.
23. Murrough, J.W., Abdallah, C.G., and Mathew, S.J. (2017). Targeting glutamate signalling in depression: progress and prospects. Nat Rev Drug Discov 16, 472-486. 10.1038/nrd.2017.16.
24. Millan, M.J., Andrieux, A., Bartzokis, G., Cadenhead, K., Dazzan, P., Fusar-Poli, P., Gallinat, J., Giedd, J., Grayson, D.R., Heinrichs, M., et al. (2016). Altering the course of schizophrenia: progress and perspectives. Nat Rev Drug Discov 15, 485-515. 10.1038/nrd.2016.28.
25. Zhang, W., Ross, P.J., Ellis, J., and Salter, M.W. (2022). Targeting NMDA receptors in neuropsychiatric disorders by drug screening on human neurons derived from pluripotent stem cells. Transl Psychiatry 12, 243. 10.1038/s41398-022-02010-z.
26. Cadinu, D., Grayson, B., Podda, G., Harte, M.K., Doostdar, N., and Neill, J.C. (2018). NMDA receptor antagonist rodent models for cognition in schizophrenia and identification of novel drug treatments, an update. Neuropharmacology 142, 41-62. 10.1016/j.neuropharm.2017.11.045.
27. Krystal, J.H., Abdallah, C.G., Sanacora, G., Charney, D.S., and Duman, R.S. (2019). Ketamine: A Paradigm Shift for Depression Research and Treatment. Neuron 101, 774-778. 10.1016/j.neuron.2019.02.005.
28. Potier, M., Georges, F., Brayda-Bruno, L., Ladépêche, L., Lamothe, V., Abed, S.A., Groc, L., and Marighetto, A. (2015). Temporal memory and its enhancement by estradiol

requires surface dynamics of hippocampal CA1 NMDA receptors. Biological Psychiatry 488, 1-12. 10.1016/j.biopsych.2015.07.017.
29. Dupuis, J.P., Nicole, O., and Groc, L. (2023). NMDA receptor functions in health and disease: Old actor, new dimensions. Neuron. 10.1016/j.neuron.2023.05.002.
30. Dore, K., Aow, J., and Malinow, R. (2015). Agonist binding to the NMDA receptor drives movement of its cytoplasmic domain without ion flow. Proc Natl Acad Sci U S A 112, 14705-14710. 10.1073/pnas.1520023112.
31. Ferreira, J.S., Papouin, T., Ladepeche, L., Yao, A., Langlais, V.C., Bouchet, D., Dulong, J., Mothet, J.P., Sacchi, S., Pollegioni, L., et al. (2017). Co-agonists differentially tune GluN2B-NMDA receptor trafficking at hippocampal synapses. Elife 6. 10.7554/eLife.25492.
32. Dore, K., Labrecque, S., Tardif, C., and De Koninck, P. (2014). FRET-FLIM investigation of PSD95-NMDA receptor interaction in dendritic spines; control by calpain, CaMKII and Src family kinase. PLoS One 9, e112170. 10.1371/journal.pone.0112170.
33. Zhang, Y., Ye, F., Zhang, T., Lv, S., Zhou, L., Du, D., Lin, H., Guo, F., Luo, C., and Zhu, S. (2021). Structural basis of ketamine action on human NMDA receptors. Nature 596, 301-305. 10.1038/s41586-021-03769-9.
34. Elias, G.M., and Nicoll, R.A. (2007). Synaptic trafficking of glutamate receptors by MAGUK scaffolding proteins. Trends Cell Biol 17, 343-352.
35. Bard, L., Sainlos, M., Bouchet, D., Cousins, S., Mikasova, L., Breillat, C., Stephenson, F.A., Imperiali, B., Choquet, D., and Groc, L. (2010). Dynamic and specific interaction between synaptic NR2-NMDA receptor and PDZ proteins. Proc Natl Acad Sci U S A 107, 19561-19566. 1002690107 10.1073/pnas.1002690107.
36. Dalmau, J., Geis, C., and Graus, F. (2017). Autoantibodies to Synaptic Receptors and Neuronal Cell Surface Proteins in Autoimmune Diseases of the Central Nervous System. Physiol Rev 97, 839-887. 10.1152/physrev.00010.2016.
37. Wollmuth, L.P., Chan, K., and Groc, L. (2021). The diverse and complex modes of action of anti-NMDA receptor autoantibodies. Neuropharmacology 194, 108624. 10.1016/j.neuropharm.2021.108624.
38. Lee, S.J., Escobedo-Lozoya, Y., Szatmari, E.M., and Yasuda, R. (2009). Activation of CaMKII in single dendritic spines during long-term potentiation. Nature 458, 299-304. 10.1038/nature07842.
39. Planaguma, J., Leypoldt, F., Mannara, F., Gutierrez-Cuesta, J., Martin-Garcia, E., Aguilar, E., Titulaer, M.J., Petit-Pedrol, M., Jain, A., Balice-Gordon, R., et al. (2015). Human N-methyl D-aspartate receptor antibodies alter memory and behaviour in mice. Brain 138, 94-109. 10.1093/brain/awu310.
40. Song, X., Jensen, M.O., Jogini, V., Stein, R.A., Lee, C.H., McHaourab, H.S., Shaw, D.E., and Gouaux, E. (2018). Mechanism of NMDA receptor channel block by MK-801 and memantine. Nature 556, 515-519. 10.1038/s41586-018-0039-9.
41. Yasuda, R., Hayashi, Y., and Hell, J.W. (2022). CaMKII: a central molecular organizer of synaptic plasticity, learning and memory. Nat Rev Neurosci 23, 666-682. 10.1038/s41583-022-00624-2.
42. Ferreira, J.S., Dupuis, J.P., Kellermayer, B., Benac, N., Manso, C., Bouchet, D., Levet, F., Butler, C., Sibarita, J.B., and Groc, L. (2020). Distance-dependent regulation of NMDAR nanoscale organization along hippocampal neuron dendrites. Proc Natl Acad Sci U S A 117, 24526-24533. 10.1073/pnas.1922477117.
43. Hosokawa, T., Liu, P.W., Cai, Q., Ferreira, J.S., Levet, F., Butler, C., Sibarita, J.B., Choquet, D., Groc, L., Hosy, E., et al. (2021). CaMKII activation persistently segregates

postsynaptic proteins via liquid phase separation. Nat Neurosci 24, 777-785. 10.1038/s41593-021-00843-3.
44. Casarotto, P.C., Girych, M., Fred, S.M., Kovaleva, V., Moliner, R., Enkavi, G., Biojone, C., Cannarozzo, C., Sahu, M.P., Kaurinkoski, K., et al. (2021). Antidepressant drugs act by directly binding to TRKB neurotrophin receptors. Cell 184, 1299-1313 e1219. 10.1016/j.cell.2021.01.034.
45. Lasic, E., Lisjak, M., Horvat, A., Bozic, M., Sakanovic, A., Anderluh, G., Verkhratsky, A., Vardjan, N., Jorgacevski, J., Stenovec, M., and Zorec, R. (2019). Astrocyte Specific Remodeling of Plasmalemmal Cholesterol Composition by Ketamine Indicates a New Mechanism of Antidepressant Action. Sci Rep 9, 10957. 10.1038/s41598-019-47459-z.
46. Wilcox, M.R., Nigam, A., Glasgow, N.G., Narangoda, C., Phillips, M.B., Patel, D.S., Mesbahi-Vasey, S., Turcu, A.L., Vazquez, S., Kurnikova, M.G., and Johnson, J.W. (2022). Inhibition of NMDA receptors through a membrane-to-channel path. Nat Commun 13, 4114. 10.1038/s41467-022-31817-z.
47. Thompson, R.J., Jackson, M.F., Olah, M.E., Rungta, R.L., Hines, D.J., Beazely, M.A., MacDonald, J.F., and MacVicar, B.A. (2008). Activation of pannexin-1 hemichannels augments aberrant bursting in the hippocampus. Science 322, 1555-1559. 10.1126/science.1165209.
48. Weilinger, N.L., Lohman, A.W., Rakai, B.D., Ma, E.M., Bialecki, J., Maslieieva, V., Rilea, T., Bandet, M.V., Ikuta, N.T., Scott, L., et al. (2016). Metabotropic NMDA receptor signaling couples Src family kinases to pannexin-1 during excitotoxicity. Nat Neurosci 19, 432-442. 10.1038/nn.4236.
49. Yan, J., Bengtson, C.P., Buchthal, B., Hagenston, A.M., and Bading, H. (2020). Coupling of NMDA receptors and TRPM4 guides discovery of unconventional neuroprotectants. Science 370. 10.1126/science.aay3302.
50. Zong, P., Feng, J., Yue, Z., Li, Y., Wu, G., Sun, B., He, Y., Miller, B., Yu, A.S., Su, Z., et al. (2022). Functional coupling of TRPM2 and extrasynaptic NMDAR exacerbates excitotoxicity in ischemic brain injury. Neuron 110, 1944-1958 e1948. 10.1016/j.neuron.2022.03.021.
51. Gardoni, F., Picconi, B., Ghiglieri, V., Polli, F., Bagetta, V., Bernardi, G., Cattabeni, F., Di Luca, M., and Calabresi, P. (2006). A critical interaction between NR2B and MAGUK in L-DOPA induced dyskinesia. J Neurosci 26, 2914-2922.
52. Milnerwood, A.J., Gladding, C.M., Pouladi, M.A., Kaufman, A.M., Hines, R.M., Boyd, J.D., Ko, R.W., Vasuta, O.C., Graham, R.K., Hayden, M.R., et al. (2010). Early increase in extrasynaptic NMDA receptor signaling and expression contributes to phenotype onset in Huntington's disease mice. Neuron 65, 178-190. 10.1016/j.neuron.2010.01.008.
53. Cisse, M., Halabisky, B., Harris, J., Devidze, N., Dubal, D.B., Sun, B., Orr, A., Lotz, G., Kim, D.H., Hamto, P., et al. (2011). Reversing EphB2 depletion rescues cognitive functions in Alzheimer model. Nature 469, 47-52. 10.1038/nature09635.
54. Lacor, P.N., Buniel, M.C., Furlow, P.W., Clemente, A.S., Velasco, P.T., Wood, M., Viola, K.L., and Klein, W.L. (2007). Abeta oligomer-induced aberrations in synapse composition, shape, and density provide a molecular basis for loss of connectivity in Alzheimer's disease. J Neurosci 27, 796-807. 10.1523/JNEUROSCI.3501-06.2007.
55. Birnbaum, J.H., Bali, J., Rajendran, L., Nitsch, R.M., and Tackenberg, C. (2015). Calcium flux-independent NMDA receptor activity is required for Abeta oligomer-induced synaptic loss. Cell Death Dis 6, e1791. 10.1038/cddis.2015.160.

56. Dore, K., Carrico, Z., Alfonso, S., Marino, M., Koymans, K., Kessels, H.W., and Malinow, R. (2021). PSD-95 protects synapses from beta-amyloid. Cell Rep 35, 109194. 10.1016/j.celrep.2021.109194.
57. Kessels, H.W., Nabavi, S., and Malinow, R. (2013). Metabotropic NMDA receptor function is required for beta-amyloid-induced synaptic depression. Proc Natl Acad Sci U S A 110, 4033-4038. 1219605110. 10.1073/pnas.1219605110.
58. Tamburri, A., Dudilot, A., Licea, S., Bourgeois, C., and Boehm, J. (2013). NMDA-receptor activation but not ion flux is required for amyloid-beta induced synaptic depression. PLoS One 8, e65350. 10.1371/journal.pone.0065350.
59. Jezequel, J., Lepleux, M., Kahn, R.S., Honnorat, J., Leboyer, M., and Groc, L. (2018). Am J Psychiatry In Press.
60. Planaguma, J., Haselmann, H., Mannara, F., Petit-Pedrol, M., Grunewald, B., Aguilar, E., Ropke, L., Martin-Garcia, E., Titulaer, M.J., Jercog, P., et al. (2016). Ephrin-B2 prevents N-methyl-D-aspartate receptor antibody effects on memory and neuroplasticity. Ann Neurol. 10.1002/ana.24721.
61. Espana, A., Seth, H., Jezequel, J., Huang, T., Bouchet, D., Lepleux, M., Grea, H., Bechter, K., Schneider, M., Hanse, E., and Groc, L. (2021). Alteration of NMDA receptor trafficking as a cellular hallmark of psychosis. Transl Psychiatry 11, 444. 10.1038/s41398-021-01549-7.
62. Johansson, E.M., Bouchet, D., Tamouza, R., Ellul, P., Morr, A.S., Avignone, E., Germi, R., Leboyer, M., Perron, H., and Groc, L. (2020). Human endogenous retroviral protein triggers deficit in glutamate synapse maturation and behaviors associated with psychosis. Sci Adv 6, eabc0708. 10.1126/sciadv.abc0708.
63. Duman, R.S., Aghajanian, G.K., Sanacora, G., and Krystal, J.H. (2016). Synaptic plasticity and depression: new insights from stress and rapid-acting antidepressants. Nat Med 22, 238-249. 10.1038/nm.4050.
64. Gould, T.D., Zarate, C.A., Jr., and Thompson, S.M. (2019). Molecular Pharmacology and Neurobiology of Rapid-Acting Antidepressants. Annu Rev Pharmacol Toxicol 59, 213-236. 10.1146/annurev-pharmtox-010617-052811.
65. Castren, E., and Monteggia, L.M. (2021). Brain-Derived Neurotrophic Factor Signaling in Depression and Antidepressant Action. Biol Psychiatry 90, 128-136. 10.1016/j.biopsych.2021.05.008.
66. Moliner, R., Girych, M., Brunello, C.A., Kovaleva, V., Biojone, C., Enkavi, G., Antenucci, L., Kot, E.F., Goncharuk, S.A., Kaurinkoski, K., et al. (2023). Psychedelics promote plasticity by directly binding to BDNF receptor TrkB. Nat Neurosci 26, 1032-1041. 10.1038/s41593-023-01316-5.
67. Zhang, H., Etherington, L.A., Hafner, A.S., Belelli, D., Coussen, F., Delagrange, P., Chaouloff, F., Spedding, M., Lambert, J.J., Choquet, D., and Groc, L. (2012). Regulation of AMPA receptor surface trafficking and synaptic plasticity by a cognitive enhancer and antidepressant molecule. Mol Psychiatry. mp201280 10.1038/mp.2012.80.
68. Fred, S.M., Moliner, R., Antila, H., Engelhardt, K.A., Schluter, O.M., Casarotto, P.C., and Castren, E. (2023). TRKB interaction with PSD95 is associated with latency of fluoxetine and 2R,6R-hydroxynorketamine. Eur J Neurosci 57, 1215-1224. 10.1111/ejn.15952.
69. Xue, S.G., He, J.G., Lu, L.L., Song, S.J., Chen, M.M., Wang, F., and Chen, J.G. (2023). Enhanced TARP-gamma8-PSD-95 coupling in excitatory neurons contributes to the rapid antidepressant-like action of ketamine in male mice. Nat Commun 14, 7971. 10.1038/s41467-023-42780-8.

70. Su, T., Lu, Y., Fu, C., Geng, Y., and Chen, Y. (2023). GluN2A mediates ketamine-induced rapid antidepressant-like responses. Nat. Neurosci. 26, 1751-1761. 10.1038/s41593-023-01436-y.
71. Ma, S., Chen, M., Jiang, Y., Xiang, X., Wang, S., Wu, Z., Li, S., Cui, Y., Wang, J., Zhu, Y., et al. (2023). Sustained antidepressant effect of ketamine through NMDAR trapping in the LHb. Nature 622, 802-809. 10.1038/s41586-023-06624-1.
72. Yang, Y., Cui, Y., Sang, K., Dong, Y., Ni, Z., Ma, S., and Hu, H. (2018). Ketamine blocks bursting in the lateral habenula to rapidly relieve depression. Nature 554, 317-322. 10.1038/nature25509.
73. Viaccoz, A., Desestret, V., Ducray, F., Picard, G., Cavillon, G., Rogemond, V., Antoine, J.C., Delattre, J.Y., and Honnorat, J. (2014). Clinical specificities of adult male patients with NMDA receptor antibodies encephalitis. Neurology 82, 556-563. WNL.0000000000000126 10.1212/WNL.0000000000000126.
74. Kaech, S., and Banker, G. (2006). Culturing hippocampal neurons. Nat Protoc 1, 2406-2415. 10.1038/nprot.2006.356.
75. Guilloux, J.P., Seney, M., Edgar, N., and Sibille, E. (2011). Integrated behavioral z-scoring increases the sensitivity and reliability of behavioral phenotyping in mice: relevance to emotionality and sex. J Neurosci Methods 197, 21-31. 10.1016/j.jneumeth.2011.01.019.
76. Heilemann, M., van de Linde, S., Schuttpelz, M., Kasper, R., Seefeldt, B., Mukherjee, A., Tinnefeld, P., and Sauer, M. (2008). Subdiffraction-resolution fluorescence imaging with conventional fluorescent probes. Angew Chem Int Ed Engl 47, 6172-6176. 10.1002/anie.200802376.
77. Kechkar, A., Nair, D., Heilemann, M., Choquet, D., and Sibarita, J.B. (2013). Real-time analysis and visualization for single-molecule based super-resolution microscopy. PLoS One 8, e62918. 10.1371/journal.pone.0062918.
78. Levet, F., Hosy, E., Kechkar, A., Butler, C., Beghin, A., Choquet, D., and Sibarita, J.B. (2015). SR-Tesseler: a method to segment and quantify localization-based super-resolution microscopy data. Nat Methods 12, 1065-1071. 10.1038/nmeth.3579.
79. Aow, J., Dore, K., and Malinow, R. (2015). Conformational signaling required for synaptic plasticity by the NMDA receptor complex. Proc Natl Acad Sci U S A 112, 14711-14716. 10.1073/pnas.1520029112.
80. Mannara, F., Radosevic, M., Planaguma, J., Soto, D., Aguilar, E., Garcia-Serra, A., Maudes, E., Pedreno, M., Paul, S., Doherty, J., et al. (2020). Allosteric modulation of NMDA receptors prevents the antibody effects of patients with anti-NMDAR encephalitis. Brain 143, 2709-2720. 10.1093/brain/awaa195.

Figure 1

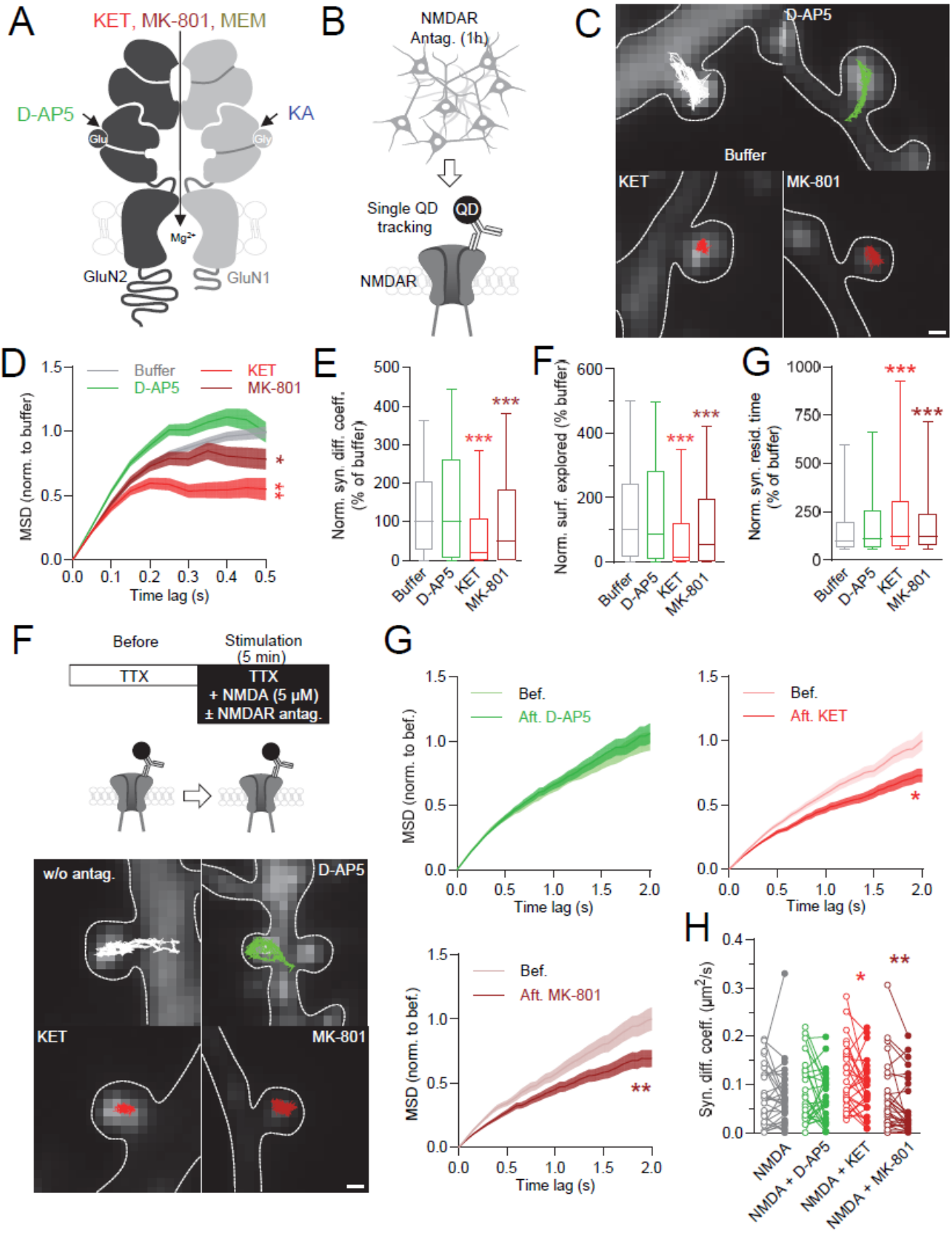
A
KET, MK-801, MEM
D-AP5
KA
Glu
Gly
Mg2+
GluN2
GluN1
B
NMDAR
Antag. (1h)
Single QD
tracking
QD
NMDAR
C
D-AP5
Buffer
KET
MK-801
D
Buffer
D-AP5
KET
MK-801
MSD (norm. to buffer)
Time lag (s)
E
Norm. syn. diff. coeff.
(% of buffer)
F
Norm. surf. explored (% buffer)
G
Norm. syn. resid. time
(% of buffer)
F
Before
Stimulation
(5 min)
TTX
TTX
+ NMDA (5 µM)
± NMDAR antag.
w/o antag.
D-AP5
KET
MK-801
G
Bef.
Aft. D-AP5
Aft. KET
Aft. MK-801
MSD (norm. to bef.)
Time lag (s)
H
Syn. diff. coeff. (µm²/s)
NMDA
NMDA + D-AP5
NMDA + KET
NMDA + MK-801

Figure 1. OCBs enhance the synaptic trapping of NMDAR

(A) Schematic representation of a GluN1/GluN2 NMDAR complex displaying the sites of action of the competitive antagonist D-2-amino-5-phosphonovalerate (D-AP5), the glycine binding site antagonist kynurenic acid (KA), and the uncompetitive open channel blockers ketamine (KET), dizocilpine (MK-801) and memantine (MEM).

(B-C) Experimental principle (B) and epifluorescence images of dendritic segments expressing Homer1c-dsRed (grey) as a synaptic marker with representative trajectories (25 s, 20 Hz acquisition rate) of endogenous quantum dot (QD)-labelled synaptic NMDAR exposed to buffer, D-AP5 (50 µM), KET (1 µM), or MK-801 (20 µM) for 1h. Scale bar, 500 nm.

(D) Normalized mean squared displacement (MSD) over time of synaptic NMDAR after 1h exposure to buffer (grey; n = 2,580 trajectories), D-AP5 (green; n = 1,010), KET (red; n = 441), or MK-801 (wine; n = 585). Kolmogorov-Smirnov test, *p<0.05, **p<0.01.

(E) Normalized instantaneous diffusion coefficients of synaptic NMDAR after 1h exposure to buffer (n = 2,631 trajectories), D-AP5 (n = 918), KET (n = 546), or MK-801 (n = 594). Data expressed as median ± 25-75% IQR (box) and 10-90% percentile (whiskers). Kruskal-Wallis followed by Dunn's multiple comparison test, ***p<0.001.

(F) Normalized surface explored by synaptic NMDAR over 100 ms after 1h exposure to buffer (n = 1,223 trajectories), D-AP5 (n = 491), KET (n = 205), or MK-801 (n = 296). Data expressed as median ± 25-75% IQR (box) and 10-90% percentile (whiskers). Kruskal-Wallis followed by Dunn's multiple comparison test, ***p<0.001.

(G) Normalized synaptic residency time of NMDAR after 1h exposure to buffer (n = 2,304 trajectories), D-AP5 (n = 1,321), KET (n = 735), or MK-801 (n = 861). Data expressed as median ± 25-75% IQR (box) and 10-90% percentile (whiskers). Kruskal-Wallis followed by Dunn's multiple comparison test, ***p<0.001.

(F) Experimental principle (top) and epifluorescence images of dendritic segments expressing Homer1c-dsRed (grey) as a synaptic marker with representative trajectories of endogenous QD-labelled synaptic NMDAR after exposure to buffer or NMDA (5 µM) combined with D-AP5 (50 µM), KET (1 µM) or MK-801 (20 µM) in the presence of TTX (1 µM). Scale bar, 500 nm.

(G) Normalized MSD over time of NMDAR before and after exposure to NMDA combined with D-AP5 (before, n = 580 trajectories; after, n = 597 trajectories), KET (before, n = 464; after, n = 459) or MK-801 (before, n = 410; after, n = 433) in the presence of TTX. Kolmogorov-Smirnov test, *p<0.05, **p<0.01.

(H) Instantaneous diffusion coefficients of synaptic NMDAR before and after exposure to NMDA alone (n = 29 cells) or combined with D-AP5 (n = 28), KET (n = 28) or MK-801 (n = 30) in the presence of TTX. Each dot represents the median diffusion coefficient for one cell, before and after treatment. Paired t-test, *p<0.05, **p<0.01.

Figure 2

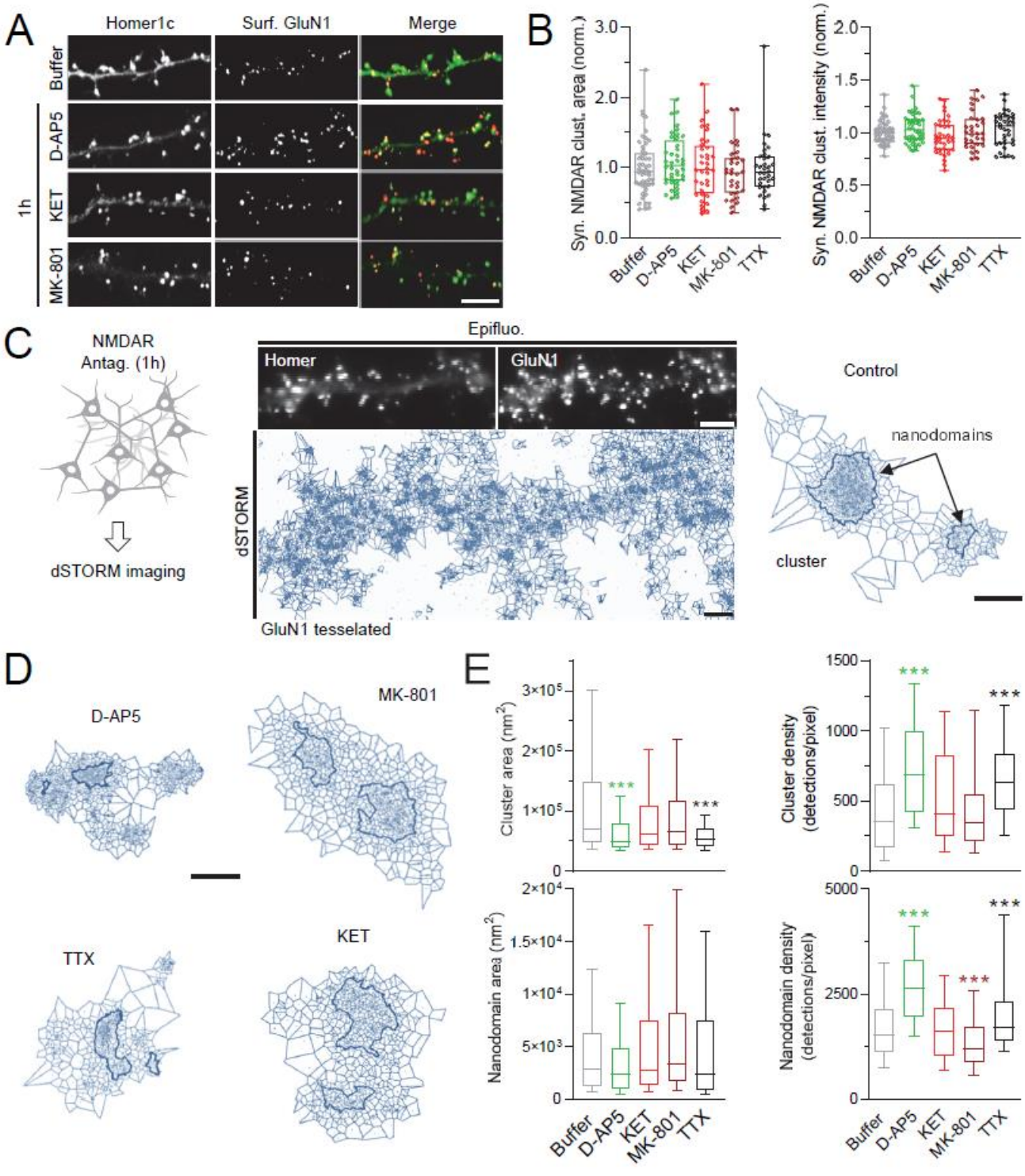
A
Homer1c
Surf. GluN1
Merge
Buffer
1h
D-AP5
KET
MK-801
B
Syn. NMDAR clust. area (norm.)
Syn. NMDAR clust. intensity (norm.)
Buffer
D-AP5
KET
MK-801
TTX
C
NMDAR
Antag. (1h)
dSTORM imaging
Epifluo.
Homer
GluN1
dSTORM
GluN1 tesselated
Control
nanodomains
cluster
D
D-AP5
MK-801
TTX
KET
E
Cluster area (nm²)
Nanodomain area (nm²)
Cluster density (detections/pixel)
Nanodomain density (detections/pixel)
***

Figure 2. Acute exposure to OCBs has a limited impact on NMDAR synaptic numbers and organization

(A) Hippocampal neurons immunostained for Homer1c-GFP (green) and flag-GluN1-NMDAR (red) after 1h exposure to buffer, D-AP5 (50 µM), KET (1 µM) or MK-801 (20 µM). Scale bar, 5 µm.

(B) Synaptic NMDAR cluster area (left) and intensity (right) after exposure to buffer (n = 50 cells), D-AP5 (n = 40), KET (n = 36), MK-801 (n = 31) or TTX (n = 41). Data expressed as median ± 25-75% IQR (box) and min to max (whiskers). Each dot represents the mean synaptic NMDAR cluster area (left) and intensity (right) for one cell, respectively.

(C) Left panel, experimental principle. Mid panel, dendritic segment with Homer1c-GFP (upper left) and flag-GluN1 (upper right), and tesselated super-resolved image of flag-GluN1 detections in dSTORM (lower panel). Scale bars, upper panels, 5 µm; lower panel, 2 µm. Right panel, a tesselated super-resolved GluN1-NMDAR cluster after exposure to buffer. Each dot represents a detection and thick outlines indicate intra-cluster nanodomains of receptors. Scale bar, 100 nm.

(D) Tesselated super-resolved GluN1-NMDAR clusters after exposure to D-AP5, KET, MK-801 or TTX. Scale bar, 100 nm.

(E) Upper panels, area (left) and density (right) of GluN1-NMDAR clusters after exposure to buffer (n = 181 clusters), D-AP5 (n = 79), KET (n = 179), MK-801 (n = 113) or TTX (n = 139). Lower panels, area (left) and density (right) of GluN1-NMDAR nanodomains after exposure to buffer (n = 561 nanodomains), D-AP5 (n = 222), KET (n = 522), MK-801 (n = 327) or TTX (n = 330). Data expressed as median ± 25-75% IQR (box) and 10-90% percentile (whiskers). Kruskal-Wallis followed by Dunn's multiple comparison test, ***p<0.001.

Figure 3

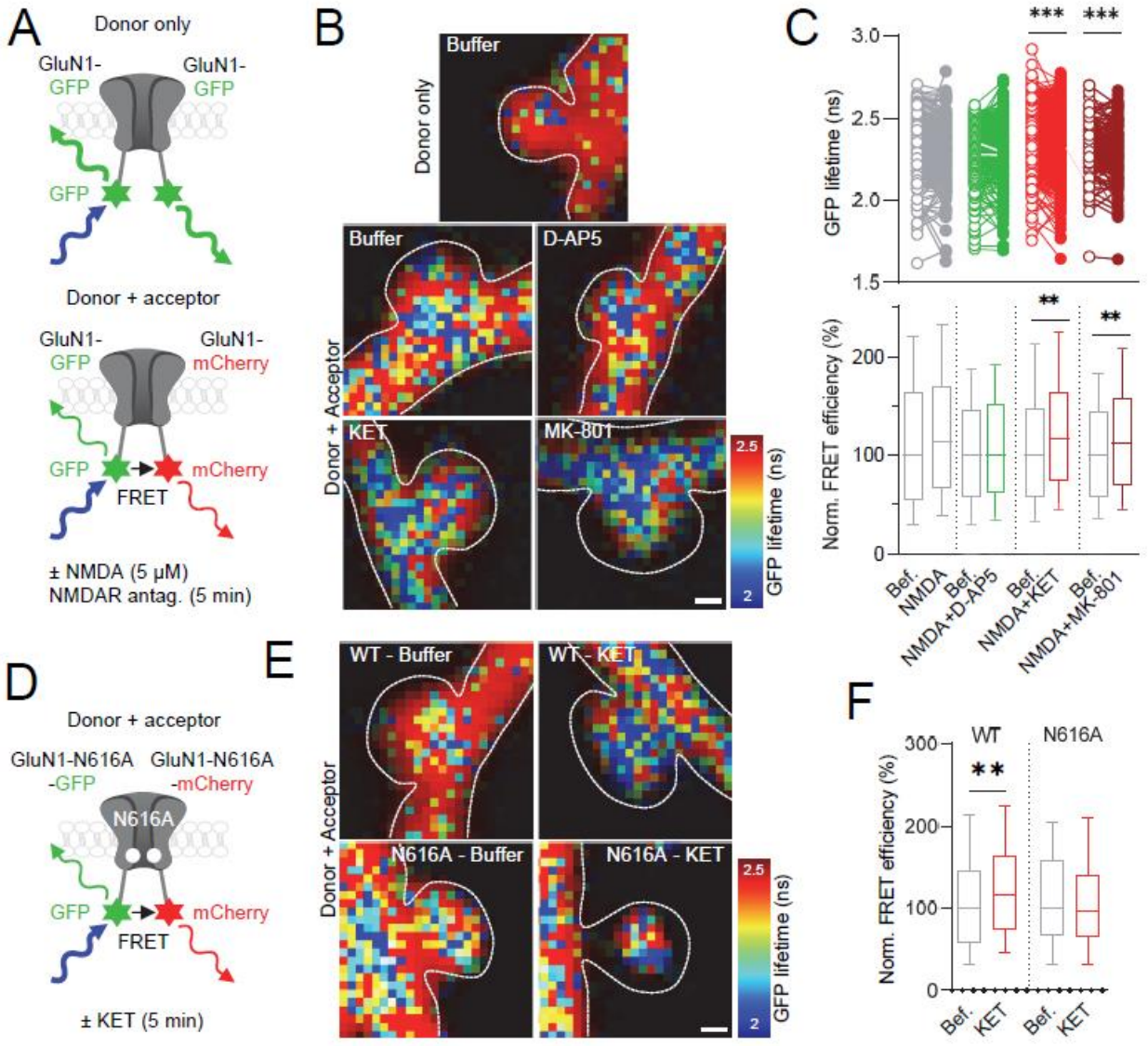
A
Donor only
GluN1-GFP
GluN1-GFP
GFP
Donor + acceptor
GluN1-GFP
GluN1-mCherry
GFP
mCherry
FRET
± NMDA (5 µM)
NMDAR antag. (5 min)
B
Donor only
Buffer
Donor + Acceptor
Buffer
D-AP5
KET
MK-801
2.5
2
GFP lifetime (ns)
C
***
***
GFP lifetime (ns)
3.0
2.5
2.0
1.5
**
**
Norm. FRET efficiency (%)
200
100
0
Bef.
NMDA
Bef.
NMDA+D-AP5
Bef.
NMDA+KET
Bef.
NMDA+MK-801
D
Donor + acceptor
GluN1-N616A -GFP
GluN1-N616A -mCherry
N616A
GFP
mCherry
FRET
± KET (5 min)
E
WT - Buffer
WT - KET
Donor + Acceptor
N616A - Buffer
N616A - KET
2.5
2
GFP lifetime (ns)
F
WT
N616A
**
Norm. FRET efficiency (%)
300
200
100
0
Bef.
KET
Bef.
KET

Figure 3. KET drives conformational changes in NMDAR cytosolic domains

(A) Principle of intra-molecular FLIM-FRET experiments.

(B) GFP lifetime in GluN1-GFP (donor only) and GluN1-GFP/GluN1-mCherry (donor + acceptor) dendritic spine clusters after exposure to buffer or NMDA (5 µM) combined with D-AP5 (50 µM), KET (1 µM) or MK-801 (20 µM). Scale bar, 1 µm.

(C) Upper panel, GFP lifetime in GluN1-GFP/GluN1-mCherry clusters before and after exposure to NMDA combined with D-AP5 (n = 373 clusters), KET (n = 498) or MK-801 (n = 239). Each dot represents the lifetime of one cluster, before and after treatment. Wilcoxon test, ***p<0.0001. Lower panel, FRET efficiency in GluN1-GFP/GluN1-mCherry clusters before and after exposure to NMDA combined with D-AP5 (n = 385 clusters), KET (n = 326) or MK-801 (n = 239). Data expressed as median ± 25-75% IQR (box) and 10-90% percentile (whiskers). Mann-Whitney test, **p<0.01.

(D) GluN1-GFP/GluN1-mCherry FRET couple incorporating the N616A point mutation.

(E) GFP lifetime in GluN1-GFP/GluN1-mCherry (WT) or GluN1-N616A-GFP/GluN1-N616A-mCherry (N616A) dendritic spine clusters after exposure to buffer or NMDA combined with KET. Scale bar, 1 µm.

(F) FRET efficiency in GluN1-GFP/GluN1-mCherry (WT, n = 326 clusters) and GluN1-N616A-GFP/GluN1-N616A-mCherry (N616A, n = 362) clusters before and after exposure to NMDA combined with KET. Data expressed as median ± 25-75% IQR (box) and 10-90% percentile (whiskers). Mann-Whitney test, **p<0.01.

Figure 4

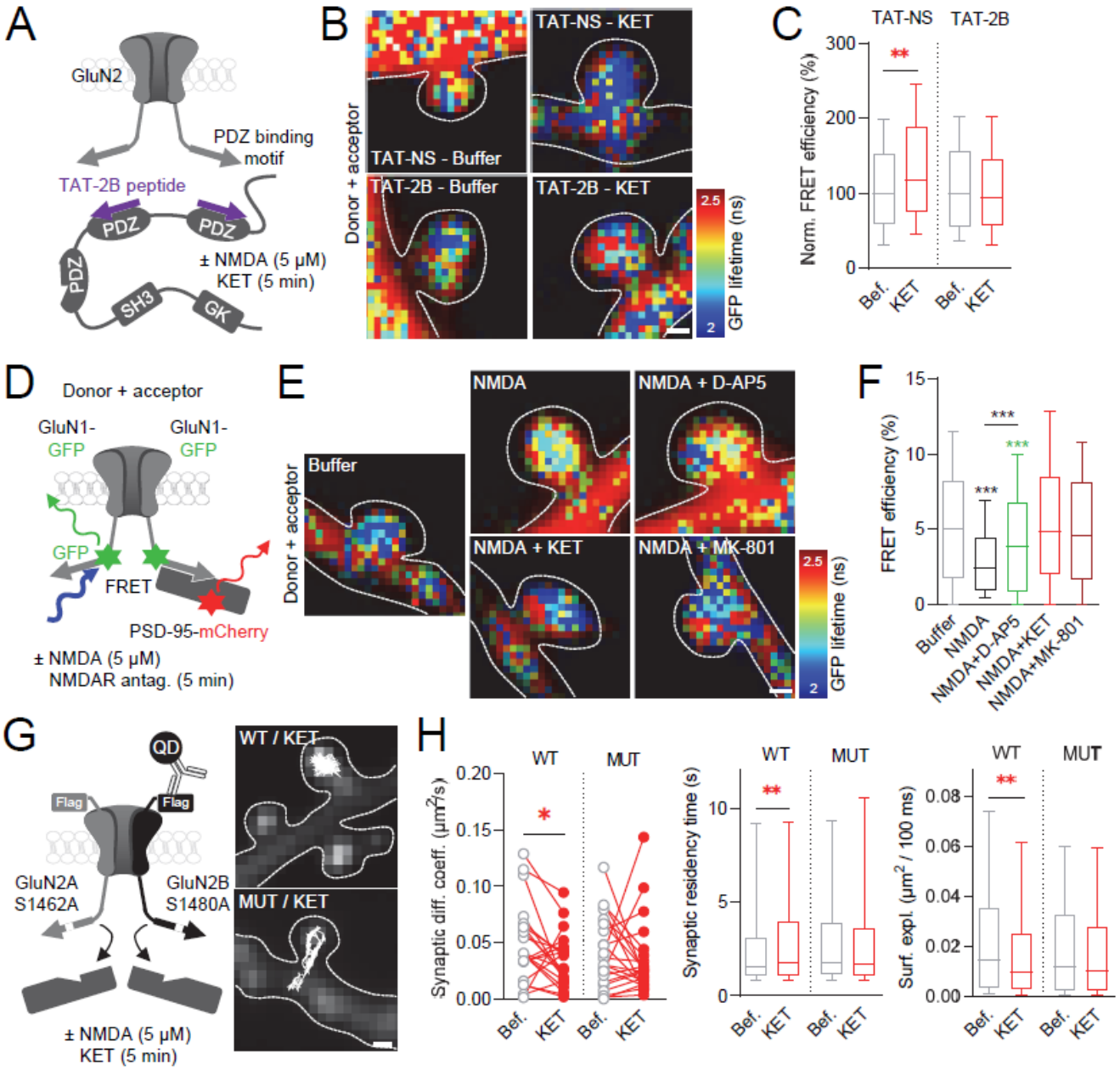
A
GluN2
PDZ binding motif
TAT-2B peptide
PDZ
PDZ
PDZ
SH3
GK
± NMDA (5 µM)
KET (5 min)
B
Donor + acceptor
TAT-NS - Buffer
TAT-NS - KET
TAT-2B - Buffer
TAT-2B - KET
2.5
2
GFP lifetime (ns)
C
TAT-NS
TAT-2B
Norm. FRET efficiency (%)
300
200
100
0
**
Bef.
KET
Bef.
KET
D
Donor + acceptor
GluN1-GFP
GluN1-GFP
GFP
FRET
PSD-95-mCherry
± NMDA (5 µM)
NMDAR antag. (5 min)
E
Donor + acceptor
Buffer
NMDA
NMDA + D-AP5
NMDA + KET
NMDA + MK-801
2.5
2
GFP lifetime (ns)
F
FRET efficiency (%)
15
10
5
0
***
***
***
Buffer
NMDA
NMDA+D-AP5
NMDA+KET
NMDA+MK-801
G
QD
Flag
Flag
GluN2A S1462A
GluN2B S1480A
± NMDA (5 µM)
KET (5 min)
WT / KET
MUT / KET
H
WT
MUT
Synaptic diff. coeff. (µm²/s)
0.20
0.15
0.10
0.05
0.00
*
Bef.
KET
Bef.
KET
WT
MUT
Synaptic residency time (s)
10
5
0
**
Bef.
KET
Bef.
KET
WT
MUT
Surf. expl. (µm² / 100 ms)
0.08
0.06
0.04
0.02
0.00
**
Bef.
KET
Bef.
KET

Figure 4. KET favors synaptic trapping through enhanced interaction with PDZ domain-containing scaffolding proteins

(A) Action of TAT-2B competing peptides.

(B) GFP lifetime in GluN1-GFP/GluN1-mCherry dendritic spine clusters before and after NMDA combined with KET in the presence of TAT-NS or TAT-2B peptides (10 µM). Scale bar, 1 µm.

(C) FRET efficiency in GluN1-GFP/GluN1-mCherry clusters before and NMDA combined with KET in the presence of scramble TAT-NS (n = 205 clusters) or TAT-2B (n = 243). Data expressed as median ± 25-75% IQR (box) and 10-90% percentile (whiskers). Mann-Whitney test, **p<0.01.

(D) Inter-molecular FLIM-FRET experiments.

(E) GFP lifetime in GluN1-GFP/PSD-95-mCherry dendritic spine clusters after exposure to buffer or NMDA alone combined with D-AP5, KET or MK-801. Scale bar, 1 µm.

(F) FRET efficiency in GluN1-GFP/PSD-95-mCherry clusters after exposure to buffer (n = 895 clusters) or NMDA (n = 761) alone or combined with D-AP5 (n = 723), KET (n = 535) or MK-801 (n = 606). Data expressed as median ± 25-75% IQR (box) and 10-90% percentile (whiskers). Kruskal-Wallis followed by Dunn's multiple comparison test, ***p<0.001.

(G) Dendritic segments expressing Homer1c-dsRed (grey) with representative trajectories of QD-labelled wild-type Flag-GluN2A/Flag-GluN2B and mutated Flag-GluN2A-S1462A/Flag-GluN2B-S1480A synaptic NMDAR exposed to NMDA combined with KET. Scale bar, 500 nm.

(H) Left panel, instantaneous diffusion coefficients of wild-type Flag-GluN2A/Flag-GluN2B (WT, n = 21 cells) and Flag-2A-S1462A/Flag-2B-S1480A (MUT, n = 22) synaptic NMDAR before and after NMDA and KET in the presence of TTX. Each dot represents the median diffusion coefficient for one cell, before and after treatment. Paired t-test, *p<0.05. Middle panel, synaptic residency time of WT (n = 21) and MUT (n = 22) synaptic NMDAR before (WT, n = 548 trajectories; MUT, n = 485) and after (WT, n = 583; MUT, n = 605) exposure to NMDA and KET. Data expressed as median ± 25-75% IQR (box) and 10-90% percentile (whiskers). Wilcoxon test, **p<0.01. Right panel, surface explored by WT (n = 21) and MUT (n = 22) synaptic NMDAR before (WT, n = 286 trajectories; MUT, n = 291) and after (WT, n = 318; MUT, n = 338) exposure to NMDA and KET. Data expressed as median ± 25-75% IQR (box) and 10-90% percentile (whiskers). Wilcoxon test, **p<0.01.

Figure 5

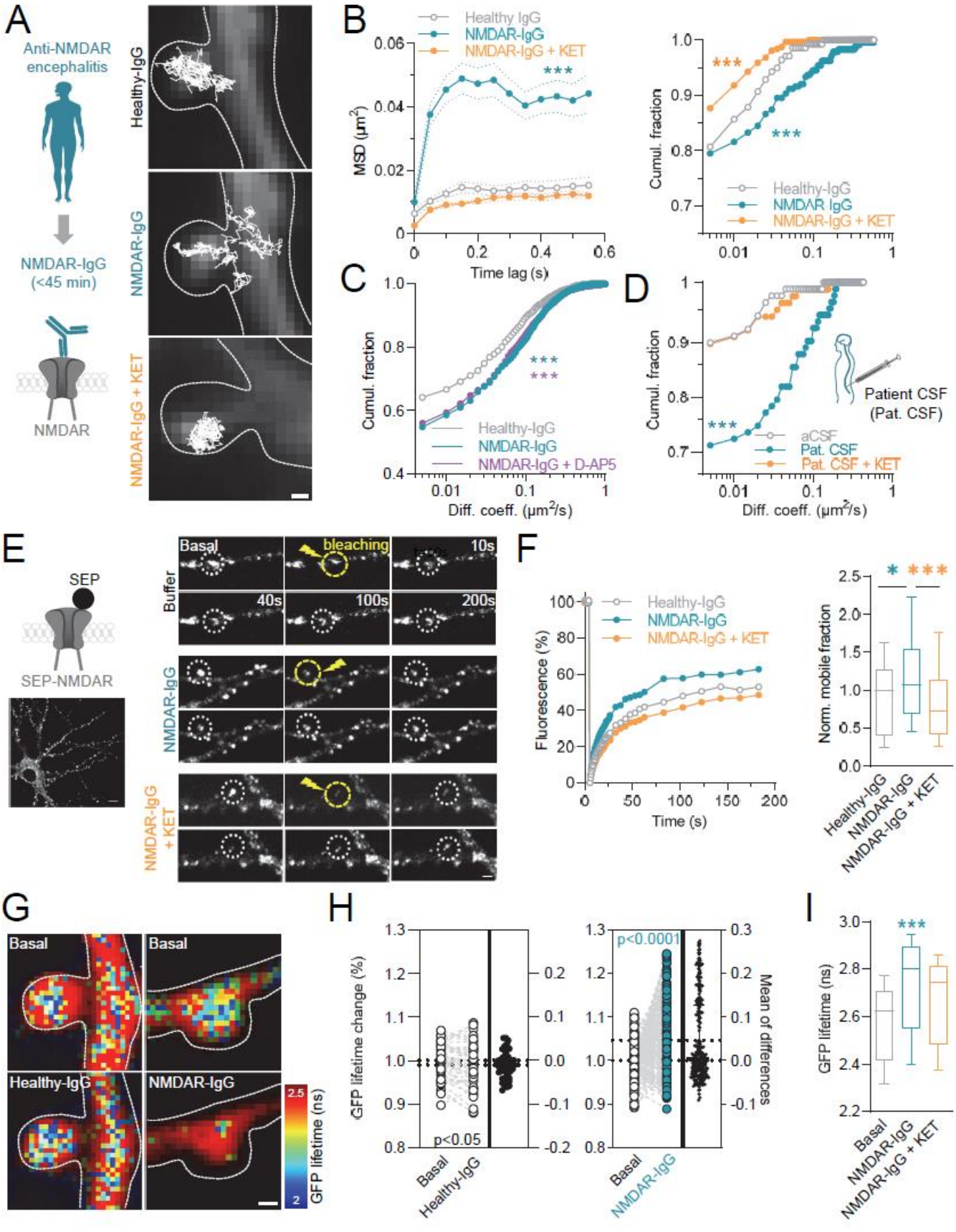
A
Anti-NMDAR encephalitis
NMDAR-IgG (<45 min)
NMDAR
Healthy-IgG
NMDAR-IgG
NMDAR-IgG + KET
B
Healthy IgG
NMDAR-IgG
NMDAR-IgG + KET
MSD (µm²)
Time lag (s)
Cumul. fraction
Healthy-IgG
NMDAR IgG
NMDAR-IgG + KET
C
Cumul. fraction
Healthy-IgG
NMDAR-IgG
NMDAR-IgG + D-AP5
Diff. coeff. (µm²/s)
D
Cumul. fraction
Patient CSF (Pat. CSF)
aCSF
Pat. CSF
Pat. CSF + KET
Diff. coeff. (µm²/s)
E
SEP
SEP-NMDAR
Buffer
NMDAR-IgG
NMDAR-IgG + KET
Basal
bleaching
10s
40s
100s
200s
F
Fluorescence (%)
Healthy-IgG
NMDAR-IgG
NMDAR-IgG + KET
Time (s)
Norm. mobile fraction
Healthy-IgG
NMDAR-IgG
NMDAR-IgG + KET
G
Basal
Healthy-IgG
NMDAR-IgG
GFP lifetime (ns)
H
GFP lifetime change (%)
p<0.05
Basal
Healthy-IgG
p<0.0001
Mean of differences
Basal
NMDAR-IgG
I
GFP lifetime (ns)
Basal
NMDAR-IgG
NMDAR-IgG + KET

Figure 5. KET prevents impairment in NMDAR synaptic trapping and conformational rearrangements caused by patient-derived anti-NMDAR antibodies

(A) Left panel, Patients' IgG purification. Right panel, dendritic segments expressing Homer1c-dsRed with representative trajectories of QD-labelled GluN2A-NMDAR after 30 min exposure to Healthy-IgG (upper panel), NMDAR-IgG (middle panel) or NMDAR-IgG + KET (10 µM; lower panel). Scale bar, 500 nm.

(B) MSD (left panel) and cumulative distributions of instantaneous diffusion coefficients (right panel) of synaptic NMDAR after exposure to Healthy-IgG (n = 140 trajectories), NMDAR-IgG (n = 240), or NMDAR-IgG + KET (n = 318). Kolmogorov-Smirnov test, ***p<0.0001.

(C) Cumulative distributions of instantaneous diffusion coefficients of synaptic NMDAR after exposure to Healthy-IgG (n = 1,578 trajectories), NMDAR-IgG (n = 1,794), or NMDAR-IgG + D-AP5 (50 µM; n = 1,881). Kolmogorov-Smirnov test, ***p<0.0001.

(D) Left panel, CSF sampling (spinal tap) from a patient suffering from anti-NMDAR encephalitis. Right panel, cumulative distributions of instantaneous diffusion coefficients of synaptic NMDAR after artificial CSF (aCSF, n = 63 trajectories), patient CSF (n = 54), or Pat. CSF + KET (n = 55). Kolmogorov-Smirnov test; ***p<0.001.

(E) Left panel, schematic representation of a SEP-tagged NMDAR and representative neuron expressing SEP-GluN2A-NMDAR. Scale bar, 10 µm. Right panel, dendritic segments illustrating recovery from photobleaching in SEP-GluN2A-NMDAR clusters (white dotted circles) after 20 min exposure to buffer, NMDAR-IgG or NMDAR-IgG + KET. Scale bar, 2 µm.

(F) Left panel, fluorescence recovery after photobleaching in SEP-GluN2A-NMDAR clusters. Each curve represents the mean of regions of interest for a representative neuron. Right panel, mobile fraction of SEP-GluN2A-NMDAR after exposure to Healthy-IgG (n = 234 ROI), NMDAR-IgG (n = 332), or NMDAR-IgG + KET (n = 262). Data expressed as median ± 25-75% IQR (box) and 10-90% percentile (whiskers). One-way ANOVA followed by Tukey's multiple comparison test, *p<0.05, ***p<0.001.

(G) GFP lifetime in GluN1-GFP/GluN1-mCherry dendritic spine clusters in basal condition and 15 min after exposure to Healthy-IgG or NMDAR-IgG. Scale bar, 1 µm.

(H) GFP lifetime in GluN1-GFP/GluN1-mCherry clusters before and 15 min after exposure to healthy-IgG (n = 50 ROI) or NMDAR-IgG (n = 174). Each dot represents the median lifetime for one cell, before and after treatment. Unpaired t-test ***p<0.001.

(I) GFP lifetime in GluN1-GFP/GluN1-mCherry clusters before and after NMDAR-IgG alone then NMDAR-IgG + KET (n = 417 clusters). Data expressed as median ± 25-75% IQR (box) and 10-90% percentile (whiskers). Paired t-test ***p<0.001.

Figure 6

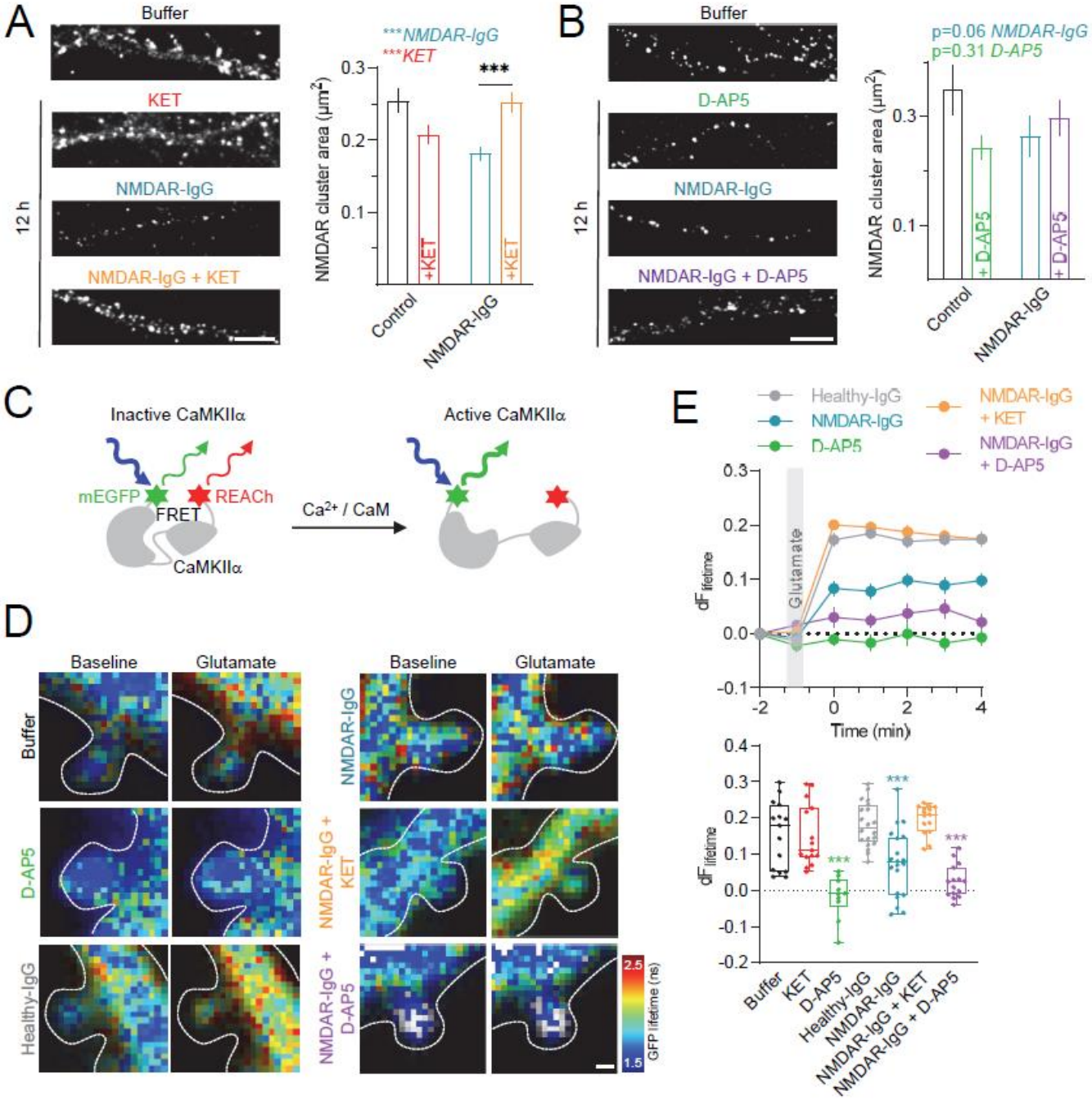
A
Buffer
KET
NMDAR-IgG
NMDAR-IgG + KET
12 h
***NMDAR-IgG
***KET
NMDAR cluster area (µm²)
0.3
0.2
0.1
***
+KET
+KET
Control
NMDAR-IgG
B
Buffer
D-AP5
NMDAR-IgG
NMDAR-IgG + D-AP5
12 h
p=0.06 NMDAR-IgG
p=0.31 D-AP5
NMDAR cluster area (µm²)
0.3
0.1
+ D-AP5
+ D-AP5
Control
NMDAR-IgG
C
Inactive CaMKIIα
Active CaMKIIα
mEGFP
REACh
FRET
CaMKIIα
Ca²⁺ / CaM
D
Baseline
Glutamate
Baseline
Glutamate
Buffer
D-AP5
Healthy-IgG
NMDAR-IgG
NMDAR-IgG + KET
NMDAR-IgG + D-AP5
2.5
1.5
GFP lifetime (ns)
E
Healthy-IgG
NMDAR-IgG
D-AP5
NMDAR-IgG + KET
NMDAR-IgG + D-AP5
Glutamate
dF lifetime
0.3
0.2
0.1
0.0
-0.1
-2
0
2
4
Time (min)
dF lifetime
0.4
0.3
0.2
0.1
0.0
-0.1
-0.2
***
***
***
Buffer
KET
D-AP5
Healthy-IgG
NMDAR-IgG
NMDAR-IgG + KET
NMDAR-IgG + D-AP5

Figure 6. KET prevents synaptic NMDAR depletion and signalling deficits caused by patient-derived anti-NMDAR antibodies

(A) Left, dendritic segments immunostained for surface GluN2B-NMDAR after buffer, KET, NMDAR-IgG or NMDAR-IgG + KET. Scale bar, 2 µm. Right, synaptic NMDAR cluster area after buffer (n = 184 clusters), KET (n = 103), NMDAR-IgG (n = 221), NMDAR-IgG + KET (n = 219). Data expressed as mean ± SD. Two-way ANOVA followed by Tukey's multiple comparison test, ***p<0.001.

(B) Left, dendritic segments immunostained for surface GluN2B-NMDAR after exposure to buffer, D-AP5, NMDAR-IgG or NMDAR-IgG + D-AP5. Scale bar, 2 µm. Right, synaptic NMDAR cluster area after buffer (n = 78 clusters), D-AP5 (n = 88), NMDAR-IgG (n = 64), NMDAR-IgG + D-AP5 (n = 93). Data expressed as mean ± SD.

(C) Principle of intra-molecular FLIM-FRET experiments.

(D) GFP lifetime in Green-Camui dendritic spine clusters before and after glutamate (25 µM) in the presence of buffer, D-AP5 (50 µM), Healthy-IgG, NMDAR-IgG, NMDAR-IgG + KET, or NMDAR-IgG + D-AP5. Scale bar, 1 µm.

(E) Timelapse (upper panel) and quantifications (timepoint 2 min; lower panel) of GFP lifetime in Green-Camui dendritic spine clusters before and after glutamate in the presence of buffer (n = 15 clusters), KET (10 µM; n = 15), D-AP5 (50 µM; n = 13), Healthy-IgG (n = 35), NMDAR-IgG (n = 35), NMDAR-IgG + KET (n = 15) or NMDAR-IgG + D-AP5 (n = 15). Data expressed as median ± 25-75% IQR (box) and 10-90% percentile (whiskers). Each dot represents the lifetime for one cluster. One-way ANOVA followed by Tukey's multiple comparison test, ***p<0.001.

Figure 7

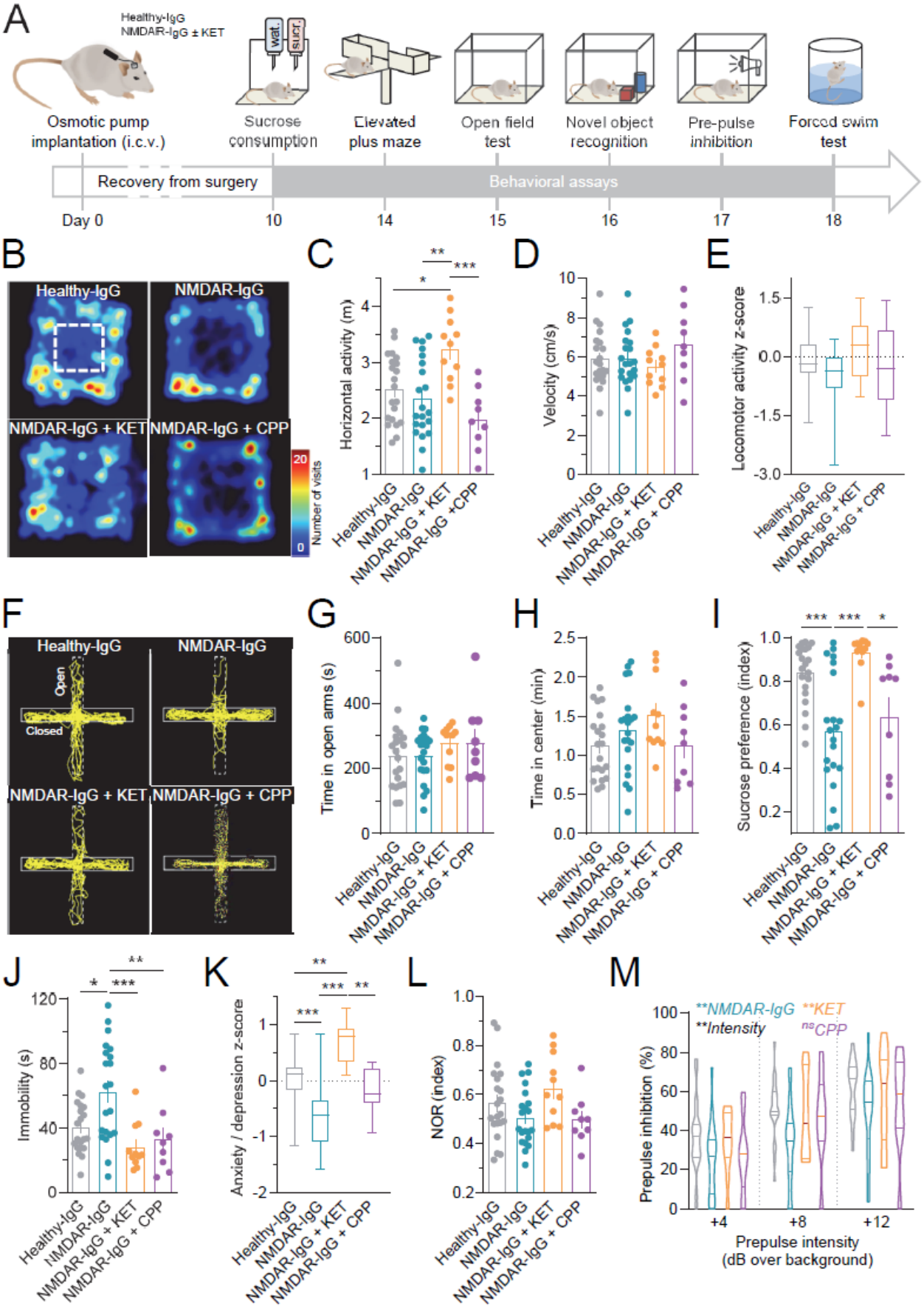
A
Healthy-IgG
NMDAR-IgG ± KET
wat.
sucr.
Osmotic pump implantation (i.c.v.)
Sucrose consumption
Elevated plus maze
Open field test
Novel object recognition
Pre-pulse inhibition
Forced swim test
Recovery from surgery
Behavioral assays
Day 0
10
14
15
16
17
18
B
Healthy-IgG
NMDAR-IgG
NMDAR-IgG + KET
NMDAR-IgG + CPP
20
0
Number of visits
C
Horizontal activity (m)
D
Velocity (cm/s)
E
Locomotor activity z-score
F
Healthy-IgG
NMDAR-IgG
Open
Closed
NMDAR-IgG + KET
NMDAR-IgG + CPP
G
Time in open arms (s)
H
Time in center (min)
I
Sucrose preference (index)
J
Immobility (s)
K
Anxiety / depression z-score
L
NOR (index)
M
**NMDAR-IgG **KET
**Intensity nsCPP
Prepulse inhibition (%)
+4
+8
+12
Prepulse intensity
(dB over background)
Healthy-IgG
NMDAR-IgG
NMDAR-IgG + KET
NMDAR-IgG + CPP

Figure 7. KET reverses anxiety- and sensorimotor gating-related behavioral deficits caused by patient antibodies

(A) Timeline of behavior experiments of rats infused with saline (Sham; n = 15 rats), IgG from healthy individuals alone (Healthy-IgG, n = 21) or combined with KET (Healthy-IgG + KET, n = 9), patient IgG (NMDAR-IgG, n = 21) alone or combined with either KET (NMDAR-IgG + KET, n = 11) or CPP (NMDAR-IgG + CPP; n = 9) during 14 days.

(B) Heatmaps of the visits in central or wall zones of the open field arena of animals exposed to either Healthy-IgG, NMDAR-IgG alone or combined with KET.

(C-E) Horizontal activity (C), velocity (D), and Z-scores for locomotor activity (E) calculated from horizontal activity and velocity measurements of animals exposed to either Healthy-IgG or NMDAR-IgG alone or combined with either KET or CPP. All data expressed as scatter dot plot with mean ± SEM except for (E) displayed as median ± 25-75% IQR (box) and 10-90% percentile (whiskers). One-way ANOVA followed by Tukey's multiple comparisons test, *p<0.05, **p<0.01, ***p<0.001.

(F) Tracks (yellow) in the open and closed arms of the elevated plus maze of animals exposed to either Healthy-IgG or NMDAR-IgG alone or combined with KET.

(G-K) Time within open arms (G, elevated plus maze), time in center zone (H, open field test), sucrose preference index (I, sucrose consumption), time spent immobile (J, forced swim test), and Z-scores for anxiety / depression calculated from sucrose consumption, forced swim, open field and elevated plus maze tests of animals exposed to either Healthy-IgG or NMDAR-IgG alone or combined with either KET or CPP. All data expressed as scatter dot plot with mean ± SEM except for (K) displayed as median ± 25-75% IQR (box) and 10-90% percentile (whiskers). One-way ANOVA followed by Tukey's multiple comparisons test, *p<0.05, **p<0.01, ***p<0.001.

(L) Novel object recognition (NOR) index of animals exposed to either Healthy-IgG or NMDAR-IgG alone or combined with KET or CPP.

(M) PPI of startle responses of animals exposed to either Healthy-IgG or NMDAR-IgG alone or combined with KET or CPP for prepulse intensities of +4 dB, +8 dB and +12 dB over background. Two-way ANOVA followed by Tukey's multiple comparisons test, **p<0.01.

STAR METHODS

RESOURCE AVAILABILITY

Lead Contact

Further information and requests for resources and reagents should be directed to Laurent Groc (laurent.groc@u-bordeaux.fr).

Materials availability

This study did not generate any unique reagents.

Data and code availability

This paper does not report original code. Any additional information required to reanalyse the data reported in this paper is available from the lead contact upon request. All materials used are commercially available.

KEY RESOURCES TABLE

REAGENT or RESOURCE	SOURCE	IDENTIFIER
Antibodies		
Anti-GFP polyclonal antibody (rabbit)	ThermoFisher Scientific	Cat# A-6455
Anti-GluN1 polyclonal antibody (rabbit)	Alomone Labs	Cat# AGC-001
Anti-K_V1.3 polyclonal antibody (rabbit)	Alomone Labs	Cat# APC-101
Anti-EphB2R polyclonal antibody (goat)	R&D systems	Cat# AF467
Anti-Flag polyclonal antibody (rabbit)	Sigma-Aldrich	Cat# F2555
Anti-Flag M2 monoclonal antibody (mouse)	Sigma-Aldrich	Cat# F1804
Anti-GluN2B polyclonal antibody (rabbit)	Alomone Labs	Cat# AGC-003
Anti-GluN2B polyclonal antibody (rabbit)	Homemade	
Anti-Homer1 polyclonal antibody (guinea pig)	Synaptic Systems	#AB 10549720
Anti-GFP polyclonal antibody (mouse)	Roche	Cat# 11814460001
Alexa 594-conjugated anti-guinea pig (goat)	Jackson ImmunoResearch	***a.*** *#AB_2337442*
Alexa 488-conjugated anti-mouse secondary antibody (goat)	ThermoFisher Scientific	***b.*** *CAT#A28175*
Alexa Fluor 647-conjugated anti-mouse IgG (donkey)	ThermoFisher Scientific	Cat# A31571

Qdot 655-conjugated anti-rabbit IgG (goat)	ThermoFisher Scientific	Cat# Q11422MP
Qdot 655-conjugated anti-goat IgG (rabbit)	ThermoFisher Scientific	Cat# Q11821MP
Equipment for *in vivo* experiments		
Osmotic pumps	Alzet	Model 2002
Forced Swim test	Noldus	
Elevated plus maze	Noldus	
Open-field arena	Home-made	54 × 54 × 40 cm
Panlab startle chamber	Harvard Apparatus	
Chemicals, peptides, and recombinant proteins		
Buprenorphine	Axience	Buprecare (0.3 mg/ml)
Meloxicam	Boehringer Ingelheim Animal Health France	Metacam (0.5 mg/m)
Ketamine hydrochloride	Virbac	Ketamine 1000 (100 mg/ml)
D-AP5	Tocris Bioscience	Cat# 0106
(+)-MK-801 maleate	Tocris Bioscience	Cat# 0924
Memantine hydrochloride	Tocris Bioscience	Cat# 0773
(RS)-CPP	Tocris Bioscience	Cat# 0173
Kynurenic acid	Sigma-Aldrich	Cat# K3375
NMDA	Sigma-Aldrich	Cat# M3262
Poly-L-lysine	Sigma-Aldrich	Cat# P4707
Gold nanobeads	Sigma-Aldrich	deposited on the agarose pads to correct Sample drift
TetraSpeck microspheres	ThermoFisher Scientific	Cat# T7279
Peptides, and Recombinant Proteins		
Biomimetic TAT-2B peptide	CASLO ApS,	YGRKKRRQRRRNGHVYEKLSSIESDV
Non-sense TAT-NS peptide	CASLO ApS	YGRKKRRQRRRGSEVILDQPVIAKPLIPALSVALSVKEEA
Recombinant DNA		
Plasmid to express mEos3.2-GluN1	Homemade	pRcCMV-mEos3.2-GluN1
Plasmid to express GFP-Homer1c	Homemade	pcDNA3.1-EGFP-Homer1c
Plasmid to express dimeric DsRed-Homer1c	Homemade	pcDNA3.1-dimeric_DsRed-Homer1c
Plasmid to express GluN1-mCherry	Paul de Koninck	pCMV-GluN1-mCherry
Plasmid to express GluN1-mGFP	Paul de Koninck	pCMV-GluN1-mGFP
Plasmid to express GluN1-N616A-mGFP	Homemade	pCMV-GluN1-N616A-mGFP
Plasmid to express GluN1-N616A-mCherry	Homemade	pCMV-GluN1-N616A-mCherry
Plasmid to express Flag-GluN1	Homemade	pCMV-Flag-GluN1
Plasmid to express Flag-GluN2B	Robert Wenthold	pCMV-Flag-GluN2B
Plasmid to express PSD-95-mCherry	Paul de Koninck	pCMV-PSD-95-mCherry

Plasmid to express Green-Camui□	Addgene	pCMV-REACh-CaMKIIa-mEGFP #26933
Plasmid to express SEP-□2	Sabine Lévi	pCMV-SEP-□2-$GABA_AR$
Plasmid to express Flag-GluN2A-S1462A	Homemade	pCMV-Flag-GluN2A-S1462A
Plasmid to express Flag-GluN2B-S1480A	Homemade	pCMV-Flag-GluN2B-S1480A
Plasmid to express SEP-GluN2A	Homemade	pCMV-SEP-GluN2A
Plasmid to express GCaMP6f	Baljit Kakh	pZac2.1-GCaMP6f
Plasmid to express mVenus-Gephyrin	Sabine Lévi	pCMV-mVenus-Gephyrin
Chemicals		
Horse serum	ThermoFisher Scientific	Waltham, MA, USA, ref. N° 26050-88
Bovine serum albumin (BSA)	Sigma-Aldrich	Cat #A3059
Fluoromount-G mounting medium containing DAPI	ThermoFisher Scientific	Cat #00-4959-52
Mowiol mounting medium	Sigma-Aldrich	Ref. #475904
Poly-L-lysine	Sigma-Aldrich	Ref. #P26361G
Neurobasal medium/B27	ThermoFisher Scientific	Ref. #12348-017/A3582901
NeuroCult SM1	Stemcell technologies	CAT#05711
BrainPhys medium	Stemcell technologies	CAT#05790
Leibovitz's L-15 medium	ThermoFisher Scientific	CAT#11415064
Hank's Balanced Salt Solution	ThermoFisher Scientific	Ref. #25300-054
Glycerol 24%	Sigma-Aldrich	Ref. #G5516
Tris-Cl	Sigma-Aldrich	CAT#15,456-3
Experimental Models: Organisms/Strains		
Sprague-Dawley rats	Janvier	Sprague-Dawley rats
Software and Algorithms		
GraphPad Prism v8.0	GraphPad	https://www.graphpad.com/
MetaMorph v7.8	Molecular Devices	https://www.moleculardevices.com/products/cellular-imaging-systems/acquisition-and-analysis-software/metamorph-microscopy
PALMTracer	Butler et al., Frontiers in Bioinformatics 2022	https://www.iins.u-bordeaux.fr/projectSIBARITA70
WaveTracer	Kechkar et al., PLoS One 2013	https://www.iins.u-bordeaux.fr/projectSIBARITA37
SR Tesseler	Levet et al., Nature Methods 2015	https://github.com/flevet/SR-Tesseler
MatLab	MathWorks	https://fr.mathworks.com/products/matlab.html

ImageJ	National Institutes of Health	https://imagej.nih.gov/ij/download.html
LI-FLIM	Lambert Instruments	https://www.lambertinstruments.com/liflim
EthoVision XT	Noldus	https://www.noldus.com/ethovision-xt

EXPERIMENTAL MODEL AND SUBJECT DETAILS

Human samples

Purified immunoglobulins (IgG) and cerebrospinal fluid (CSF) samples were collected from patients with anti-NMDAR encephalitis at the national reference center for auto-immune neurological diseases (Pr J. Honnorat, Lyon) upon early symptom presentation before any treatment was administrated. They were stored at -80°C at the NeuroBioTec center for biological ressources (Hospices Civils de Lyon, France). Analysis on patient CSF included detection of NMDAR-IgG and titration of cell counts, proteins, glucose, as well as CSF/serum albumin ratio which is an indicator of blood-brain barrier impairment. Patients also underwent a tumor screening. Serum samples were tested for the presence of NMDAR-IgG using a cell-based assay on human embryonic kidney cells (HEK293) expressing both GluN1- and GluN2B-NMDAR subunits, as previously described.[17,73] To detect NMDAR-IgG in CSF samples, cells were fixed (4% PFA, 10 min) and incubated with patient CSF (1:50 dilution in saturation buffer, 90 min). Samples were considered as positive when a clear staining was confirmed by 3 different readers in 3 independent assays. Serum samples were dialyzed against phosphate buffered saline, and solutions were used at pH of 7.4. Sera were purified in order to extract IgG isotype antibodies and dialyzed against phosphate buffer saline. Immunoglobulins from three different patients were pooled together, whereas CSFs were kept separate. Written informed consent was obtained from all participating subjects.

Animal experiments

Animal procedures were conducted in accordance with the European Community guidelines (Directive 2010/63/EU) regulating animal research, and were approved by the local Bordeaux Ethics Committee (APAFIS #23521-2019120616502664). For *in vivo* experiments, 2-months old male Sprague-Dawley rats (Janvier, France) were used. Experiments were conducted during the light cycle (05:00 to 17:00) by the same experimenter who handled the animals throughout the whole duration of the experiment. Rats were kept at ambient temperature (21° ± 1°C) with *ad libitum* access to food and water. Every effort was made to minimize the number of animals used and their suffering. Rats were housed two by cage with the same litter and

with the same treatment/cage. All animals were acclimatized to the room for at least 1 hour before the onset of each test. During open field and pre-pulse inhibition (PPI) tests, the experimenter was not blind to the animal's condition but behavioural data were collected using a computer-controlled system. The 86 rats (15 sham, 21 Healthy-IgG, 21 NMDAR-IgG, 11 NMDAR-IgG + KET, 9 Healthy-IgG + KET, 9 NMDAR-IgG + CPP) underwent surgery to implant a sub-cutaneous osmotic pump (200 µl) connected to an intracerebral catheter perfusing the right ventricle during 14 days. Behavioural tests were conducted following following a recovery period at 10 (sucrose preference), 14 (elevated plus maze), 15 (open field), 16 (novel object recognition), 17 (prepulse inhibition), and 18 (forced swim test) days after surgery. Animals were sacrificed at 21 days post-surgery and there brains were collected for further analysis. All drugs were dissolved in the same vehicle (sterile water).

Primary hippocampal cell cultures

Hippocampal cultures were prepared from embryonic day 18 Sprague-Dawley rat pups. Embryo brains were quickly removed and put in a dish with Leibovitz's L-15 medium. The hippocampus was isolated and incubated at 37°C for 15 min with a trypsin solution. Cerebral tissue was immersed in Hank's Balanced Salt Solution (HBSS) (KCl 5.33 mM, KH_2PO_4 0.44 mM, $NaHCO_3$ 4.16 mM, NaCl 137.93 mM, Na_2HPO_4 0.33 mM, D-Glucose 5.55 mM) (ThermoFisher Scientific) for dissection. The cell suspension - containing neurons and glia - was diluted in 60 mm sterile petri dishes containing pre-warmed Neurobasal culture medium supplemented with horse serum and poly-L-lysine coated 18 mm cover-slips, at a density of 250-275.10^3 cells per ml. Dishes were maintained at 37°C in 5% CO_2 in a humidity-controlled incubator. For standard primary cultures, a full medium exchange with serum-free Neurobasal/B-27 culture medium was performed at 3 days *in vitro* (DIV). Full media exchanges continued twice weekly until use. For neuronal cultures following the protocol of Kaech & Banker (2006),[74] coverslips were flipped onto astrocyte feeder layers 3 hours after plating and maintained in this inverted configuration. At DIV 3, a full medium exchange with serum-free Neurobasal/B-27 culture medium containing 5 µM cytosine arabinoside was performed to prevent astrocyte proliferation. The protocol was used for experiments in which astrocytic expression of target surface proteins could interfere with data collection or add extraneous noise to imaging of neuronal cells.

Cerebroventricular infusions

Cerebroventricular infusions were performed using osmotic pumps (model 2002, Alzet®) with the following characteristics: volume 200 µl, flow rate 0.5 µl/h, and total duration 14 days. The day before surgery, osmotic pumps (one per animal) were loaded with 20 µl (100 µg) of human NMDAR-IgG or Healthy-IgG in presence or absence of 180 µl of KET hydrochloride (100

mg/ml, Virbac®, France) or CPP (0.8 mM final; Tocris Bioscience, UK). The saline control received 0.9% NaCl solution. The volume of KET hydrochloride was 180 µl, equivalent to a pump concentration of 380 mM. The pumps were then connected to a polyethylene tube (brain infusion kit2, Alzet®) and left 4h in sterile physiological serum at +4°C. Rats were anaesthetized by isoflurane inhalation and subcutaneously injected with buprenorphine (0.1 mg/kg) and meloxicam (1 mg/kg). They were placed on a stereotaxic frame, and after drilling the skull bone, the catheter was inserted into the right ventricle (0.9 mm anterior and 1.1 mm lateral from bregma, depth 0.32 mm). The arm of the catheter was connected to the osmotic pump which was subcutaneously implanted on the back. Appropriate ventricular placement of the catheters was assessed in randomly selected rat injecting methylene blue through the catheter. Twenty-one days following surgery, animals were anesthetized with pentobarbital (50 mg/kg) and transcardially perfused with 4% paraformaldehyde. Brains were removed and postfixed overnight at 4°C. For immunohistochemistry, 18 µm-thick coronal tissue sections were cut on a microtome-cryostat (Leica CM3050S), thaw-mounted onto adapted slides (superfrost ultra plus, Thermo Scientific Labs), and stored at -20°C until further processing.

Behaviour experiments

Sucrose preference test

The sucrose preference test was performed 10 days after surgery. On the four days before the test, two bottles of water, one with 2% sucrose and the other without, were placed in the cage. Every day the position of the bottles was exchanged and the consumption from each bottle was measured. On the day of the test, the two bottles were placed in the cage again and the consumption from each bottle was recorded after 24 h. The preference for sucrose was calculated as the relative amount of water with sucrose versus total liquid (water with and without sucrose) consumed by the rats.

Elevated plus maze test

The elevated plus maze test was performed 14 days after surgery. This test measures the conflict between the natural tendency of animals to avoid an illuminated and elevated surface, and their natural tendency to explore new environments. We used a rat elevated plus maze (Imetronic®, Pessac France) made of medium-density fiberboard with a matte grey acrylic surface, which consists of four arms (two open arms without walls and two arms enlosed by 30 cm-high walls) with the following dimensions: 50 cm long and 10 cm wide. The closed arms received a 10 lux light intensity whereas the open arms received 200 lux. Rats were placed at the junction of the open and closed arms, facing the open arm opposite to where the experimenter was located. The behaviour of each animal was tracked for 10 min and analysed

using a video camera connected to a computer interface equipped with a video tracking software (EthoVision XT, Noldus®). The following parameters were monitored: time spent in open or in closed arms, entries made in open or in closed arms, and total entries made.

Open field test

The open field test was performed 15 days after surgery. The locomotor activity was measured in a homemade open field arena (54 long × 54 wide × 40 cm high) with light settings at approximately 20 lux. Novelty-induced locomotion was assessed by video tracking rats that freely explored the empty arena during 10 min. From the recordings, anxiety was evaluated as the time spent within a center zone comprising 50% of the arena during the first 10 min. Adaptation to context was assessed as a decrease in locomotor activity. The total distance travelled and velocity were tracked and analyzed using a video camera connected to a computer interface equipped with a video tracking software (EthoVision XT, Noldus®).

Novel object recognition test

The novel object recognition test was performed 16 days after surgery in a homemade open field arena (54 long × 54 wide × 40 cm high). Rats were placed into the open field arena for 10 min while two identical objects were presented and the time spent by the rat exploring each object was recorded. After a retention phase of 3 h, rats were placed for another 10 min into the open field arena but one of the familiar objects was replaced by a novel object and the total time spent exploring each object (novel and familiar) was registered. Objects were positioned in the opposite corners of those used in the training phase and the novel object was presented in 50% of trials on the right and in 50% of trials on the left side. Object exploration was defined as the orientation of the nose towards the object within a distance of less than 2 cm. A discrimination index was calculated as the difference between the time spent exploring the novel and the time spent exploring the familiar object divided by the total time exploring both objects. A higher discrimination index is considered to reflect better memory retention for the familiar object.

Pre-pulse inhibition (PPI) test

The PPI test was performed using a Panlab startle chamber (Harvard Apparatus) 17 days after surgery. Each PPI session lasted for approximately 40 min and began with a 5 min acclimatization period with a constant background noise. The session consisted of 8 different trial types: a no pulse, a startle pulse (120 dB at 8 kHz, 40 ms) that was preceded by 3 prepulses at +4, +8, and +12 dB above a 74 dB background noise (20 ms, interval of 100 ms). Each session started with 10 startle pulses (intertrial intervals (ITIsec) of 70 s) followed by a counterbalanced pseudorandom order of the 8 trials × 6 and ended with a final block of 10

startle pulses. Baseline data from different groups were pooled. Potentiation in the response to the prepulses was observed in different animal groups, and these animals were excluded from the final dataset. Prepulse inhibition is expressed as % PPI and was calculated as (100*((S − PP)/S)), where S is the average response on startle only trials and PP is the average response on prepulse + startle trials.

Forced swim test

The forced swim test was performed 18 days after surgery to assess depressive-like behaviour. Rats were placed in a plastic cylinder containing warm water (27-28° C), deep enough to prevent touching the bottom of the cylinder and forcing the rats to swim. The trial lasted 5 min and the total time of immobility after 2 min was recorded. Immobility was defined as the time that the animal stopped swimming and only used minimal movements to keep the head above the water.

Z-score calculations

As previously described,[75] z-scores were calculated as a set of converging behavioral observations. The z-score represent the value for each animal minus the mean of the control group, divided by the standard deviation of the control group. The z-score for anxiety/depression-like behavior was calculated as the mean of z-scores of each animal taking into consideration the sucrose preference test (index sweet water/total water consumption: percentage of sucrose preference), the elevated plus maze test (index open/closed arms: percentage of time in open arms), the open field test (percentage of time spent in the center zone) and the forced swim test (percentage of time spent immobile). The z-score for locomotor activity was calculated as the mean of z-scores of each animal taking into consideration the horizontal activity (distance covered during 10 min) and the velocity (average velocity over 10 min) in the open field test.

METHODS DETAILS

Transfection

For live imaging experiments, cultured hippocampal neurons were transfected at days *in vitro* (DIV) 7-10 using the calcium-phosphate method. Precipitates containing 1 mg plasmidic DNA (see key resources table) were prepared using the following solutions: TE (1 M Tris-HCl pH 7.3, 1 mM EDTA), $CaCl_2$ (2.5 M $CaCl_2$ in 10 M HEPES, pH 7.2), 2X HEPES-buffered saline (HEBS; 12 mM dextrose, 50 mM HEPES, 10 mM KCl, 280 mM NaCl and 1.5 mM Na_2HPO_4-$2H_2O$, pH = 7.2). Coverslips were transferred to 12-well plates containing 250 µl/well of conditioned culture medium supplemented with 2 mM kynurenic acid (Sigma-Aldrich), and 50 µl of DNA precipitate

solution was added to each well. Cells were incubated for 1 h at 37°C, then washed with unsupplemented Neurobasal medium containing 2 mM kynurenic acid and moved back to their original culture dishes. Transfection was monitored following at least 3 days.

Immunostaining

Cultured hippocampal neurons from E14 rat embryos were plated at a density of 2.75-3.25 x 10^5 neurons/mL in 60 mm Petri dishes containing 18 mm glass coverslips pre-coated with poly-L-lysine (Sigma-Aldrich). Neurons were maintained at 37°C and 5% CO_2 for up to 21 days. A 3% Horse Serum (ThermoFisher Scientific) solution was present in the culture medium until 4-7 days in vitro (DIV). Neurons were cultured in Neurobasal™ medium (ThermoFisher Scientific) supplemented with NeuroCult™ SM1 (Stemcell technologies). Progressively, Neurobasal was partially replaced with equally supplemented BrainPhys™ medium (Stemcell technologies). Cultured neurons at DIV 13-15 were incubated 6-12 h with human control or NMDAR-IgG at 37°C with or without NMDAR antagonists. Surface exogenous flag-GluN1 NMDAR were immunostained in live neurons using a mouse monoclonal anti-flag antibody (Sigma-Aldrich; 10 min at 37°C). Neurons were then fixed in 4% PFA for 15 min at room temperature. Fixed samples were carefully washed and immersed in a PBS 1X-NH_4Cl 50 mM quenching solution for 10 min. Samples were subsequently labeled for 1h with an anti-mouse Alexa 647-conjugated secondary antibody (ThermoFisher Scientific; 1/500) in a PBS 1X-BSA 1% blocking solution. Coverslips were carefully washed again and mounted onto glass slides with Mowiol mounting medium (composed of: Mowiol 4-88 9.6% (w/v), Glycerol 24% (w/v), and Tris-Cl (0.2 M, pH 8.5) 0.1 M). Surface endogenous GluN2B, exogenous SEP-GluN2A or SEP-GluN1 NMDAR were specifically immunostained using a monoclonal antibody against GluN2B (Alomone Labs, 1/500, 12 min, 37°C; homemade antibodies 2 mg/ml, Agro-Bio Labs, 1:20) or against GFP for SEP-containing subunits (Roche Labs, 1/500, 12 min, 37°C). Primary antibodies were incubated for 2 h followed by secondary staining with Alexa 488-conjugated anti-mouse secondary antibody (Invitrogen, 1/500, 30 min). In order to label the post-synaptic density, neurons were fixed (4% PFA, 15 min), permeabilized with Triton-BSA 1% (5 min) and successively incubated with anti-Homer1c antibody (Synaptic Systems; 1:500, 30 min) and a secondary anti-guinea pig Alexa 594 antibody (Jackson ImmunoResearch, 1/500, 30 min). Fluorescence acquisitions were performed using a Yokogawa CSU-X1 spinning-disk system (Yokogawa Electric Corporation, Tokyo, Japan) mounted on a Leica DMI6000B microscope (Leica Microsystems, Wetzlar, Germany). Samples were excited using a diode-pumped solid-state 491 laser (200 mW, 8.5-10% power, 100-200 ms exposure time) and a 642-laser diode (100 mW, 7-7.5% power, 500 ms exposure time). Images were acquired using a Plan Apo 63x oil immersion objective (NA 1.4-0.6), the appropriate excitation/emission filters and an Evolve EMCCD camera (Teledyne Photometrics). An initial experiment (1 out of 4) was p/rformed using a coolSNAP HQ2 CCD camera (Teledyne

Photometrics), a Plan Apo 100x oil immersion objective (NA 1.4-0.7), and diode-pumped solid-state 491 (100 mW, 30% power, 700 ms exposure time) and 642 (50 mW, 50% power, 800 ms exposure time) lasers. 10-15 cells per condition from independent experiments were selected. From each neuron, only one dendrite was chosen for fluorescence quantification analysis. Images were subjected to a user-defined intensity threshold for cluster selection and background subtraction. The mean fluorescence intensity was measured for all clusters of the selected region. Synaptic clusters were determined as overlapping thresholded Homer1c clusters. All analyses were done blind to treatment condition. For surface cluster analysis, dendritic branches were chosen manually in a blinded manner and cluster areas and numbers were obtained using a manual threshold approach based on integrated fluorescence levels in ImageJ (NIH).

Calcium imaging

Dissociated hippocampal neurons were transfected with GCaMP6f and DsRed-Homer1c between DIV 8 and 10 using the calcium-phosphate coprecipitation method. On the day of experiment (DIV 15-19), coverslips were transferred to a RC-41LP recording chamber (Harvard Apparatus; Cat# 64-0368). Cells were maintained in a pre-heated and equilibrated (37 °C / 5% CO_2) Tyrode solution composed of the following (in mM): 110 NaCl, 5 KCl, 2 $MgCl_2$, 2 $CaCl_2$, 15 D-Glucose, 25 HEPES (pH 7.4; 276 mOsm). Three time-lapse movies (3,000 frames, 20 Hz frame rate) were successively recorded on a widefield Nikon eclipse Ti microscope (Nikon France) equipped with a Plan Apo 60X oil immersion objective (NA 1.40) using a mercury lamp, appropriate excitation/emission filters and an Evolve EMCCD camera (Teledyne Photometrics). Cells were imaged before (baseline) and after being exposed to NMDA combined with either D-AP5 (50 µM), MK-801 (20 µM), KET (1 µM) or MEM (1 µM) for 5 min. D-AP5 was then added in the imaging chamber for 5 min to obtain a baseline recording free of NMDAR-dependent calcium transients. Dendritic spines were visually identified using DsRed-Homer1c signal to avoid bias towards more active spines, and average fluorescence (F) values for each spine were recorded over time. Time-lapse movies were concatenated and realigned in ImageJ (PoorMan3DReg plugin, Michael Liebling, and Template Matching plugin, Qingzong Tseng). Fluorescence from calcium transients vs. time was measured within individual ROIs manually defined by the experimenter (ImageJ, NIH). All pixels within each ROI were averaged to give a single value time course associated to the ROI. Mean normalized fluorescence (ΔF/F) was calculated by subtracting each value with the mean of the previous 5 s values lower than P_{50} (µ) and dividing the result by µ. Positive calcium transients were identified following a two-step procedure: initially, ΔF/F traces were smoothened by convoluting the raw signal with a 10 s squared kernel. True positives (with minimal intervals of 1s between transients) were then defined on an automated basis using custom-written

MATLAB (MathWorks) routines where the threshold was set at 5 times the standard deviation of the corresponding D-AP5 average trace.

Photo-activated localization microscopy (PALM)

Dissociated hippocampal neurons were prepared from E18 Sprague-Dawley rats and plated on 18 mm poly-lysine-pre-coated coverslips, as previously described.[17] Neurons were transfected with mEos3.2-GluN1 and GFP-Homer1c between DIV 8 and 10 using the calcium-phosphate coprecipitation method. On the day of experiment (DIV 14-15), coverslips were mounted on a Ludin chamber (Life Imaging Services). Cells were maintained in a pre-heated and equilibrated (37 °C / 5% CO_2) Tyrode solution composed of the following (in mM): 108 NaCl, 5 KCl, 2 $MgCl_2$, 2 $CaCl_2$, 15 D-Glucose, 25 HEPES (pH 7.4; 276 mOsm). Image acquisitions were performed on a Nikon Ti-Eclipse microscope (Nikon France) equipped with an incubator box and an air heating system (Life Imaging Services), a Perfect Focus System (PFS), a motorized stage TI-S-ER, and an azymuthal Ilas² TIRF arm (Gataca Systems) coupled to a laser bench containing 405 nm (100 mW), 488 nm (150 mW), 532 nm (1 W), 561 nm (200 mW) and 642 nm (1 W) diodes. Photo-conversion of mEos3.2 was achieved using the 405 nm laser and photo-converted single molecule fluorescence was excited with the 561 nm laser. Both lasers illuminated the sample simultaneously and their respective powers were adjusted to maintain the number of stochastically-activated molecules constant during acquisitions. The angle of illumination was adjusted in oblique configuration to detect mEos3.2 signals at the cell surface and to decrease background noise. Fluorescence signals were detected using an Apo TIRF 100X NA 1.49 oil-immersion objective and a Fusion BT sCMOS camera (Hamamatsu Photonics). The microscope and image acquisition were driven by the Metamorph software (Molecular Devices). Redistributions of mEos3.2-GluN1 at the neuronal surface were monitored for 4000 frames at 20 Hz acquisition rate (200 s recordings). Each neuronal field was imaged twice, i.e. before and after a 5 min exposure to NMDA (5 µM) alone or combined with either D-AP5 (50 µM), KET (1 µM), MK-801 (20 µM) or memantine (1 µM). Drugs were added directly into the bath after the first acquisition. Trajectory reconstruction and data extraction were performed using the PALMTracer plug-in running under the Metamorph software environment (J.B. Sibarita, Bordeaux). The two-dimensional trajectories of single molecules in the plane of focus were constructed by correlation analysis between consecutive images using a Vogel algorithm. For each trajectory, the instantaneous diffusion coefficient ‘D’ was calculated from linear fits of the first 4 points of the mean-square-displacement versus time function using $MSD(t) = \langle r2 \rangle (t) = 4Dt$. Synaptic areas were defined by wavelet image segmentation from fluorescence images of the GFP-Homer1c postsynaptic marker.

Direct Stochastic Optical Reconstruction Microscopy (dSTORM)

Dissociated hippocampal neurons were transfected with GFP-Homer1c and Flag-GluN1 between DIV 8 and 10 using the calcium-phosphate coprecipitation method. On DIV 14-17, neurons were exposed to TTX (1 µM), D-AP5 (50 µM), KET (1 µM), MK-801 (20 µM) or MEM (1 µM) for 1h. Neurons were then incubated with blocking agents (HEPES 10 mM, BSA 1%; 5 min, 37°C) and labeled using a mouse monoclonal anti-Flag antibody (Sigma-Aldrich, Saint-Louis, MO, USA, Cat# N° F1804, 1/500, 10 min, 37°C) in the presence of different drugs. Samples were fixed in 4% PFA (15 min, RT) and carefully washed in a quenching solution (PBS-1X, NH_4Cl 50 mM). Unspecific antibody binding sites were masked using a blocking solution (1.5% BSA, 0.1% fish gel, 0.1% Triton-100X; 45 min, RT). Samples were labeled with an anti-mouse Alexa 647-conjugated secondary antibody (ThermoFisher Scientific, 1/500; 1h, RT). Coverslips were carefully washed and stored in PBS 1X at 4°C until imaging. Multicolor fluorescent TetraSpeck™ microspheres were added to the samples before image acquisition (ThermoFisher Scientific, Cat# T7279; 1/500; 10 min, at RT). Imaging sessions were performed on a Nikon Eclipse Ti microscope (Nikon France) equipped with a Perfect Focus System (PFS), an azymuthal Ilas² TIRF arm and scanner system (Gataca Systems), a Ti-S-ER motorized stage controlled by MetaMorph software (Molecular Devices), an Apo TIRF 100X oil-immersion objective (NA 1.49) and an Evolve EMCCD camera (Teledyne Photometrics) with a final pixel size of 160 nm. Alexa 647 fluorophores were converted into the dark state using a 642 nm fiber laser at maximum power (1,000 mW), and a stable optimized rate of stochastically-activated molecules per frame was achieved by controlling the power of a diode-pumped solid-state 405 nm laser (1,000 mW) while fixing the 642 nm laser power to around 30% of maximum. Samples were illuminated in TIRF mode and images were obtained with an exposure time of 20 ms (50 Hz frame rate) up to 80,000 consecutive frames. Imaging was carried out at RT in a closed Ludin chamber (Life Imaging Services) using a pH-adjusted extracellular solution containing oxygen scavengers and reducing agents.[76] Single-molecule localization and reconstruction was performed online with automatic feedback control of the lasers using the WaveTracer module, enabling optimal single-molecule density during the acquisition.[77] The acquisition and localization sequences were driven by MetaMorph software in streaming mode using a region of interest of 256 x 256 pixels. Super-resolved images were reconstructed with the PALMTracer software plugin for MetaMorph using a Gaussian fit (xy sigma) to determine the centroid-coordinates of a single molecule and lateral drift correction was achieved using the positions of the photostable TetraSpeck™ beads. SR-Tesseler software was used to quantify protein clustering from the detected fluorophore coordinates.[78] This method uses a Voronoi diagram to decompose a super-resolved image into polygons of various sizes, which are drawn by equally dividing the distances between all adjacent detections. From those polygons, several parameters can be

extracted, such as the first-rank density σi^1 of a detected molecule i. Automatic segmentation of clusters was performed by selecting sets of detections having a density σi^1 higher than $2\sigma^d$, with σ^d being the average density of a user-defined region (containing one dendrite). All selected neighboring molecules were merged and only clusters having a minimum area of 1.25 px^2 (minimum area of 180 nm^2 based on the size of GluN1 clusters in epifluorescence) and a minimum number of localizations of 5, as previously defined.[8] were considered. For each cluster j, automatic segmentation of the nanodomains was achieved by applying $\sigma_{(i,j)}{}^1 > 1\sigma_j{}^o$, with $\sigma_j{}^o$ the average density of the cluster j and $\sigma_{(i,j)}{}^1$ the density of its i^{th} molecule. As for clusters, all selected neighboring molecules were merged and only nanodomains having a minimum area of 0.00625 px^2 (minimum area of 12.65 nm^2 based on the size of an NMDAR) and a minimum number of localizations of 25 based on the number of times a single emitter is expected to blink during the total length of an acquisition were considered.[8] Size parameters of both the clusters and the nanodomains were extracted by principal component analysis. Local detection densities were calculated as the number of localizations divided by the respective area of the cluster or nanodomain. Synaptic NMDAR clusters were identified manually by superimposing an epifluorescence image of GFP-Homer1c to a super-resolved image of Flag-GluN1 clusters.

Fluorescence recovery after photobleaching (FRAP)

Dissociated hippocampal neurons were transfected with SEP-GluN2A between DIV 8 and 10 using the calcium-phosphate coprecipitation method. On DIV 14-16, neurons were exposed to NMDAR-IgG, with or without KET (10 µM) or D-AP5 (50 µM) for either 20 min or 12 h, and were subsequently imaged on an inverted confocal Leica DMI6000B microscope (Leica Microsystems) with a Yokogawa CSU-X1 spinning-disk system (Yokogawa Electric Corporation). Acquisitions were performed using a Plan Apo 63x oil immersion objective (NA 1.4) and a Prime 95B camera (Teledyne Photometrics, Tucson, AZ, USA). A 488 nm laser (400 mW) at 50% intensity was used to photobleach locally. Recovery from photobleaching was monitored by three consecutive acquisition periods at 2, 0.5, and 0.1 Hz acquisition rates, respectively, using the appropriate excitation/emission filters. Clusters were imaged over a period of 180 s. Fluorescence intensity was measured using MetaMorph software (Molecular Devices) and corrected for acquisitional photobleaching. Image analysis and background noise were performed using homemade plugins in ImageJ (NIH).

Frequency domain based fluorescence lifetime imaging microscopy of Förster resonance energy transfer (FLIM-FRET)

Dissociated hippocampal neurons were transfected between DIV 8 and 10 using the calcium-phosphate precipitation method. For experiments designed to probe NMDAR conformational

rearrangements elicited by antagonists or antibodies, neurons were co-transfected to express recombinant NMDAR complexes incorporating C-terminus-tagged GluN1-GFP (donor fluorophore) and GluN1-mCherry (acceptor fluorophore; gifts from Paul de Koninck) together with flag-tagged GluN2B subunits (gift from Robert Wenthold), as previously described.[31,79] Causality between drug binding to the receptor and changes in conformation was tested by expressing GluN1-N616A-GFP and GluN1-N616A-mCherry incorporating a point mutation within the binding site for KET.[33] For intermolecular FRET experiments designed to assess whether antagonists affect interactions between NMDAR and MAGUK, neurons were co-transfected to express GluN1-GFP (donor fluorophore) and PSD-95-mCherry (acceptor fluorophore; gifts from Paul de Koninck).[32] For intramolecular FRET experiments designed to explore if KET would prevent NMDAR-IgG-elicited impairment in CaMKIIα activity, neurons were transfected to express the FRET-based sensor Green-Camuiα in which the N- and C-termini of CaMKIIα are labelled with monomeric enhanced GFP (mEGFP, donor fluorophore) and resonance energy-accepting chromoprotein (REACh, acceptor fluorophore), respectively.[38] On the day of experiment (DIV 12-15), coverslips were mounted on a Ludin chamber (Life Imaging Services, Basel, Switzerland). Cells were maintained in a pre-heated and equilibrated (37 °C / 5% CO_2) Tyrode solution composed of the following (in mM): 108 NaCl, 5 KCl, 2 $MgCl_2$, 2 $CaCl_2$, 15 D-Glucose, 25 HEPES (pH 7.4; 276 mOsm). Image acquisitions were performed at 37°C on an inverted Leica DMI6000B microscope (Leica Microsystems) equipped with an incubator box and an air heating system (Life Imaging Services), a Yokogawa CSU-X1 spinning-disk system (Yokogawa Electric Corporation, Tokyo, Japan), a motorized stage controlled with MetaMorph software (Molecular Devices, Sunnyvale, USA), and using a LIFA frequency domain lifetime attachment and the LI-FLIM software (Lambert Instruments BV). Cells were excited using a sinusoidally modulated (36 MHz) 478 nm LED (1 W) under wide-field illumination. Emissions were collected using HCX Plan Apo CS 63X (NA 1.4) or HCX Plan Apo 100X (NA 1.4) oil immersion objectives, an appropriate filter set and an intensified Li2CAM CCD camera (Lambert Instruments BV, Groningen, The Netherlands). Lifetimes were calibrated using a solution of erythrosin B (1 mg/ml) as a reference (0.086 ns; 30 ms exposure time). GFP lifetimes of the samples were determined from the fluorescence phase-shift between the sample and the reference from a set of 12 phase settings using LI-FLIM software (Lambert Instruments BV). FRET efficiency was calculated as $EFRET = 1 - (\tau_{DA}/\tau_D)$, where τ_{DA} is the lifetime of the donor fluorophore (GFP) in the presence of the acceptor (mCherry) and τ_D is the average lifetime of the donor alone, as previously described.[32] Depending on experimental configurations, neuronal fields were selected based on the expression of GluN1-GFP, GluN1-N616A-GFP, Green-Camuiα, GluN1-mCherry, GluN1-N616A-mCherry and PSD-95-mCherry which were excited using either 491

nm (GFP) or 561 nm (mCherry) diode lasers (100 mW). Fluorescence signals were visualized using an appropriate filter set and an Evolve EMCCD camera (Teledyne Photometrics), and acquisitions were carried out using MetaMorph. GFP lifetimes were measured using the LI-FLIM software from 20 to 30 dendritic spines manually defined using ImageJ (NIH) based on the presence of GluN1-GFP and GluN1-mCherry clusters, blind to the FLIM image. In experiments probing NMDAR conformational rearrangements elicited by antagonists, each neuronal field was imaged twice, i.e. before and 5 min after exposure to NMDA (5 µM) alone or combined with either D-AP5 (50 µM), KET (1 µM), MK-801 (20 µM) or MEM (1 µM). Drugs were added directly into the bath after the first acquisition. To explore the contribution of interactions between NMDAR and MAGUK in KET-induced conformational rearrangements, neurons were pre-incubated for 1h either with a nonsense (TAT-NS; YGRKKRRQRRRGSEVILDQPVIAKPLIPALSVALSVKEEA, 10 µM; CASLO ApS, Kongens Lyngby, Denmark) or a biomimetic peptide (TAT-2B; YGRKKRRQRRRNGHVYEKLSSIESDV, 10 µM) competing with GluN2B for the binding to PDZ domains.[35] GFP lifetimes were acquired in the presence of the peptides before and 5 min after application of NMDA (5 µM) together with KET (1 µM). The ability of KET to compensate for antibody-elicited conformational rearrangements in NMDAR cytosolic domains was probed through repeated measures of GFP lifetime. After a first acquisition in Tyrode medium, Healthy-IgG or NMDAR-IgG were added to the bath and incubated for 15 min before a second acquisition was performed. KET (10 µM) was then added to the bath for 15 min and a third measurement was achieved. Repeated measures of GFP lifetime were also implemented with the Green-Camuiα FRET-based sensor to assess the ability of KET and D-AP5 to prevent NMDAR-IgG-elicited impairment in CaMKIIα activity. Prior to imaging, cells were pre-incubated for 1h with either buffer, KET (10 µM), D-AP5 (50 µM), Healthy-IgG, NMDAR-IgG, or NMDAR-IgG combined with KET or D-AP5. GFP lifetimes were then acquired every minute before (two baseline timepoints) and after addition of glutamate (25 µM) to the bath to stimulate NMDAR-mediated recruitment of CaMKIIα activity.

Single particle tracking (SPT)

Single particle tracking of endogenous or recombinant NMDAR, γ2-$GABA_AR$, EphB2R and $K_V1.3$ was performed as previously described.[17] For experiments involving recombinant proteins, neurons were transfected between DIV 8 and 10 to express SEP-□2, Flag-GluN2A-WT, Flag-GluN2B-WT, Flag-GluN2A-S1462A, Flag-GluN2B-S1480A or SEP-GluN2A using the calcium-phosphate coprecipitation method. DsRed-Homer1c and mVenus-Gephyrin were expressed as exogenous markers of excitatory and inhibitory synapses, respectively. On DIV 13-15, dissociated hippocampal neurons were incubated for 10 min (37°C, 5% CO2) with polyclonal antibodies against either GluN1 (rabbit; Alomone Labs; 1:200), EphB2R (goat; R&D

systems; 1:200), K_V1.3 (rabbit; Alomone Labs; 1:200), GFP (rabbit; ThermoFisher Scientific; 1:50,000) or Flag (rabbit; Sigma-Aldrich, 1:10,000). Neurons were then washed and incubated for 10 min with either F(ab')2-goat anti-rabbit IgG (H+L) secondary antibody, Qdot 655 (ThermoFisher Scientific; 1:10,000) or F(ab')2-rabbit anti-goat IgG (H+L) secondary antibody, Qdot 655 (ThermoFisher Scientific; 1:10,000). Non-specific binding was blocked by adding 1% BSA (Sigma-Aldrich) to the labelling solutions. All incubations were performed in pre-heated Tyrode solution containing (in mM): 110 NaCl, 5 KCl, 2 MgCl2, 2 CaCl2, 12 D-glucose, 25 HEPES, pH 7.4, 1% BSA. Coverslips were transferred to a RC-41LP recording chamber (Harvard Apparatus; Cat# 64-0368) and perfused with pre-heated and equilibrated (37 °C / 5% CO_2) Tyrode medium. Drugs, peptides and antibodies were either pre-incubated or added directly into the bath, as indicated. Image acquisitions were performed on a Nikon Ti-U Eclipse microscope (Nikon France). QD were detected using a mercury lamp and appropriate excitation/emission filters. Images were acquired using an exposure time of 50 ms (20 Hz) with up to 500 consecutive frames. Signals were detected using an Evolve EMCCD camera (Teledyne Photometrics) controlled by MetaMoprh software (Molecular Devices). Tracking was performed on randomly-selected dendritic regions for up to 20 min. The instantaneous diffusion coefficient 'D' was calculated for each trajectory, from linear fits of the first 4 points of the mean-square-displacement versus time function using MSD(t) = <r2> (t) = 4Dt. The two-dimensional trajectories of single molecules in the plane of focus were constructed by correlation analysis between consecutive images using a Vogel algorithm.

Statistical analysis

Statistical analysis was performed using GraphPad Prism (GraphPad Software Corporation, San Diego, CA, USA). For behaviour experiments, a predetermined sample size was based on previous studies and the literature [39,80]. A sample size of 10 to 15 rats was used, which corresponds to a power factor of 0.6. A D'Agostino and Pearson omnibus normality test was applied to determine the normality of the data. For normally distributed data, the following parametric tests were applied: for unpaired data, Student t-test; for paired data, Paired t-test test; for unmatched grouped data, One-way ANOVA followed by Tukey's multiple comparison test. For data that did not follow a normal distribution, the following non-parametric tests were applied: for unpaired data, Mann-Whitney test; for paired data, Wilcoxon matched-pairs signed rank test; for unmatched grouped data, Kruskal-Wallis test followed by Dunn's multiple comparison test. For distribution comparisons a Kolmogorov-Smirnov test was used. Statistically significant differences between conditions are represented as asterisks ($p>0.05$, *$p>0.05$, **$p<0.01$, ***$p<0.001$).

Preparation of figures and analysis

Figures were assembled in ImageJ (NIH), only contrast and brightness were adjusted to optimize the image quality. All statistical analysis was performed in GraphPad Prism 9.2 (GraphPad Software, San Diego, USA).

Figure S1

Related to Fig. 1

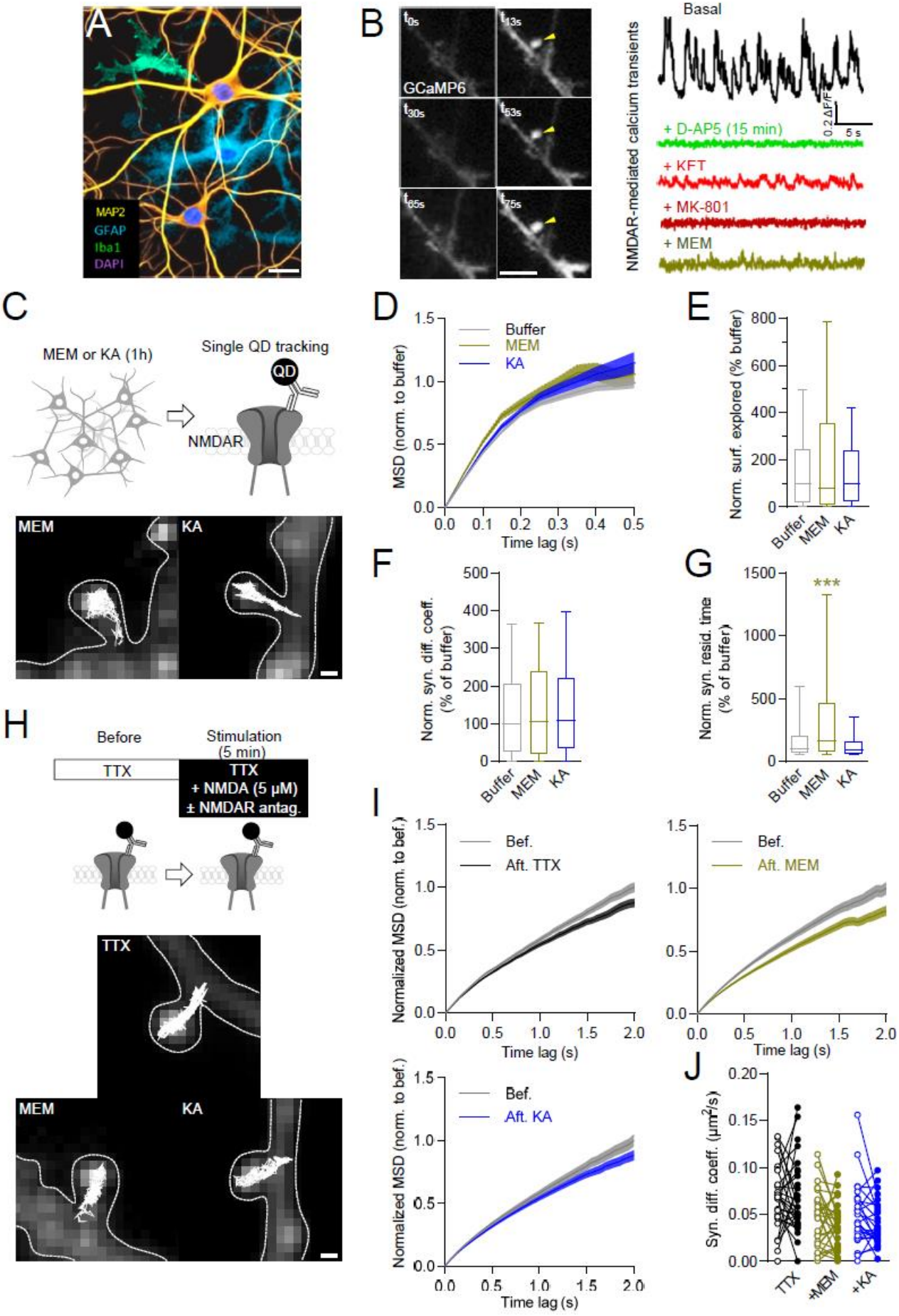

Figure S1: Acute action of OCBs on the synaptic trapping of NMDAR

(A) Representative illustration of mixed primary cultures prepared from E18 rat hippocampi containing neuronal (MAP2-positive cells, yellow), glial (GFAP-positive cells, blue) and microglial (Iba1-positive, green) cells. DAPI, nuclear staining (purple). Scale bar, 20 µm.

(B) Left panel, representative example of spontaneous calcium activity (20 Hz acquisition rate) monitored over time in a dendritic spine (yellow arrow) using the genetically-encoded GCaMP6f calcium sensor. Scale bar, 5 µm. Right panel, representative example traces of NMDAR-mediated calcium transients in single spines (DF/F) after incubation with NMDA (5 µM) alone (Basal) or combined with D-AP5 (50 µM, green), KET (1 µM, red), MK-801 (20 µM, wine) or memantine (MEM, 1 µM, yellow).

(C) Experimental principle (top) and epifluorescence images of dendritic segments expressing Homer1c-dsRed (grey) as a synaptic marker with representative trajectories (25 s, 20 Hz acquisition rate) of endogenous quantum dot (QD)-labelled synaptic NMDAR exposed to MEM (1 µM), or KA (10 µM) for 1h. Scale bar, 500 nm.

(D) Normalized mean squared displacement (MSD) over time of synaptic NMDAR after 1h exposure to buffer (grey; n = 2580 trajectories), MEM (yellow; n = 838 trajectories), or KA (blue; n = 683).

(E) Normalized surface explored by synaptic NMDAR over 100 ms after 1h exposure to buffer (n = 1,223 trajectories), MEM (n = 477), or KA (n = 326). Data expressed as median ± 25-75% IQR (box) and 10-90% percentile (whiskers).

(F) Normalized instantaneous diffusion coefficients of synaptic NMDAR after 1h exposure to buffer (n = 2,631 trajectories), MEM (n = 632), or KA (n = 631). Data expressed as median ± 25-75% IQR (box) and 10-90% percentile (whiskers).

(G) Normalized synaptic residency time of NMDAR after 1h exposure to buffer (n = 2304 trajectories), MEM (n = 750), or KA (n = 631). Data expressed as median ± 25-75% IQR (box) and 10-90% percentile (whiskers). Kruskal-Wallis followed by Dunn's multiple comparison test, ***$p<0.001$.

(H) Experimental principle (top) and epifluorescence images of dendritic segments expressing Homer1c-dsRed (grey) as a synaptic marker with representative trajectories of endogenous QD-labelled synaptic NMDAR after exposure to TTX (1 µM) or NMDA (5 µM) combined with MEM (1 µM) or KA (10 µM) in the presence of TTX. Scale bar, 500 nm.

(I) Normalized MSD over time of NMDAR before and after exposure to TTX or NMDA combined with MEM (before, n = 827 trajectories; after, n = 941 trajectories) or KA (before, n = 883; after, n = 975) in the presence of TTX.

(J) Instantaneous diffusion coefficients of synaptic NMDAR before and after exposure to TTX or NMDA combined with MEM (n = 30 cells) or KA (n = 27) in the presence of TTX. Each dot represents the median diffusion coefficient for one cell, before and after treatment.

Figure S2

Related to Fig. 1

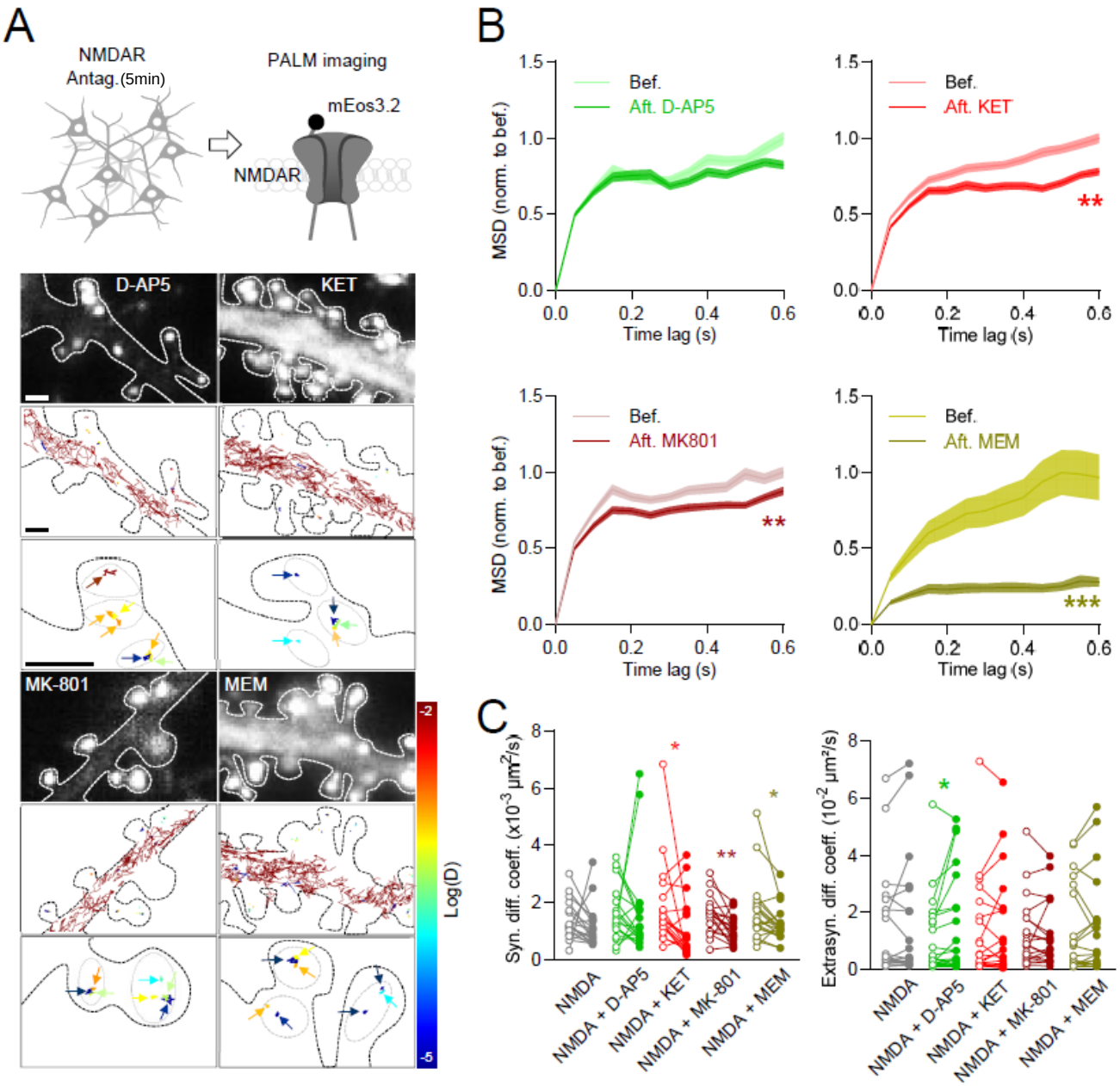

Figure S2: OCBs enhance the synaptic trapping of NMDAR

(A) Experimental principle (top) and epifluorescence images (upper panels) of dendritic segments expressing Homer1c-GFP (grey) with color-coded representative total (middle panels) and synaptic (lower panels) trajectories of GluN1-mEos3.2-NMDAR after 5 min exposure to NMDA combined with D-AP5, KET, MK-801 or MEM. Scale bars, 1 µm.

(B) Normalized MSD over time of synaptic NMDAR before and after exposure to NMDA combined with D-AP5 (before, n = 5,164 trajectories; after, n = 6,636 trajectories), KET (before, n = 11,594; after, n = 9,039), MK-801 (before, n = 8,000; after, n = 7,748), or MEM (before, n = 9,713; after, n = 5,757). Kolmogorov-Smirnov test, **p<0.01, ***p<0.001.

(C) Instantaneous diffusion coefficients of synaptic (left panel) and extrasynaptic (right panel) NMDAR before and after exposure to NMDA alone (n = 19 cells) or combined with D-AP5 (n = 19), KET (n = 20), MK-801 (n = 20), or MEM (n = 19). Each dot represents the median diffusion coefficient for one cell, before and after treatment. Paired t-test, *p<0.05, **p<0.01.

Figure S3

Related to Fig. 1

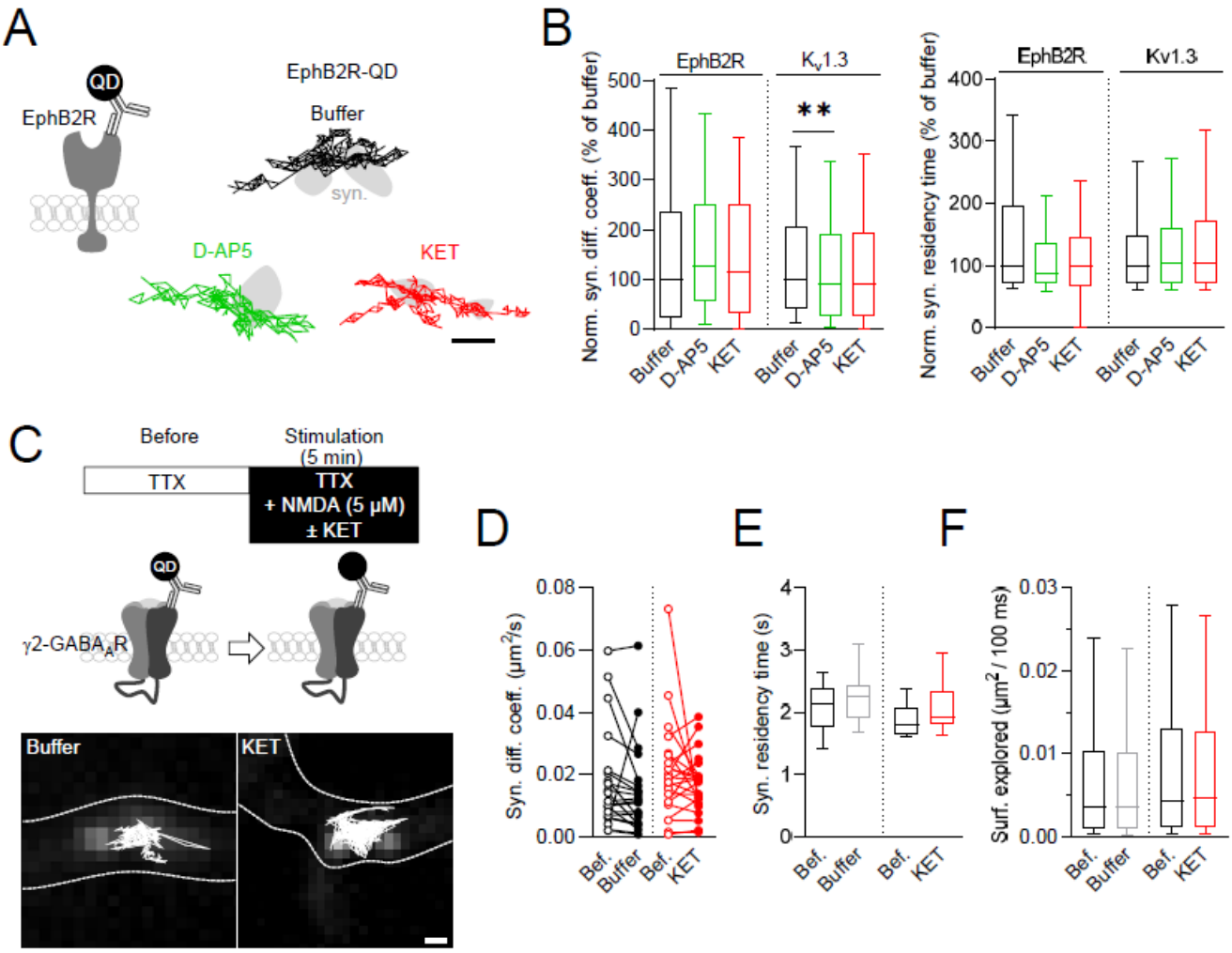

Figure S3: OCBs selectively enhance the trapping of NMDAR at excitatory synapses

(A) Principle of EphB2R SPT experiments and representative individual trajectories (25 s, 20 Hz acquisition rate) of quantum dot (QD)-labelled surface EphB2R at synapses labelled with Homer1c-dsRed as a marker (syn., grey areas) after a 1h exposure to buffer (black), D-AP5 (50 µM, green) or KET (1 µM, red). Scale bar, 500 nm.

(B) Left panel, normalized instantaneous diffusion coefficients of synaptic EphB2R and K_V1.3 (normalization to buffer) after 1h exposure to buffer (black; EphB2R, n = 207 trajectories; K_V1.3, n = 1,179 trajectories), D-AP5 (50 µM, green; EphB2R, n = 363 trajectories; K_V1.3, n = 1,041 trajectories) or KET (1 µM, red; EphB2R, n = 184 trajectories; K_V1.3, n = 507 trajectories). Right panel, normalized synaptic residency time of EphB2R and K_V1.3 (normalization to buffer) after 1h exposure to buffer (black; EphB2R, n = 207 trajectories; K_V1.3, n = 1,179 trajectories), D-AP5 (50 µM, green; EphB2R, n = 253 trajectories; K_V1.3, n = 1,041 trajectories) or KET (1 µM, red; EphB2R, n = 143 trajectories; K_V1.3, n = 507 trajectories). Data expressed as median ± 25-75% IQR (box) and 10-90% percentile (whiskers). Kruskal-Wallis followed by Dunn's multiple comparison test, **p<0.01.

(C) Experimental principle (top) and epifluorescence images of dendritic segments expressing Gephyrin-dsRed (grey) as a synaptic marker with representative trajectories (25 s, 20 Hz acquisition rate) of quantum dot (QD)-labelled γ2-$GABA_A$R at inhibitory synapses after a 5 min exposure to buffer (white) or KET (1 µM, red) combined with NMDA (5 µM) in the presence of TTX (1 µM). Scale bar, 500 nm.

(D) Instantaneous diffusion coefficients of γ2-$GABA_A$R at inhibitory synapses before and 5 min after exposure to buffer (black; N = 23 cells) or KET (1 µM, red; N = 23 cells) combined with NMDA (5 µM) in the presence of TTX (1 µM). Each dot represents the median diffusion coefficient for one cell, before and after treatment.

(E) Residency time of γ2-$GABA_A$R at inhibitory synapses before and 5 min after exposure to buffer (grey; N = 23 cells) or KET (1 µM, red; N = 23 cells) combined with NMDA (5 µM) in the presence of TTX (1 µM). Data expressed as median ± 25-75% IQR (box) and 10-90% percentile (whiskers).

(F) Surface explored by γ2-$GABA_A$R at inhibitory synapses before and 5 min after exposure to buffer (grey; Bef., n = 1,573 trajectories; Buffer, n = 1,404 trajectories; N = 23 cells) or KET (1 µM, red; Bef., n = n = 1,551 trajectories; KET, n = 1,486 trajectories; N = 23 cells) combined with NMDA (5 µM) in the presence of TTX (1 µM). Data expressed as median ± 25-75% IQR (box) and 10-90% percentile (whiskers).

Figure S4

Related to Fig. 2

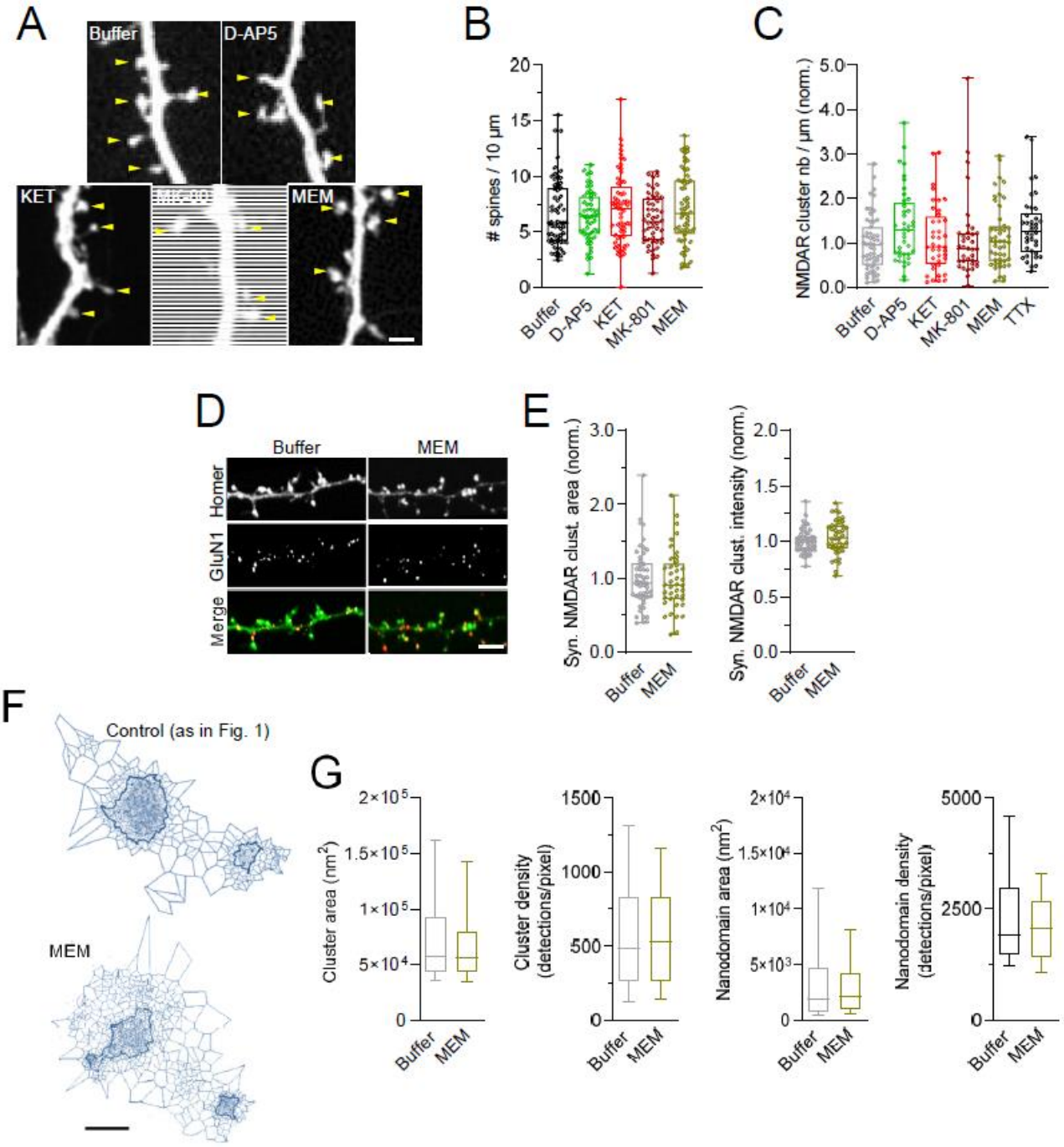

Figure S4: Acute exposure to OCBs has a limited impact on dendritic spines, NMDAR synaptic numbers and organization

(A) Representative dendritic stretches from GFP-expressing neurons in each experimental condition. Yellow arrows indicate visually-identified dendritic spines. Scale bar, 1 µm.

(B) Number of dendritic spines per 10 µm after 1h exposure to buffer (black; n = 63 dendrites, N = 30 cells), D-AP5 (50 µM, green; n = 52 dendrites, N = 28 cells), KET (1 µM, red; n = 60 dendrites, N = 30 cells), MK-801 (20 µM, wine; n = 50 dendrites, N = 25 cells) or memantine (MEM, 1 µM, yellow; n = 60 dendrites, N = 30 cells). Data expressed as median ± 25-75% IQR (box) and min to max (whiskers). Each dot represents the mean number of spines per 10 µm for one dendritic stretch.

(C) NMDAR cluster number per micron (normalized to buffer) after 1h exposure to buffer (grey; n = 55 cells), D-AP5 (50 µM, green; n = 40 cells), KET (1 µM, red; n = 40 cells), MK-801 (20 µM, wine; N = 35 cells), memantine (1 µM, yellow; n = 47 cells) or TTX (1 µM, black; n = 38 cells). Data expressed as median ± 25-75% IQR (box) and min to max (whiskers). Each dot represents the mean number of clusters per micron for one cell.

(D) Representative dendritic segments of hippocampal neurons immunostained for Homer1c-GFP (green) and flag-GluN1 NMDAR (red) after 1h exposure to buffer or memantine (MEM, 1 µM). Scale bar, 5 µm.

(E) Synaptic NMDAR cluster area (left panel) and intensity (right panel) after 1h exposure to buffer (grey; N = 50 cells) or memantine (1 µM, yellow; N = 41 cells). Data normalized to buffer and expressed as median ± 25-75% IQR (box) and min to max (whiskers). Each dot represents the mean synaptic NMDAR cluster area (left) and synaptic NMDAR cluster intensity (right) for one cell, respectively.

(F) Representative example of a tesselated super-resolved post-synaptic GluN1-NMDAR cluster after a 1h exposure to memantine (MEM, 1 µM). Each dot represents a detection and thick outlines indicate intra-cluster nanodomains of receptors. Scale bar, 100 nm.

(G) Area (left panel) and density (middle left panel) of post-synaptic GluN1-NMDAR clusters after a 1h exposure to either buffer (grey; n = 59 clusters, N = 8 cells), or memantine (1 µM, yellow; n = 164 clusters, N = 7 cells). Area (middle right panel) and density (right panel) of post-synaptic GluN1-NMDAR nanodomains after a 1h exposure to either buffer (grey; n = 149 nanodomains, N = 8 cells), or memantine (1 µM, yellow; n = 574 nanodomains, N = 7 cells). Data expressed as median ± 25-75% IQR (box) and 10-90% percentile (whiskers).

Figure S5

Related to Fig. 3

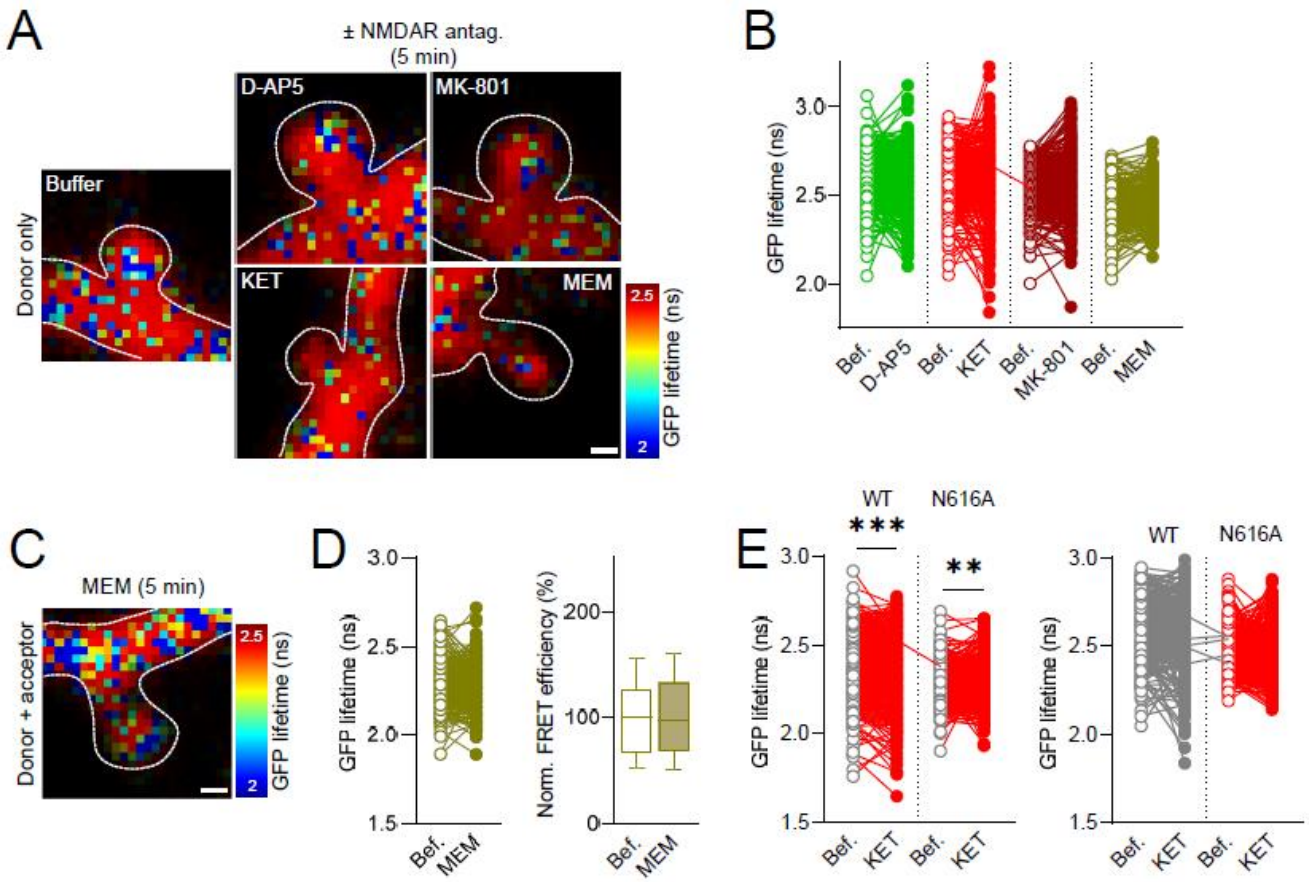

Figure S5: NMDAR antagonists do not impact the fluorescence lifetime of the donor fluorophore and memantine has no impact on the conformation of NMDAR cytosolic domains

(A) Representative illustrations of GFP lifetime in GluN1-GFP (donor only) dendritic spine clusters 5 min after exposure to buffer or NMDA (5 µM) combined with either D-AP5 (50 µM), KET (1 µM), MK-801 (20 µM), or memantine (MEM, 1 µM). Scale bar, 1 µm.

(B) GFP lifetime in GluN1-GFP clusters before and 5 min after exposure to NMDA (5 µM) combined with D-AP5 (50 µM, green; n = 488 clusters, N = 28 cells), KET (1 µM, red; n = 310 clusters, N = 43 cells), MK-801 (20 µM, wine; n = 389 clusters, N = 17 cells), or memantine (1 µM, yellow; n = 207 clusters, N = 53 cells). Each dot represents the lifetime for one cluster, before and after treatment. (C) Representative illustration of GFP lifetime in a GluN1-GFP/GluN1-mCherry (donor + acceptor) dendritic spine cluster 5 min after exposure to NMDA (5 µM) combined with memantine (MEM, 1 µM). Scale bar, 1 µm.

(D) Left panel, GFP lifetime in GluN1-GFP/GluN1-mCherry clusters before and 5 min after exposure to NMDA (5 µM) combined with memantine (1 µM, yellow; n = 298 clusters, N = 72 cells). Each dot represents the lifetime for one cluster, before and after treatment. Right panel, normalized FRET efficiency in GluN1-GFP/GluN1-mCherry clusters before and 5 min after exposure to NMDA (5 µM) combined with memantine (1 µM, yellow; n = 218 clusters, N = 72 cells). Data expressed as median ± 25-75% IQR (box) and 10-90% percentile (whiskers).

(E) Left panel, GFP lifetime in GluN1-GFP/GluN1-mCherry (n = 326 clusters, N = 19 cells) and GluN1-N616A-GFP/GluN1-N616A-mCherry (n = 362 clusters, N = 26 cells) clusters before and 5 min after exposure to NMDA (5 µM) combined with KET (1 µM, red). Right panel, GFP lifetime in GluN1-GFP (n = 326 clusters, N = 22 cells) and GluN1-N616A-GFP (n = 362 clusters, N = 34 cells) clusters before and 5 min after exposure to NMDA (5 µM) combined with KET (1 µM, red). Each dot represents the lifetime for one cluster, before and after treatment. Wilcoxon test, ***p<0.001, **p<0.01.

Figure S6

Related to Fig. 4

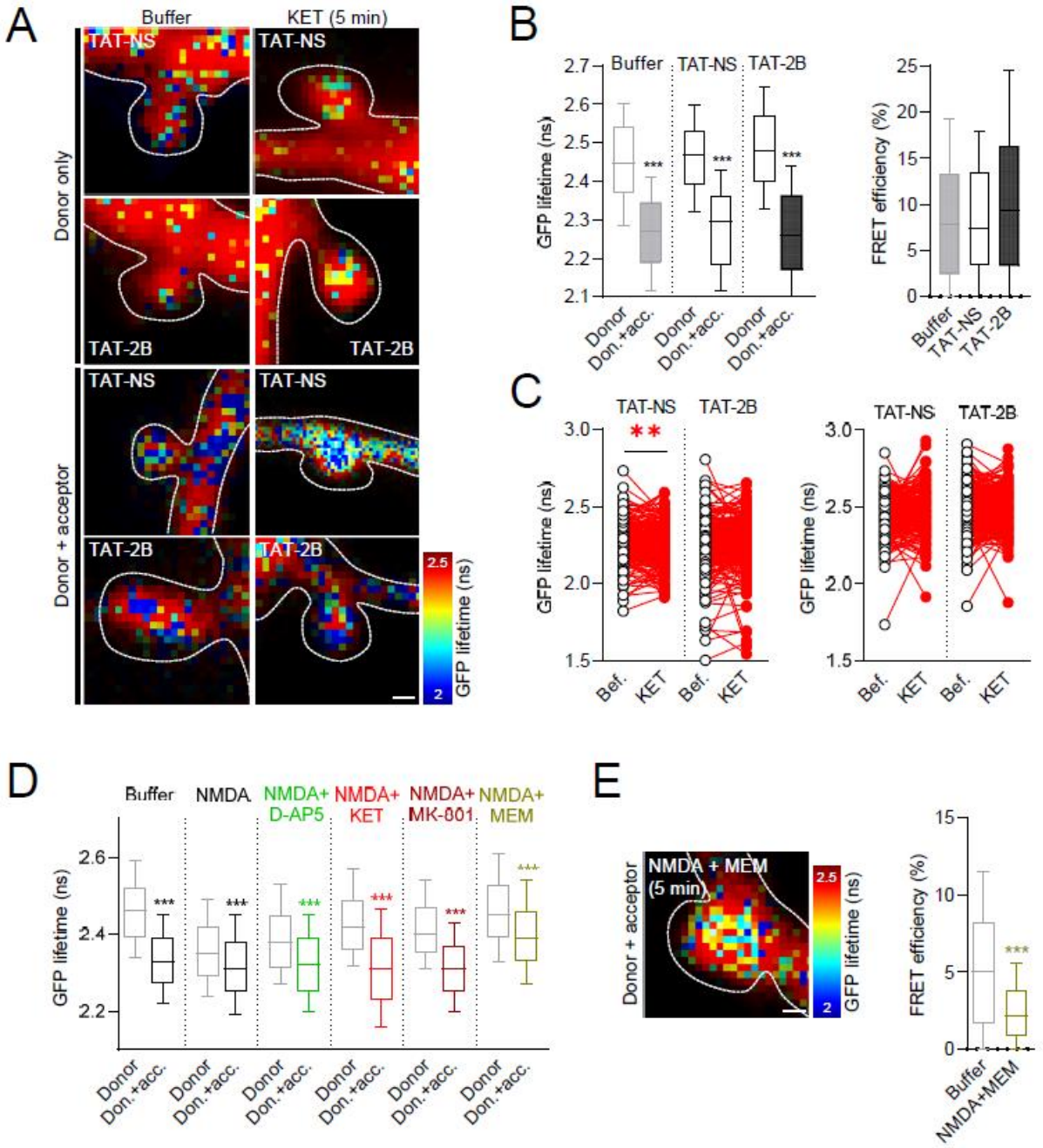

Figure S6: Peptides and NMDAR antagonists do not impact the fluorescence lifetime of the donor fluorophore

(A) Representative illustrations of GFP lifetime in GluN1-GFP (donor only, upper panels) or GluN1-GFP/GluN1-mCherry (donor + acceptor, lower panels) dendritic spine clusters before and 5 min after exposure to buffer or NMDA (5 µM) combined with KET (1 µM) in the presence of TAT-NS or TAT-2B peptides (10 µM). Scale bar, 1 µm.

(B) Left panel, GFP lifetime in GluN1-GFP (donor) and GluN1-GFP/GluN1-mCherry (don.+acc.) clusters in the presence of buffer (grey; donor, n = 207 clusters, N = 53 cells; don.+acc., n = 285 clusters, N = 72 cells), TAT-NS (10 µM, white; donor, n = 318 clusters, N = 83 cells; don.+acc., n = 195 clusters, N = 81 cells), or TAT-2B (10 µM, black; donor, n = 327 clusters, N = 77 cells; don.+acc., n = 234 clusters, N = 88 cells) peptides. Right panel, FRET efficiency in GluN1-GFP/GluN1-mCherry clusters in the presence of buffer (grey; n = 207 clusters, N = 72 cells), TAT-NS (10 µM, white; n = 195 clusters, N = 81 cells) or TAT-2B (10 µM, black; n = 234 clusters, N = 88 cells) peptides. Data expressed as median ± 25-75% IQR (box) and 10-90% percentile (whiskers). Kruskal-Wallis followed by Dunn's multiple comparison test, ***p<0.001.

(C) Left panel, GFP lifetime in GluN1-GFP/GluN1-mCherry clusters before and 5 min after exposure to NMDA (5 µM) combined with KET (1 µM, red) in the presence of scramble TAT-NS (10 µM; n = 205 clusters, N = 81 cells) or biomimetic TAT-2B (10 µM; n = 243 clusters, N = 88 cells) peptides. Right panel, GFP lifetime in GluN1-GFP clusters before and 5 min after exposure to NMDA (5 µM) combined with KET (1 µM, red) in the presence of TAT-NS (10 µM; n = 318 clusters, N = 83 cells), or TAT-2B (10 µM; n = 327 clusters, N = 77 cells) peptides. Each dot represents the lifetime for one cluster, before and after treatment. Wilcoxon test, **p<0.01.

(D) GFP lifetime in GluN1-GFP (donor) and GluN1-GFP/PSD95-mCherry (don.+acc.) clusters after exposure to buffer (dark grey; donor, n = 887 clusters, N = 38 cells; don.+acc., n = 887 clusters, N = 38 cells) or NMDA alone (5 µM, light grey; donor, n = 1,145 clusters, N = 45 cells; don.+acc., n = 761 clusters, N = 43 cells) or combined with D-AP5 (50 µM, green; donor, n = 881 clusters, N = 45 cells; don.+acc., n = 723 clusters, N = 41 cells), KET (1 µM, red; donor, n = 967 clusters, N = 30 cells; don.+acc., n = 535 clusters, N = 33 cells), MK-801 (20 µM, wine; donor, n = 860 clusters, N = 30 cells; don.+acc., n = 606 clusters, N = 26 cells) or MEM (1 µM, yellow; donor, n = 876 clusters, N = 32 cells; don.+acc., n = 791 clusters, N = 34 cells). Data expressed as median ± 25-75% IQR (box) and 10-90% percentile (whiskers). Mann-Whitney test, ***p<0.0001.

(E) Left panel, representative illustration of GFP lifetime in a GluN1-GFP/PSD95-mCherry dendritic spine cluster 5 min after exposure to NMDA (5 µM) combined with memantine (MEM, 1 µM). Scale bar, 1 µm. Right panel, FRET efficiency in GluN1-GFP/PSD95-mCherry clusters

before and 5 min after exposure to buffer (grey; n = 895 clusters, N = 38 cells) or NMDA (5 µM) combined with memantine (1 µM, yellow; n = 791 clusters, N = 31 cells). Data expressed as median ± 25-75% IQR (box) and 10-90% percentile (whiskers). Mann-Whitney test, ***p<0.0001.

Figure S7

Related to Fig. 5

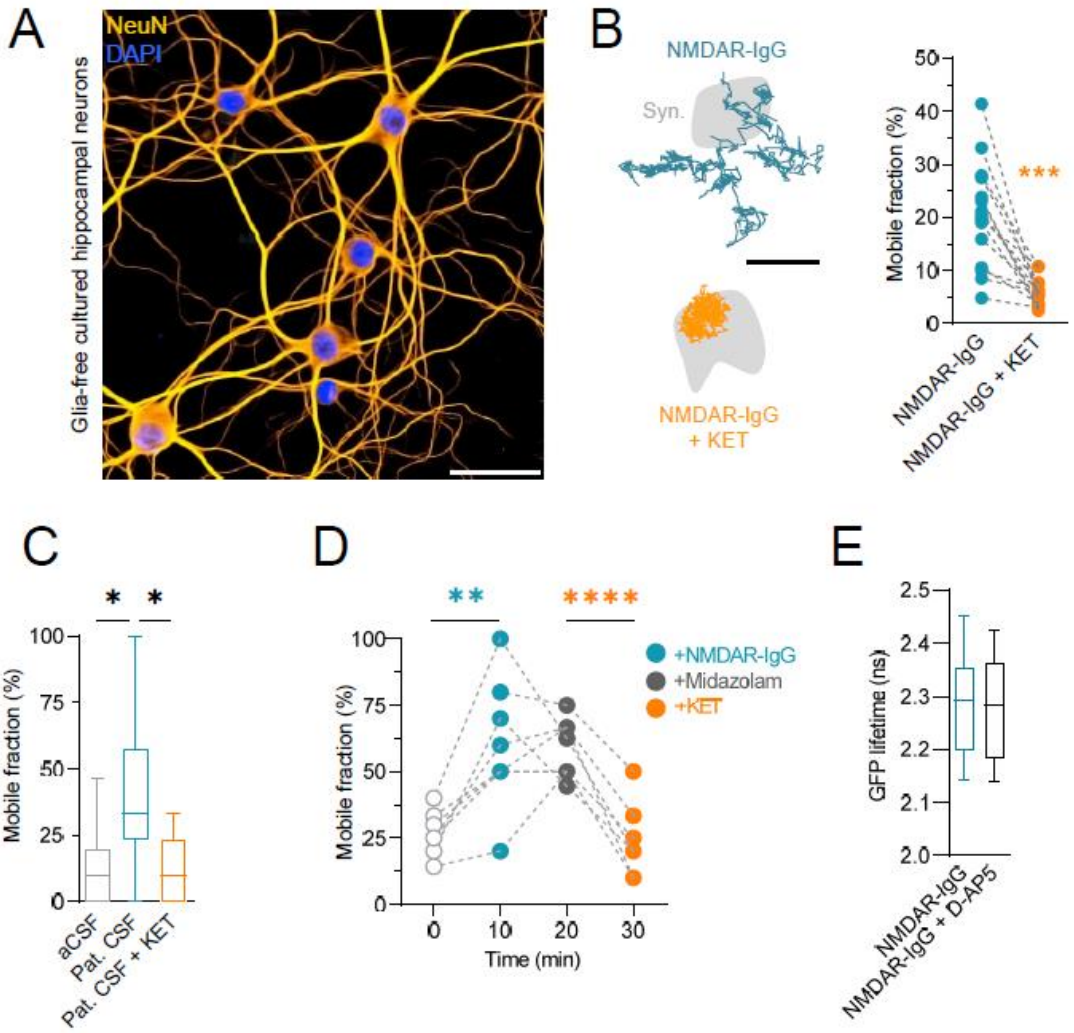

Figure S7: KET prevents impairment in NMDAR synaptic trapping and conformational rearrangements caused by patient-derived anti-NMDAR antibodies

(A) Representative illustration of glia-free Banker cultures prepared from E18 rat hippocampi. NeuN, neuronal staining (yellow); DAPI, nuclear staining (blue). Scale bar, 30 µm.

(B) Left, representative trajectories (25 s, 20 Hz acquisition rate) of quantum dot (QD)-labelled surface GluN2A-NMDAR at synapses labelled with Homer1c-dsRed as a marker (syn., grey areas) after 30 min exposure to NMDAR-IgG (blue) or NMDAR-IgG + KET (10µM; orange). Scale bar, 500 nm. Right, mobile fraction of GluN2A-NMDAR at excitatory synapses of glia-free neurons exposed to NMDAR-IgG for 12h), before and 15 min after application of KET (10 µM; n = 15 cells). Each dot represents the lifetime for one cell, before and after treatment. Paired t-test, ***p<0.001.

(C) Mobile fraction of synaptic GluN2A-NMDAR after 30 min exposure to aCSF (grey; N = 8 cells), Pat. CSF (blue; N=12 cells) or Pat. CSF + KET (10 µM, orange; N = 18 cells). Data expressed as median ± 25-75% IQR (box) and 10-90% percentile (whiskers). Kruskal-Wallis followed by Dunn's multiple comparison test, *p<0.05.

(D) Mobile fraction of synaptic GluN2A-NMDAR before and 10 min after exposure to NMDAR-IgG (blue), then midazolam (10 µM, dark grey), then KET (10 µM, orange) (N = 8 cells). Each dot represents the median mobile fraction for one cell, before and after treatment. Paired t-test, **p<0.01, ***p<0.0001.

(E) GFP lifetime in GluN1-GFP/GluN1-mCherry clusters before and 15 min after exposure to D-AP5 (50 µM) in the presence of NMDAR-IgG (n = 68 clusters, N = 13 cells). Data expressed as median ± 25-75% IQR (box) and 10-90% percentile (whiskers). Paired t-test ***p<0.001.

Figure S8

Related to Fig. 6

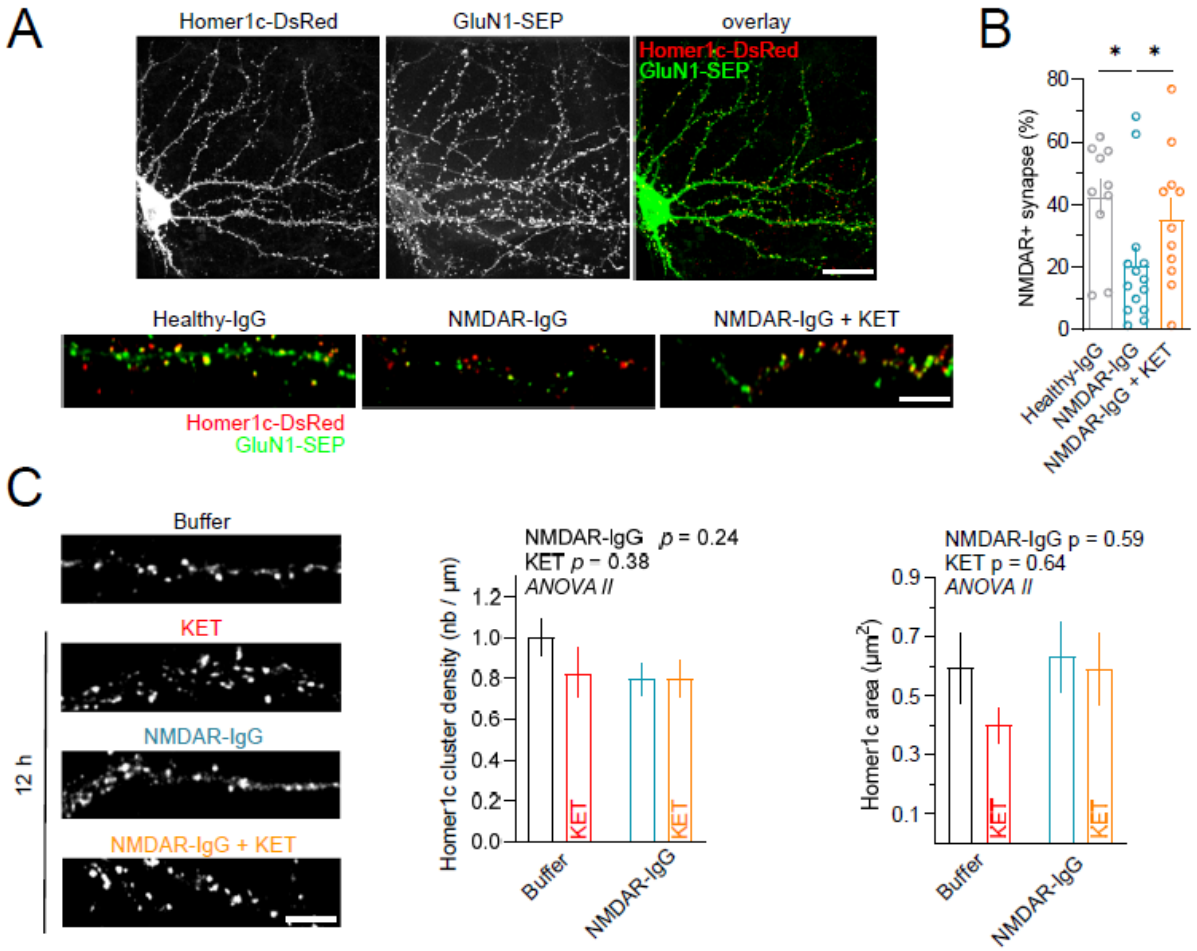

Figure S8: KET prevents synaptic NMDAR depletion and signalling deficits caused by patient-derived anti-NMDAR antibodies

(A) Upper panels, epifluorescence images of a neuron expressing Homer-DsRed and SEP-GluN1. Scale bar, 10 µm. Lower panels, representative epifluorescence images of Homer-DsRed (red) and SEP-GluN1 (green) expression on dendritic segments after 12h exposure to Healthy-IgG, NMDAR-IgG or NMDAR-IgG + KET (10 µM). Scale bar, 2 µm.

(B) Fraction of NMDAR cluster-positive synapses after 12h exposure to Healthy-IgG (grey; n = 10 cells), NMDAR-IgG (blue; n = 18 cells), NMDAR-IgG + KET (10 µM, orange; n = 11 cells). Data expressed as mean ± SEM. One-way ANOVA followed by Tukey's multiple comparison test, *$p < 0.05$.

(C) Left, representative epifluorescence images of dendritic segments immunostained for surface Homer1c after 12h exposure to buffer, KET (10 µM), NMDAR-IgG or NMDAR-IgG + KET (10 µM). Scale bar, 2 µm. Middle, Homer1c cluster density after 12h exposure to buffer (black; n = 35 cells), KET (10 µM, red; n = 19 cells), NMDAR-IgG (black; n = 44 cells), NMDAR-IgG + KET (10 µM, red; n = 41 cells). Right, Homer1c cluster area after 12h exposure to buffer (black; n = 40 cells), KET (10 µM, red; n = 36 cells), NMDAR-IgG (black; n = 36 cells), NMDAR-IgG + KET (10 µM, red; n = 37 cells). Data expressed as mean ± SEM.

Figure S9

Related to Fig. 7

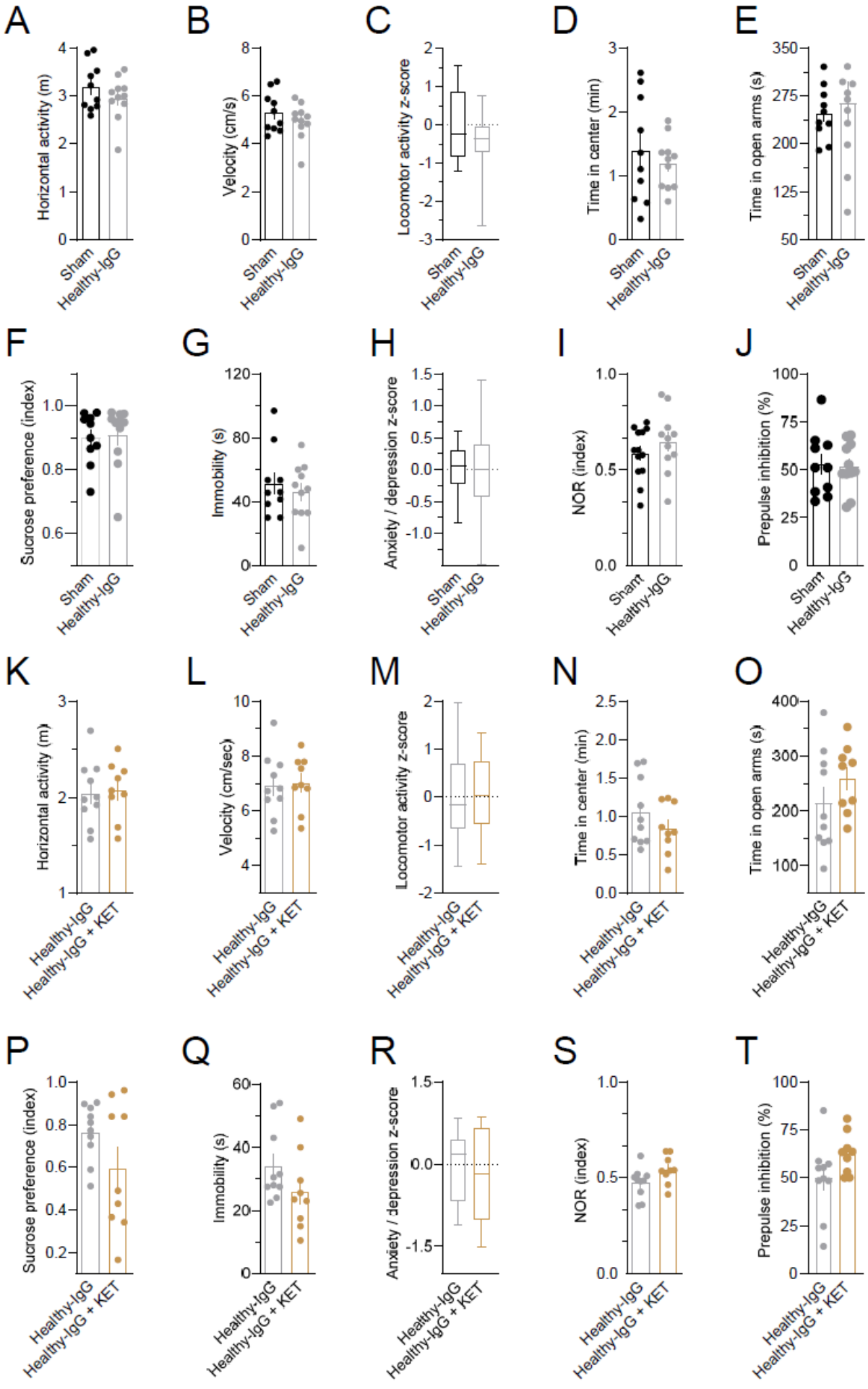

Figure S9: Immunoglobulins G from healthy individuals have no impact on behavioral performances

(A-J) Horizontal activity (A, open field), velocity (B, open field), Z-scores for locomotor activity (C) calculated from horizontal activity and velocity measurements, time in center zone (D, open field), time in open arms (E, elevated plus maze), sucrose preference index (F, sucrose consumption), time spent immobile (G, forced swim test), Z-scores for anxiety / depression (H) calculated from sucrose consumption, forced swim, open field and elevated plus maze tests, novel object recognition (I, NOR) index and prepulse inhibition of startle responses (J) of animals exposed to either saline (n = 10 rats) or Healthy-IgG (n = 11 rats). All data expressed as scatter dot plot with mean ± SEM except for (C) and (H) displayed as median ± 25-75% IQR (box) and 10-90% percentile (whiskers).

(K-T) Horizontal activity (K, open field), velocity (L, open field), Z-scores for locomotor activity (M) calculated from horizontal activity and velocity measurements, time in center zone (N, open field), time in open arms (O, elevated plus maze), sucrose preference index (P, sucrose consumption), time spent immobile (Q, forced swim test), Z-scores for anxiety / depression (R) calculated from sucrose consumption, forced swim, open field and elevated plus maze tests, novel object recognition (S, NOR) index and prepulse inhibition of startle responses (T) of animals exposed to either Healthy-IgG alone (n = 10 rats) or combined with KET (n = 9 rats). All data expressed as scatter dot plot with mean ± SEM except for (M) and (R) displayed as median ± 25-75% IQR (box) and 10-90% percentile (whiskers).

Results II: EXPLORING THE CONTRIBUTION OF DRUG-EVOKED NMDAR REDISTRIBUTIONS IN THE ANTIDEPRESSANT ACTION OF KETAMINE

Introduction

Major depressive disorder (MDD) is a leading cause of disability worldwide that affects about 7% of adults (Nemeroff, 2008). Current treatments, which include psychotherapies and pharmacological agents targeting aminergic systems (such as SSRIs, SNRIs, and MAOIs), often have a delayed onset of action, typically requiring several weeks to achieve significant clinical effects (Machado-Vieira et al., 2010). More importantly, still up to one-third of patients are resistant to these treatments (Insel and Wang, 2009). Thus, the recent discovery that a subanesthetic dose of ketamine, a non-competitive N-methyl-D-aspartate glutamate receptor (NMDAR) antagonist, induce a rapid-acting and sustained antidepressant effect has risen new hopes for the treatment of depression (Berman et al., 2000; Carlos A Zarate et al., 2006). Ketamine antidepressant and global psychotomimetic effects were initially thought to result from NMDAR inhibition but accumulating evidence suggests that additional mechanisms beyond receptor blockade are involved (Abdallah et al., 2018; Yang et al., 2018; Zanos et al., 2016). Ketamine may promote synaptic plasticity and enhance neural connectivity, particularly in brain regions involved in mood regulation, i.e. cortico-meso-limbic-striatal structures (Duman and Aghajanian, 2012). However, this is rather counterintuitive since ketamine blocks ion flow through NMDAR, and the exact mechanisms through which it alleviates symptoms in these brain regions remain unclear. Recent studies demonstrated that NMDAR-dependent synaptic plasticity may not invariably require calcium influx through the ion channel pore (Nabavi et al., 2013; Stein et al., 2020). Indeed, diffusion-based surface redistributions of NMDAR support their activity and therefore regulate synaptic plasticity processes supporting memory and cognition (Dupuis et al., 2014; Kellermayer et al., 2018). Moreover, disruptions in these NMDAR surface redistributions may play a crucial role in the development of neuropsychiatric diseases. Such impairment can cause profound cognitive and behavioral deficits, as observed in the presence of circulating anti-NMDAR antibodies from patients diagnosed with anti-NMDAR encephalitis (Jézéquel et al., 2017; Mikasova et al., 2012). We have previously shown than beyond the inhibition of ionotropic function, ketamine enhances NMDAR synaptic trapping, reducing anxio-depressive behavioral deficits caused by autoantibodies from patients with anti-NMDAR encephalitis (Villega et al, accepted in Neuron). Thus, we hypothesized that ketamine-elicited changes in NMDAR synaptic distribution may contribute to rearrangements in the functional connectivity of cortico-meso-limbic structures, supporting alleviation of depressive symptoms.

Materials and Methods

In vitro experiments

Cortical cultures

Primary cultures of cortical neurons mixed with glial cells were prepared from 14 embryonic day (E14) C57BL/6 mouse embryos. Cortical tissues underwent dissection and mechanical dissociation following a 15-minute treatment at 37°C with 0.05% Trypsin-EDTA 1X solution containing Penicillin-Streptomycin and HEPES. Neurons were plated at a density of 600 000 cells per dish onto poly-L-lysine pre-coated glass coverslips in 60 mm Petri dishes, using Neurobasal Plus Medium supplemented with 0.5 mM GlutaMAX, 1X B-27 Plus Supplement, and 1,5% horse serum. Full media exchange with Neurobasal Plus Medium supplemented with 1X B-27 Plus Supplement was done at 3 days in vitro (DIV). Overall, cultures were maintained at 37°C in 5% CO2 for up to14 days. Cells were exposed to either β-cyclodextrin (0.45%; solubilizing agent for CORT) alone (VEH) or combined with CORT (100 nM) for 72h. Ketamine (KET) was added to the medium and incubated for 90 min or 24 hours before imaging, at a concentration of 1 µM, which is within the range measurable in brain tissue following i.p injection of a subanesthetic dose that induces an antidepressant effect in mice (10 mg/kg).

Transfection

To incorporate specific DNA plasmids into neuronal cultures, neurons were transfected at DIV 11 following a calcium phosphate transfection method. DNA precipitates were prepared by mixing Homer-GFP, GluN1-mEos 3.2, GluN2A-mEos 3.2 and/or GluN2B-mEos 3.2 plasmids (at the concentration of 1 µg/coverslip) with the following solutions: TE buffer (1 mM Tris-HCl pH 7.3, 1 mM EDTA), $CaCl_2$ (2.5 M $CaCl_2$ in 10 mM HEPES, pH 7.2) and 2X HEPES-buffered saline (HEBS; 12 mM dextrose, 50 mM HEPES, 10 mM KCl, 280 mM NaCl and 1.5 mM Na2HPO4-2H2O, pH 7.2). Coverslips were transferred to 12-well plates containing 250µL/well of conditioned culture medium supplemented with 2 mM kynurenic acid (Sigma-Aldrich Labs, Saint-Louis, MO, USA, ref. N°K3375). 50µl of DNA precipitate solution was added to each well. Cells were incubated for 1 h at 37°C, then washed with supplemented Neurobasal medium containing 2 mM kynurenic acid. Coverslips were then transferred back to their original culture dishes filled with BrainPhys medium supplemented with B-27 Plus Supplement.

Photo-activated localization microscopy (PALM)

All PALM experiments were performed between DIV13 and DIV15. Coverslips were mounted on a Ludin chamber (Life Imaging Services, Basel, Switzerland) in 1 mL of their medium.

Images were acquired with a Nikon Ti-Eclipse microscope encased in an incubator box and an air heating system (Life Imaging Services). The microscope is also equipped with a Perfect Focus System (PFS), an Ilas² TIRF arm (Gataca Systems, Massy, France), an Apo TIRF 100X NA 1.49 oil-immersion objective, and an ORCA-Fusion BT sCMOS camera (Hamamatsu Photonics, Massy, France). First, transfected cells expressing Homer-GFP were detected with a 488 nm laser. Then, cells were simultaneously illuminated with two different lasers to allow for the detection of mEos 3.2 proteins: a 405 nm laser responsible for the photo-conversion and a 561 nm laser responsible for the excitation of these photo-converted molecules. The powers of both lasers were adjusted to maintain a constant stochastic activation of the molecules all along the acquisition. Images were acquired with Metamorph software (Molecular Devices, Sunnyvale, USA), mEos 3.2 dynamics were recorded for 2000 frames at 20 Hz acquisition rate.

Analyses and statistics

Data was processed with the PALMTracer plug-in running under the Metamorph software environment (J.B. Sibarita). Single molecules localizations were first performed by Gaussian fitting of mEos3.2 fluorescent signals. The two-dimensional trajectories (10 frames minimum) of single molecules in the plane of focus were then constructed by correlation analysis between consecutive images using a Vogel algorithm. For each track, the diffusion coefficient D was calculated by applying a linear fit on the first 4 points of the mean-square-displacement (MSD) versus time interval function using $MSD(t) = \langle r2(t) \rangle = 4Dt$. Image segmentation of Homer-labeled synaptic regions was performed to discriminate between synaptic and extrasynaptic compartments. Statistical analyses were performed with GraphPad Prism 8 software. ANOVA two-ways were performed to assess how corticosterone (first factor) and ketamine (second factor) affect the median diffusion coefficient D. For MSD distributions comparison, a Kolmogorov-Smirnov test was used. Significance levels were defined as $*p \leq 0.05$, $**p < 0.01$, $***p < 0.001$.

Ex vivo experiments

Animals

The ex vivo experiments were performed on a pharmacological model of depression (Brachman et al., 2016). Corticosterone (CORT) (Sigma Aldrich) was dissolved in its vehicle (cyclodextrine 0.45%) at a concentration of 35 µg/mL. C57BL/6 male mice were drinking either CORT or vector solution as a control for 5 weeks. Then, animals were sacrificed and transcardially perfused with 4% PFA. Brains were post-fixed for one night, rinsed, and kept in PBS at 4°C until further processing.

Immunolabeling and tissue clearing (iDISCO+)

Samples were prepared using the iDISCO+ procedure developed by Nicolas Renier (Renier et al., 2016, 2014). Briefly, samples first underwent a pre-clearing step for 5 days: samples were progressively dehydrated using increasing concentrations of methanol (MeOH), delipidated with a 66% dichloromethane (DCM)/ 33 % MeOH mix, bleached in a MeOH solution containing 5% hydrogen peroxide (H2O2) and progressively rehydrated in PBS. Then, samples were incubated for 10 days with a rabbit primary antibody directed against the immediate early gene *c-fos*, whose expression reflects neuronal activity (c-Fos antibody 226 008, Synaptic Systems). Once the primary antibody was washed, samples were incubated for 7 days with a donkey anti-rabbit secondary antibody Alexa Fluor 647 (ThermoFisher Scientific). Finally, samples were washed and dehydrated for 2 days with respectively PBS washes and H_2O/MeOH growing concentrations. On the last day, samples are incubated in a 66% DCM/ 33 % MeOH solution and transferred in dibenzyl ether (DBE) for storage until 3D imaging.

Light-sheet Microscopy

Samples were imaged using a light-sheet imaging microscope comprising an Andor Neo sCMOS camera and an Olympus MVPLAPO 2X objective (Ultramicroscope I, LaVision Biotec). Samples were first mounted on a specific holder and maintained with a crew in a position allowing sagittal optical sectioning. They were then placed under the microscope and were immersed in an ethyl-cinnamate bath that matched their refractive index (1.56) and oriented perpendicular to the light path. Acquisitions were done with ImspectorPro software (LaVision Biotec). For each sample, the left hemisphere was imaged by 3 light sheets of different angles that excite the sample from the right side with a vertical step size of 6 µm (NA 0.035). First, a 0.8X autofluorescence scan of the sample was performed with a 488 nm laser for 900 frames at 5 Hz acquisition rate for a final pixel size of 4.062*4.062*6 µm. Then, *c-fos-positive* cells were detected performing a 2X mosaic acquisition (5% overlap) with a 640 nm laser for 900 frames at a 33,3 Hz acquisition rate for a final pixel size of 1.625*1.625*6 µm.

Data extraction

Mosaic acquisitions were stitched using the Stitchy software (Translucence Bio). Quantifications were performed with the developed open-source ClearMap software (Renier et al, 2016). Image registration of the autofluorescence scan to the 3D annotated brain mouse atlas (Mouse P56 sagittal, Allen Institute Brain Atlases) and subsequent alignment to the *c-fos* scan were performed to identify brain areas. Detection of *c-fos*-positive cells involved cell nucleus identification via background subtraction, filtration and 3D peak detection to locate the nuclei accurately. We chose a threshold of 10 voxels for the cell size. A disk-shaped structure

element of 6 pixels of diameter was applied by subtraction to remove the background pixels below an intensity cutoff of 1000.

Data analyses

Analyses have been restricted to 17 regions shown to be involved in depression: basolateral amygdala (BLA), hippocampus (Hipp), lateral hypothalamus (LH), dorsomedial hypothalamus (DMH), subparaventricular zone of the hypothalamus (SPZ), suprachiasmatic nucleus (SCN), anterior cingulate cortex (ACC), infralimbic cortex (IF), prelimbic cortex (PL), dorsal raphe nucleus (DRN), ventral tegmental area (VTA), ventral pallidum (VP), laterodorsal tegmental nucleus (LTDg), pedunculopontine nucleus (PPN), central amygdala (CeM), nucleus accumbens (Nac) and lateral habenula (LHb). *c-fos* densities were calculated for each area by dividing the number of *c-fos* positive cells by the volume of the corresponding region (cells/mm^3). Functional connectivity has been analyzed for each condition to study network connectivity changes within meso-cortico-limbic-striatal circuits. Pearson correlation coefficients (r) were calculated for all pairs of possible correlations, 136 in total. Coefficients were then computed for all pairwise correlations at the level of 9 broad brain regions by grouping some of ROI: hippocampus (Hipp), medial prefrontal cortex (mPFC; grouping of anterior cingulate cortex (ACC), infralimbic cortex (IF) and prelimbic cortex (PL)) (Figure 2C), basolateral amygdala (BLA), hypothalamus (grouping of lateral hypothalamus (LH), dorsomedial hypothalamus (DMH), subparaventricular zone (SPZ) and suprachiasmatic nucleus (SCN)), midbrain (grouping of ventral tegmental area (VTA) and dorsal raphe nucleus (DRN)), ventral pallidum (VP), pons (grouping of pedunculopontine nucleus (PPN) and laterodorsal tegmental nucleus (LTDg)), striatum (grouping of central amygdala (CeM) and nucleus accumbens (Nac)) and lateral habenula (LHb). Connectivity matrices were generated from the values of the colour-coded r coefficients for all 17 ROI: negative correlations are represented by r values from -1 to 0, positive correlations are represented by r values from 0 to 1. From these matrices were built functional connectivity networks using significant correlations ($p<0.05$). Network density D was calculated using the number of regions involved in the network (nodes, N) and the number of correlations (edges, E) with the following formula: $D = (2*E) / (N*(N-1))$.

In vivo experiments

Animals

Ex vivo experiments were performed on a pharmacological model of depression (Brachman 2016). Corticosterone (CORT) (Sigma Aldrich) was dissolved in its vehicle (cyclodextrine 0.45%) at a concentration of 35 µg/mL. C57BL/6 male mice were drinking either CORT or

vector solution as a control for 5 weeks. Mice were maintained on a 12L:12D schedule (50-70% humidity, 25-26°C) and were housed with ad libitum access to food and water supplemented with either β-cyclodextrin (0.45%; solubilizing agent for CORT) alone for control groups (vehicle, VEH) or combined with CORT (35 µg/mL). After 5 weeks, animals were injected with either KET (10 mg/kg i.p) or vehicle. The battery of tests used to characterize anxiety/depression-like behavioral manifestations started 24 hours after injection. The experimental plan and all procedures were in accordance with the European guide for the care and use of laboratory animals and approved by the ethics committee of the University of Bordeaux (CE50) and the French Ministry of Research under the n ° APAFIS 27675.

Behavior

Before each experiment, mice were taken to the test room to acclimate them for at least 30 min to the room conditions. We performed a battery of tests designed to evaluate different modalities of the depressive-like phenotype. Arenas were cleaned with specific disinfectant surfactant between each trial (Aniospray surf 29).

Elevated O-maze

This test was performed on day 1, 24 h after the ketamine injection. The elevated O-maze was used to evaluate anxiety, indeed it is testing the conflict between the natural propensities of rodents for exploration and fear (Braun et al., 2011). Experiments were performed in a 50 cm diameter elevated O-maze containing 2 open sections without walls and 2 sections enclosed by 15 cm high walls. Each section was 40 cm long and 5 cm wide. The arena was illuminated with a dim light to have approximately a 50-lux light in open sections and a 30-lux light in closed sections. Mice were always placed at the entry of the same closed arm, their exploratory behavior was recorded for 10 min using a camera connected to the video tracking software EthoVision XT (Noldus). The time spent in open arms were subsequently measured.

Open field test

To measure anxiety and locomotor behavior, experiments were performed on day 2 in a homemade grey plexiglass open-field arena (45 cm long × 45 cm wide × 45 cm high) heterogeneously illuminated with a dim light to have around 50 lux in the center and 35 lux in the corners. Animals were always placed in the same corner to start the experiment. Mice were able to explore the empty arena for 10 min and novelty-induced locomotion was recorded by a camera connected to the video tracking software EthoVision XT (Noldus). For the analysis, the arena was virtually divided into an anxiety-provoking center zone (square comprising 50% of the arena) and a wall zone (the rest of the arena along the borders) usually

considered safer for the animals. The extracted parameters are the total traveled distance in meters and the velocity in cm/sec.

Novelty-suppressed feeding test

Experiments were performed on day 3 after the ketamine injection. Animals were food-deprived for a minimum of 12 hours, depending on the order of passage into the test of anxiety-related behavior. Two open homemade arenas filled with litter where a food pellet was placed in the brightly illuminated (around 200 lux) middle of the arena were used to monitor the behavior of two animals at the same time for 10 min. Animals were always placed in the same corner of the arena and the latency to eat the food pellet was subsequently measured.

Sucrose preference test

On the day preceding the test, mice were placed individually for 2 hours of habituation in cages containing 2 bottles of water, of which one with 1% sucrose. Mice were then water-deprived for 12 hours before the test. The following day (day 4), all the bottles were weighed and water-deprived mice were placed again in those cages for 4 hours, at the end of which bottles were weighed again to determine the volume consumption. Results are expressed in percentages, measuring the proportion of sucrose water intake relative to the total fluid intake consumed by the animals: sucrose preference (%) = $V_{(\text{sucrose intake})}/[V_{(\text{sucrose intake})}+V_{(\text{water intake})}] \times 100$.

Tail suspension test

Experiments were performed on day 5 after ketamine injection. Adhesive tape was placed approximately 1 cm from the end of the tail of the mice. Animals were then suspended approximately 10 cm above the floor in a homemade box and their escaping-related behavior was recorded for 6 min. Detection of movements to measure mobility time was then performed and subtracted from the total time of recording to identify immobility time. Small punctual movements of the head and the front paws were not considered as escape-intended behavior.

Z-score calculation

In order to normalize each behavioral test, a Z-score for all conditions in each test was calculated using the following formula : $Z = ((\text{value}_{\text{considered animal}})-(\text{mean}_{\text{CTRL group}}))/(SD_{\text{CTRL group}})$ (Guilloux et al., 2011). Z-scores from all behaviorals were then averaged for each animal in order to have a more global indication of the depressive-like behavior for each animal. Parameters considered to calculate the Z-score in each test were: % time in closed arms for the O-maze, cumulative duration in wall zones for the open-field, latency to eat for the novelty-suppressed feeding test, % water preference in sucrose preference test and immobility time in tail suspension test (Highland et al., 2021).

Results

Ketamine alleviates depression-like behavioral deficits caused by prolonged exposure to corticosterone

We first explored whether ketamine (KET) has the ability to improve depression-like behavioral manifestations in our experimental settings. To do so, we used a pharmacological model of depression where mice were provided with either vehicle (cyclodextrin, CTRL)- or corticosterone (CORT)-supplemented drinking water for 5 weeks (David et al., 2009). Animals then received either a vehicle (NaCl) or a KET (10 mg/kg) intraperitoneal (IP) injection and were submitted to a battery of tests starting 24h post-injection that were designed to evaluate the expression of different modalities characterizing a depression-like phenotype, i.e. expression of anxiety (elevated plus maze, open field, novelty-suppressed feeding test), anhedonia (sucrose consumption) and despair (tail suspension test) (Figure 1A).

For each test, ketamine injection in mice that were drinking vector solution (CTRL KET) did not induce behavioral changes by itself when compared to CTRL animals, as measured by the depression-like behavior Z-score calculated from a combination of all tests (Figure 1G). However, mice drinking CORT spent significantly less time in anxiogenic areas as measured in the O-maze and the open field (Figures 1B, 1D) and ketamine efficiently compensated for these deficits in the O-maze, as illustrated by KET improvement of CORT-induced decreased number of entries of animals in open arms highlighting the ability of KET to reduce anxiety-like behavior (Figure 1B). Food-deprived mice under CORT also displayed a significantly longer latency to reach food pellets in the center of the arena in the novelty-suppressed feeding test (NSFT), which was however not counteracted by KET (Figure 1C). Similarly, CORT induced despair in mice that was not significantly alleviated by KET, as reflected by the decreased latency to first immobility compared to other experimental conditions in the tail suspension test (Figure 1F).

Altogether, these data show that CORT does promote a depressive-like state in exposed mice, while KET efficiently compensates for only some of the modalities of the depression-like phenotype, i.e. anxiety-related behavioral deficits induced by chronic exposure to CORT (Figure 1G).

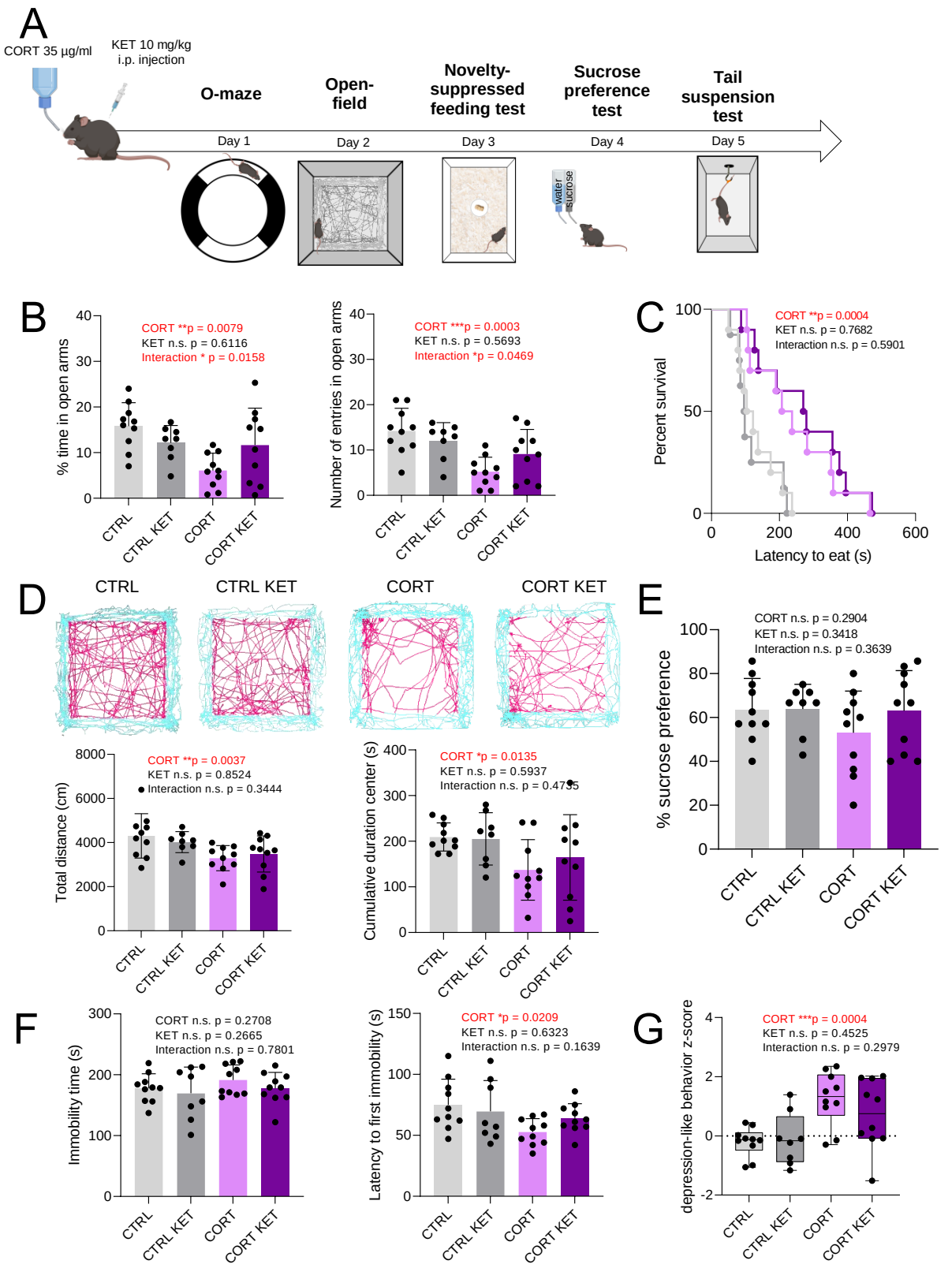

Figure 1: Ketamine alleviates depression-like behavioral deficits caused by prolonged exposure to corticosterone. (**A**) Timeline of behavioral testing. (**B**) Time in open arms (%) and number of entries in open arms performed by animals in the O-maze. (**C**) Kaplan-Meier survival curves for each group of animals representing the latency to eat (% of animals which did not eat as a function of time) in the novelty suppressed feeding test. (**D**) Upper panel, representative tracks of animals in the center zone (pink) and the wall zone (blue) of the open field arena. Lower panel, total distance traveled (cm, left) and cumulative duration in the center zone (s, right) of animals. (**E**) Sucrose preference percentage (uptake of sucrose water/total liquid uptake) of animals. (**F**) Time spent immobile (left panel) and latency to first immobility (right panel) of animals in the tail suspension test. (**G**) Z-scores for depression-like behavior calculated from the combination of all behavioral tasks (CTRL n = 10 animals; CTRL KET n = 8 animals; CORT n = 10 animals; CORT KET n = 10 animals). Statistics in each behavioral test: two-way ANOVA, * p < 0,05; ** p < 0,01; *** p < 0,001.

Chronic CORT exposure and 24h KET change functional connectivity in meso-cortico-limbic-striatal networks

KET is believed to alleviate depressive-like manifestations by inducing a wave of plasticity in meso-cortico-limbic neuronal networks supporting reward and mood where excitatory transmission is weakened in depression (Thompson, 2023). Using the same experimental paradigm, we investigated the changes in patterns of activity within these networks underlying the depressive-like behavioral manifestations caused by chronic CORT exposure and the antidepressant action resulting from KET IP injection. To do so, we relied on protocols developed by Renier and colleagues demonstrating that changes in brain activity, whether triggered by behavioral task or pharmacological treatment, can be visualized using a combination of tissue optical clearing, immediate early gene (IEG) labelling and light sheet microscopy (Renier et al., 2016)(Figure 2A). Expression of the IEG *c-fos* is a commonly-used molecular marker of neuronal activity. Indeed, functional connectivity has been widely assessed by examining *c-fos* expression patterns across regions after specific stimuli, hence revealing statistical relationships between neural activities, indicating how brain regions interact and communicate (Barth, 2007).

We limited the analysis of *c-fos* expression correlations to 17 regions of interest (ROI) shown to be involved in the expression of depression-like phenotypes in rodents (Figure 2B). First, we compared the impact of CORT, 24h KET, or their combination, on the correlation strengths of various ROI by examining the distribution of Pearson r values between groups. Overall, both CORT and KET treatments significantly decreased correlations in the 17 ROIs compared to CTRL, alike the combination of both treatments (Figure 2C).

Next, we performed a similar analysis at the level of 9 broader brain regions by grouping some ROI: hippocampus (Hipp), medial prefrontal cortex (mPFC; including anterior cingulate cortex (ACC), infralimbic cortex (IF), and prelimbic cortex (PL)), basolateral amygdala (BLA), hypothalamus (including lateral hypothalamus (LH), dorsomedial hypothalamus (DMH), subparaventricular zone (SPZ), and suprachiasmatic nucleus (SCN)), midbrain (including ventral tegmental area (VTA) and dorsal raphe nucleus (DRN)), ventral pallidum (VP), pons (including pedunculopontine nucleus (PPN) and laterodorsal tegmental nucleus (LTDg)), striatum (including central amygdala (CeM) and nucleus accumbens (Nac)), and lateral habenula (LHb) (Annex, Figure 1).

Some areas, such as the hippocampus and VP, did not show differences in correlation across treatments (Figure 2C, Annex Figure 1). However, 24 h KET significantly decreased r values in the mPFC, BLA, hypothalamus, midbrain, pons, striatum, and LHb. The interaction between

CORT and KET in the CORT KET mice was observed only in the mPFC, BLA, midbrain, pons, and striatum, with mostly a decreased r value compared to the CORT condition alone (Figure 2C, Annex Figure 1).

Interestingly, the mPFC and BLA were the only brain regions where KET compensated for the CORT-induced reduction in r values where in addition, mPFC was initially demonstrated a significant decrease in r values with CORT alone (Figure 2C, Annex Figure 1).

Next, to build correlation matrices, we focused the investigation on the 17 specific ROI, we were therefore investigating a total number of 136 possible correlations. Analyses of correlations matrices built for each condition revealed that the number of significant correlations vary between the groups, respectively: 64 positive correlations for CTRL group; 38 positive correlations for CTRL KET group; 36 positive correlations for CORT group; 40 positive correlations and 4 negative correlations for CORT KET group (Figure 2D). Percentages of involvement of each structure for each network are described in annex, table 1 (Figure 2E).

Functional connectivity network for CTRL group is the denser and more homogeneous network of all conditions (network density D = 0.47), showing a preferential involvement of BLA and LH whereas LHb is not involved in the network (Figure 2E; Annex, table 1). Functional connectivity matrix in the CTRL KET (D = 0.28) condition reveals more than 50% decorrelations of structures within the network compared to CTRL condition (38 correlations versus 64 correlations), with SPZ and PL being the main involved in the CTRL KET network (Figure 2D, 2E; Annex, table 1). Functional connectivity matrix in CORT-exposed animals reveals more than 50% decorrelations of structures within the network compared to CTRL condition (36 correlations versus 64 correlations), with SPZ and VP being the main structures involved in the CORT network (D = 0.26) (Figure 2D, 2E; Annex, table 1). These two observations suggest alterations of connectomes by CORT alone and KET alone. These alterations are similarly organized, with a loss of correlations within and with the striatum, pons, pallidum, midbrain and cortical subplate general anatomic areas (Figure 2B, 2E). However, when initially not part of the network in CTRL condition, LHb takes part respectively slightly in CTRL KET network and predominantly in CORT patterns of activity (Figure 2E). Compared to CORT group, CORT KET mice show the appearance of 4 negative correlations involving SCN with ACC, IL, VTA and Nac with VTA (Figure 2D, 2E). Furthermore, CORT KET network (D = 0.32) shows major involvements of BLA, LH, ACC and IF (Annex, table 1), and a loss of involvement of LHb in the network compared to CORT condition (Figure 2E).

Investigation of the involvement of each region into patterns of activities revealed that major involvement of mPFC areas is consistently found in the presence of ketamine; respectively PL in CTRL KET group and ACC, IF for CORT KET.

Altogether, these data suggest that the mPFC is a preferential target in the effects mediated by ketamine on meso-cortico-limbic-striatal circuit activity.

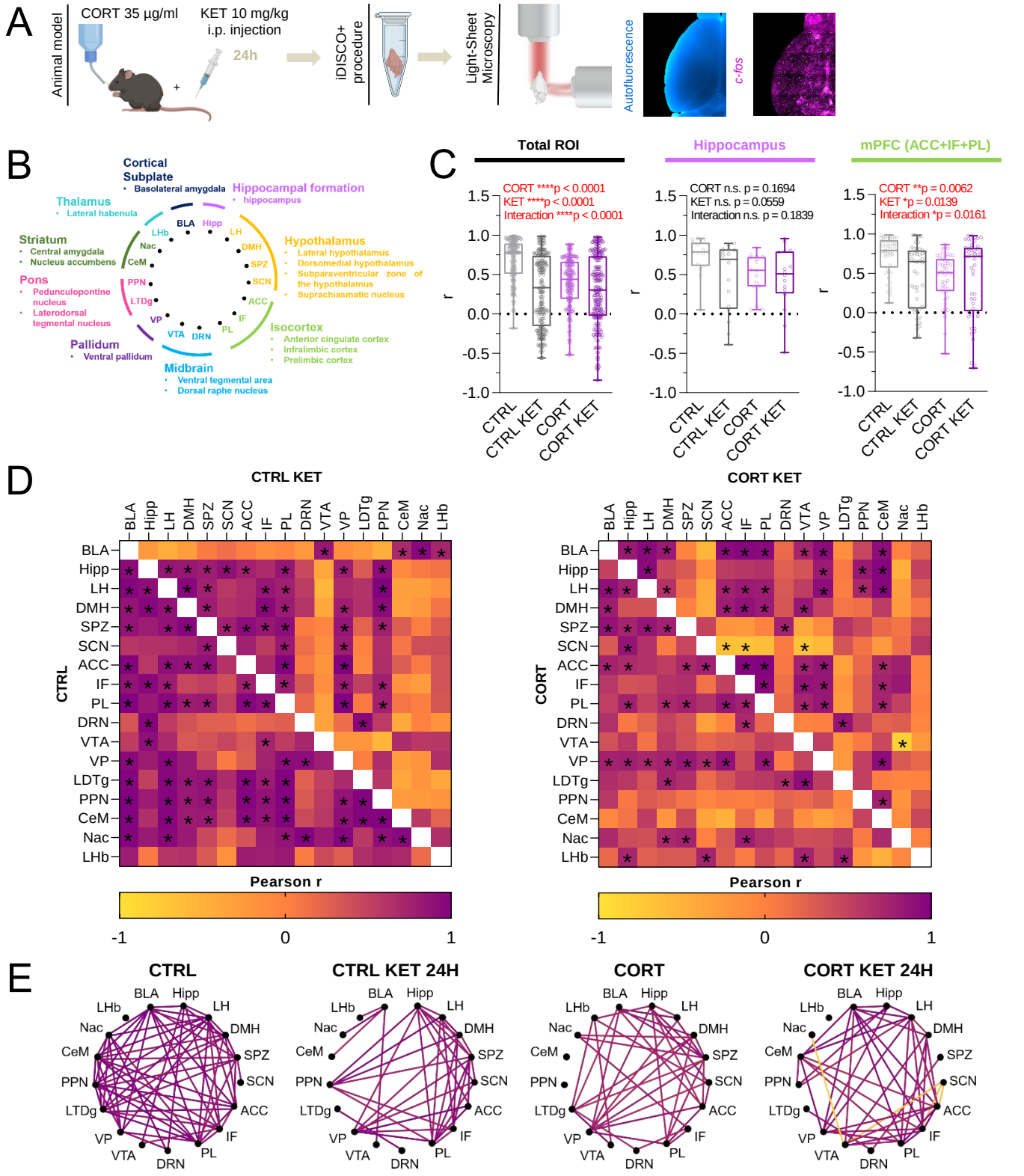

Figure 2: Ketamine induces changes in correlated activities within meso-cortico-limbic-striatal systems 24 hours after exposure. (A) Design of the experiment, mice are drinking corticosterone for 5 weeks and receive a ketamine injection. 24 hours after, brains are perfused and undergo iDISCO+ protocol before being imaged at the light-sheet microscope. (**B**) Chosen regions of interest (ROI) and their color-coded anatomic region origin according to the mouse Allen Brain Atlas (ABA). (**C**) Interregional correlation values (r) for all regions of interest (ROI, left), the hippocampus (middle) and the medial prefrontal cortex (mPFC), considered as the grouping of anterior cingulate cortex (ACC), infralimbic cortex (IF) and prelimbic cortex (PL) (right). Two-way ANOVA, ns, *p<0,05, **p<0,01, ****p<0,0001. (**D**) Matrices of functional connectivity revealing patterns of *c-fos* correlations according to conditions (CTRL n = 8; CTRL KET n = 9; CORT n = 10; CORT KET n = 9). (**E**) Network for each group built from significant correlations revealed in the matrices (*p<0.05). Purple connections represent positive correlations while yellow connections represent negative correlations. BLA: basolateral amygdala; Hipp: hippocampus; LH: lateral hypothalamus; DMH: dorsomedial hypothalamus; SPZ: subparaventricular zone of the hypothalamus; SCN: suprachiasmatic nucleus; ACC: anterior cingulate cortex; IF: infralimbic cortex; PL: prelimbic cortex; DRN: dorsal raphe nucleus; VTA: ventral tegmental area; VP: ventral pallidum; LTDg: laterodorsal tegmental nucleus; PPN: pedunculopontine nucleus; CeM: central amygdala; Nac: nucleus accumbens; LHb: lateral habenula.

Prolonged exposure (24h) to KET selectively enhances the synaptic trapping of GluN2A-NMDAR

NMDAR-dependent plasticity mechanisms in the PFC participate in the antidepressant action of KET (Thompson, 2023). We have previously shown that the initiation of NMDAR-dependent synaptic plasticity and cognitive functions such as memory formation involve activity-elicited, surface diffusion-based rearrangements in synaptic NMDAR (Dupuis et al., 2014). Building up on our observation that KET-elicited enhancement in NMDAR synaptic trapping restores synaptic signaling impairment and alleviates depression-related behavioral manifestations caused by patient antibodies (cf. Results I, Villéga et al., Neuron, in press), we then explored whether the stabilization of NMDAR at synapses was affected in our experimental conditions using photoactivated localization microscopy (PALM) on dissociated cortical neurons. In order to match *in vivo* experimental settings, cortical neurons were chronically incubated with either vehicle or corticosterone (CORT) for 3 days and KET (1 µM) or buffer was added to the culture medium after two days of treatment, i.e. 24 h before recordings (Figure 3A). As GluN2A- and GluN2B-subunit-containing receptors predominate in the cortex where their balance at synapses controls the threshold for plasticity, we focused our attention on these receptor subtypes and monitored the surface dynamics of recombinant GluN2A- and GluN2B-containing NMDAR labeled with the photoconvertible fluorescent protein mEos3.2 (Figure 3B).

Chronic CORT treatment had a limited impact on GluN2A-NMDAR and GluN2B-NMDAR surface diffusion properties both at synaptic and extrasynaptic sites, although enhanced synaptic confinement of GluN2B-NMDAR was observed when comparing CTRL and CORT conditions but without significant changes on diffusion coefficients (Figures 3C, 3D). However, administration of KET for 24h triggered a decrease in the diffusion and an increase in the confinement of GluN2A-NMDAR at synapses whether it was applied in the presence of CORT or not, with both CTRL and CORT conditions being significantly different from CTRL KET and CORT KET conditions, respectively (Figure 3C). It also enhanced confinement of extrasynaptic GluN2A-NMDAR when comparing CORT and CORT KET conditions but with no alteration to diffusion coefficients (Figure 3C). Interestingly, KET administration had no impact on the diffusion or confinement of synaptic GluN2B-NMDAR, suggesting that its action on synaptic GluN2A-NMDAR is subtype-selective (Figure 3D). Extrasynaptic GluN2B-NMDAR, though, displayed higher diffusion rates after 24h KET with or without CORT, as observed when comparing diffusion coefficient values of CTRL and CORT conditions with those of CTRL KET and CORT KET conditions, respectively, consistent with a decreased level of confinement in the CTRL KET condition compared to the CTRL condition on the MSD versus lag time plot (Figure 3D).

Importantly, the antidepressant action of KET has been proposed to rely on its metabolites rather than the drug itself (Zanos et al., 2016). In order to investigate whether the impact of KET on GluN2A-NMDAR was due to the molecule itself or to its by-products, we tested the effect of the metabolite mainly reported to have antidepressant action, (2R,6R)-HNK (10 µM), on both CTRL and CORT-exposed neurons (Figure 4A). PALM recordings revealed that (2R,6R)-HNK did not replicate KET-elicited synaptic trapping of GluN2A-NMDAR, supporting a direct action of the drug on the receptors (Figure 4B).

Altogether these results reveal that chronic CORT exposure does not affect NMDAR dynamics at the cell surface, while 24 h KET selectively enhances the synaptic retention of GluN2A-NMDAR and decreases the confinement of GluN2B-NMDAR in extrasynaptic compartments, whether applied in conjunction with CORT or not.

Observing a preferential retention of GluN2A-NMDAR at synapses 24 hours after ketamine, a time point when the drug is no longer present in its initial form in the cultures, led us to question the impact of ketamine in the short term, specifically during the initiation of the antidepressant effects reported by patients.

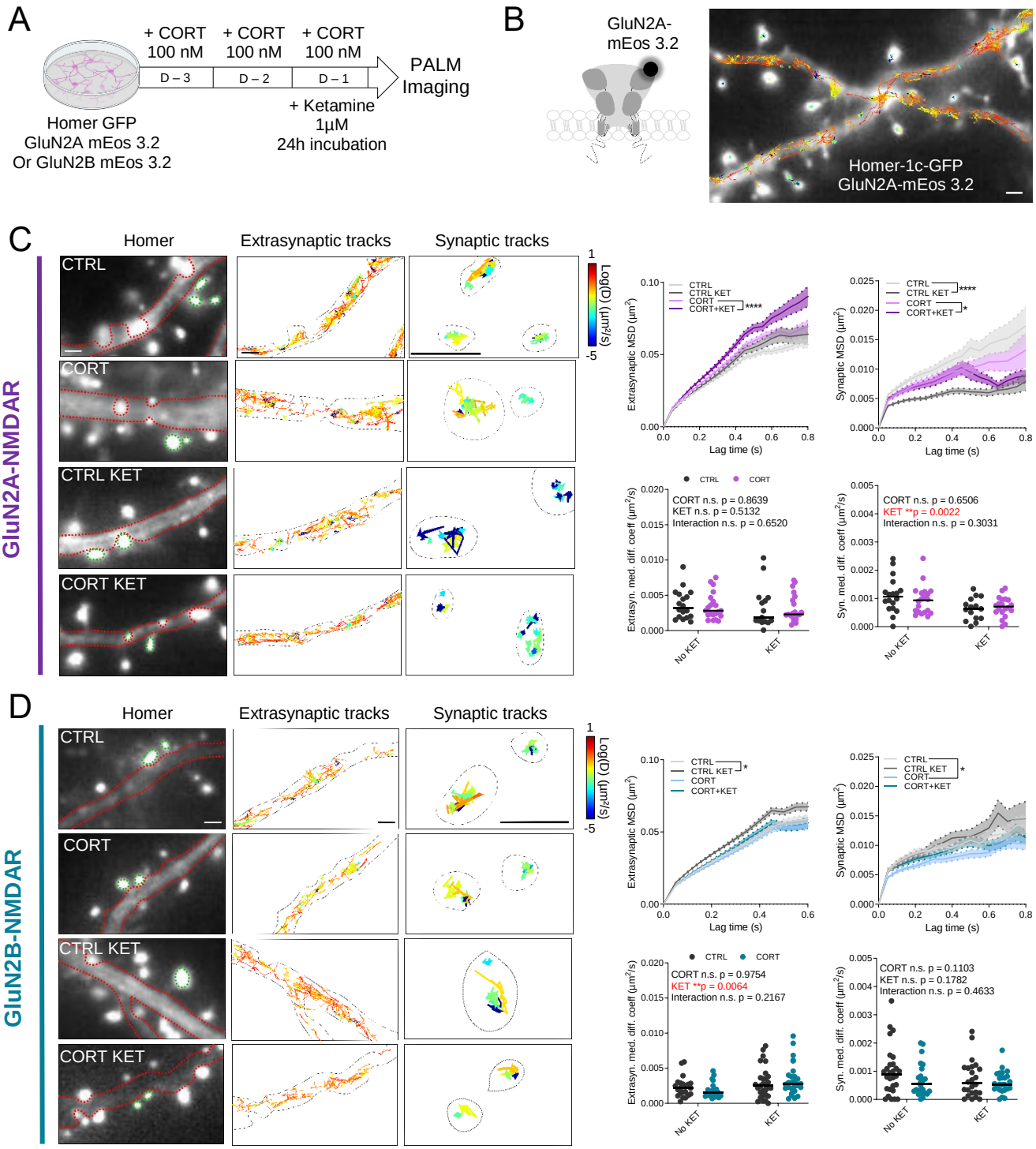

Figure 3: Prolonged exposure (24h) to KET selectively enhances the synaptic trapping of GluN2A-NMDAR. (**A**) Design of the experiment. Neurons were transfected with Homer GFP and GluN2A mEos 3.2 (or GluN2B mEos 3.2) and exposed to CORT for 3 days before the experiment. Ketamine was added 24h before the experiment. D = Day of the PALM live imaging experiment. (**B**) Left, schematic representation of GluN2A-NMDAR labelled with mEos 3.2. Right, superimposition of randomly colored GluN2A-mEos 3.2 trajectories along a cortical neuron dendrite labelled with Homer-1C-GFP as a synaptic marker. Scale bar, 1 µm. (**C**) Left, images of Homer synaptic labelling, extrasynaptic trajectories and synaptic trajectories of GluN2A-NMDAR according to conditions. Right, extrasynaptic and synaptic MSD curves (upper panels; data represented as mean ± SEM; Kolmogorov-Smirnov test, *p<0.05, ****p<0.0001) and median diffusion coefficients (lower panels; data represented as median ± min to max, two-way ANOVA, **p < 0,01) in CTRL (n = 18 neurons), CTRL KET (n = 15 neurons), CORT (n = 21 neurons), CORT KET (n = 21 neurons). (**D**) Left, images of Homer synaptic labelling, extrasynaptic trajectories and synaptic trajectories of GluN2B-NMDAR according to conditions. Right, extrasynaptic and synaptic MSD curves (upper panels; data represented as mean ± SEM; Kolmogorov-Smirnov, *p<0.05) and median diffusion coefficient (lower panels; data represented as median ± min to max; two-way ANOVA, **p < 0,01) in CTRL (n = 22 neurons), CTRL KET (n = 29 neurons), CORT (n = 22 neurons), CORT KET (n = 28 neurons) conditions.

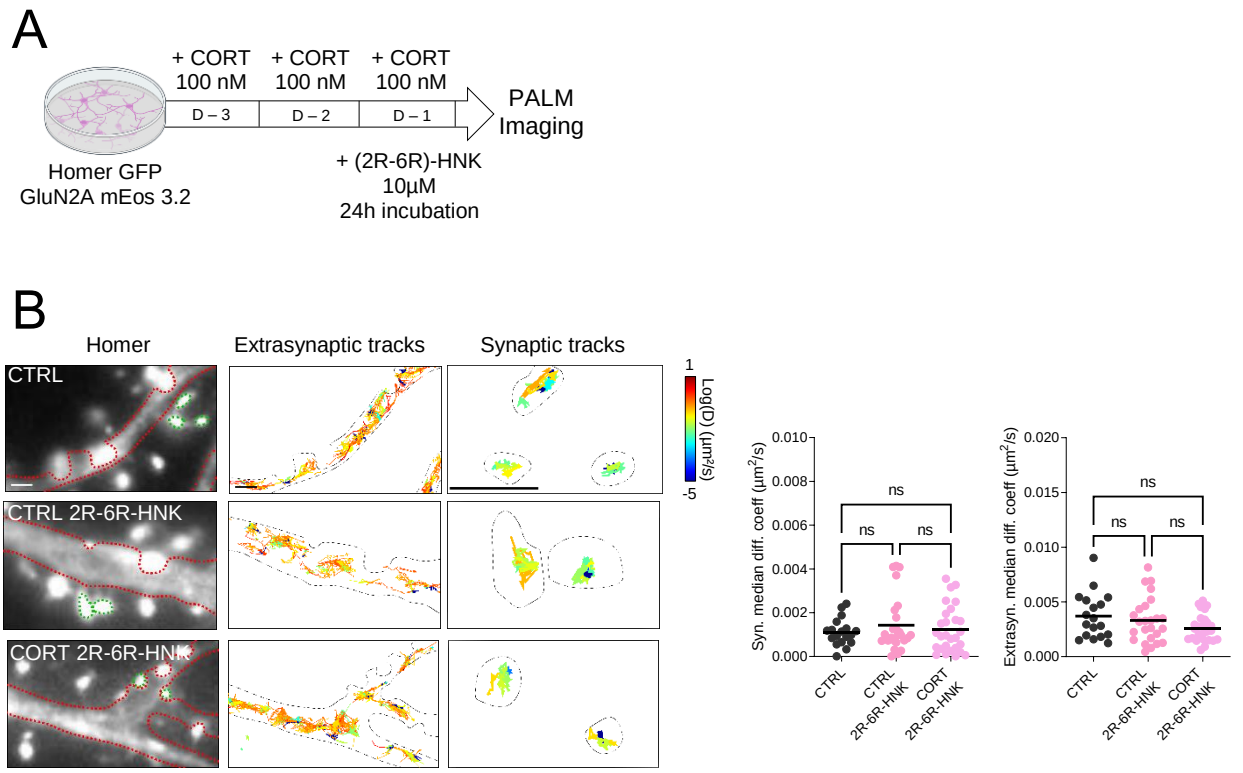

Figure 4: (2R-6R)-HNK does not recapitulate KET-elicited synaptic trapping of GluN2A-NMDAR. (A) Design of the experiment. Neurons were transfected with Homer GFP and GluN2A mEos 3.2 and exposed to CORT for 3 days before the experiment. The metabolite (2R-6R)-HNK was added 24 h before the live imaging. D = Day of the PALM live imaging experiment. (**B**) Left panels, images of Homer synaptic labelling, extrasynaptic trajectories and synaptic trajectories of GluN2A-NMDAR according to conditions. Right panels, synaptic and extrasynaptic median diffusion coefficients (data represented as median ± min to max, Kruskal-Wallis; p = 0.8555 for synaptic compartment; p = 0.1866 for extrasynaptic compartment) in CTRL (n = 18 neurons), CTRL (2R-6R)-HNK (n = 25 neurons), CORT (2R-6R)-HNK (n = 27 neurons) conditions. Note that the CTRL group is the same as CTRL group in Figure 3, as all 6 conditions have been performed at the same time on identical cultures.

Acute exposure (90 min) to KET selectively enhances the synaptic trapping of GluN2B-NMDAR

To better characterize the molecular mechanisms underlying the early onset of the antidepressant action of ketamine, we performed the similar experiment but adjusted the exposure time of KET from 24 h to 90 min (Figure 5).

Chronic CORT administration had limited impact on the surface diffusion properties of synaptic GluN2A-NMDAR and GluN2B-NMDAR, though it triggered an enhanced confinement of synaptic GluN2A-NMDAR when comparing CTRL and CORT conditions but with no impact on diffusion coefficients (Figures 5C, 5D). While it did not affect extrasynaptic GluN2B-NMDAR either, the CORT treatment produced a significant decrease in the diffusion and an increase in the confinement of GluN2A-NMDAR at extrasynaptic locations whether KET was co-applied or not, with both CTRL and CTRL KET conditions being significantly different from CORT and CORT KET conditions, respectively (Figure 5C). Acute (90 min) KET application also had little influence on the diffusion properties of synaptic GluN2A-NMDAR, although it enhanced their confinement as observed when comparing MSD distributions of CTRL and CORT conditions with those of CTRL KET and CORT KET conditions, respectively (Figure 5C). However, the administration of KET triggered a significant decrease in the diffusion and an increase in the confinement of both synaptic and extrasynaptic GluN2B-NMDAR regardless of the presence of CORT, with both CTRL and CORT conditions being significantly different from CTRL KET and CORT KET conditions in the two compartments, respectively (Figure 5D).

Together, these results indicate that acute exposure to KET favors the trapping of GluN2B-NMDAR, both at synaptic and extrasynaptic sites and regardless of the application of CORT. They also show that chronic CORT enhances the confinement of extrasynaptic GluN2A-NMDAR, suggesting that both molecules may act on the regulation of NMDAR diffusion-trapping but through independent and non-compensatory pathways.

We next sought to investigate if these preferential effects of KET at 90 min had a repercussion at the brain activity level.

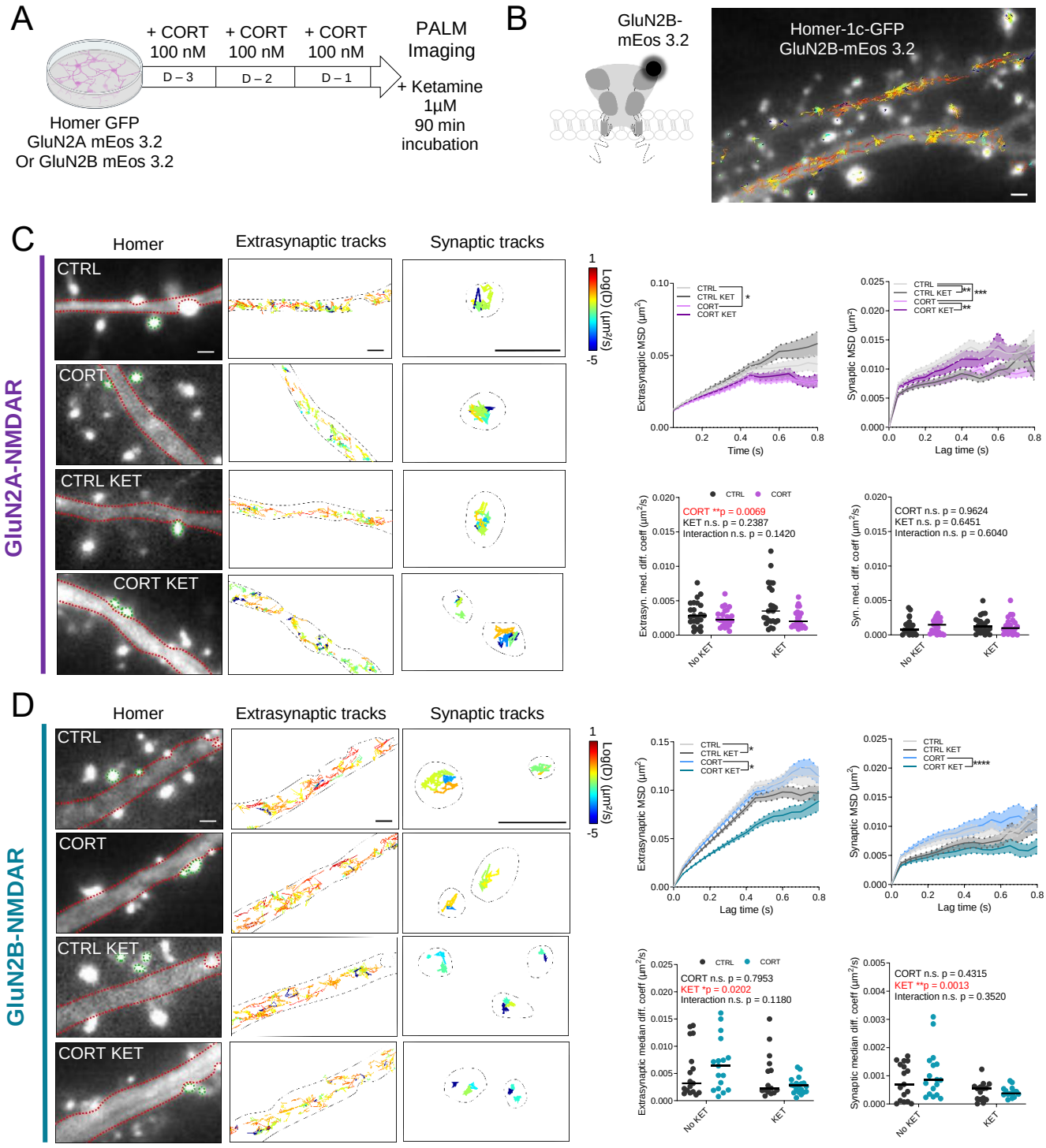

Figure 5: Acute exposure (90 min) to KET selectively enhances the synaptic trapping of GluN2B-NMDAR. (A) Design of the experiment. Neurons were transfected with Homer GFP and GluN2A mEos 3.2 (or GluN2B mEos 3.2) and exposed to CORT for 3 days before the experiment. Ketamine was added 90 min before the live imaging. D = Day of the PALM live imaging experiment. (B) Left, schematic representation of GluN2B-NMDAR labelled with mEos 3.2. Right, superimposition of randomly colored GluN2B-mEos 3.2 trajectories along a cortical neuron dendrite labelled with Homer-1C-GFP as a synaptic marker. Scale bar, 1 µm. (**C**) **Data acquisition and analysis by Lina Sikouk, M2 intern**. Left, images of Homer synaptic labelling, extrasynaptic trajectories and synaptic trajectories of GluN2A-NMDAR according to conditions. Right, extrasynaptic and synaptic MSD curves (upper panels; data represented as mean ± SEM; Kolmogorov-Smirnov *p<0.05, **p<0.01, ***p<0.001) and median diffusion coefficients (lower panels; data represented as median ± min to max, two-way ANOVA, **p<0,01) (CTRL n = 23 neurons, CTRL KET n = 24; CORT n = 23; CORT KET n = 22). (**D**) Left, images of Homer synaptic labelling, extrasynaptic trajectories and synaptic trajectories of GluN2B-NMDAR according to conditions. Right, extrasynaptic and synaptic GluN2B-NMDA MSD curves (mean ± SEM, *p<0.05, ****p<0.0001; Kolmogorov-Smirnov) and median diffusion coefficient (median ± min to max, two-way ANOVA, *p<0,05, **p<0,01) in CTRL (n = 17 neurons), CTRL KET (n = 15 neurons), CORT (n = 17 neurons), CORT KET (n = 19 neurons).

Meso-cortico-limbic-striatal functional connectivity shows fewer changes 90 min after KET

Observing preferential retention of GluN2B-NMDAR at synapses following 90 min of ketamine exposure suggested an early initiation of activity changes. Therefore, we sought to investigate whether functional connectivity within brains of different conditions was varying concomitantly with NMDAR dynamic changes. Therefore, we performed, as previously shown on figure 2A, a combination of *c-fos* labelling, tissue clearing and light-sheet imaging on depressive-like mice exposed to 5 weeks on CORT (35 µg/ml) and receiving an injection of KET (10 mg/kg). Brains were perfused 90 min after the ketamine injection.

We limited the analysis of *c-fos* expression correlations to 17 ROI known to be involved in depression-like phenotypes in rodents (Figure 2B). First, we compared the impact of CORT, 90 min KET, or their combination on the ROI correlation strengths by examining the distribution of Pearson r values between groups. Overall, only the 90 min KET exposure significantly decreased correlations in the 17 ROI compared to CTRL (Figure 6A).

Next, we performed a similar analysis at the level of 9 broader brain regions by grouping some ROI, as previously done (Figure 6A, Annex Figure 2). Only the basolateral amygdala (BLA) did not show differences in correlation across treatments (Annex Figure 2). In the mPFC, both CORT and KET individually decreased r values compared to CTRL, with no significant effect of their interaction (Figure 6A). The interaction between CORT and KET in the CORT KET mice was observed only in the lateral habenula (LHb) and pons. In the pons, the r value decreased compared to CORT alone, while in the LHb, KET counteracted the effect of CORT by increasing correlations of the structure with the rest of the network (Annex Figure 2).

Then, to build correlation matrices, we focused the investigation on the 17 specific ROI, we were therefore investigating a total number of 136 possible correlations. Analyses of correlations matrices built for each condition revealed that the number of significant correlations vary between the groups, respectively: 83 positive correlations for CTRL group; 76 positive correlations for CTRL KET group; 86 positive correlations for CORT group; 55 positive correlations for CORT KET group (Figure 6B). Percentages of involvement of each structure for each network are described in annex table 2 (Figure 6B).

The functional connectivity networks in CTRL (D = 0.61), CTRL KET (D = 0.56), and CORT (D = 0.63) conditions were dense, homogeneous, and quite similar, whereas the CORT KET network appeared less dense and homogeneous (D = 0.40) (Figure 6C). Although different animals were used, both the CTRL and CORT groups were processed under the same

conditions as shown in Figure 2. However, the results in Figure 5 revealed different patterns. LH and SPZ were mainly involved in CTRL networks while VP, CeM and Nac were mainly involved in CORT networks (Annex, Table 2). The only consistent predominant structure involved in both CORT networks is VP (Annex, Tables 1, 2). LHb only take part CORT KET network, and not in depressive-like mice of CORT group (Figure 6C).

Ninety minutes after KET administration, Nac is the predominant actor in the CTRL KET network, while Hipp is the predominant actor in the CORT KET network (Annex, Table 2).

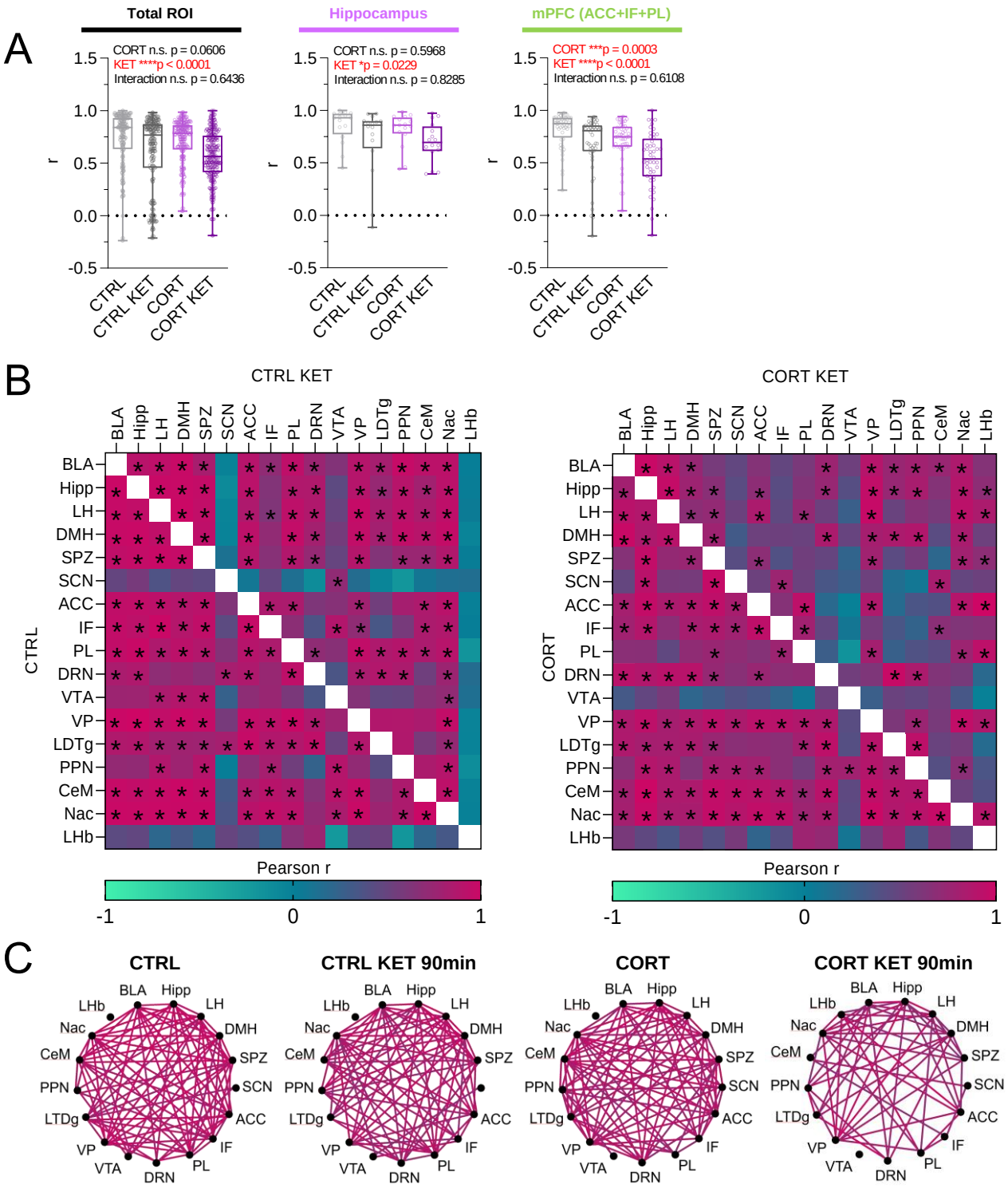

Figure 6: Acute exposure (90 min) to KET induces few changes in correlated activities within meso-cortico-limbic-striatal systems. (**A**) Interregional correlation values (r) for all regions of interest (ROI, left), the hippocampus (middle) and the medial prefrontal cortex (mPFC), considered as the grouping of anterior cingulate cortex (ACC), infralimbic cortex (IF) and prelimbic cortex (PL) (right). Two-way ANOVA, ns, *p<0,05, ***p<0,001, ****p<0,0001. (**B**) Matrices of functional connectivity revealing patterns of *c-fos* correlations according to conditions (CTRL n = 7; CTRL KET n = 9; CORT n = 8; CORT KET n = 10). (**C**) Network for each group built from significant correlations revealed in the matrices. Connections are color-coded according to pearson r value (*p<0.05). BLA: basolateral amygdala; Hipp: hippocampus; LH: lateral hypothalamus; DMH: dorsomedial hypothalamus; SPZ: subparaventricular zone of the hypothalamus; SCN: suprachiasmatic nucleus; ACC: anterior cingulate cortex; IF: infralimbic cortex; PL: prelimbic cortex; DRN: dorsal raphe nucleus; VTA: ventral tegmental area; VP: ventral pallidum; LTDg: laterodorsal tegmental nucleus; PPN: pedunculopontine nucleus; CeM: central amygdala; Nac: nucleus accumbens; LHb: lateral habenula.

Discussion

Choosing the corticosterone model to study depression at different scales

We chose to work on a neuroendocrine model of depression by chronically exposing C57BL/6 mice to corticosterone. This approach allowed us to compare our *in vivo* and *in vitro* studies more efficiently. Using a pharmacological strategy helps ensured establishment of the neurochemical environment of depression, making it consistent with the investigation of molecular mechanisms and neural circuitry. Usually, behavioral models of depression such as the chronic mild stress (CMS) model and the chronic social defeat stress (CSDS) are preferred and more commonly used. They both rely on exposure to environmental factors, with CSDS being more ethologically valid (Qiao 2016). However, even if these models are closer to real-life conditions under which patients develop depression, i.e. etiological validity, these protocols can be complicated to reproduce. For instance, CMS model presents high variability due to individual vulnerability and concomitant presence of susceptible genes, and the nature and intensity of stressors used (Willner, 2017). Similarly, the CSDS model requires careful animals handling and pairing of aggressors with the tested mouse, a lack of pairing consistency as well as aggressor behaviors increase variability of responses (Kim 2017). In contrast, the CORT model that we used tends to present high reproducibility for several reasons. First, dose and exposure time of corticosterone are controlled. Second, it triggers a consistent behavioral phenotype. Third, it is physiologically relevant as high levels of cortisol consequently to HPA axis hyperactivation are present in 73% of depressed patients (Stetler and Miller, 2011). Furthermore, it has been demonstrated that serum cortisol levels are proportional to the severity of the disease, this has been concluded from the observation of a significant positive correlation between serum cortisol levels and severity of symptoms measured by the HDRS scale (Zobel, 2001). Both models share common outcomes, for example CMS and CORT model are altering hippocampal neurogenesis (Willner, 2017). While the CORT model replicates certain modalities of the disease, it does not reproduce the entire range of physiological alterations and symptoms seen in clinics. Consequently, because of the multifactorial nature of depression, relying on a single model is not ideal and combining at least two models would provide more complete insights.

Another notable point in our study is that we limited the investigations to male mice, despite depression being more prevalent in women (Kuehner, 2017). The CORT model of depression displays major sex differences, making its use limited in females. Indeed, prolonged CORT exposure in females does not produce anxio-depressive-like behaviors, and it has been suggested that females may develop a tolerance to high dosages of CORT (Mekiri et al., 2017). This tolerance is believed to be influenced by hormonal differences (Seney et al., 2012).

Furthermore, the CORT model is not the only one displaying sex differences. For instance, the social defeat model successfully induces a depressive phenotype in male mice, but not in females, where aggressive behaviors are less common (Solomon, 2017). Similarly, female sensitivity to CMS is variable and highly dependent on the mouse strain and the behavioral tests used (Mineur et al., 2006). Consequently, obtaining data on the mechanisms of depression in females remains challenging.

CORT-exposed mice present deficits in each test except in the sucrose preference test (SPT)

We performed a series of behavioral tests designed to evaluate different aspects of depressive-like behavior. As revealed by the O-maze, open field, NSFT, TST and the ultimate calculation of a Z-score, 5 weeks of CORT did induce a depressive-like phenotype in mice, as previously reported (David et al., 2009; Hache et al., 2012). However, the effect was not recapitulated in the fourth test, the sucrose preference (SP) test. This test indexes anhedonia, which is a core symptom of depression characterized by a diminished ability to experience pleasure and happiness. In animal models of depression, a reduction in sucrose preference is a strong and reliable indicator of depressive-like phenotype. Therefore, it is puzzling that we did not observed any changes in the sucrose preference of CORT-exposed mice. Due to logistic constraint relative to the serial aspect of our battery in a short time, animals have been habituated for 4 hours in individual cages the day before the test. We then measured SP the following day, by placing the animals back in their individual cages for 4 hours. However, cage changes is not optimal as they can cause leakage of solutions, ultimately leading to increased variability in the results (Serchov et al., 2016). According to a meta-analysis, baseline levels of SP are usually above 80% for control animals while depressed-like mice under chronic mild stress (CMS) for 4 weeks display an impaired SP of 40 to 50% (Antoniuk et al., 2019). In our study, baseline levels in CTRL mice exposed solely to vehicle (cyclodextrine 0.45%) were above 60% while CORT-exposed mice displayed 53% preference for sucrose. This indicates a lack of specificity, which could be due to insufficient habituation or measurement time, or the fact that mice were subjected to other behavioral tests in the preceding three days. Typically, SP testing involves a longer acclimatization period to the two-bottle choice setup, ranging from 24 hours to 5-7 days (Ding et al., 2018; Serchov et al., 2016). However, a 2-hour SP test (1%) of mice exposed for 21 days to a CORT solution at a dose lower than ours (25 µg/ml vs 35 µg/ml) is sufficient to observe significant anhedonic behavior (Zhao et al., 2024). This suggests that our inability to measure anhedonia is more likely due to insufficient acclimatization time rather than the measurement duration. Furthermore, other adjustments can be made to increase SPT resolution in our study, such as, i) the establishment of a baseline level for SP prior to CORT exposure to reduce individual variability, meaning that changes in SP can be

better attributed to CORT treatment rather than pre-existing differences in animals; ii) switching bottle positions in the middle of the testing to reduce potential side preference effect; iii) avoiding to perform NSFT before SPT to avoid sequential food deprivation followed by water deprivation; iv) introducing the animals to sucrose taste before data collection to reduce the effect of neophobia, either by the establishment of a baseline level (see i)) or by increasing sucrose concentration during habituation (Strekalova and Steinbusch, 2010).

On a final note, some tests can be less sensitive to CORT treatments, guiding our choices in behavioral assessments. For instance, while both the tail suspension test (TST) and the forced swim test (FST) measure behavioral despair, the TST shows increased sensitivity for the detection of antidepressant effects compared to the FST (Castagné et al., 2011). In a mouse model of schizophrenia, the effects of a single dose of ketamine are detected in the TST but not in the FST, indicating that the TST is better suited for measuring the impact of acute neurochemical changes (Chatterjee et al., 2012). In addition, chronic CORT exposure in mice produces a depressive-like phenotype measured in the open field (OF) and novelty-suppressed feeding test (NSFT) but not in the FST (David et al., 2009). One aspect missing in our study is the impact on working memory (WM). Indeed, WM deficits are major cognitive impairment observed in MDD patients (Chen et al., 2023). Radial arm maze (RAM) and T maze are commonly used to assess working spatial memory in rodents (Dominguez et al., 2019; Kohler et al., 2022).

Ketamine compensates for modalities of depression-like phenotype

Ketamine fully reversed anxiety-related deficits in the O-maze test. However, this effect did not persist in subsequent tests. When calculating Z-scores, we observed a distinct response to ketamine between our two cohorts within the CORT KET group: the first cohort did not respond to ketamine treatment, as its Z-score was comparable to the CORT group, while the second cohort Z-score aligned with the CTRL group, suggesting an antidepressant response. Conducting the experiment once more in a third cohort of animals is necessary to validate the long-lasting ketamine antidepressant effects under our experimental conditions.

We used a racemic mixture of (R,S)-ketamine, composed of equal parts of (R)-ketamine and (S)-ketamine (esketamine). In 2019, the FDA approved esketamine as an adjunct treatment for patients with treatment-resistant depression (TRD) alongside a primary oral antidepressant (Cristea and Naudet, 2019). (S)-ketamine has a fourfold higher affinity for NMDAR (Ki = 0.30 µM) and possesses three to four times greater anesthetic potency compared to (R)-ketamine (Ki = 1.40 µM) (Domino, 2010; Domino et al., 1965). A racemic mixture of (R,S)-ketamine displays an intermediate affinity for NMDAR (Ki = 0.53 µM) (Ebert et al., 1997). Research has

primarily focused on esketamine due to its NMDAR-blocking property, which is believed to underlie its antidepressant effects (Li et al., 2010; Wilkinson and Kitay, 2020). In TRD patients, esketamine has shown rapid antidepressant effects that can last up to two months, and it also reduces suicidal ideation (Canuso et al., 2018; Daly et al., 2018). However, the precise molecular mechanisms behind esketamine antidepressant action remain unclear. In healthy subjects, esketamine can cause severe psychomimetic side effects by increasing cerebral metabolic rates of glucose (CMRglu) (Vollenweider et al., 1997). In contrast, (R)-ketamine induces lower CMRglu levels in the brain, resulting in fewer psychomimetic side effects and a lower potential for abuse (Vollenweider et al., 1997; Yang et al., 2015).

In animal models, comparison studies of the antidepressant effect of (R,S)-ketamine, (R)-ketamine and (S)-ketamine have been conducted. For instance, (R,S)-ketamine (10 mg/kg) and (R)-ketamine (10 mg/kg), but not (S)-ketamine (10 mg/kg), reversed the depressive-like behavior of rats exposed to chronic CORT injections for 21 days, in the FST 24 h after a single i.p. injection (Fukumoto et al., 2017). Furthermore, in the tail suspension test (TST) in mice, (R,S)-ketamine and (R)-ketamine continued to exhibit antidepressant effects 48 hours after injection, whereas (S)-ketamine did not (Fukumoto et al., 2017). This suggests that (R,S)-ketamine and (R)-ketamine exhibit more antidepressant potency than (S)-ketamine. These results have been confirmed on mice undergoing chronic social defeat stress (CSDS) with a single intranasal administration of the different compounds at the same doses of 10 mg/kg (Chang et al., 2019). Analyses of FST results 24 hours post-treatment indicated that the order of antidepressant potency is (R)-ketamine > (R,S)-ketamine > (S)-ketamine, while the order of psychomimetic potency is (S)-ketamine > (R,S)-ketamine > (R)-ketamine (Chang et al., 2019).

Collectively, these data support a rapid-onset and lasting antidepressant action of (R)-ketamine, which is free of the psychomimetic effects seen with (S)-ketamine and, to a lesser extent, (R,S)-ketamine. To note, the potency of antidepressant effect of ketamine isomers does not appear to correlate with their NMDAR antagonism potency, indicating that NMDAR blocking may not be the main mechanisms underlying the antidepressant action of ketamine. A recent meta-analysis reviewing 24 clinical trials confirmed that (R,S)-ketamine exhibit greater responses and remission rates than esketamine (Bahji et al., 2021).

Lastly, there is still no clear consensus on the molecular mechanisms that explain the different antidepressant potencies of (R)-ketamine and (S)-ketamine. Unlike (S)-ketamine, the antidepressant effect of (R)-ketamine was believed to be mediated by the activation of TrkB receptors through BDNF enhancement, while other studies suggested that the antidepressant

actions of both isomers involve BDNF-TrkB activation (Rafało-Ulińska and Pałucha-Poniewiera, 2022; Yang et al., 2015). Moreover, contradictory results also suggest the involvement of mTOR and ERK pathways in the antidepressant effects of (R)-ketamine and (S)-ketamine, attempting to explain the differences in their potencies, but a clear conclusion is still lacking (Rafało-Ulińska and Pałucha-Poniewiera, 2022; Yang et al., 2018). Hence, our inability to reproduce the long-lasting antidepressant effect of (R,S)-ketamine beyond 24 hours in subsequent tests may be due to the different susceptibilities of the isomers in CORT-exposed mice.

Ketamine-induced brain functional connectivity rewiring is different between initial and later phase of the establishment of the antidepressant effect

To assess the global impact of ketamine antidepressant effects, we selected two specific timepoints for measuring brain functional connectivity: 90 minutes and 24 hours. We chose to investigate the establishment of the antidepressant effect at 90 minutes, as it aligns with the onset of symptom relief observed in patients (Lapidus et al., 2014; Carlos A Zarate et al., 2006). Additionally, c-Fos protein levels are known to peak between 1.5 to 2 hours after neural activity induction (Chaudhuri et al., 2000). At 24 hours, we focused on connectivity changes to coincide with the conclusion of the synaptic plasticity window triggered by ketamine, once the drug has been metabolized, signifying the onset of the antidepressant maintenance phase (Moda-Sava et al., 2019). Moreover, c-Fos protein levels remain detectable at this stage, as observed in studies on chronic stress (Lin et al., 2018; Matsuda et al., 1996). Our methodology combines *c-fos* detection with light sheet microscopy to measure these changes.

Ketamine at 90 min versus at 24 hours produced different network rearrangements within meso-cortico-limbic-striatal systems. Ketamine mainly enhances nucleus accumbens (Nac) and hippocampus (Hipp) connectivity within 90 min while active regions at 24 hours involve the subparaventricular zone (SPZ), basolateral amygdala (BLA), lateral hypothalamus (LH) and most of all medial prefrontal cortex (mPFC).

The Nac (nucleus accumbens) is a brain region within the ventral striatum that, along with the ventral tegmental area (VTA), forms the well-characterized VTA-Nac dopaminergic pathway, a crucial element of the reward circuit (Russo and Nestler, 2013). This pathway also connects midbrain areas, such as the laterodorsal tegmentum (LTDg) and the rostromedial tegmentum (RMTg), to other limbic and cortical areas like BLA and Hipp, thereby driving reward-related behaviors through various types of neurotransmitter modulation processes (Berridge and Kringelbach, 2015; Russo and Nestler, 2013). The Nac has been implicated in the psychomimetic effects of phencyclidine, the parent compound of ketamine, which shares

ketamine binding site on NMDAR (Steinpreis and Salamone, 1993). The psychomimetic effects of a subanesthetic dose of ketamine typically occur within an hour following the infusion in depressed patients (Berman et al., 2000). More precisely, psychiatric symptoms measured by the Brief Psychiatric Rating Scale (BPRS) occur during the first 30 to 60 minutes after ketamine exposure in depressed patients in 72 % of studies (Tashakkori et al., 2021). Nac activity is likely to decrease gradually, rendering this region a minor actor in the maintenance of antidepressant effects 24 hours post-exposure, as we observe in our study.

Additionally, as the Nac is dysfunctioning in MDD, ketamine may target this area among others to modulate its activity. Indeed, MDD patients display Nac hypertrophy compared to healthy humans (Abdallah et al., 2017). And considering the network dimension, functional connectivity between Nac and mPFC are driving anhedonia modality in depression, as well as in antidepressant response. A recent study shows that ketamine (administered as a single i.p injection of 10 mg/kg) enhances functional connectivity, 24 hours post exposure, between glutamatergic inputs from the mPFC and Hipp to dopaminergic neurons in the Nac thereby reducing anhedonia in mice exposed to chronic CORT (Lucantonio et al., 2023). In our study, we observed Nac involvement in the 90 minutes network, which has been reduced in the 24 hours network. Hence, our study supports the idea that counteracting Nac dysfunction induced by depression may be a crucial role of ketamine in establishing and maintaining its antidepressant effect.

Sleep disturbances and MDD are bidirectionally related. Beyond being a consistent symptom of the disease, sleep dysfunction can serve as a predictor, as individuals with sleep disturbances have twice the risk of developing MDD (Baglioni et al., 2011). The most common sleep disturbance in MDD patients is insomnia (88%), highlighting the ability of depression to disrupt sleep patterns and circadian rhythms (Song and Zhu, 2021). In addition to its antidepressant effects, ketamine has been shown to improve sleep quality in depressed patients (Duncan et al., 2019). The suprachiasmatic nuclei (SCN) and its main efferent target, the subparaventricular zone of the hypothalamus (SPZ), are key structures in regulating circadian rhythms and controlling sleep/wake cycle parameters (Lu et al., 2001). Modulation of their activity, notably by the anesthetic isoflurane, has been suggested to be associated with dysregulated circadian rhythms and sleep-wake alternation (Hu et al., 2024). Hence, the increased involvement of the SPZ in CTRL KET and CORT 24 h networks suggests modifications in sleep patterns and circadian rhythms.

5 weeks of CORT did not have a consistent effect on brain networks

In our study, we observed that CORT impacted brain networks more deeply at the 24 h timepoint compared to the 90 min timepoint, despite the conditions being identical for both experiments. Indeed, the CORT network was denser in the 90 min experiment (D = 0.63) compared to the 24 h experiment (D = 0.26). When considering changes in correlation strength in broad brain regions, the effect of CORT was less clear, as it was occurring in only the midbrain, LHb and mPFC in the 90 min experiment, whereas it affected the mPFC, hypothalamus, pons, and striatum in the 24 h experiment. Notably, the mPFC is the more consistent target across all analyses in these experiments.

One explanation of these differences could be related to *c-fos* expression. Although still detectable up to one week after activation, protein levels of expression are weaker than after 30-60 min, indicating a transient activation (Lin et al., 2018). Indeed, *c-fos* detection technique is known for its low temporal resolution, peaking approximately 2 hours after induction, which limits its ability to capture rapid neuronal activity changes occurring within minutes (Kovács, 2008). Additionally, although *c-fos* is more expressed in excitatory neurons than inhibitory neurons in the cerebral cortex and hippocampus, it does not allow to decipher neuron subtypes, thereby limiting interpretations regarding involvement in different neurotransmitter systems at the brain level (Filipkowski et al., 2000).

The use of transgenic mice, like FosTRAP2 mice, would allow for direct labelling of *c-fos* positive cells and provide finer control of its temporal window of expression through tamoxifen administration (DeNardo et al., 2019). Furthermore, in order to enhance temporal resolution and gain deeper insights into the dynamics of changes following KET treatment *in vivo*, functional *c-fos* imaging using superparamagnetic iron oxide nanoparticles (SPIONs) hybridizing with *c-fos* mRNA and detectable in real-time MRI could be a complementary approach (Liu et al., 2007).

The medial prefrontal cortex (mPFC) as a hub for the maintenance of the antidepressant effect

We show that ketamine is able to counteract CORT-induced activity dysregulations in the mPFC, 24 hours after exposure, once the antidepressant effect has been established. The mPFC governs high executive functions and plays key roles in various cognitive processes such as decision making, attention, memory and emotional control (Bittar and Labonté, 2021; Euston et al., 2012). It is thus not surprising that impairment in mPFC functioning and structure are consistently found in MDD patients, with consensual evidence of volume reduction and functional connectivity alterations (Pizzagalli and Roberts, 2022).

Over the years and with functional magnetic resonance imaging (fMRI) development, the investigation of brain dysregulations in depression has evolved. Indeed, initially focused on segregated structural and functional changes, researchers now have a broader approach by examining brain interactions and connectivity patterns changes. This shift has led to an update of the concept of depression as a network-based disorder (Mulders et al., 2015). Two different types of network organizations in the human brain operate in balance: a resting state network (RSN) or default mode network (DMN), and task positive networks (TPN)(Di and Biswal, 2014). The DMN corresponds to a pattern of coordinated brain region activity when a person is at rest and not involved in a task but rather in self-referential mental activities (Davey et al., 2016). This network includes the precuneus/posterior cingulate cortex (PCC), the medial prefrontal cortex (MPF), and medial, lateral, and inferior parietal cortex (Raichle et al., 2001).

Depressed patients present an hyperactivity of the DMN, thought to lead to excessive self-focus and rumination, and a decreased connectivity within TPN (Knyazev et al., 2018). More precisely, the central executive network (CEN) and the salience network (SN) are the main hypoactivated TPN in MDD (Mulders et al., 2015). The CEN consists of the lateral prefrontal cortex, the posterior parietal cortex (PPC), the frontal eye fields (FEF) and part of the dorsomedial prefrontal cortex (dmPFC) and is involved in attention and working memory while the SN includes the fronto-insular cortex, the dorsal ACC, the amygdala and temporal poles and is implicated in emotion regulation (Mulders et al., 2015).

Besides being characterized as a hub region for the expression of depressive symptoms in humans, complementary evidence from clinical studies supports the mPFC as a key structure in mediating antidepressant effects. In humans, alleviation of depressive symptoms by electroconvulsive therapy (ECT) has been related to improved connectivity in DMN, where network-based analysis show decreased brain activity in the PFC and prominent changes in its functional connectivity (Qi et al., 2020). Regarding pharmacotherapies, the prefrontal cortex serves as an imaging biomarker of therapeutic response in MDD patients (Fonseka et al., 2018). Indeed, reductions in prefrontal activity are consistent among responders and absent in non-responders, indicating its crucial role in mediating antidepressant effects (Cook and Leuchter, 2001).

The effect of ketamine in healthy subjects has been well described but to a lesser extent in the context of depression. However, this has implications for the antidepressant action of ketamine, as the molecule decreases functional connectivity of the DMN (Scheidegger et al., 2012). Furthermore, recent reports suggest that ketamine adjusts prefrontal brain functional

connectivity in depressed patients. 24h after a 45-min infusion of ketamine at the subanesthetic dose of 0.5 mg/kg, MDD patients exhibit enhanced connectivity between the subgenual anterior cingulate cortex (sgACC) and the right lateral PFC, associated to relief of depressive symptoms (Gärtner et al., 2019). In TRD patients, ketamine infusion (0.5 mg/kg over 40 min) increased functional connectivity of the sgACC with the perigenual ACC (pgACC) and anterior ventromedial PFC (vmPFC), and this correlates with an improvement in anhedonia scores (Alexander et al., 2023). In a recent study of TRD patients, ketamine increased connectivity between frontal and limbic regions 24 hours post-infusion, associated to an improvement of the depressive symptoms (Rengasamy et al., 2024). Thus, ketamine modulates both intraconnectivity within prefrontal areas and interconnectivity with other brain regions, highlighting the medial prefrontal cortex (mPFC) as a central hub in depressed patients.

Ketamine enhancement of prefrontal regions functioning is also supported by molecular studies in rodents. Despite distinct anatomical definition of prefrontal regions between humans and rodent, functional homology has been identified. These regions are involved in both species in executive functions, decision-making, working memory, and social behaviors (Euston et al., 2012; Kesner and Churchwell, 2011) More specifically, the rodent infralimbic (IF) cortex is analogous to the human subgenual ACC (sgACC); the prelimbic (PL) area corresponds to the perigenual ACC (pgACC); both IL and PL are also analogous to the human ventromedial PFC (vmPFC); and the rodent ACC is analogous to both the human dorsal ACC (dACC) and ventral ACC (vACC) (Alexander et al., 2023; Laubach et al., 2018). Hence, even if cross-species comparisons are challenging, rodent studies on prefrontal areas provide valuable insights in the understanding of the neurobiological basis of anti-depressant effects of molecules like ketamine. In our study, we investigated the IF, PL, and ACC separately and, for simplification, referred to their combination as the medial prefrontal cortex (mPFC).

At the network level, 24 hours after ketamine, we observed a recovery of the functional connectivity between IF and ACC that was lost in CORT-mice, consistent the pivotal role of the sgACC in ketamine-mediated antidepressant effect in depressed patients. Furthermore, ketamine uniquely increased connectivity within the mPFC (ACC+IF+PL), counteracting CORT-induced decrease in connectivity. In rats, a 10 mg/kg ketamine injection increased BOLD signal connectivity within prefrontal and hippocampal regions, particularly the IF, within 15 minutes (Gass et al., 2014). Accumulating evidence suggest that ketamine promotes synaptic plasticity via mTORC1 signaling and synaptogenesis, which mitigates behavioral deficits in rodents (Duman et al., 2016). In fact, chronic CORT exposure in rats induces functional and structural changes in the mPFC, which are counteracted 24 hours after a 10

mg/kg injection of ketamine (Mingardi et al., 2023). Hence, a subanesthetic dose of ketamine impact both neuronal synaptic plasticity processes and broader patterns of functional connectivity across the brain.

CORT has no effect on GluN2A- or GluN2B-NMDAR diffusion

In depressed patients, hypercortisolemia and abnormal glucocorticoid receptor (GR) and mineralocorticoid receptor (MR) signaling are key factors in the hyperactivation of the HPA axis. In rodents, corticosterone (CORT) is the major glucocorticoid hormone secreted by the adrenal gland as part of the hypothalamic-pituitary-adrenal (HPA) axis response to stress (Nandam et al., 2020). To mimic the *in vivo* conditions of stressed mice, we modeled chronic stress in cultures by chronically applying for 72 hours CORT to cortical cultures.

Regarding glucocorticoids, their effects in the brain can vary depending on the dose and duration of exposure. CORT demonstrates a U-shaped dose-response relationship in the brain (Joëls, 2006). In organotypic hippocampal cultures, CORT induces apoptosis at a concentration of 1 µM and necrosis at 10 µM over a 72-hour period role of the mPFC (Kurek et al., 2016). Therefore, we selected a concentration of 100 nM based on previous research, aiming to saturate glucocorticoid receptors (GR, Kd ~ 1-5 nM; MR, Kd ~ 0.3 nM) and to avoid the pro-apoptotic effects observed at higher concentrations of CORT (Joëls, 2006; Mikasova et al., 2017).

At 100 nM, CORT enhances GluR2-AMPAR synaptic content through increased lateral diffusion in rat hippocampal cultured neurons, concomitant with an increase in the amplitude of miniature excitatory postsynaptic currents (mEPSCs) (Groc et al., 2008; Karst and Joëls, 2005). Furthermore, acute CORT administration for 20 minutes rapidly regulates GluN2B-NMDAR surface dynamics and synaptic content through MR signaling in hippocampal neurons, which is associated with an enhancement of NMDAR-mediated mEPSCs (Mikasova et al., 2017). Here, we show that chronic CORT exposure (72 hours) has no impact on GluN2A-NMDAR or GluN2B-NMDAR surface diffusion in cortical neurons.

CORT mainly mediate its effects in the brain through the activation of high-affinity mineralocorticoid receptors (MR) and low-affinity glucocorticoid receptors (GR), which can thereby either modulate specific gene expression (genomic action) or directly act on the intracellular environment notably through signaling pathway activation (non-genomic action) (Panettieri et al., 2019). GR and MR are expressed differently across human and rodent brains. In the human central nervous system, GR are primarily expressed in the frontal cortex, hypothalamus, hippocampus, and cerebellum, while MR are mostly expressed in the

hippocampus and limbic lobe (Singh et al., 2023). In rodents, GR are widely expressed throughout the brain, whereas MR expression is predominantly in limbic regions such as the hippocampus, amygdala, and lateral septum (McCann et al., 2021).

CORT lack of effect on NMDAR surface dynamics in our cortical neuronal cultures may be attributed to the predominant expression of glucocorticoid receptor (GR) rather than mineralocorticoid receptor (MR), which has been shown to mediate CORT action on NMDAR surface diffusion (Mikasova et al., 2017). Alternatively, this lack of effect could also be due to the difference in exposure duration (20 minutes versus 72 hours), suggesting that longer exposures may induce compensatory mechanisms aimed at promoting homeostasis.

Synaptic trapping of NMDAR as a therapeutic target

In cortical cultures, we observed that a subanesthetic dose of ketamine sequentially enhances the trapping of GluN2B-NMDAR shortly after exposure. Subsequently, the trapping of GluN2A-NMDAR occurs, aligning with the persistence of these effects even after the drug has been eliminated, i.e. 24 hours after.

GluN2A- and GluN2B-NMDAR form distinct protein complexes and initiate different signaling cascades, resulting in distinct contributions of these two NMDAR subtypes to synaptic plasticity processes. (Dupuis et al., 2023; Kellermayer et al., 2018). As a consequence, their regulation governs synaptic plasticity driven-processes, such as brain development, memory, and cognitive functions (Paoletti et al., 2013). More specifically, GluN2B-NMDAR function and organization are notably regulated by its interaction with CaMKII. This interaction favors GluN2B-NMDAR trapping and the intracellular redistribution of CaMKII, promoting the induction of long-term potentiation (LTP) at glutamatergic synapses (Dupuis et al., 2014; Shipton and Paulsen, 2014). On the other hand, GluN2A-NMDAR are less crucial for LTP induction but are still important for its maintenance. They primarily act as ionotropic calcium providers in the postsynaptic density (PSD), generating distinct calcium dynamics in the postsynapse (Franchini et al., 2020; Sun et al., 2017). Indeed, GluN2A-NMDAR allow for a moderate and transient influx of Ca^{2+} whereas GluN2B-NMDAR facilitate rapid and substantial Ca^{2+} influx (Deep et al., 2019; Paul and Connor, 2010).

Thus, the preferential retention of GluN2B-NMDAR at synapses following 90 minutes of ketamine exposure aligns with early synaptic plasticity processes that support the onset of its antidepressant effect (Duman et al., 2016). Similarly, the preferential anchoring of GluN2A-NMDAR at synapses may sustain these effects through the maintenance of synaptic plasticity, consistent with the prolonged antidepressant effect lasting several days to a week. (Berman

et al., 2000; Carlos A Zarate et al., 2006). As a next step, we aim to investigate whether manipulating initial synaptic trapping of GluN2B-NMDAR with competing peptides can prevent ketamine-induced redistributions, thereby examining its therapeutic implications.

Indeed, the enhancement of synaptic receptors associated with plasticity processes has emerged as a promising therapeutic strategy. Ketamine and fluoxetine have the ability to bind receptors for BDNF, i.e. TrkB receptors (TrkBR). Through allosteric modulation, they promote TrkB membrane trafficking to favor their cell surface expression and subsequent BDNF signaling involved in the antidepressant effect (Casarotto et al., 2021). Furthermore, a recent study conducted by Moliner and colleagues (2023) show that lysergic acid diethylamide (LSD) and psilocin (PSI) enhance the retention of TrkBR at synapses. Indeed, these psychedelics bind with high affinity to TrkBR and through positive allosteric modulation, stabilize these receptors in an active conformation. This maintains their anchoring in membrane lipid rafts, thus promoting prolonged BDNF signaling and synaptic plasticity (Moliner et al., 2023).

Therefore, our data support the idea that various types of psychoactive molecules, such as ketamine, mediate antidepressant effects independently of direct action on the signaling function of post-synaptic receptors at synapses and that these receptor surface reorganizations may explain their prolonged effects.

Ketamine effect on NMDAR retention at synapses may not involve metabolites action

As other NMDAR antagonists failed to replicate the antidepressant effect of ketamine, accumulating evidence points to its mediation through the action of its metabolites, particularly hydroxynorketamines (HNK), i.e. (2R-6R)-HNK and to a less extent (2S-6S)-HNK (Highland et al., 2021). Thus, we investigated if ketamine-elicited NMDAR were attributable to the molecule itself or the action of (2R-6R)-HNK. We show that the antidepressant dose of 10 µM in CORT chronically exposed neurons did not reproduce the anchoring effect on GluN2A-NMDAR of ketamine, 24 hours after exposure.

Similarly to ketamine, a single injection of the metabolite (2R,6R)-HNK (10 mg/kg) has been shown to alleviate anhedonic behaviors in rats exposed to chronic CORT, without reproducing its psychoactive side effects (Zanos et al., 2016). This study further demonstrate that the metabolite enhances glutamatergic signaling independently of NMDAR signaling, but rather through a synaptic upregulation of AMPAR in the hippocampus (Zanos et al., 2016). The impact of (2R,6R)-HNK of AMPAR signaling has also been shown in other structures like the mesencephale or the nucleus accumbens, but whether this may be associated with its antidepressant effect remain unclear (Qu et al., 2021).

In our study, complementary experiments assessing (2R,6R)-HNK impact on GluN2B-NMDAR or AMPAR surface trafficking would allow for better understanding of its underlying molecular mechanisms.

Conclusion

To conclude, we provide valuable insights into the molecular mechanisms and network functional connectivity reorganizations that may contribute to the antidepressant effect of ketamine. The manipulation of NMDAR synaptic trapping within specific brain areas may directly compensate for depression-induced connectivity alterations, opening new therapeutic strategies that avoid the undesirable side effects associated with direct signaling alterations attributable to current psychoactive molecules.

Annexes

Regions of interest	CTRL group	CTRL KET group	CORT group	CORT KET group
BLA	18.75	10.52631579	13.88888889	20.45454545
Hipp	9.375	21.05263158	19.44444444	11.36363636
LH	18.75	15.78947368	11.11111111	20.45454545
DMH	14.0625	18.42105263	16.66666667	13.63636364
SPZ	14.0625	23.68421053	22.22222222	2.272727273
SCN	1.5625	10.52631579	11.11111111	6.818181818
ACC	14.0625	10.52631579	16.66666667	20.45454545
IF	14.0625	15.78947368	8.333333333	20.45454545
PL	17.1875	23.68421053	16.66666667	18.18181818
DRN	4.6875	2.631578947	5.555555556	2.272727273
VTA	3.125	2.631578947	5.555555556	15.90909091
VP	10.9375	18.42105263	22.22222222	15.90909091
LTDg	14.0625	2.631578947	11.11111111	2.272727273
PPN	17.1875	15.78947368	0	6.818181818
CeM	17.1875	2.631578947	0	18.18181818
Nac	10.9375	2.631578947	8.333333333	2.272727273
LHb	0	2.631578947	11.11111111	0

Table 1: Percentage of involvement of each region of interest in the network for each condition for the 24h experiment. The number of significant correlations for each area has been counted and divided by the total number of significant correlations for the considered group, then transformed into percentages. In orange has been underlined the regions that show the largest involvement in the network for each condition. Linked to figure 2C.

Regions of interest	CTRL group	CTRL KET group	CORT group	CORT KET group
BLA	14.45783133	17.10526316	11.62790698	16.36363636
Hipp	14.45783133	15.78947368	15.11627907	20
LH	15.6626506	17.10526316	11.62790698	16.36363636
DMH	14.45783133	15.78947368	12.79069767	16.36363636
SPZ	15.6626506	14.47368421	13.95348837	12.72727273
SCN	2.409638554	1.315789474	9.302325581	3.636363636
ACC	14.45783133	13.15789474	13.95348837	12.72727273
IF	14.45783133	9.210526316	11.62790698	5.454545455
PL	14.45783133	15.78947368	6.976744186	10.90909091
DRN	8.43373494	13.15789474	12.79069767	9.090909091
VTA	7.228915663	3.947368421	1.162790698	0
VP	14.45783133	13.15789474	16.27906977	18.18181818
LTDg	13.25301205	9.210526316	12.79069767	9.090909091
PPN	7.228915663	10.52631579	12.79069767	12.72727273
CeM	14.45783133	11.84210526	16.27906977	5.454545455
Nac	14.45783133	18.42105263	16.27906977	18.18181818
LHb	0	0	0	12.72727273

Table 2: Percentage of involvement of each region of interest in the network for each condition for the 90 min experiment. The number of significant correlations for each area has been counted and divided by the total number of significant correlations for the considered group, then transformed into percentages. In orange has been underlined the regions that show the largest involvement in the network for each condition. Linked to figure 3A.

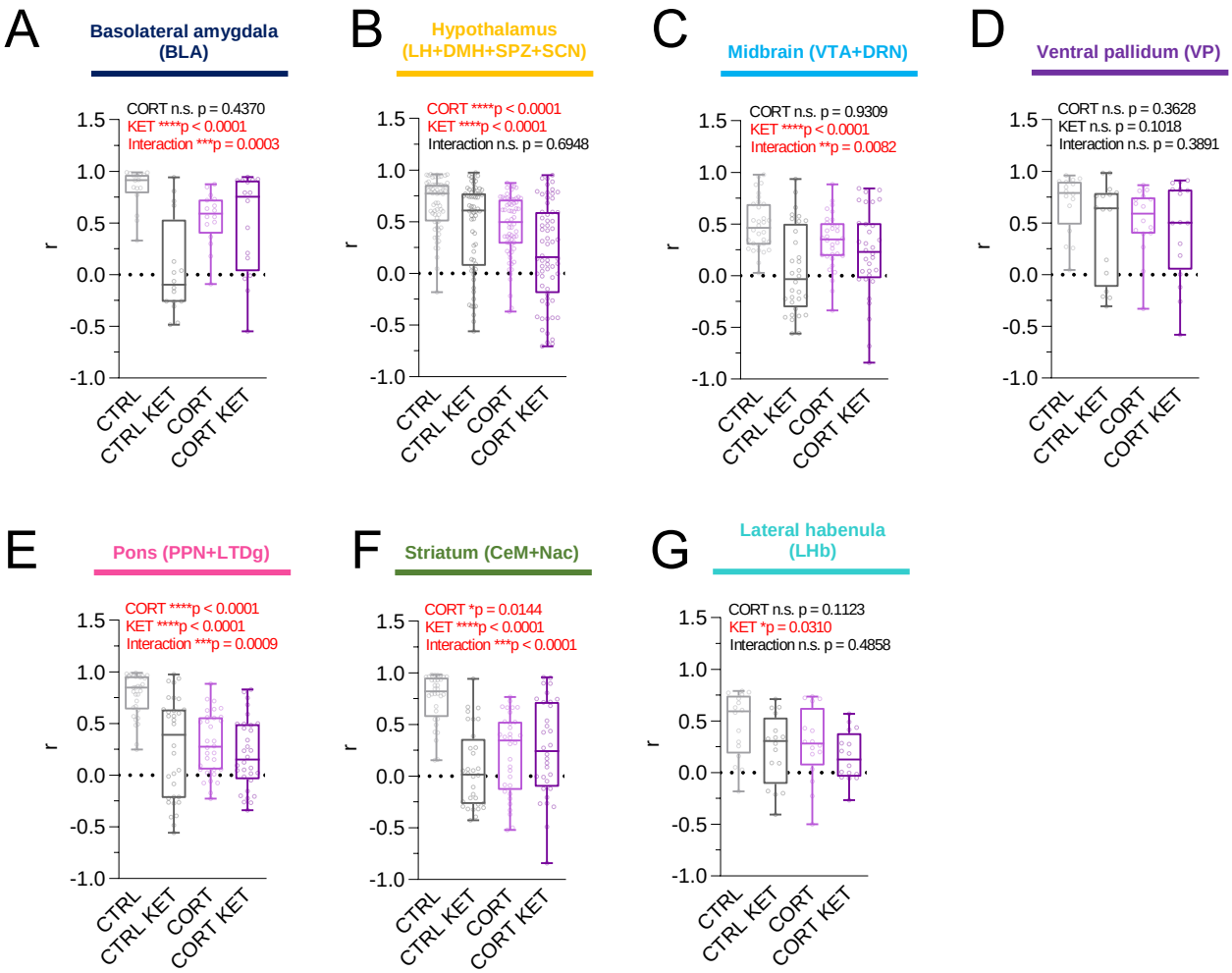

Figure 1: Changes in correlated activities within meso-cortico-limbic-striatal systems after 5 weeks of CORT and 24h of KET. (**A**) r values of interregional correlations of the basolateral amygdala (BLA) according to conditions (Two-way ANOVA, ns, ***p<0,001, ****p<0,0001). (**B**) r values of interregional correlations of hypothalamic regions, considered as the grouping of lateral hypothalamus (LH), dorsomedial hypothalamus (DMH), subparaventricular zone (SPZ) and suprachiasmatic nucleus (SCN), according to conditions (Two-way ANOVA, ns, ****p<0,0001). (**C**) r values of interregional correlations of midbrain area, considered as the grouping of ventral tegmental area (VTA) and dorsal raphe nucleus (DRN), according to conditions (Two-way ANOVA, ns, **p<0,01,****p<0,0001). (**D**) r values of interregional correlations of the ventral pallidum (VP) according to conditions (Two-way ANOVA, ns). (**E**) r values of interregional correlations of pons regions, considered as the grouping of pedunculopontine nucleus (PPN) and laterodorsal tegmental nucleus (LTDg) according to conditions (Two-way ANOVA, ***p<0,001,****p<0,0001). (**F**) r values of interregional correlations of striatal regions, considered as the grouping of central amygdala (CeM) and nucleus accumbens (Nac), according to conditions (Two-way ANOVA, *p<0,05,***p<0,001, ****p<0,0001). (**B**) r values of interregional correlations of the lateral habenula (LHb) according to conditions (Two-way ANOVA, ns, *p<0,05). Conditions for all graphs: CTRL (n = 8 brains), CTRL KET (n = 9 brains), CORT (n = 10 brains) and CORT KET (n = 9 brains).

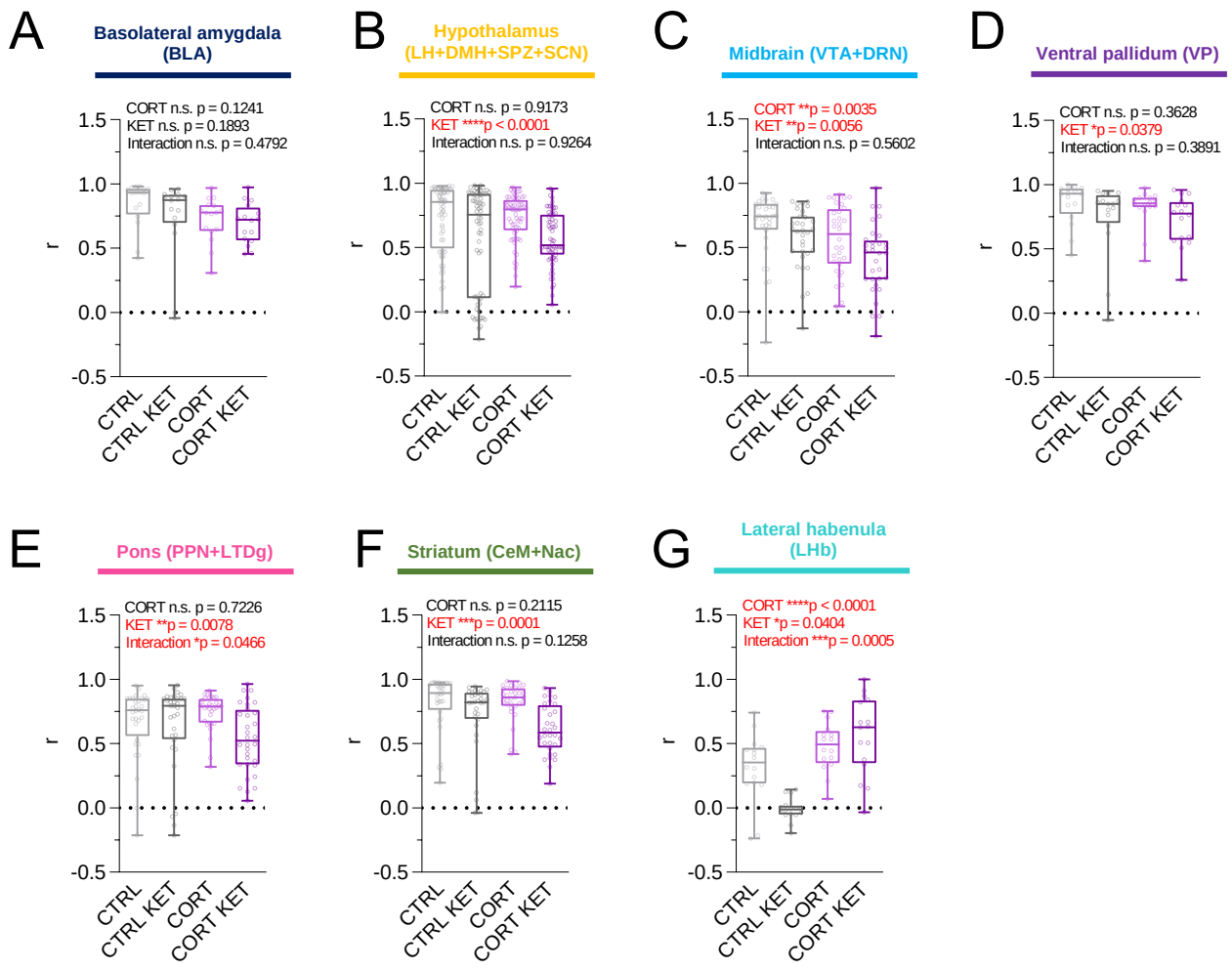

Figure 2: Changes in correlated activities within meso-cortico-limbic-striatal systems after 5 weeks of CORT and 90min of KET. (**A**) r values of interregional correlations of the basolateral amygdala (BLA) according to conditions (Two-way ANOVA, ns). (**B**) r values of interregional correlations of hypothalamic regions, considered as the grouping of lateral hypothalamus (LH), dorsomedial hypothalamus (DMH), subparaventricular zone (SPZ) and suprachiasmatic nucleus (SCN), according to conditions (Two-way ANOVA, ns, ****p<0,0001). (**C**) r values of interregional correlations of midbrain area, considered as the grouping of ventral tegmental area (VTA) and dorsal raphe nucleus (DRN), according to conditions (Two-way ANOVA, ns, **p<0,01). (**D**) r values of interregional correlations of the ventral pallidum (VP) according to conditions (Two-way ANOVA, ns, *p<0,05). (**E**) r values of interregional correlations of pons regions, considered as the grouping of pedunculopontine nucleus (PPN) and laterodorsal tegmental nucleus (LTDg) according to conditions (Two-way ANOVA, *p<0,05,**p<0,01). (**F**) r values of interregional correlations of striatal regions, considered as the grouping of central amygdala (CeM) and nucleus accumbens (Nac), according to conditions (Two-way ANOVA,***p<0,001). (**B**) r values of interregional correlations of the lateral habenula (LHb) according to conditions (Two-way ANOVA, *p<0,05, ***p<0,001, ****p<0,0001). Conditions for all graphs: CTRL (n = 7 brains), CTRL KET (n = 9 brains), CORT (n = 8 brains) and CORT KET (n = 10 brains).

References

Abdallah, C.G., Jackowski, A., Salas, R., Gupta, S., Sato, J.R., Mao, X., Coplan, J.D., Shungu, D.C., Mathew, S.J., 2017. The Nucleus Accumbens and Ketamine Treatment in Major Depressive Disorder. Neuropsychopharmacology 42, 1739–1746. https://doi.org/10.1038/npp.2017.49

Abdallah, C.G., Sanacora, G., Duman, R.S., Krystal, J.H., 2018. The neurobiology of depression, ketamine and rapid-acting antidepressants: Is it glutamate inhibition or activation? Pharmacol. Ther. 190, 148–158. https://doi.org/10.1016/j.pharmthera.2018.05.010

Alexander, L., Hawkins, P.C.T., Evans, J.W., Mehta, M.A., Zarate, C.A., 2023. Preliminary evidence that ketamine alters anterior cingulate resting-state functional connectivity in depressed individuals. Transl. Psychiatry 13, 1–10. https://doi.org/10.1038/s41398-023-02674-1

Aljuwaiser, M., Alayadhi, N., Ozidu, V., Shafik Zakhari, S.A., Rushdy, R., Naguy, A., 2023. Clinical Indications of Memantine in Psychiatry-Science or Art? Psychopharmacol. Bull. 53, 30–38.

Anderson, R.J., Freedland, K.E., Clouse, R.E., Lustman, P.J., 2001. The Prevalence of Comorbid Depression in Adults With Diabetes. Diabetes Care 24, 1069–1078. https://doi.org/10.2337/diacare.24.6.1069

Andrade, C., 2017. Ketamine for Depression, 4: In What Dose, at What Rate, by What Route, for How Long, and at What Frequency? J. Clin. Psychiatry 78, e852–e857. https://doi.org/10.4088/JCP.17f11738

Antonijevic, I.A., 2006. Depressive disorders—is it time to endorse different pathophysiologies? Psychoneuroendocrinology 31, 1–15. https://doi.org/10.1016/j.psyneuen.2005.04.004

Antoniuk, S., Bijata, M., Ponimaskin, E., Wlodarczyk, J., 2019. Chronic unpredictable mild stress for modeling depression in rodents: Meta-analysis of model reliability. Neurosci. Biobehav. Rev. 99, 101–116. https://doi.org/10.1016/j.neubiorev.2018.12.002

Autry, A.E., Adachi, M., Nosyreva, E., Na, E.S., Los, M.F., Cheng, P., Kavalali, E.T., Monteggia, L.M., 2011. NMDA receptor blockade at rest triggers rapid behavioural antidepressant responses. Nature 475, 91–95. https://doi.org/10.1038/nature10130

Baglioni, C., Battagliese, G., Feige, B., Spiegelhalder, K., Nissen, C., Voderholzer, U., Lombardo, C., Riemann, D., 2011. Insomnia as a predictor of depression: a meta-analytic evaluation of longitudinal epidemiological studies. J. Affect. Disord. 135, 10–19. https://doi.org/10.1016/j.jad.2011.01.011

Bahji, A., Vazquez, G.H., Zarate, C.A., 2021. Comparative efficacy of racemic ketamine and esketamine for depression: A systematic review and meta-analysis. J. Affect. Disord. 278, 542–555. https://doi.org/10.1016/j.jad.2020.09.071

Bard, L., Sainlos, M., Bouchet, D., Cousins, S., Mikasova, L., Breillat, C., Stephenson, F.A., Imperiali, B., Choquet, D., Groc, L., 2010. Dynamic and specific interaction between synaptic NR2-NMDA receptor and PDZ proteins. Proc. Natl. Acad. Sci. 107, 19561–19566. https://doi.org/10.1073/pnas.1002690107

Barth, J., Munder, T., Gerger, H., Nüesch, E., Trelle, S., Znoj, H., Jüni, P., Cuijpers, P., 2013. Comparative Efficacy of Seven Psychotherapeutic Interventions for Patients with Depression: A Network Meta-Analysis. PLoS Med. 10, e1001454. https://doi.org/10.1371/journal.pmed.1001454

Becker, M., Pinhasov, A., Ornoy, A., 2021. Animal Models of Depression: What Can They Teach Us about the Human Disease? Diagnostics 11, 123. https://doi.org/10.3390/diagnostics11010123
Bénac, N., Ezequiel Saraceno, G., Butler, C., Kuga, N., Nishimura, Y., Yokoi, T., Su, P., Sasaki, T., Petit-Pedrol, M., Galland, R., Studer, V., Liu, F., Ikegaya, Y., Sibarita, J.-B., Groc, L., 2024. Non-canonical interplay between glutamatergic NMDA and dopamine receptors shapes synaptogenesis. Nat. Commun. 15, 27. https://doi.org/10.1038/s41467-023-44301-z
Beneyto, M., Kristiansen, L.V., Oni-Orisan, A., McCullumsmith, R.E., Meador-Woodruff, J.H., 2007. Abnormal Glutamate Receptor Expression in the Medial Temporal Lobe in Schizophrenia and Mood Disorders. Neuropsychopharmacology 32, 1888–1902. https://doi.org/10.1038/sj.npp.1301312
Beneyto, M., Meador-Woodruff, J.H., 2008. Lamina-Specific Abnormalities of NMDA Receptor-Associated Postsynaptic Protein Transcripts in the Prefrontal Cortex in Schizophrenia and Bipolar Disorder. Neuropsychopharmacology 33, 2175–2186. https://doi.org/10.1038/sj.npp.1301604
Berman, R.M., Cappiello, A., Anand, A., Oren, D.A., Heninger, G.R., Charney, D.S., Krystal, J.H., 2000. Antidepressant effects of ketamine in depressed patients. Biol. Psychiatry 47, 351–354. https://doi.org/10.1016/S0006-3223(99)00230-9
Berridge, K.C., Kringelbach, M.L., 2015. Pleasure systems in the brain. Neuron 86, 646–664. https://doi.org/10.1016/j.neuron.2015.02.018
Beurel, E., Toups, M., Nemeroff, C.B., 2020. The Bidirectional Relationship of Depression and Inflammation: Double Trouble. Neuron 107, 234–256. https://doi.org/10.1016/j.neuron.2020.06.002
Bipolar disorders, 2018. . Nat. Rev. Dis. Primer 4, 18009. https://doi.org/10.1038/nrdp.2018.9
Bittar, T.P., Labonté, B., 2021. Functional Contribution of the Medial Prefrontal Circuitry in Major Depressive Disorder and Stress-Induced Depressive-Like Behaviors. Front. Behav. Neurosci. 15. https://doi.org/10.3389/fnbeh.2021.699592
Borsellino, P., Krider, R.I., Chea, D., Grinnell, R., Vida, T.A., 2023. Ketamine and the Disinhibition Hypothesis: Neurotrophic Factor-Mediated Treatment of Depression. Pharmaceuticals 16, 742. https://doi.org/10.3390/ph16050742
Brachman, R.A., McGowan, J.C., Perusini, J.N., Lim, S.C., Pham, T.H., Faye, C., Gardier, A.M., Mendez-David, I., David, D.J., Hen, R., Denny, C.A., 2016. Ketamine as a Prophylactic Against Stress-Induced Depressive-like Behavior. Biol. Psychiatry 79, 776–786. https://doi.org/10.1016/j.biopsych.2015.04.022
Braun, A.A., Skelton, M.R., Vorhees, C.V., Williams, M.T., 2011. Comparison of the elevated plus and elevated zero mazes in treated and untreated male Sprague–Dawley rats: Effects of anxiolytic and anxiogenic agents. Pharmacol. Biochem. Behav. 97, 406–415. https://doi.org/10.1016/j.pbb.2010.09.013
Brunello, N., Mendlewicz, J., Kasper, S., Leonard, B., Montgomery, S., Nelson, J.C., Paykel, E., Versiani, M., Racagni, G., 2002. The role of noradrenaline and selective noradrenaline reuptake inhibition in depression. Eur. Neuropsychopharmacol. 12, 461–475. https://doi.org/10.1016/S0924-977X(02)00057-3
Burgdorf, J., Zhang, X. -l., Weiss, C., Gross, A., Boikess, S.R., Kroes, R.A., Khan, M.A., Burch, R.M., Rex, C.S., Disterhoft, J.F., Stanton, P.K., Moskal, J.R., 2015. The long-lasting antidepressant effects of rapastinel (GLYX-13) are associated with a metaplasticity process in the medial prefrontal cortex and hippocampus. Neuroscience 308, 202–211. https://doi.org/10.1016/j.neuroscience.2015.09.004

Burstein, O., Doron, R., 2018. The Unpredictable Chronic Mild Stress Protocol for Inducing Anhedonia in Mice. J. Vis. Exp. 58184. https://doi.org/10.3791/58184
Cai, S.X., 2006. Glycine/NMDA receptor antagonists as potential CNS therapeutic agents: ACEA-1021 and related compounds. Curr. Top. Med. Chem. 6, 651–662. https://doi.org/10.2174/156802606776894465
Campayo, A., Gómez-Biel, C.H., Lobo, A., 2011. Diabetes and Depression. Curr. Psychiatry Rep. 13, 26–30. https://doi.org/10.1007/s11920-010-0165-z
Carmack, S.A., Kim, J.S., Sage, J.R., Thomas, A.W., Skillicorn, K.N., Anagnostaras, S.G., 2013. The competitive NMDA receptor antagonist CPP disrupts cocaine-induced conditioned place preference, but spares behavioral sensitization. Behav. Brain Res. 239, 155–163. https://doi.org/10.1016/j.bbr.2012.10.042
Carrillo, P., Petit, A.-C., Gaillard, R., Vinckier, F., 2020. Psychotropes du futur : de l'imipramine à la kétamine. Bull. Académie Natl. Médecine 204, 1034–1042. https://doi.org/10.1016/j.banm.2020.09.038
Casarotto, P.C., Girych, M., Fred, S.M., Kovaleva, V., Moliner, R., Enkavi, G., Biojone, C., Cannarozzo, C., Sahu, M.P., Kaurinkoski, K., Brunello, C.A., Steinzeig, A., Winkel, F., Patil, S., Vestring, S., Serchov, T., Diniz, C.R.A.F., Laukkanen, L., Cardon, I., Antila, H., Rog, T., Piepponen, T.P., Bramham, C.R., Normann, C., Lauri, S.E., Saarma, M., Vattulainen, I., Castrén, E., 2021. Antidepressant drugs act by directly binding to TRKB neurotrophin receptors. Cell 184, 1299-1313.e19. https://doi.org/10.1016/j.cell.2021.01.034
Chang, L., Zhang, K., Pu, Y., Qu, Y., Wang, S., Xiong, Z., Ren, Q., Dong, C., Fujita, Y., Hashimoto, K., 2019. Comparison of antidepressant and side effects in mice after intranasal administration of (R,S)-ketamine, (R)-ketamine, and (S)-ketamine. Pharmacol. Biochem. Behav. 181, 53–59. https://doi.org/10.1016/j.pbb.2019.04.008
Chaudhuri, A., Zangenehpour, S., Rahbar-Dehgan, F., Ye, F., 2000. Molecular maps of neural activity and quiescence. Acta Neurobiol. Exp. (Warsz.) 60, 403–410. https://doi.org/10.55782/ane-2000-1359
Chaudhury, D., Liu, H., Han, M.-H., 2015. Neuronal correlates of depression. Cell. Mol. Life Sci. 72, 4825–4848. https://doi.org/10.1007/s00018-015-2044-6
Chen, L., Wang, Q., Xu, T., 2023. Working memory function in patients with major depression disorder: A narrative review. Clin. Psychol. Psychother. 30, 281–293. https://doi.org/10.1002/cpp.2811
Choquet, D., Triller, A., 2013. The Dynamic Synapse. Neuron 80, 691–703. https://doi.org/10.1016/j.neuron.2013.10.013
Chowdhury, G.M.I., Zhang, J., Thomas, M., Banasr, M., Ma, X., Pittman, B., Bristow, L., Schaeffer, E., Duman, R.S., Rothman, D.L., Behar, K.L., Sanacora, G., 2017. Transiently increased glutamate cycling in rat PFC is associated with rapid onset of antidepressant-like effects. Mol. Psychiatry 22, 120–126. https://doi.org/10.1038/mp.2016.34
Citri, A., Malenka, R.C., 2008. Synaptic Plasticity: Multiple Forms, Functions, and Mechanisms. Neuropsychopharmacology 33, 18–41. https://doi.org/10.1038/sj.npp.1301559
Collingridge, G.L., Kehl, S.J., McLennan, H., 1983. The antagonism of amino acid-induced excitations of rat hippocampal CA1 neurones in vitro. J. Physiol. 334, 19–31. https://doi.org/10.1113/jphysiol.1983.sp014477
Cook, I.A., Leuchter, A.F., 2001. Prefrontal changes and treatment response prediction in depression. Semin. Clin. Neuropsychiatry 6, 113–120. https://doi.org/10.1053/scnp.2001.21844
Crawley, O., Conde-Dusman, M.J., Pérez-Otaño, I., 2022. GluN3A NMDA receptor subunits: more enigmatic than ever? J. Physiol. 600, 261–276. https://doi.org/10.1113/JP280879

Cuijpers, P., Quero, S., Dowrick, C., Arroll, B., 2019. Psychological Treatment of Depression in Primary Care: Recent Developments. Curr. Psychiatry Rep. 21, 129. https://doi.org/10.1007/s11920-019-1117-x
Dalmau, J., Tüzün, E., Wu, H., Masjuan, J., Rossi, J.E., Voloschin, A., Baehring, J.M., Shimazaki, H., Koide, R., King, D., Mason, W., Sansing, L.H., Dichter, M.A., Rosenfeld, M.R., Lynch, D.R., 2007. Paraneoplastic anti-N-methyl-D-aspartate receptor encephalitis associated with ovarian teratoma. Ann. Neurol. 61, 25–36. https://doi.org/10.1002/ana.21050
Davey, C.G., Pujol, J., Harrison, B.J., 2016. Mapping the self in the brain's default mode network. NeuroImage 132, 390–397. https://doi.org/10.1016/j.neuroimage.2016.02.022
David, D.J., Samuels, B.A., Rainer, Q., Wang, J.-W., Marsteller, D., Mendez, I., Drew, M., Craig, D.A., Guiard, B.P., Guilloux, J.-P., Artymyshyn, R.P., Gardier, A.M., Gerald, C., Antonijevic, I.A., Leonardo, E.D., Hen, R., 2009. Neurogenesis-Dependent and -Independent Effects of Fluoxetine in an Animal Model of Anxiety/Depression. Neuron 62, 479–493. https://doi.org/10.1016/j.neuron.2009.04.017
Davies, J., Evans, R.H., Herrling, P.L., Jones, A.W., Olverman, H.J., Pook, P., Watkins, J.C., 1986. CPP, a new potent and selective NMDA antagonist. Depression of central neuron responses, affinity for [3H]D-AP5 binding sites on brain membranes and anticonvulsant activity. Brain Res. 382, 169–173. https://doi.org/10.1016/0006-8993(86)90127-7
Dawbarn, D., Pycock, C.J., 1981. Motor effects following application of putative excitatory amino acid antagonists to the region of the mesencephalic dopamine cell bodies in the rat. Naunyn. Schmiedebergs Arch. Pharmacol. 318, 100–104. https://doi.org/10.1007/BF00508833
De Aquino, J.P., Londono, A., Carvalho, A.F., 2018. An Update on the Epidemiology of Major Depressive Disorder Across Cultures, in: Kim, Y.-K. (Ed.), Understanding Depression. Springer Singapore, Singapore, pp. 309–315. https://doi.org/10.1007/978-981-10-6580-4_25
de Wit, J., Ghosh, A., 2016. Specification of synaptic connectivity by cell surface interactions. Nat. Rev. Neurosci. 17, 4–4. https://doi.org/10.1038/nrn.2015.3
Dean, J., Keshavan, M., 2017. The neurobiology of depression: An integrated view. Asian J. Psychiatry 27, 101–111. https://doi.org/10.1016/j.ajp.2017.01.025
Deep, S.N., Mitra, S., Rajagopal, S., Paul, S., Poddar, R., 2019. GluN2A-NMDA receptor–mediated sustained Ca2+ influx leads to homocysteine-induced neuronal cell death. J. Biol. Chem. 294, 11154–11165. https://doi.org/10.1074/jbc.RA119.008820
DeNardo, L.A., Liu, C.D., Allen, W.E., Adams, E.L., Friedmann, D., Fu, L., Guenthner, C.J., Tessier-Lavigne, M., Luo, L., 2019. Temporal Evolution of Cortical Ensembles Promoting Remote Memory Retrieval. Nat. Neurosci. 22, 460–469. https://doi.org/10.1038/s41593-018-0318-7
Di, X., Biswal, B.B., 2014. Modulatory interactions between the default mode network and task positive networks in resting-state. PeerJ 2, e367. https://doi.org/10.7717/peerj.367
Dinis-Oliveira, R.J., 2017. Metabolism and metabolomics of ketamine: a toxicological approach. Forensic Sci. Res. 2, 2–10. https://doi.org/10.1080/20961790.2017.1285219
Dityatev, A., Schachner, M., Sonderegger, P., 2010. The dual role of the extracellular matrix in synaptic plasticity and homeostasis. Nat. Rev. Neurosci. 11, 735–746. https://doi.org/10.1038/nrn2898
Dominguez, G., Henkous, N., Prevot, T., David, V., Guillou, J.-L., Belzung, C., Mons, N., Béracochéa, D., 2019. Sustained corticosterone rise in the prefrontal cortex is a key factor for chronic stress-induced working memory deficits in mice. Neurobiol. Stress 10, 100161. https://doi.org/10.1016/j.ynstr.2019.100161

Domino, E.F., 2010. Taming the ketamine tiger. 1965. Anesthesiology 113, 678–684. https://doi.org/10.1097/ALN.0b013e3181ed09a2
Domino, E.F., Chodoff, P., Corssen, G., 1965. PHARMACOLOGIC EFFECTS OF CI-581, A NEW DISSOCIATIVE ANESTHETIC, IN MAN. Clin. Pharmacol. Ther. 6, 279–291. https://doi.org/10.1002/cpt196563279
Domino, E.F., Zsigmond, E.K., Domino, L.E., Domino, K.E., Kothary, S.P., Domino, S.E., 1982. Plasma levels of ketamine and two of its metabolites in surgical patients using a gas chromatographic mass fragmentographic assay. Anesth. Analg. 61, 87–92.
Dosemeci, A., Weinberg, R.J., Reese, T.S., Tao-Cheng, J.-H., 2016. The Postsynaptic Density: There Is More than Meets the Eye. Front. Synaptic Neurosci. 8. https://doi.org/10.3389/fnsyn.2016.00023
Downey, D., Dutta, A., McKie, S., Dawson, G.R., Dourish, C.T., Craig, K., Smith, M.A., McCarthy, D.J., Harmer, C.J., Goodwin, G.M., Williams, S., Deakin, J.F.W., 2016. Comparing the actions of lanicemine and ketamine in depression: key role of the anterior cingulate. Eur. Neuropsychopharmacol. J. Eur. Coll. Neuropsychopharmacol. 26, 994–1003. https://doi.org/10.1016/j.euroneuro.2016.03.006
Duman, R.S., Aghajanian, G.K., 2012. Synaptic Dysfunction in Depression: Potential Therapeutic Targets. Science 338, 68–72. https://doi.org/10.1126/science.1222939
Duman, R.S., Aghajanian, G.K., Sanacora, G., Krystal, J.H., 2016. Synaptic plasticity and depression: new insights from stress and rapid-acting antidepressants. Nat. Med. 22, 238–249. https://doi.org/10.1038/nm.4050
Duncan, W.C., Ballard, E.D., Zarate, C.A., 2019. Ketamine-Induced Glutamatergic Mechanisms of Sleep and Wakefulness: Insights for Developing Novel Treatments for Disturbed Sleep and Mood. Handb. Exp. Pharmacol. 253, 337–358. https://doi.org/10.1007/164_2017_51
Dupuis, J.P., Ladepeche, L., Seth, H., Bard, L., Varela, J., Mikasova, L., Bouchet, D., Rogemond, V., Honnorat, J., Hanse, E., Groc, L., 2014. Surface dynamics of GluN2B-NMDA receptors controls plasticity of maturing glutamate synapses. EMBO J. 33, 842–861. https://doi.org/10.1002/embj.201386356
Dupuis, J.P., Nicole, O., Groc, L., 2023. NMDA receptor functions in health and disease: Old actor, new dimensions. Neuron 111, 2312–2328. https://doi.org/10.1016/j.neuron.2023.05.002
Ebert, B., Mikkelsen, S., Thorkildsen, C., Borgbjerg, F.M., 1997. Norketamine, the main metabolite of ketamine, is a non-competitive NMDA receptor antagonist in the rat cortex and spinal cord. Eur. J. Pharmacol. 333, 99–104. https://doi.org/10.1016/S0014-2999(97)01116-3
Elderon, L., Whooley, M.A., 2013. Depression and Cardiovascular Disease. Prog. Cardiovasc. Dis. 55, 511–523. https://doi.org/10.1016/j.pcad.2013.03.010
Elias, G.M., Nicoll, R.A., 2007. Synaptic trafficking of glutamate receptors by MAGUK scaffolding proteins. Trends Cell Biol. 17, 343–352. https://doi.org/10.1016/j.tcb.2007.07.005
Espana, A., Seth, H., Jézéquel, J., Huang, T., Bouchet, D., Lepleux, M., Gréa, H., Bechter, K., Schneider, M., Hanse, E., Groc, L., 2021. Alteration of NMDA receptor trafficking as a cellular hallmark of psychosis. Transl. Psychiatry 11, 444. https://doi.org/10.1038/s41398-021-01549-7
Euston, D.R., Gruber, A.J., McNaughton, B.L., 2012. The Role of Medial Prefrontal Cortex in Memory and Decision Making. Neuron 76, 1057–1070. https://doi.org/10.1016/j.neuron.2012.12.002

Falkenberg, T., Lindefors, N., Camilli, F., Metsis, M., Ungerstedt, U., 1996. Glutamate release correlates with brain-derived neurotrophic factor and trkB mRNA expression in the CA1 region of rat hippocampus. Brain Res. Mol. Brain Res. 42, 317–327. https://doi.org/10.1016/s0169-328x(96)00134-9
Fattore, L., Amchova, P., Fadda, P., Ruda-Kucerova, J., 2023. Olfactory Bulbectomy Model of Depression Lowers Responding for Food in Male and Female Rats: The Modulating Role of Caloric Restriction and Response Requirement. Biomedicines 11, 2481. https://doi.org/10.3390/biomedicines11092481
Fava, M., Davidson, K.G., 1996. DEFINITION AND EPIDEMIOLOGY OF TREATMENT-RESISTANT DEPRESSION. Psychiatr. Clin. North Am. 19, 179–200. https://doi.org/10.1016/S0193-953X(05)70283-5
Ferrari, F., Villa, R.F., 2017. The Neurobiology of Depression: an Integrated Overview from Biological Theories to Clinical Evidence. Mol. Neurobiol. 54, 4847–4865. https://doi.org/10.1007/s12035-016-0032-y
Ferreira, J.S., Dupuis, J.P., Kellermayer, B., Bénac, N., Manso, C., Bouchet, D., Levet, F., Butler, C., Sibarita, J.-B., Groc, L., 2020. Distance-dependent regulation of NMDAR nanoscale organization along hippocampal neuron dendrites. Proc. Natl. Acad. Sci. 117, 24526–24533. https://doi.org/10.1073/pnas.1922477117
Ferreira, J.S., Papouin, T., Ladépêche, L., Yao, A., Langlais, V.C., Bouchet, D., Dulong, J., Mothet, J.-P., Sacchi, S., Pollegioni, L., Paoletti, P., Oliet, S.H.R., Groc, L., 2017. Co-agonists differentially tune GluN2B-NMDA receptor trafficking at hippocampal synapses. eLife 6, e25492. https://doi.org/10.7554/eLife.25492
Feyissa, A.M., Chandran, A., Stockmeier, C.A., Karolewicz, B., 2009. Reduced levels of NR2A and NR2B subunits of NMDA receptor and PSD-95 in the prefrontal cortex in major depression. Prog. Neuropsychopharmacol. Biol. Psychiatry 33, 70–75. https://doi.org/10.1016/j.pnpbp.2008.10.005
Filipkowski, R.K., Rydz, M., Berdel, B., Morys, J., Kaczmarek, L., 2000. Tactile Experience Induces c-fos Expression in Rat Barrel Cortex. Learn. Mem. 7, 116–122. https://doi.org/10.1101/lm.7.2.116
Fonseka, T.M., MacQueen, G.M., Kennedy, S.H., 2018. Neuroimaging biomarkers as predictors of treatment outcome in Major Depressive Disorder. J. Affect. Disord. 233, 21–35. https://doi.org/10.1016/j.jad.2017.10.049
Fox, K., Armstrong-James, M., 1986. The role of the anterior intralaminar nuclei and N-methyl D-aspartate receptors in the generation of spontaneous bursts in rat neocortical neurones. Exp. Brain Res. 63, 505–518. https://doi.org/10.1007/BF00237474
Franchini, L., Carrano, N., Di Luca, M., Gardoni, F., 2020. Synaptic GluN2A-Containing NMDA Receptors: From Physiology to Pathological Synaptic Plasticity. Int. J. Mol. Sci. 21, 1538. https://doi.org/10.3390/ijms21041538
Fukui, M., Rodriguiz, R.M., Zhou, J., Jiang, S.X., Phillips, L.E., Caron, M.G., Wetsel, W.C., 2007. *Vmat2* Heterozygous Mutant Mice Display a Depressive-Like Phenotype. J. Neurosci. 27, 10520–10529. https://doi.org/10.1523/JNEUROSCI.4388-06.2007
Fukumoto, K., Fogaça, M.V., Liu, R.-J., Duman, C., Kato, T., Li, X.-Y., Duman, R.S., 2019. Activity-dependent brain-derived neurotrophic factor signaling is required for the antidepressant actions of (2R,6R)-hydroxynorketamine. Proc. Natl. Acad. Sci. U. S. A. 116, 297–302. https://doi.org/10.1073/pnas.1814709116
Fukumoto, K., Toki, H., Iijima, M., Hashihayata, T., Yamaguchi, J., Hashimoto, K., Chaki, S., 2017. Antidepressant Potential of (R)-Ketamine in Rodent Models: Comparison with (S)-Ketamine. J. Pharmacol. Exp. Ther. 361, 9–16. https://doi.org/10.1124/jpet.116.239228

Furukawa, H., Singh, S.K., Mancusso, R., Gouaux, E., 2005. Subunit arrangement and function in NMDA receptors. Nature 438, 185–192. https://doi.org/10.1038/nature04089
Gao, M., Rejaei, D., Liu, H., 2016. Ketamine use in current clinical practice. Acta Pharmacol. Sin. 37, 865–872. https://doi.org/10.1038/aps.2016.5
Gardier, A.M., Guiard, B.P., Guilloux, J.-P., Repérant, C., Coudoré, F., David, D.J., 2009. Interest of using genetically manipulated mice as models of depression to evaluate antidepressant drugs activity: a review. Fundam. Clin. Pharmacol. 23, 23–42. https://doi.org/10.1111/j.1472-8206.2008.00640.x
Gardoni, F., Di Luca, M., 2021. Protein-protein interactions at the NMDA receptor complex: From synaptic retention to synaptonuclear protein messengers. Neuropharmacology 190, 108551. https://doi.org/10.1016/j.neuropharm.2021.108551
Gärtner, M., Aust, S., Bajbouj, M., Fan, Y., Wingenfeld, K., Otte, C., Heuser-Collier, I., Böker, H., Hättenschwiler, J., Seifritz, E., Grimm, S., Scheidegger, M., 2019. Functional connectivity between prefrontal cortex and subgenual cingulate predicts antidepressant effects of ketamine. Eur. Neuropsychopharmacol. 29, 501–508. https://doi.org/10.1016/j.euroneuro.2019.02.008
Gass, N., Schwarz, A.J., Sartorius, A., Schenker, E., Risterucci, C., Spedding, M., Zheng, L., Meyer-Lindenberg, A., Weber-Fahr, W., 2014. Sub-Anesthetic Ketamine Modulates Intrinsic BOLD Connectivity Within the Hippocampal-Prefrontal Circuit in the Rat. Neuropsychopharmacology 39, 895–906. https://doi.org/10.1038/npp.2013.290
Gerhard, D.M., Pothula, S., Liu, R.-J., Wu, M., Li, X.-Y., Girgenti, M.J., Taylor, S.R., Duman, C.H., Delpire, E., Picciotto, M., Wohleb, E.S., Duman, R.S., 2020. GABA interneurons are the cellular trigger for ketamine's rapid antidepressant actions. J. Clin. Invest. 130, 1336–1349. https://doi.org/10.1172/JCI130808
Ghasemi, M., Phillips, C., Trillo, L., De Miguel, Z., Das, D., Salehi, A., 2014. The role of NMDA receptors in the pathophysiology and treatment of mood disorders. Neurosci. Biobehav. Rev. 47, 336–358. https://doi.org/10.1016/j.neubiorev.2014.08.017
Global, regional, and national burden of 12 mental disorders in 204 countries and territories, 1990–2019: a systematic analysis for the Global Burden of Disease Study 2019, 2022. . Lancet Psychiatry 9, 137–150. https://doi.org/10.1016/S2215-0366(21)00395-3
Groc, L., Choquet, D., 2020. Linking glutamate receptor movements and synapse function. Science 368, eaay4631. https://doi.org/10.1126/science.aay4631
Groc, L., Choquet, D., 2006. AMPA and NMDA glutamate receptor trafficking: multiple roads for reaching and leaving the synapse. Cell Tissue Res. 326, 423–438. https://doi.org/10.1007/s00441-006-0254-9
Groc, L., Choquet, D., Chaouloff, F., 2008. The stress hormone corticosterone conditions AMPAR surface trafficking and synaptic potentiation. Nat. Neurosci. 11, 868–870. https://doi.org/10.1038/nn.2150
Groc, L., Heine, M., Cousins, S.L., Stephenson, F.A., Lounis, B., Cognet, L., Choquet, D., 2006. NMDA receptor surface mobility depends on NR2A-2B subunits. Proc. Natl. Acad. Sci. 103, 18769–18774. https://doi.org/10.1073/pnas.0605238103
Groc, L., Lafourcade, M., Heine, M., Renner, M., Racine, V., Sibarita, J.-B., Lounis, B., Choquet, D., Cognet, L., 2007. Surface Trafficking of Neurotransmitter Receptor: Comparison between Single-Molecule/Quantum Dot Strategies. J. Neurosci. 27, 12433–12437. https://doi.org/10.1523/JNEUROSCI.3349-07.2007
Guilloux, J.-P., Seney, M., Edgar, N., Sibille, E., 2011. Integrated behavioral z-scoring increases the sensitivity and reliability of behavioral phenotyping in mice: relevance to

emotionality and sex. J. Neurosci. Methods 197, 21–31. https://doi.org/10.1016/j.jneumeth.2011.01.019
Gutknecht, L., Popp, S., Waider, J., Sommerlandt, F.M.J., Göppner, C., Post, A., Reif, A., Van Den Hove, D., Strekalova, T., Schmitt, A., Colaço, M.B.N., Sommer, C., Palme, R., Lesch, K.-P., 2015. Interaction of brain 5-HT synthesis deficiency, chronic stress and sex differentially impact emotional behavior in Tph2 knockout mice. Psychopharmacology (Berl.) 232, 2429–2441. https://doi.org/10.1007/s00213-015-3879-0
Hache, G., Guiard, B.P., Le Dantec, Y., Orvoën, S., David, D.J., Gardier, A.M., Coudoré, F., 2012. Antinociceptive effects of fluoxetine in a mouse model of anxiety/depression. Neuroreport 23, 525–529. https://doi.org/10.1097/WNR.0b013e328353d70a
Haenisch, B., Bönisch, H., 2011. Depression and antidepressants: Insights from knockout of dopamine, serotonin or noradrenaline re-uptake transporters. Pharmacol. Ther. 129, 352–368. https://doi.org/10.1016/j.pharmthera.2010.12.002
Hansen, K.B., Wollmuth, L.P., Bowie, D., Furukawa, H., Menniti, F.S., Sobolevsky, A.I., Swanson, G.T., Swanger, S.A., Greger, I.H., Nakagawa, T., McBain, C.J., Jayaraman, V., Low, C.-M., Dell'Acqua, M.L., Diamond, J.S., Camp, C.R., Perszyk, R.E., Yuan, H., Traynelis, S.F., 2021. Structure, Function, and Pharmacology of Glutamate Receptor Ion Channels. Pharmacol. Rev. 73, 1469–1658. https://doi.org/10.1124/pharmrev.120.000131
Hellweg, R., Zueger, M., Fink, K., Hörtnagl, H., Gass, P., 2007. Olfactory bulbectomy in mice leads to increased BDNF levels and decreased serotonin turnover in depression-related brain areas. Neurobiol. Dis. 25, 1–7. https://doi.org/10.1016/j.nbd.2006.07.017
Highland, J.N., Zanos, P., Riggs, L.M., Georgiou, P., Clark, S.M., Morris, P.J., Moaddel, R., Thomas, C.J., Zarate, C.A., Pereira, E.F.R., Gould, T.D., 2021. Hydroxynorketamines: Pharmacology and Potential Therapeutic Applications. Pharmacol. Rev. 73, 763–791. https://doi.org/10.1124/pharmrev.120.000149
Horak, M., Petralia, R.S., Kaniakova, M., Sans, N., 2014. ER to synapse trafficking of NMDA receptors. Front. Cell. Neurosci. 8. https://doi.org/10.3389/fncel.2014.00394
Hu, Y., Du, W., Qi, J., Luo, H., Zhang, Z., Luo, M., Wang, Y., 2024. Comparative brain-wide mapping of ketamine- and isoflurane-activated nuclei and functional networks in the mouse brain. eLife 12, RP88420. https://doi.org/10.7554/eLife.88420
Hunter, D., Jamet, Z., Groc, L., 2021. Autoimmunity and NMDA receptor in brain disorders: Where do we stand? Neurobiol. Dis. 147, 105161. https://doi.org/10.1016/j.nbd.2020.105161
Iacobucci, G.J., Popescu, G.K., 2019. Spatial Coupling Tunes NMDA Receptor Responses via Ca2+ Diffusion. J. Neurosci. 39, 8831–8844. https://doi.org/10.1523/JNEUROSCI.0901-19.2019
Ikram, H., Haleem, D.J., 2017. Repeated treatment with reserpine as a progressive animal model of depression. Pak. J. Pharm. Sci. 30, 897–902.
Insel, T.R., Wang, P.S., 2009. The STAR*D trial: revealing the need for better treatments. Psychiatr. Serv. Wash. DC 60, 1466–1467. https://doi.org/10.1176/ps.2009.60.11.1466
Jamet, Z., Mergaux, C., Meras, M., Bouchet, D., Villega, F., Kreye, J., Prüss, H., Groc, L., 2024. NMDA receptor autoantibodies primarily impair the extrasynaptic compartment. Brain J. Neurol. awae163. https://doi.org/10.1093/brain/awae163
Jang, S., Lee, H., Kim, E., 2017. Synaptic adhesion molecules and excitatory synaptic transmission. Curr. Opin. Neurobiol. 45, 45–50. https://doi.org/10.1016/j.conb.2017.03.005
Jeon, S.W., Kim, Y.K., 2016. Neuroinflammation and cytokine abnormality in major depression: Cause or consequence in that illness? World J. Psychiatry 6, 283–293. https://doi.org/10.5498/wjp.v6.i3.283

Jézéquel, J., Johansson, E.M., Dupuis, J.P., Rogemond, V., Gréa, H., Kellermayer, B., Hamdani, N., Le Guen, E., Rabu, C., Lepleux, M., Spatola, M., Mathias, E., Bouchet, D., Ramsey, A.J., Yolken, R.H., Tamouza, R., Dalmau, J., Honnorat, J., Leboyer, M., Groc, L., 2017. Dynamic disorganization of synaptic NMDA receptors triggered by autoantibodies from psychotic patients. Nat. Commun. 8, 1791. https://doi.org/10.1038/s41467-017-01700-3
Jiménez-Sánchez, L., Campa, L., Auberson, Y.P., Adell, A., 2014. The Role of GluN2A and GluN2B Subunits on the Effects of NMDA Receptor Antagonists in Modeling Schizophrenia and Treating Refractory Depression. Neuropsychopharmacology 39, 2673–2680. https://doi.org/10.1038/npp.2014.123
Joëls, M., 2006. Corticosteroid effects in the brain: U-shape it. Trends Pharmacol. Sci. 27, 244–250. https://doi.org/10.1016/j.tips.2006.03.007
Joëls, M., Karst, H., Sarabdjitsingh, R.A., 2018. The stressed brain of humans and rodents. Acta Physiol. Oxf. Engl. 223, e13066. https://doi.org/10.1111/apha.13066
Johansson, E.M., Bouchet, D., Tamouza, R., Ellul, P., Morr, AS., Avignone, E., Germi, R., Leboyer, M., Perron, H., Groc, L., 2020. Human endogenous retroviral protein triggers deficit in glutamate synapse maturation and behaviors associated with psychosis. Sci. Adv. 6, eabc0708. https://doi.org/10.1126/sciadv.abc0708
Kapitein, L.C., Hoogenraad, C.C., 2011. Which way to go? Cytoskeletal organization and polarized transport in neurons. Mol. Cell. Neurosci. 46, 9–20. https://doi.org/10.1016/j.mcn.2010.08.015
Karolewicz, B., Stockmeier, C.A., Ordway, G.A., 2005. Elevated Levels of the NR2C Subunit of the NMDA Receptor in the Locus Coeruleus in Depression. Neuropsychopharmacol. Off. Publ. Am. Coll. Neuropsychopharmacol. 30, 1557–1567. https://doi.org/10.1038/sj.npp.1300781
Karst, H., Joëls, M., 2005. Corticosterone slowly enhances miniature excitatory postsynaptic current amplitude in mice CA1 hippocampal cells. J. Neurophysiol. 94, 3479–3486. https://doi.org/10.1152/jn.00143.2005
Kawatake-Kuno, A., Li, H., Inaba, H., Hikosaka, M., Ishimori, E., Ueki, T., Garkun, Y., Morishita, H., Narumiya, S., Oishi, N., Ohtsuki, G., Murai, T., Uchida, S., 2024. Sustained antidepressant effects of ketamine metabolite involve GABAergic inhibition-mediated molecular dynamics in aPVT glutamatergic neurons. Neuron 112, 1265-1285.e10. https://doi.org/10.1016/j.neuron.2024.01.023
Kellermayer, B., Ferreira, J.S., Dupuis, J., Levet, F., Grillo-Bosch, D., Bard, L., Linarès-Loyez, J., Bouchet, D., Choquet, D., Rusakov, D.A., Bon, P., Sibarita, J.-B., Cognet, L., Sainlos, M., Carvalho, A.L., Groc, L., 2018. Differential Nanoscale Topography and Functional Role of GluN2-NMDA Receptor Subtypes at Glutamatergic Synapses. Neuron 100, 106-119.e7. https://doi.org/10.1016/j.neuron.2018.09.012
Kesner, R.P., Churchwell, J.C., 2011. An analysis of rat prefrontal cortex in mediating executive function. Neurobiol. Learn. Mem. 96, 417–431. https://doi.org/10.1016/j.nlm.2011.07.002
Kessels, H.W., Nabavi, S., Malinow, R., 2013. Metabotropic NMDA receptor function is required for β-amyloid–induced synaptic depression. Proc. Natl. Acad. Sci. 110, 4033–4038. https://doi.org/10.1073/pnas.1219605110
Kessler, R.C., Chiu, W.T., Demler, O., Walters, E.E., 2005. Prevalence, Severity, and Comorbidity of 12-Month DSM-IV Disorders in the National Comorbidity Survey Replication. Arch. Gen. Psychiatry 62, 617. https://doi.org/10.1001/archpsyc.62.6.617

Kiloh, L.G., Child, J.P., Latner, G., 1960. A controlled trial of iproniazid in the treatment of endogenous depression. J. Ment. Sci. 106, 1139–1144. https://doi.org/10.1192/bjp.106.444.1139
Kim, J., Schwartz, T.L., 2020. Psychiatric Comorbidity in Major Depressive Disorder, in: Major Depressive Disorder. Elsevier, pp. 91–102. https://doi.org/10.1016/B978-0-323-58131-8.00007-0
Kim, J., Wulschner, L.E.G., Oh, W.C., Ko, J., 2022. Trans-synaptic mechanisms orchestrated by mammalian synaptic cell adhesion molecules. BioEssays News Rev. Mol. Cell. Dev. Biol. 44, e2200134. https://doi.org/10.1002/bies.202200134
Kimura, H., Okamoto, K., Sakai, Y., 1985. Pharmacological evidence for L-aspartate as the neurotransmitter of cerebellar climbing fibres in the guinea-pig. J. Physiol. 365, 103–119. https://doi.org/10.1113/jphysiol.1985.sp015761
Knyazev, G.G., Savostyanov, A.N., Bocharov, A.V., Brak, I.V., Osipov, E.A., Filimonova, E.A., Saprigyn, A.E., Aftanas, L.I., 2018. Task-positive and task-negative networks in major depressive disorder: A combined fMRI and EEG study. J. Affect. Disord. 235, 211–219. https://doi.org/10.1016/j.jad.2018.04.003
Kohler, J., Mei, J., Banneke, S., Winter, Y., Endres, M., Emmrich, J.V., 2022. Assessing spatial learning and memory in mice: Classic radial maze versus a new animal-friendly automated radial maze allowing free access and not requiring food deprivation. Front. Behav. Neurosci. 16. https://doi.org/10.3389/fnbeh.2022.1013624
Koolschijn, P.C.M.P., van Haren, N.E.M., Lensvelt-Mulders, G.J.L.M., Hulshoff Pol, H.E., Kahn, R.S., 2009. Brain volume abnormalities in major depressive disorder: A meta-analysis of magnetic resonance imaging studies. Hum. Brain Mapp. 30, 3719–3735. https://doi.org/10.1002/hbm.20801
Kovács, K.J., 2008. Measurement of Immediate-Early Gene Activation- c-fos and Beyond. J. Neuroendocrinol. 20, 665–672. https://doi.org/10.1111/j.1365-2826.2008.01734.x
Krieger, J., Bahar, I., Greger, I.H., 2015. Structure, Dynamics, and Allosteric Potential of Ionotropic Glutamate Receptor N-Terminal Domains. Biophys. J. 109, 1136–1148. https://doi.org/10.1016/j.bpj.2015.06.061
Kuehner, C., 2017. Why is depression more common among women than among men? Lancet Psychiatry 4, 146–158. https://doi.org/10.1016/S2215-0366(16)30263-2
Kurek, A., Kucharczyk, M., Detka, J., Ślusarczyk, J., Trojan, E., Głombik, K., Bojarski, B., Ludwikowska, A., Lasoń, W., Budziszewska, B., 2016. Pro-apoptotic Action of Corticosterone in Hippocampal Organotypic Cultures. Neurotox. Res. 30, 225–238. https://doi.org/10.1007/s12640-016-9630-8
Kuring, J.K., Mathias, J.L., Ward, L., 2018. Prevalence of Depression, Anxiety and PTSD in People with Dementia: a Systematic Review and Meta-Analysis. Neuropsychol. Rev. 28, 393–416. https://doi.org/10.1007/s11065-018-9396-2
Lacor, P.N., Buniel, M.C., Furlow, P.W., Clemente, A.S., Velasco, P.T., Wood, M., Viola, K.L., Klein, W.L., 2007. Abeta oligomer-induced aberrations in synapse composition, shape, and density provide a molecular basis for loss of connectivity in Alzheimer's disease. J. Neurosci. Off. J. Soc. Neurosci. 27, 796–807. https://doi.org/10.1523/JNEUROSCI.3501-06.2007
Ladepeche, L., Dupuis, J.P., Bouchet, D., Doudnikoff, E., Yang, L., Campagne, Y., Bézard, E., Hosy, E., Groc, L., 2013. Single-molecule imaging of the functional crosstalk between surface NMDA and dopamine D1 receptors. Proc. Natl. Acad. Sci. U. S. A. 110, 18005–18010. https://doi.org/10.1073/pnas.1310145110

Lapidus, K.A.B., Levitch, C.F., Perez, A.M., Brallier, J.W., Parides, M.K., Soleimani, L., Feder, A., Iosifescu, D.V., Charney, D.S., Murrough, J.W., 2014. A randomized controlled trial of intranasal ketamine in major depressive disorder. Biol. Psychiatry 76, 970–976. https://doi.org/10.1016/j.biopsych.2014.03.026
Lau, W.K., Lui, P.W., Wong, C.K.C., Chan, Y.S., Yung, K.K.L., 2003. Differential expression of N-methyl-D-aspartate receptor subunit messenger ribonucleic acids and immunoreactivity in the rat neostriatum during postnatal development. Neurochem. Int. 43, 47–65. https://doi.org/10.1016/s0197-0186(02)00191-2
Laubach, M., Amarante, L.M., Swanson, K., White, S.R., 2018. What, If Anything, Is Rodent Prefrontal Cortex? eNeuro 5, ENEURO.0315-18.2018. https://doi.org/10.1523/ENEURO.0315-18.2018
Le Daré, B., Pelletier, R., Morel, I., Gicquel, T., 2022. [History of Ketamine: An ancient molecule that is still popular today]. Ann. Pharm. Fr. 80, 1–8. https://doi.org/10.1016/j.pharma.2021.04.005
Lee, F.J.S., Xue, S., Pei, L., Vukusic, B., Chéry, N., Wang, Y., Wang, Y.T., Niznik, H.B., Yu, X., Liu, F., 2002. Dual Regulation of NMDA Receptor Functions by Direct Protein-Protein Interactions with the Dopamine D1 Receptor. Cell 111, 219–230. https://doi.org/10.1016/S0092-8674(02)00962-5
LeMoult, J., Humphreys, K.L., Tracy, A., Hoffmeister, J.-A., Ip, E., Gotlib, I.H., 2020. Meta-analysis: Exposure to Early Life Stress and Risk for Depression in Childhood and Adolescence. J. Am. Acad. Child Adolesc. Psychiatry 59, 842–855. https://doi.org/10.1016/j.jaac.2019.10.011
Lesept, F., Chevilley, A., Jezequel, J., Ladépêche, L., Macrez, R., Aimable, M., Lenoir, S., Bertrand, T., Rubrecht, L., Galea, P., Lebouvier, L., Petersen, K.-U., Hommet, Y., Maubert, E., Ali, C., Groc, L., Vivien, D., 2016. Tissue-type plasminogen activator controls neuronal death by raising surface dynamics of extrasynaptic NMDA receptors. Cell Death Dis. 7, e2466–e2466. https://doi.org/10.1038/cddis.2016.279
Levine, J., Panchalingam, K., Rapoport, A., Gershon, S., McClure, R.J., Pettegrew, J.W., 2000. Increased cerebrospinal fluid glutamine levels in depressed patients. Biol. Psychiatry 47, 586–593. https://doi.org/10.1016/s0006-3223(99)00284-x
Li, C.-T., 2023. Chapter 1 - Overview of treatment-resistant depression, in: Li, C.-T., Cheng, C.-M. (Eds.), Progress in Brain Research, Treatment-Resistant Depression Part A. Elsevier, pp. 1–23. https://doi.org/10.1016/bs.pbr.2023.03.007
Li, L., Vlisides, P.E., 2016. Ketamine: 50 Years of Modulating the Mind. Front. Hum. Neurosci. 10, 612. https://doi.org/10.3389/fnhum.2016.00612
Li, L.-J., Hu, R., Lujan, B., Chen, J., Zhang, J.-J., Nakano, Y., Cui, T.-Y., Liao, M.-X., Chen, J.-C., Man, H.-Y., Feng, H., Wan, Q., 2016. Glycine Potentiates AMPA Receptor Function through Metabotropic Activation of GluN2A-Containing NMDA Receptors. Front. Mol. Neurosci. 9, 102. https://doi.org/10.3389/fnmol.2016.00102
Li, N., Lee, B., Liu, R.-J., Banasr, M., Dwyer, J.M., Iwata, M., Li, X.-Y., Aghajanian, G., Duman, R.S., 2010. mTOR-Dependent Synapse Formation Underlies the Rapid Antidepressant Effects of NMDA Antagonists. Science 329, 959–964. https://doi.org/10.1126/science.1190287
Li, Q., Takeuchi, Y., Wang, J., Gellért, L., Barcsai, L., Pedraza, L.K., Nagy, A.J., Kozák, G., Nakai, S., Kato, S., Kobayashi, K., Ohsawa, M., Horváth, G., Kékesi, G., Lőrincz, M.L., Devinsky, O., Buzsáki, G., Berényi, A., 2023. Reinstating olfactory bulb-derived limbic gamma oscillations alleviates depression-like behavioral deficits in rodents. Neuron 111, 2065-2075.e5. https://doi.org/10.1016/j.neuron.2023.04.013

Li, W., Ali, T., He, K., Liu, Z., Shah, F.A., Ren, Q., Liu, Y., Jiang, A., Li, S., 2021a. Ibrutinib alleviates LPS-induced neuroinflammation and synaptic defects in a mouse model of depression. Brain. Behav. Immun. 92, 10–24. https://doi.org/10.1016/j.bbi.2020.11.008
Li, W., Ali, T., Zheng, C., Liu, Z., He, K., Shah, F.A., Ren, Q., Rahman, S.U., Li, N., Yu, Z.-J., Li, S., 2021b. Fluoxetine regulates eEF2 activity (phosphorylation) via HDAC1 inhibitory mechanism in an LPS-induced mouse model of depression. J. Neuroinflammation 18, 38. https://doi.org/10.1186/s12974-021-02091-5
Li, X., Mu, F., Liu, D., Zhu, J., Yue, S., Liu, M., Liu, Y., Wang, J., 2022. Predictors of suicidal ideation, suicide attempt and suicide death among people with major depressive disorder: A systematic review and meta-analysis of cohort studies. J. Affect. Disord. 302, 332–351. https://doi.org/10.1016/j.jad.2022.01.103
Lin, X., Itoga, C.A., Taha, S., Li, M.H., Chen, R., Sami, K., Berton, F., Francesconi, W., Xu, X., 2018. c-Fos mapping of brain regions activated by multi-modal and electric foot shock stress. Neurobiol. Stress 8, 92–102. https://doi.org/10.1016/j.ynstr.2018.02.001
Liu, C.H., Kim, Y.R., Ren, J.Q., Eichler, F., Rosen, B.R., Liu, P.K., 2007. Imaging cerebral gene transcripts in live animals. J. Neurosci. Off. J. Soc. Neurosci. 27, 713–722. https://doi.org/10.1523/JNEUROSCI.4660-06.2007
Liu, R.-J., Duman, C., Kato, T., Hare, B., Lopresto, D., Bang, E., Burgdorf, J., Moskal, J., Taylor, J., Aghajanian, G., Duman, R.S., 2017. GLYX-13 Produces Rapid Antidepressant Responses with Key Synaptic and Behavioral Effects Distinct from Ketamine. Neuropsychopharmacol. Off. Publ. Am. Coll. Neuropsychopharmacol. 42, 1231–1242. https://doi.org/10.1038/npp.2016.202
Liu, Y., Lin, D., Wu, B., Zhou, W., 2016. Ketamine abuse potential and use disorder. Brain Res. Bull. 126, 68–73. https://doi.org/10.1016/j.brainresbull.2016.05.016
Lochmann, D., Richardson, T., 2018. Selective Serotonin Reuptake Inhibitors, in: Macaluso, M., Preskorn, S.H. (Eds.), Antidepressants, Handbook of Experimental Pharmacology. Springer International Publishing, Cham, pp. 135–144. https://doi.org/10.1007/164_2018_172
Lodge, D., Watkins, J.C., Bortolotto, Z.A., Jane, D.E., Volianskis, A., 2019. The 1980s: d-AP5, LTP and a Decade of NMDA Receptor Discoveries. Neurochem. Res. 44, 516–530. https://doi.org/10.1007/s11064-018-2640-6
Lombion-Pouthier, S., Vandel, P., Nezelof, S., Haffen, E., Millot, J.-L., 2006. Odor perception in patients with mood disorders. J. Affect. Disord. 90, 187–191. https://doi.org/10.1016/j.jad.2005.11.012
Lopez-Munoz, F., Alamo, C., 2009. Monoaminergic Neurotransmission: The History of the Discovery of Antidepressants from 1950s Until Today. Curr. Pharm. Des. 15, 1563–1586. https://doi.org/10.2174/138161209788168001
Lovinger, D.M., 2008. Communication Networks in the Brain 31.
Lu, J., Zhang, Y.-H., Chou, T.C., Gaus, S.E., Elmquist, J.K., Shiromani, P., Saper, C.B., 2001. Contrasting Effects of Ibotenate Lesions of the Paraventricular Nucleus and Subparaventricular Zone on Sleep–Wake Cycle and Temperature Regulation. J. Neurosci. 21, 4864–4874. https://doi.org/10.1523/JNEUROSCI.21-13-04864.2001
Lucantonio, F., Li, S., Lu, J., Roeglin, J., Bontempi, L., Shields, B.C., Zarate, C.A., Tadross, M.R., Pignatelli, M., 2023. Ketamine rescues anhedonia by cell-type and input specific adaptations in the Nucleus Accumbens (preprint). Neuroscience. https://doi.org/10.1101/2023.06.08.544088

Lüscher, C., Malenka, R.C., 2012. NMDA receptor-dependent long-term potentiation and long-term depression (LTP/LTD). Cold Spring Harb. Perspect. Biol. 4, a005710. https://doi.org/10.1101/cshperspect.a005710
MacGillavry, H.D., Song, Y., Raghavachari, S., Blanpied, T.A., 2013. Nanoscale Scaffolding Domains within the Postsynaptic Density Concentrate Synaptic AMPA Receptors. Neuron 78, 615–622. https://doi.org/10.1016/j.neuron.2013.03.009
Machado-Vieira, R., Baumann, J., Wheeler-Castillo, C., Latov, D., Henter, I.D., Salvadore, G., Zarate, C.A., 2010. The Timing of Antidepressant Effects: A Comparison of Diverse Pharmacological and Somatic Treatments. Pharmaceuticals 3, 19–41. https://doi.org/10.3390/ph3010019
Majláth, Z., Török, N., Toldi, J., Vécsei, L., 2016. Memantine and Kynurenic Acid: Current Neuropharmacological Aspects. Curr. Neuropharmacol. 14, 200–209. https://doi.org/10.2174/1570159X14666151113123221
Malhi, G.S., Mann, J.J., 2018. Depression. Lancet Lond. Engl. 392, 2299–2312. https://doi.org/10.1016/S0140-6736(18)31948-2
Matsuda, S., Peng, H., Yoshimura, H., Wen, T.C., Fukuda, T., Sakanaka, M., 1996. Persistent c-fos expression in the brains of mice with chronic social stress. Neurosci. Res. 26, 157–170.
Mauri, M.C., Ferrara, A., Boscati, L., Bravin, S., Zamberlan, F., Alecci, M., Invernizzi, G., 1998. Plasma and platelet amino acid concentrations in patients affected by major depression and under fluvoxamine treatment. Neuropsychobiology 37, 124–129. https://doi.org/10.1159/000026491
Mayer, M.L., Westbrook, G.L., Guthrie, P.B., 1984. Voltage-dependent block by Mg2+ of NMDA responses in spinal cord neurones. Nature 309, 261–263. https://doi.org/10.1038/309261a0
Maynard, S.A., Ranft, J., Triller, A., 2023. Quantifying postsynaptic receptor dynamics: insights into synaptic function. Nat. Rev. Neurosci. 24, 4–22. https://doi.org/10.1038/s41583-022-00647-9
McCann, K.E., Lustberg, D.J., Shaughnessy, E.K., Carstens, K.E., Farris, S., Alexander, G.M., Radzicki, D., Zhao, M., Dudek, S.M., 2021. Novel role for mineralocorticoid receptors in control of a neuronal phenotype. Mol. Psychiatry 26, 350–364. https://doi.org/10.1038/s41380-019-0598-7
Michaluk, P., Mikasova, L., Groc, L., Frischknecht, R., Choquet, D., Kaczmarek, L., 2009. Matrix Metalloproteinase-9 Controls NMDA Receptor Surface Diffusion through Integrin β1 Signaling. J. Neurosci. 29, 6007–6012. https://doi.org/10.1523/JNEUROSCI.5346-08.2009
Mikasova, L., De Rossi, P., Bouchet, D., Georges, F., Rogemond, V., Didelot, A., Meissirel, C., Honnorat, J., Groc, L., 2012. Disrupted surface cross-talk between NMDA and Ephrin-B2 receptors in anti-NMDA encephalitis. Brain 135, 1606–1621. https://doi.org/10.1093/brain/aws092
Mikasova, L., Xiong, H., Kerkhofs, A., Bouchet, D., Krugers, H.J., Groc, L., 2017. Stress hormone rapidly tunes synaptic NMDA receptor through membrane dynamics and mineralocorticoid signalling. Sci. Rep. 7, 8053. https://doi.org/10.1038/s41598-017-08695-3
Miller, A.H., Maletic, V., Raison, C.L., 2009. Inflammation and its discontents: the role of cytokines in the pathophysiology of major depression. Biol. Psychiatry 65, 732–741. https://doi.org/10.1016/j.biopsych.2008.11.029
Miller, O.H., Yang, L., Wang, C.-C., Hargroder, E.A., Zhang, Y., Delpire, E., Hall, B.J., 2014. GluN2B-containing NMDA receptors regulate depression-like behavior and are critical for the

rapid antidepressant actions of ketamine. eLife 3, e03581. https://doi.org/10.7554/eLife.03581
Mingardi, J., Ndoj, E., Bonifacino, T., Misztak, P., Bertoli, M., La Via, L., Torazza, C., Russo, I., Milanese, M., Bonanno, G., Popoli, M., Barbon, A., Musazzi, L., 2023. Functional and Molecular Changes in the Prefrontal Cortex of the Chronic Mild Stress Rat Model of Depression and Modulation by Acute Ketamine. Int. J. Mol. Sci. 24, 10814. https://doi.org/10.3390/ijms241310814
Mion, G., 2017. History of anaesthesia: The ketamine story – past, present and future. Eur. J. Anaesthesiol. 34, 571–575. https://doi.org/10.1097/EJA.0000000000000638
Mion, G., Villevieille, T., 2013. Ketamine Pharmacology: An Update (Pharmacodynamics and Molecular Aspects, Recent Findings). CNS Neurosci. Ther. 19, 370–380. https://doi.org/10.1111/cns.12099
Moda-Sava, R.N., Murdock, M.H., Parekh, P.K., Fetcho, R.N., Huang, B.S., Huynh, T.N., Witztum, J., Shaver, D.C., Rosenthal, D.L., Alway, E.J., Lopez, K., Meng, Y., Nellissen, L., Grosenick, L., Milner, T.A., Deisseroth, K., Bito, H., Kasai, H., Liston, C., 2019. Sustained rescue of prefrontal circuit dysfunction by antidepressant-induced spine formation. Science 364, eaat8078. https://doi.org/10.1126/science.aat8078
Moghaddam, B., Adams, B., Verma, A., Daly, D., 1997. Activation of glutamatergic neurotransmission by ketamine: a novel step in the pathway from NMDA receptor blockade to dopaminergic and cognitive disruptions associated with the prefrontal cortex. J. Neurosci. Off. J. Soc. Neurosci. 17, 2921–2927. https://doi.org/10.1523/JNEUROSCI.17-08-02921.1997
Moliner, R., Girych, M., Brunello, C.A., Kovaleva, V., Biojone, C., Enkavi, G., Antenucci, L., Kot, E.F., Goncharuk, S.A., Kaurinkoski, K., Kuutti, M., Fred, S.M., Elsilä, L.V., Sakson, S., Cannarozzo, C., Diniz, C.R.A.F., Seiffert, N., Rubiolo, A., Haapaniemi, H., Meshi, E., Nagaeva, E., Öhman, T., Róg, T., Kankuri, E., Vilar, M., Varjosalo, M., Korpi, E.R., Permi, P., Mineev, K.S., Saarma, M., Vattulainen, I., Casarotto, P.C., Castrén, E., 2023. Psychedelics promote plasticity by directly binding to BDNF receptor TrkB. Nat. Neurosci. 26, 1032–1041. https://doi.org/10.1038/s41593-023-01316-5
Mony, L., Paoletti, P., 2023. Mechanisms of NMDA receptor regulation. Curr. Opin. Neurobiol. 83, 102815. https://doi.org/10.1016/j.conb.2023.102815
Mony, L., Zhu, S., Carvalho, S., Paoletti, P., 2011. Molecular basis of positive allosteric modulation of GluN2B NMDA receptors by polyamines. EMBO J. 30, 3134–3146. https://doi.org/10.1038/emboj.2011.203
Monyer, H., Burnashev, N., Laurie, D.J., Sakmann, B., Seeburg, P.H., 1994. Developmental and regional expression in the rat brain and functional properties of four NMDA receptors. Neuron 12, 529–540. https://doi.org/10.1016/0896-6273(94)90210-0
Morris, L.S., Mehta, M., Ahn, C., Corniquel, M., Verma, G., Delman, B., Hof, P.R., Jacob, Y., Balchandani, P., Murrough, J.W., 2022. Ventral tegmental area integrity measured with high-resolution 7-Tesla MRI relates to motivation across depression and anxiety diagnoses. NeuroImage 264, 119704. https://doi.org/10.1016/j.neuroimage.2022.119704
Mössner, R., Mikova, O., Koutsilieri, E., Saoud, M., Ehlis, A.-C., Müller, N., Fallgatter, A.J., Riederer, P., 2007. Consensus paper of the WFSBP Task Force on Biological Markers: biological markers in depression. World J. Biol. Psychiatry Off. J. World Fed. Soc. Biol. Psychiatry 8, 141–174. https://doi.org/10.1080/15622970701263303
Muetzelfeldt, L., Kamboj, S.K., Rees, H., Taylor, J., Morgan, C.J.A., Curran, H.V., 2008. Journey through the K-hole: Phenomenological aspects of ketamine use. Drug Alcohol Depend. 95, 219–229. https://doi.org/10.1016/j.drugalcdep.2008.01.024

Mulders, P.C., van Eijndhoven, P.F., Schene, A.H., Beckmann, C.F., Tendolkar, I., 2015. Resting-state functional connectivity in major depressive disorder: A review. Neurosci. Biobehav. Rev. 56, 330–344. https://doi.org/10.1016/j.neubiorev.2015.07.014
Murillo, A., Navarro, A.I., Puelles, E., Zhang, Y., Petros, T.J., Pérez-Otaño, I., 2021. Temporal Dynamics and Neuronal Specificity of Grin3a Expression in the Mouse Forebrain. Cereb. Cortex N. Y. N 1991 31, 1914–1926. https://doi.org/10.1093/cercor/bhaa330
Nabavi, S., Kessels, H.W., Alfonso, S., Aow, J., Fox, R., Malinow, R., 2013. Metabotropic NMDA receptor function is required for NMDA receptor-dependent long-term depression. Proc. Natl. Acad. Sci. 110, 4027–4032. https://doi.org/10.1073/pnas.1219454110
Nai, Q., Li, S., Wang, S.-H., Liu, J., Lee, F.J.S., Frankland, P.W., Liu, F., 2010. Uncoupling the D1-N-Methyl-D-Aspartate (NMDA) Receptor Complex Promotes NMDA-Dependent Long-Term Potentiation and Working Memory. Biol. Psychiatry 67, 246–254. https://doi.org/10.1016/j.biopsych.2009.08.011
Nair, D., Hosy, E., Petersen, J.D., Constals, A., Giannone, G., Choquet, D., Sibarita, J.-B., 2013. Super-Resolution Imaging Reveals That AMPA Receptors Inside Synapses Are Dynamically Organized in Nanodomains Regulated by PSD95. J. Neurosci. 33, 13204–13224. https://doi.org/10.1523/JNEUROSCI.2381-12.2013
Nandam, L.S., Brazel, M., Zhou, M., Jhaveri, D.J., 2020. Cortisol and Major Depressive Disorder—Translating Findings From Humans to Animal Models and Back. Front. Psychiatry 10. https://doi.org/10.3389/fpsyt.2019.00974
Nemeroff, C.B., 2008. the Pathophysiology of Depression. F O C U J. LIFELONG Learn. PSYCHIATRY.
Niswender, C.M., Conn, P.J., 2010. Metabotropic glutamate receptors: physiology, pharmacology, and disease. Annu. Rev. Pharmacol. Toxicol. 50, 295–322. https://doi.org/10.1146/annurev.pharmtox.011008.145533
Nordvall, G., Forsell, P., Sandin, J., 2022. Neurotrophin-targeted therapeutics: A gateway to cognition and more? Drug Discov. Today 27, 103318. https://doi.org/10.1016/j.drudis.2022.07.003
Nosyreva, E., Szabla, K., Autry, A.E., Ryazanov, A.G., Monteggia, L.M., Kavalali, E.T., 2013. Acute Suppression of Spontaneous Neurotransmission Drives Synaptic Potentiation. J. Neurosci. 33, 6990–7002. https://doi.org/10.1523/JNEUROSCI.4998-12.2013
Nowak, L., Bregestovski, P., Ascher, P., Herbet, A., Prochiantz, A., 1984. Magnesium gates glutamate-activated channels in mouse central neurones. Nature 307, 462–465. https://doi.org/10.1038/307462a0
Ogden, K.K., Traynelis, S.F., 2011. New advances in NMDA receptor pharmacology. Trends Pharmacol. Sci. 32, 726–733. https://doi.org/10.1016/j.tips.2011.08.003
Otte, C., Gold, S.M., Penninx, B.W., Pariante, C.M., Etkin, A., Fava, M., Mohr, D.C., Schatzberg, A.F., 2016. Major depressive disorder. Nat. Rev. Dis. Primer 2, 16065. https://doi.org/10.1038/nrdp.2016.65
Pachernegg, S., Strutz-Seebohm, N., Hollmann, M., 2012. GluN3 subunit-containing NMDA receptors: not just one-trick ponies. Trends Neurosci. 35, 240–249. https://doi.org/10.1016/j.tins.2011.11.010
Pan, P.M., Sato, J.R., Paillère Martinot, M.-L., Martinot, J.-L., Artiges, E., Penttilä, J., Grimmer, Y., van Noort, B.M., Becker, A., Banaschewski, T., Bokde, A.L.W., Desrivières, S., Flor, H., Garavan, H., Ittermann, B., Nees, F., Papadopoulos Orfanos, D., Poustka, L., Fröhner, J.H., Whelan, R., Schumann, G., Westwater, M.L., Grillon, C., Cogo-Moreira, H., Stringaris, A., Ernst, M., IMAGEN Consortium, 2022. Longitudinal Trajectory of the Link

Between Ventral Striatum and Depression in Adolescence. Am. J. Psychiatry 179, 470–481. https://doi.org/10.1176/appi.ajp.20081180
Pan, P.M., Sato, J.R., Salum, G.A., Rohde, L.A., Gadelha, A., Zugman, A., Mari, J., Jackowski, A., Picon, F., Miguel, E.C., Pine, D.S., Leibenluft, E., Bressan, R.A., Stringaris, A., 2017. Ventral Striatum Functional Connectivity as a Predictor of Adolescent Depressive Disorder in a Longitudinal Community-Based Sample. Am. J. Psychiatry 174, 1112–1119. https://doi.org/10.1176/appi.ajp.2017.17040430
Panettieri, R.A., Schaafsma, D., Amrani, Y., Koziol-White, C., Ostrom, R., Tliba, O., 2019. NON-GENOMIC EFFECTS OF GLUCOCORTICOIDS: AN UPDATED VIEW. Trends Pharmacol. Sci. 40, 38–49. https://doi.org/10.1016/j.tips.2018.11.002
Paoletti, P., Bellone, C., Zhou, Q., 2013. NMDA receptor subunit diversity: impact on receptor properties, synaptic plasticity and disease. Nat. Rev. Neurosci. 14, 383–400. https://doi.org/10.1038/nrn3504
Papouin, T., Ladépêche, L., Ruel, J., Sacchi, S., Labasque, M., Hanini, M., Groc, L., Pollegioni, L., Mothet, J.-P., Oliet, S.H.R., 2012. Synaptic and extrasynaptic NMDA receptors are gated by different endogenous coagonists. Cell 150, 633–646. https://doi.org/10.1016/j.cell.2012.06.029
Park, D.K., Stein, I.S., Zito, K., 2022. Ion flux-independent NMDA receptor signaling. Neuropharmacology 210, 109019. https://doi.org/10.1016/j.neuropharm.2022.109019
Parker, G.F., 2014. DSM-5 and Psychotic and Mood Disorders. J. Am. Acad. Psychiatry Law 42.
Parsons, C.G., Stöffler, A., Danysz, W., 2007. Memantine: a NMDA receptor antagonist that improves memory by restoration of homeostasis in the glutamatergic system - too little activation is bad, too much is even worse. Neuropharmacology 53, 699–723. https://doi.org/10.1016/j.neuropharm.2007.07.013
Paul, S., Connor, J.A., 2010. NR2B-NMDA receptor-mediated increases in intracellular Ca2+ concentration regulate the tyrosine phosphatase, STEP, and ERK MAP kinase signaling. J. Neurochem. 114, 1107–1118. https://doi.org/10.1111/j.1471-4159.2010.06835.x
Pause, B.M., Miranda, A., Göder, R., Aldenhoff, J.B., Ferstl, R., 2001. Reduced olfactory performance in patients with major depression. J. Psychiatr. Res. 35, 271–277. https://doi.org/10.1016/s0022-3956(01)00029-2
Peltoniemi, M.A., Hagelberg, N.M., Olkkola, K.T., Saari, T.I., 2016. Ketamine: A Review of Clinical Pharmacokinetics and Pharmacodynamics in Anesthesia and Pain Therapy. Clin. Pharmacokinet. 55, 1059–1077. https://doi.org/10.1007/s40262-016-0383-6
Perroy, J., Raynaud, F., Homburger, V., Rousset, M.-C., Telley, L., Bockaert, J., Fagni, L., 2008. Direct Interaction Enables Cross-talk between Ionotropic and Group I Metabotropic Glutamate Receptors *. J. Biol. Chem. 283, 6799–6805. https://doi.org/10.1074/jbc.M705661200
Petersen, J.D., Chen, X., Vinade, L., Dosemeci, A., Lisman, J.E., Reese, T.S., 2003. Distribution of postsynaptic density (PSD)-95 and Ca2+/calmodulin-dependent protein kinase II at the PSD. J. Neurosci. Off. J. Soc. Neurosci. 23, 11270–11278. https://doi.org/10.1523/JNEUROSCI.23-35-11270.2003
Petit-Pedrol, M., Groc, L., 2021. Regulation of membrane NMDA receptors by dynamics and protein interactions. J. Cell Biol. 220, e202006101. https://doi.org/10.1083/jcb.202006101
Petralia, R.S., Al-Hallaq, R.A., Wenthold, R.J., 2009. Trafficking and Targeting of NMDA Receptors, in: Van Dongen, A.M. (Ed.), Biology of the NMDA Receptor, Frontiers in Neuroscience. CRC Press/Taylor & Francis, Boca Raton (FL).

Petralia, R.S., Wang, Y.-X., Hua, F., Yi, Z., Zhou, A., Ge, L., Stephenson, F.A., Wenthold, R.J., 2010. Organization of NMDA receptors at extrasynaptic locations. Neuroscience 167, 68–87. https://doi.org/10.1016/j.neuroscience.2010.01.022
Pham, T.H., Defaix, C., Xu, X., Deng, S.-X., Fabresse, N., Alvarez, J.-C., Landry, D.W., Brachman, R.A., Denny, C.A., Gardier, A.M., 2018. Common Neurotransmission Recruited in (R,S)-Ketamine and (2R,6R)-Hydroxynorketamine-Induced Sustained Antidepressant-like Effects. Biol. Psychiatry 84, e3–e6. https://doi.org/10.1016/j.biopsych.2017.10.020
Pizzagalli, D.A., Roberts, A.C., 2022. Prefrontal cortex and depression. Neuropsychopharmacology 47, 225–246. https://doi.org/10.1038/s41386-021-01101-7
Pothula, S., Kato, T., Liu, R.-J., Wu, M., Gerhard, D., Shinohara, R., Sliby, A.-N., Chowdhury, G.M.I., Behar, K.L., Sanacora, G., Banerjee, P., Duman, R.S., 2021. Cell-type specific modulation of NMDA receptors triggers antidepressant actions. Mol. Psychiatry 26, 5097–5111. https://doi.org/10.1038/s41380-020-0796-3
Potier, M., Georges, F., Brayda-Bruno, L., Ladépêche, L., Lamothe, V., Abed, A.S.A., Groc, L., Marighetto, A., 2016. Temporal Memory and Its Enhancement by Estradiol Requires Surface Dynamics of Hippocampal CA1 N-Methyl-D-Aspartate Receptors. Biol. Psychiatry 79, 735–745. https://doi.org/10.1016/j.biopsych.2015.07.017
Prescott, D., White, N.D., 2017. When Is Pharmacotherapy Initiation Beneficial in Patients With Depressive Disorders? Am. J. Lifestyle Med. 11, 220–222. https://doi.org/10.1177/1559827616686051
Qi, S., Abbott, C.C., Narr, K.L., Jiang, R., Upston, J., McClintock, S.M., Espinoza, R., Jones, T., Zhi, D., Sun, H., Yang, X., Sui, J., Calhoun, V.D., 2020. Electroconvulsive therapy treatment responsive multimodal brain networks. Hum. Brain Mapp. 41, 1775–1785. https://doi.org/10.1002/hbm.24910
Qian, X., Zhong, Z., Lu, S., Zhang, Y., 2023. Repeated reserpine treatment induces depressive-like behaviors accompanied with hippocampal impairment and synapse deficit in mice. Brain Res. 1819, 148541. https://doi.org/10.1016/j.brainres.2023.148541
Qu, Y., Shan, J., Wang, S., Chang, L., Pu, Y., Wang, X., Tan, Y., Yamamoto, M., Hashimoto, K., 2021. Rapid-acting and long-lasting antidepressant-like action of (R)-ketamine in Nrf2 knock-out mice: a role of TrkB signaling. Eur. Arch. Psychiatry Clin. Neurosci. 271, 439–446. https://doi.org/10.1007/s00406-020-01208-w
Raichle, M.E., MacLeod, A.M., Snyder, A.Z., Powers, W.J., Gusnard, D.A., Shulman, G.L., 2001. A default mode of brain function. Proc. Natl. Acad. Sci. U. S. A. 98, 676–682. https://doi.org/10.1073/pnas.98.2.676
Regan, M.C., Romero-Hernandez, A., Furukawa, H., 2015. A structural biology perspective on NMDA receptor pharmacology and function. Curr. Opin. Struct. Biol. 33, 68–75. https://doi.org/10.1016/j.sbi.2015.07.012
Regehr, W.G., Tank, D.W., 1990. Postsynaptic NMDA receptor-mediated calcium accumulation in hippocampal CA1 pyramidal cell dendrites. Nature 345, 807–810. https://doi.org/10.1038/345807a0
Reiner, A., Levitz, J., 2018. Glutamatergic Signaling in the Central Nervous System: Ionotropic and Metabotropic Receptors in Concert. Neuron 98, 1080–1098. https://doi.org/10.1016/j.neuron.2018.05.018
Rengasamy, M., Mathew, S., Howland, R., Griffo, A., Panny, B., Price, R., 2024. Neural connectivity moderators and mechanisms of ketamine treatment among treatment-resistant depressed patients: a randomized controlled trial. eBioMedicine 99. https://doi.org/10.1016/j.ebiom.2023.104902

Renier, N., Adams, E.L., Kirst, C., Wu, Z., Azevedo, R., Kohl, J., Autry, A.E., Kadiri, L., Venkataraju, K.U., Zhou, Y., Wang, V.X., Tang, C.Y., Olsen, O., Dulac, C., Osten, P., Tessier-Lavigne, M., 2016. Mapping of brain activity by automated volume analysis of immediate early genes. Cell 165, 1789–1802. https://doi.org/10.1016/j.cell.2016.05.007
Renier, N., Wu, Z., Simon, D.J., Yang, J., Ariel, P., Tessier-Lavigne, M., 2014. iDISCO: A Simple, Rapid Method to Immunolabel Large Tissue Samples for Volume Imaging. Cell 159, 896–910. https://doi.org/10.1016/j.cell.2014.10.010
Roca, M., Del Amo, A.R.-L., Riera-Serra, P., Pérez-Ara, M.A., Castro, A., Roman Juan, J., García-Toro, M., García-Pazo, P., Gili, M., 2019. Suicidal risk and executive functions in major depressive disorder: a study protocol. BMC Psychiatry 19, 253. https://doi.org/10.1186/s12888-019-2233-1
Romero-Hernandez, A., Simorowski, N., Karakas, E., Furukawa, H., 2016. Molecular Basis for Subtype Specificity and High-Affinity Zinc Inhibition in the GluN1-GluN2A NMDA Receptor Amino-Terminal Domain. Neuron 92, 1324–1336. https://doi.org/10.1016/j.neuron.2016.11.006
Rothstein, J.D., Dykes-Hoberg, M., Pardo, C.A., Bristol, L.A., Jin, L., Kuncl, R.W., Kanai, Y., Hediger, M.A., Wang, Y., Schielke, J.P., Welty, D.F., 1996. Knockout of glutamate transporters reveals a major role for astroglial transport in excitotoxicity and clearance of glutamate. Neuron 16, 675–686. https://doi.org/10.1016/s0896-6273(00)80086-0
Russo, S.J., Nestler, E.J., 2013. The brain reward circuitry in mood disorders. Nat. Rev. Neurosci. 14, 609–625. https://doi.org/10.1038/nrn3381
Sanacora, G., Smith, M.A., Pathak, S., Su, H.-L., Boeijinga, P.H., McCarthy, D.J., Quirk, M.C., 2014. Lanicemine: a low-trapping NMDA channel blocker produces sustained antidepressant efficacy with minimal psychotomimetic adverse effects. Mol. Psychiatry 19, 978–985. https://doi.org/10.1038/mp.2013.130
Sans, N., Petralia, R.S., Wang, Y.-X., Blahos, J., Hell, J.W., Wenthold, R.J., 2000. A Developmental Change in NMDA Receptor-Associated Proteins at Hippocampal Synapses. J. Neurosci. 20, 1260–1271. https://doi.org/10.1523/JNEUROSCI.20-03-01260.2000
Sarbassov, D.D., Ali, S.M., Sabatini, D.M., 2005. Growing roles for the mTOR pathway. Curr. Opin. Cell Biol. 17, 596–603. https://doi.org/10.1016/j.ceb.2005.09.009
Savitz, J., Drevets, W.C., 2009. Bipolar and Major Depressive Disorder: Neuroimaging the Developmental-Degenerative Divide. Neurosci. Biobehav. Rev. 33, 699–771. https://doi.org/10.1016/j.neubiorev.2009.01.004
Scheidegger, M., Walter, M., Lehmann, M., Metzger, C., Grimm, S., Boeker, H., Boesiger, P., Henning, A., Seifritz, E., 2012. Ketamine Decreases Resting State Functional Network Connectivity in Healthy Subjects: Implications for Antidepressant Drug Action. PLoS ONE 7, e44799. https://doi.org/10.1371/journal.pone.0044799
Schmaal, L., Veltman, D.J., van Erp, T.G.M., Sämann, P.G., Frodl, T., Jahanshad, N., Loehrer, E., Tiemeier, H., Hofman, A., Niessen, W.J., Vernooij, M.W., Ikram, M.A., Wittfeld, K., Grabe, H.J., Block, A., Hegenscheid, K., Völzke, H., Hoehn, D., Czisch, M., Lagopoulos, J., Hatton, S.N., Hickie, I.B., Goya-Maldonado, R., Krämer, B., Gruber, O., Couvy-Duchesne, B., Rentería, M.E., Strike, L.T., Mills, N.T., de Zubicaray, G.I., McMahon, K.L., Medland, S.E., Martin, N.G., Gillespie, N.A., Wright, M.J., Hall, G.B., MacQueen, G.M., Frey, E.M., Carballedo, A., van Velzen, L.S., van Tol, M.J., van der Wee, N.J., Veer, I.M., Walter, H., Schnell, K., Schramm, E., Normann, C., Schoepf, D., Konrad, C., Zurowski, B., Nickson, T., McIntosh, A.M., Papmeyer, M., Whalley, H.C., Sussmann, J.E., Godlewska, B.R., Cowen, P.J., Fischer, F.H., Rose, M., Penninx, B.W.J.H., Thompson, P.M., Hibar, D.P., 2016. Subcortical brain alterations in major depressive disorder: findings from the ENIGMA Major

Depressive Disorder working group. Mol. Psychiatry 21, 806–812. https://doi.org/10.1038/mp.2015.69
Schmidt, M.V., Wang, X.-D., Meijer, O.C., 2011. Early life stress paradigms in rodents: potential animal models of depression? Psychopharmacology (Berl.) 214, 131–140. https://doi.org/10.1007/s00213-010-2096-0
Seeburg, P.H., Burnashev, N., Köhr, G., Kuner, T., Sprengel, R., Monyer, H., 1995. The NMDA Receptor Channel: Molecular Design of a Coincidence Detector, in: Proceedings of the 1993 Laurentian Hormone Conference. Elsevier, pp. 19–34. https://doi.org/10.1016/B978-0-12-571150-0.50006-8
Serchov, T., Van Calker, D., Biber, K., 2016. Sucrose Preference Test to Measure Anhedonic Behaviour in Mice. BIO-Protoc. 6. https://doi.org/10.21769/BioProtoc.1958
Setou, M., Nakagawa, T., Seog, D.-H., Hirokawa, N., 2000. Kinesin Superfamily Motor Protein KIF17 and mLin-10 in NMDA Receptor-Containing Vesicle Transport. Science 288, 1796–1802. https://doi.org/10.1126/science.288.5472.1796
Shamon, S.D., Perez, M.I., 2016. Blood pressure-lowering efficacy of reserpine for primary hypertension. Cochrane Database Syst. Rev. 2016, CD007655. https://doi.org/10.1002/14651858.CD007655.pub3
Shankar, G.M., Li, S., Mehta, T.H., Garcia-Munoz, A., Shepardson, N.E., Smith, I., Brett, F.M., Farrell, M.A., Rowan, M.J., Lemere, C.A., Regan, C.M., Walsh, D.M., Sabatini, B.L., Selkoe, D.J., 2008. Amyloid-β protein dimers isolated directly from Alzheimer's brains impair synaptic plasticity and memory. Nat. Med. 14, 837–842. https://doi.org/10.1038/nm1782
Sheng, M., Kim, E., 2011. The Postsynaptic Organization of Synapses. Cold Spring Harb. Perspect. Biol. 3, a005678–a005678. https://doi.org/10.1101/cshperspect.a005678
Shipton, O.A., Paulsen, O., 2014. GluN2A and GluN2B subunit-containing NMDA receptors in hippocampal plasticity. Philos. Trans. R. Soc. B Biol. Sci. 369, 20130163. https://doi.org/10.1098/rstb.2013.0163
Singh, M., Agarwal, V., Jindal, D., Pancham, P., Agarwal, S., Mani, S., Tiwari, R.K., Das, K., Alghamdi, B.S., Abujamel, T.S., Ashraf, G.M., Jha, S.K., 2023. Recent Updates on Corticosteroid-Induced Neuropsychiatric Disorders and Theranostic Advancements through Gene Editing Tools. Diagnostics 13, 337. https://doi.org/10.3390/diagnostics13030337
Sinner, B., Graf, B.M., 2008. Ketamine. Handb. Exp. Pharmacol. 313–333. https://doi.org/10.1007/978-3-540-74806-9_15
Smith, E.G., Deligiannidis, K.M., Ulbricht, C.M., Landolin, C.S., Patel, J.K., Rothschild, A.J., 2013. Antidepressant augmentation using the N-methyl-D-aspartate antagonist memantine: a randomized, double-blind, placebo-controlled trial. J. Clin. Psychiatry 74, 966–973. https://doi.org/10.4088/JCP.12m08252
Solomon, M.B., 2017. Evaluating social defeat as a model for psychopathology in adult female rodents. J. Neurosci. Res. 95, 763–776. https://doi.org/10.1002/jnr.23971
Song, B., Zhu, J.-C., 2021. Mechanisms of the Rapid Effects of Ketamine on Depression and Sleep Disturbances: A Narrative Review. Front. Pharmacol. 12, 782457. https://doi.org/10.3389/fphar.2021.782457
Song, C., Leonard, B.E., 2005. The olfactory bulbectomised rat as a model of depression. Neurosci. Biobehav. Rev., Animal Models of Depression and Antidepressant Activity 29, 627–647. https://doi.org/10.1016/j.neubiorev.2005.03.010
Sotelo, J.L., Musselman, D., Nemeroff, C., 2014. The biology of depression in cancer and the relationship between depression and cancer progression. Int. Rev. Psychiatry 26, 16–30. https://doi.org/10.3109/09540261.2013.875891

Stein, I.S., Park, D.K., Flores, J.C., Jahncke, J.N., Zito, K., 2020. Molecular Mechanisms of Non-ionotropic NMDA Receptor Signaling in Dendritic Spine Shrinkage. J. Neurosci. Off. J. Soc. Neurosci. 40, 3741–3750. https://doi.org/10.1523/JNEUROSCI.0046-20.2020
Steinpreis, R.E., Salamone, J.D., 1993. The role of nucleus accumbens dopamine in the neurochemical and behavioral effects of phencyclidine: a microdialysis and behavioral study. Brain Res. 612, 263–270. https://doi.org/10.1016/0006-8993(93)91671-e
Strekalova, T., Steinbusch, H.W.M., 2010. Measuring behavior in mice with chronic stress depression paradigm. Prog. Neuropsychopharmacol. Biol. Psychiatry 34, 348–361. https://doi.org/10.1016/j.pnpbp.2009.12.014
Su, T., Lu, Y., Fu, C., Geng, Y., Chen, Y., 2023. GluN2A mediates ketamine-induced rapid antidepressant-like responses. Nat. Neurosci. 26, 1751–1761. https://doi.org/10.1038/s41593-023-01436-y
Sun, Y., Cheng, X., Zhang, L., Hu, J., Chen, Y., Zhan, L., Gao, Z., 2017. The Functional and Molecular Properties, Physiological Functions, and Pathophysiological Roles of GluN2A in the Central Nervous System. Mol. Neurobiol. 54, 1008–1021. https://doi.org/10.1007/s12035-016-9715-7
Sutton, M.A., Ito, H.T., Cressy, P., Kempf, C., Woo, J.C., Schuman, E.M., 2006. Miniature neurotransmission stabilizes synaptic function via tonic suppression of local dendritic protein synthesis. Cell 125, 785–799. https://doi.org/10.1016/j.cell.2006.03.040
Tang, A.-H., Chen, H., Li, T.P., Metzbower, S.R., MacGillavry, H.D., Blanpied, T.A., 2016. A trans-synaptic nanocolumn aligns neurotransmitter release to receptors. Nature 536, 210–214. https://doi.org/10.1038/nature19058
Tang, X.-H., Zhang, G.-F., Xu, N., Duan, G.-F., Jia, M., Liu, R., Zhou, Z.-Q., Yang, J.-J., 2020. Extrasynaptic CaMKIIα is involved in the antidepressant effects of ketamine by downregulating GluN2B receptors in an LPS-induced depression model. J. Neuroinflammation 17, 181. https://doi.org/10.1186/s12974-020-01843-z
Tashakkori, M., Ford, A., Dragovic, M., Gabriel, L., Waters, F., 2021. The time course of psychotic symptom side effects of ketamine in the treatment of depressive disorders: a systematic review and meta-analysis. Australas. Psychiatry Bull. R. Aust. N. Z. Coll. Psychiatr. 29, 80–87. https://doi.org/10.1177/1039856220961642
Teng, C.T., Demetrio, F.N., 2006. Memantine may acutely improve cognition and have a mood stabilizing effect in treatment-resistant bipolar disorder. Rev. Bras. Psiquiatr. Sao Paulo Braz. 1999 28, 252–254. https://doi.org/10.1590/s1516-44462006000300020
Thompson, S.M., 2023. Plasticity of synapses and reward circuit function in the genesis and treatment of depression. Neuropsychopharmacology 48, 90–103. https://doi.org/10.1038/s41386-022-01422-1
Urani, A., Chourbaji, S., Gass, P., 2005. Mutant mouse models of depression: Candidate genes and current mouse lines. Neurosci. Biobehav. Rev. 29, 805–828. https://doi.org/10.1016/j.neubiorev.2005.03.020
Ventriglio, A., Bhugra, D., Sampogna, G., Luciano, M., De Berardis, D., Sani, G., Fiorillo, A., 2020. From dysthymia to treatment-resistant depression: evolution of a psychopathological construct. Int. Rev. Psychiatry 32, 471–476. https://doi.org/10.1080/09540261.2020.1765517
Vogelzangs, N., Beekman, A.T.F., Boelhouwer, I.G., Bandinelli, S., Milaneschi, Y., Ferrucci, L., Penninx, B.W.J.H., 2011. Metabolic Depression: A Chronic Depressive Subtype? Findings From the InCHIANTI Study of Older Persons. J. Clin. Psychiatry 72, 598–604. https://doi.org/10.4088/JCP.10m06559
Warnet, X.L., Bakke Krog, H., Sevillano-Quispe, O.G., Poulsen, H., Kjaergaard, M., 2021. The C-terminal domains of the NMDA receptor: How intrinsically disordered tails affect

signalling, plasticity and disease. Eur. J. Neurosci. 54, 6713–6739. https://doi.org/10.1111/ejn.14842
Watanabe, M., Inoue, Y., Sakimura, K., Mishina, M., 1993. Distinct distributions of five N-methyl-D-aspartate receptor channel subunit mRNAs in the forebrain. J. Comp. Neurol. 338, 377–390. https://doi.org/10.1002/cne.903380305
Wee, K.S.-L., Tan, F.C.K., Cheong, Y.-P., Khanna, S., Low, C.-M., 2016. Ontogenic Profile and Synaptic Distribution of GluN3 Proteins in the Rat Brain and Hippocampal Neurons. Neurochem. Res. 41, 290–297. https://doi.org/10.1007/s11064-015-1794-8
Wenthold, R.J., Prybylowski, K., Standley, S., Sans, N., Petralia, R.S., 2003. Trafficking of NMDA Receptors1. Annu. Rev. Pharmacol. Toxicol. 43, 335–358. https://doi.org/10.1146/annurev.pharmtox.43.100901.135803
White, P.F., Ham, J., Way, W.L., Trevor, A.J., 1980. Pharmacology of ketamine isomers in surgical patients. Anesthesiology 52, 231–239. https://doi.org/10.1097/00000542-198003000-00008
Widman, A.J., McMahon, L.L., 2018. Disinhibition of CA1 pyramidal cells by low-dose ketamine and other antagonists with rapid antidepressant efficacy. Proc. Natl. Acad. Sci. 115. https://doi.org/10.1073/pnas.1718883115
Willner, P., 2017. The chronic mild stress (CMS) model of depression: History, evaluation and usage. Neurobiol. Stress 6, 78–93. https://doi.org/10.1016/j.ynstr.2016.08.002
Willner, P., Mitchell, P.J., 2002. The validity of animal models of predisposition to depression: Behav. Pharmacol. 13, 169–188. https://doi.org/10.1097/00008877-200205000-00001
Wyllie, D.J.A., Livesey, M.R., Hardingham, G.E., 2013. Influence of GluN2 subunit identity on NMDA receptor function. Neuropharmacology 74, 4–17. https://doi.org/10.1016/j.neuropharm.2013.01.016
Yang, B., Qin, J., Nie, Y., Chen, J., 2018. Sustained antidepressant action of the N-methyl-D-aspartate receptor antagonist MK-801 in a chronic unpredictable mild stress model. Exp. Ther. Med. https://doi.org/10.3892/etm.2018.6876
Yin, R., Zhang, K., Li, Y., Tang, Z., Zheng, R., Ma, Y., Chen, Z., Lei, N., Xiong, L., Guo, P., Li, G., Xie, Y., 2023. Lipopolysaccharide-induced depression-like model in mice: meta-analysis and systematic evaluation. Front. Immunol. 14, 1181973. https://doi.org/10.3389/fimmu.2023.1181973
Yohn, C.N., Gergues, M.M., Samuels, B.A., 2017. The role of 5-HT receptors in depression. Mol. Brain 10, 28. https://doi.org/10.1186/s13041-017-0306-y
Zanos, P., Gould, T.D., 2018. Mechanisms of ketamine action as an antidepressant. Mol. Psychiatry 23, 801–811. https://doi.org/10.1038/mp.2017.255
Zanos, P., Moaddel, R., Morris, P.J., Georgiou, P., Fischell, J., Elmer, G.I., Alkondon, M., Yuan, P., Pribut, H.J., Singh, N.S., Dossou, K.S.S., Fang, Y., Huang, X.-P., Mayo, C.L., Wainer, I.W., Albuquerque, E.X., Thompson, S.M., Thomas, C.J., Zarate Jr, C.A., Gould, T.D., 2016. NMDAR inhibition-independent antidepressant actions of ketamine metabolites. Nature 533, 481–486. https://doi.org/10.1038/nature17998
Zanos, P., Moaddel, R., Morris, P.J., Riggs, L.M., Highland, J.N., Georgiou, P., Pereira, E.F.R., Albuquerque, E.X., Thomas, C.J., Zarate, C.A., Gould, T.D., 2018. Ketamine and Ketamine Metabolite Pharmacology: Insights into Therapeutic Mechanisms. Pharmacol. Rev. 70, 621–660. https://doi.org/10.1124/pr.117.015198
Zarate, C.A., Brutsche, N., Laje, G., Luckenbaugh, D.A., Venkata, S.L.V., Ramamoorthy, A., Moaddel, R., Wainer, I.W., 2012. Relationship of ketamine's plasma metabolites with

response, diagnosis, and side effects in major depression. Biol. Psychiatry 72, 331–338. https://doi.org/10.1016/j.biopsych.2012.03.004
Zarate, Carlos A, Singh, J.B., Carlson, P.J., Brutsche, N.E., Ameli, R., Luckenbaugh, D.A., Charney, D.S., Manji, H.K., 2006. A Randomized Trial of an N-methyl-D-aspartate Antagonist in Treatment-Resistant Major Depression. ARCH GEN PSYCHIATRY 63.
Zarate, Carlos A., Singh, J.B., Quiroz, J.A., De Jesus, G., Denicoff, K.K., Luckenbaugh, D.A., Manji, H.K., Charney, D.S., 2006. A double-blind, placebo-controlled study of memantine in the treatment of major depression. Am. J. Psychiatry 163, 153–155. https://doi.org/10.1176/appi.ajp.163.1.153
Zhang, B., Yang, X., Ye, L., Liu, R., Ye, B., Du, W., Shen, F., Li, Q., Guo, Fan, Liu, J., Guo, Fei, Li, Y., Xu, Z., Liu, Z., 2021. Ketamine activated glutamatergic neurotransmission by GABAergic disinhibition in the medial prefrontal cortex. Neuropharmacology 194, 108382. https://doi.org/10.1016/j.neuropharm.2020.108382
Zhou, C., Tajima, N., 2023. Structural insights into NMDA receptor pharmacology. Biochem. Soc. Trans. 51, 1713–1731. https://doi.org/10.1042/BST20230122
Zhu, S., Paoletti, P., 2015. Allosteric modulators of NMDA receptors: multiple sites and mechanisms. Curr. Opin. Pharmacol. 20, 14–23. https://doi.org/10.1016/j.coph.2014.10.009

Title: **Exploring the molecular determinants of behavioral changes induced by ketamine at the nanoscale**

Abstract: In the central nervous system (CNS), NMDA receptors (NMDAR), part of the ionotropic glutamate receptors family, mediate the majority of fast excitatory neuronal transmission. By allowing calcium influx into neuronal cells and subsequent activation of signaling pathways, NMDAR play a central role in synaptic plasticity events that occur during development and underly cognition and memory processes. Recent advances in super resolution microscopy have revealed unexpected dimensions of NMDAR signaling beyond their ionotropic function, which contribute to synaptic physiology. Indeed, NMDAR adopt a precise and dynamically regulated nanoscale organization at synapses which regulates their plasticity and controls memory formation, thereby raising the question whether NMDAR synaptic organization can be of therapeutic interest. Moreover, competitive and non-competitive antagonists like open channel blockers (OCBs) elicit similar inhibition of NMDAR signaling but result in distinct behavioral outcomes, suggesting mechanisms independent of ion flux blocking. Using a combination of super resolution microscopy techniques and behavioral testing, we demonstrate the non-competitive NMDAR antagonist ketamine enhances the synaptic trapping of receptors, and thereby alleviates anxiety/depression-like behavioral deficits caused by autoantibodies from psychotic patients. We then examined whether these changes in NMDAR distribution at synapses may contribute to ketamine-elicited rearrangements in brain connectivity supporting its antidepressant properties. Major depressive disorder is a leading cause of disability worldwide and is believed to be the consequence of abnormal activity in key structures supporting mood and reward, namely cortico-meso-limbic structures. Current treatments, such as serotonin-based pharmacotherapies and psychotherapies, have a delayed onset of action and still up to one-third of patients are resistant. Thus, the recent discovery that a subanesthetic dose of ketamine induce a rapid-acting and sustained antidepressant effect has risen new hopes for the treatment of depression. Despite intense investigation, the mechanisms through which ketamine acts on NMDAR signaling within the cortico-meso-limbic network to produce its antidepressant effect remain unclear. To address this, we have developed a multi-level approach combining single-molecule imaging to monitor NMDAR synaptic redistributions and detection of immediate early gene expression in a pharmacological model of depression using light-sheet microscopy to identify network rearrangements induced by ketamine. Overall, we provide new molecular mechanisms supporting ketamine-elicited behavioral changes, offering NMDAR synaptic distribution manipulation as a therapeutic strategy for both autoantibody-induced pathological deficits and depressive-associated deficits.

Keywords: NMDA receptor, ketamine, nanoscale organization, depression

---

Unité de recherche

Institut Interdisciplinaire de Neurosciences, Université de Bordeaux, UMR5297, Centre Broca Nouvelle Aquitaine, 146 rue Léo Saignat 33076 Bordeaux Cedex (France